Technische Universität München

Fakultät für Maschinenwesen

Lehrstuhl für Windenergie

Sensing from rotor harmonics — Application to wind estimation and imbalance correction

Marta Bertelè

Vollständiger Abdruck der von der Fakultät für Maschinenwesen der Technischen Universität München zur Erlangung des akademischen Grades eines

Doktor-Ingenieurs (Dr.-Ing.)

genehmigten Dissertation.

Vorsitzender:	Prof. Dr.-Ing. Steffen Marburg
Prüfer der Dissertation:	Prof. Dr. Carlo L. Bottasso
Zweiter Prüfer der Dissertation:	Prof. Dr. Po Wen Cheng

Die Dissertation wurde am 22.06.2020 bei der Technischen Universität München eingereicht und durch die Fakultät für Maschinenwesen am 20.10.2020 angenommen.

Technische Universität München
Fakultät für Maschinenwesen
Lehrstuhl für Windenergie
Boltzmannstraße 15
D-85748 Garching bei München
Germany
Tel.: +49 (0) 89 / 289 – 16681
Fax.: +49 (0) 89 / 289 – 16611
Email: info@wind.tum.de
Web: www.wind.mw.tum.de

ABSTRACT

The aim of this dissertation is to exploit the useful information present in the rotor harmonic response to develop new simple and cost effective tools for control and operation and maintenance.
In a nutshell, this means extracting additional valuable information from the measurements already available on the turbine. By thinking outside the box, this information can then be exploited for a variety of different applications, as long as the relation between the rotor harmonic response and the problem at hand is identified.
In this work, this concept was applied to two main research topics, leading to the development of two new methodologies.
First, a wind sensing technology is formulated to estimate the inflow at the rotor disk starting from one per revolution (1P) of out and in-plane blade root bending moments. Indeed, nowadays turbines are not fully aware of the ambient conditions in which they operate. Point-wise measurements of wind direction and shear can be provided for example by met-mast towers, but rarely a complete description of the inflow, measured for example by LiDARs (Light Detection And Ranging), is available. This new wind sensing technology, on the other hand, allows, with no additional hardware costs, to estimate online both vertical and horizontal shears and misalignments once the blade loads are measured. This wind-load relationship can be mapped through system identification once a small training set is available, therefore without the need for a finite element model of the turbine nor for sensitive turbine information. This so called *wind state observer* was extensively validated in a simulation environment, considering a variety of different turbulence intensities and seeds. Moreover, a successful validation was also performed on wind tunnel data and, within its limitation, also on field data. The wind observer proved capable of estimating the fast shear fluctuations, while following the mean trends in wind misalignments. Therefore, the wind observer could represent a useful tool for wind turbine and wind farm control. For example, it could be used to better realign the rotor to the wind, to detect the presence of impinging wakes or, more generally, to provide with reliable information about the inflow within a wind farm.
In addition, a second methodology was developed to first detect and then automatically correct for rotor imbalances starting from measurements on the fixed frame. Indeed, any imbalance, no matter its root cause, will generate additional vibrations on the machine, leading in turn to increased loading and fatigue. Therefore, an imbalance-response model was formulated to relate the 1P fore-aft acceleration on the main bearing to the gravity of the imbalance and also to its location. As a consequence, this linear model can be exploited not only to detect an imbalance, but also to remotely correct for it once access to the machine pitch system is granted. This represents a very important advantage: a remote correction allows to avoid both downtime and very expensive on-site inspections. Once again, the model identification does not require any sensitive turbine information, since it can be performed online just from two measurement points. This rotor rebalancing algorithm was extensively validated in a simulation environment including different turbulence intensities, turbulence seeds and also signal to noise ratios. The method proved very robust and capable of significantly reducing the rotor imbalance within few iterations. As a proof of concept, the algorithm was also tested on a scaled wind turbine model, confirming the results obtained with synthetic data.

I would like to thank my supervisor Professor Carlo L. Bottasso, who granted me this opportunity in the first place. Your guidance and assistance were extremely valuable, both on a professional and on a personal level.
I also want to thank all the current and historic members of the Wind Energy Institute at TUM: Alberto, Bastian, Bruno, Carlo S., Chengyu, Elli, Filippo, Franz, Helena, Jesse, Johannes, Manos, Pietro, Stefan, Stefano, Robin and Vlaho. Thank you for your collaboration, your help and your support, but also for the good times we have had outside the office.
My thanks also go to the students I had the possibility to supervise: Ali, Carlos, Chirag, Irene, Jose, Marco, Max, Mohammad, Onur, Tiasa and Umut. I learned a lot from all of you.
Finally, I would like to thank my friends and my family. Your support and patience led me to where I am today.

Contents

CHAPTER 1

Introduction

The steady growth in energy demand and the increasing awareness of global warming and its consequences present the world with critical and complex challenges. Indeed, sustaining a technological and economic growth while meeting the climate goals ratified in 2015 with the Paris Agreement [1] requires both developed and developing countries to consider CO_2 emissions a main design driver in each aspect of society.
Among others, the power production sector is one of the most relevant in the transition toward sustainability. Looking at the installed capacity in Europe within the last decade, Fig.1.1, more and more importance is placed on renewable sources such as wind and solar, whereas a decrease in new installations can be seen for coal and natural gases [2]. In fact, both solar and wind not only have become more and more cost competitive, but also have the lowest lifecycle CO_2 emissions [3] when compared to other standard and renewable technologies.
Focusing only on wind power, at the end of 2019 there were about 651 GW of installed capacity worldwide, 10% more than the previous year [4]. Europe could count on 205 GW of installed capacity, 183 GW onshore and 22 GW offshore, with a 27% increase with respect to the previous year [5].

To keep the increase in temperature below 2°C [1], the *International Energy Agency* predicts that by 2040 solar and wind will have to supply half of the world electricity demand [6]. Considering that nowadays wind covers a relatively small fraction of the energy demand – 4% of the world energy demand in 2017 [7], while in Europe it supplied about 15% in 2018 and 2019 [2, 5] – wind and solar energy are expected to grow in the coming years. To meet the proposed goals, wind energy needs therefore to continue developing, aiming at further increasing the power production while reducing costs. Moreover, wind energy will also need to address issues that recently became concerns to the public opinion, such as concerns about noise, impact on wildlife, landscape and mental well-being. Indeed, these issues already contributed to stricter regulations in a few countries, causing a contraction in installation in 2019 for example in Germany [5].

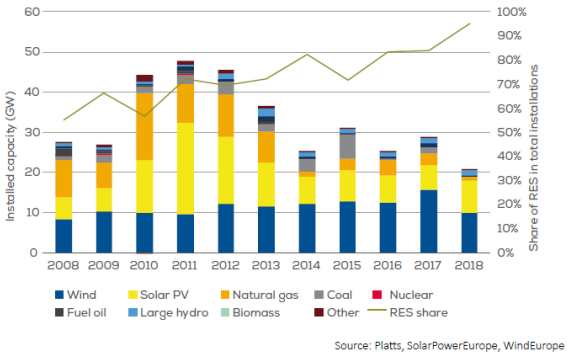

Figure 1.1: Annual installed capacity and renewable share (RES) in EU-28 [2].

1.1 Research topics and innovative content

Within this very complex scenario, this work aims at analysing the rotor harmonic response to develop new methodologies useful both for control and maintenance applications.

Nowadays, modern turbines are equipped with a wide variety of sensors both in the fixed and in the rotating frame. Each of these sensors is installed for one or more specific purposes: strain gages are used to monitor excessive loading, temperature sensors can be used to detect faults, while accelerometers are used for vibration monitoring but also to track the integrity of structural components. Taking a generic bearing as example, one just needs to analyse the measured acceleration signal in terms of the bearing characteristic frequencies to monitor its performance. Indeed, different types of bearing faults – in the inner race, outer race etc. – will occur with different characteristic frequencies, so that one can detect the presence of a fault and also its root cause [8].
But no matter their specific application, all these sensors are actually continuously measuring the response of the turbine during operation. Consequently, by thinking outside the box, these measurements could also be analysed in terms of the rotor rotational speed, to extract other useful information with no additional hardware costs.
Therefore, throughout this dissertation, the generic turbine measurements will be analysed as a function of the turbine rotational frequency, and the resulting frequency spectra will be referred to in the text as *rotor* or *turbine harmonic response*.

This information could be used for a variety of different applications. For example, considering a wind turbine as an input-output system, the analysis of the system output in terms of the rotor rotational frequency could provide information about some of its input, such as the incoming flow. Additionally, once this harmonic response has been characterized, deviations from the expected frequency spectrum could signal the presence of faults, like a rotor imbalance. Moreover, as in the example of a rotating bearing, also in this case different inputs/fault locations could cause different frequency responses: a pitch misalignment on blade one will generate a different harmonic response than a pitch misalignment on the other blades. Therefore, if one were to understand the relationship between the given input/fault and the turbine response, the turbine harmonics could be exploited to estimate the desired input or detect the desired fault.
Taking all this into account, in this thesis the rotor harmonic response will be exploited to answer two research questions.

Can the rotor harmonic response be used to estimate the impinging inflow at the rotor disk?
To answer this question, the relation between rotor harmonics and ambient conditions is analysed first, developing a methodology capable of estimating the incoming inflow starting from measured blade loads. This so called *wind sensing* technology could be exploited to improve wind turbine and wind farm control, thus increasing power production and decreasing fatigue. In addition, by increasing the power capture per surface area, this methodology could also lead to a decrease in the turbine impact on landscape and wildlife.

Can the rotor harmonic response be used not only to detect but also correct for a rotor imbalance?
Exploiting accelerometers installed in the fixed frame, a new procedure is developed to both detect a rotor imbalance – here simulated by a fault in the pitch system – and to remotely correct for it once access to the turbine pitch system is granted. A remote correction constitutes a significant advantage, since vibrations and fatigue can be reduced without a long downtime and expensive on-site inspections.

While in the past most turbines were not equipped with accelerometers and especially blade load sensors, nowadays these instrumentation is becoming more common. Indeed, if not already planned for in the design and manufacturing phase, these sensors can be installed also as a retro-fit on existing machines. In fact, many companies target their condition monitoring systems directly to operators, including therefore the installation of additional sensors. Accelerometers are a standard component of these systems and are usually exploited for vibration monitoring. They are also particularly easy to install, for example either with glue or magnetic mounting, so that a typical installation could take from 30 to 60 minutes [9]. But also blade load sensors can be installed as a retro-fit if needed, not only at the blade root [10, 11] but also at different stations along the blade [12].
Therefore, if these sensors were already installed on a wind turbine for condition or load monitoring purposes, both methodologies described within this dissertation would only consist in a software upgrade.

The following sections will provide a brief overview of the state of the art of both research areas, highlighting the innovative contributions of this work.

1.1.1 Wind sensing

State of the art

Reliable information about the ambient wind conditions impinging the turbine rotor and within a wind farm can be highly beneficial for both wind turbine and wind farm control, but also for lifetime assessment and fatigue consumption estimation, as well as for power and wind forecasting.
Being aware of the actual horizontal misalignment of the rotor with respect to the incoming flow (yaw misalignment angle) can help to correctly realign the rotor to the wind, thus increasing harvested power and decreasing machine loading, and with it reducing vibrations and fatigue. From the point of view of a wind farm controller, a reliable measurement of the yaw misalignment is fundamental for wake redirection strategies [13, 14], where the wake is deflected from the downstream turbines by purposely yawing the upstream ones. Moreover, the presence of a horizontally sheared flow can be used as a detection parameter to identify both the presence and the position of an impinging wake, whereas information about the vertical shear can be used to estimate the stability of the atmosphere, and with it the wake recovery rate. An estimate of the vertical shear can also be used to better tune individual pitch control (IPC) strategies and further reduce loading and fatigue, as well as information about the vertical wind misalignment (upflow angle) becomes especially relevant in complex terrain.

Nowadays, the standard equipment used to measure the incoming inflow consists of cup or sonic anemometers and wind vanes, measuring wind speed and horizontal wind direction at the specific point. When installed on the nacelle, the measurements have the advantage of being recorded at the turbine location but the disadvantage of being affected by several phenomena like blade-passing, nacelle interference or wake-induced flow deformation. Although ad-hoc filtering and tuned transfer functions can be used to correct for these effects, these measurements remain point-wise.
Meteorological towers, i.e. met-masts, generally record several point-wise measurements at different heights (usually up until hub height), providing also a description of the sheared inflow. Nevertheless, met-masts are usually located diameters away from the turbine, so that the evolution of the flow and also wind direction-dependent orographic effects could make the inflow at the mast very different than the one at the turbine.
More complex instrumentation, such as LiDARs and SoDARs [15–17] can be used to obtain a more complete description of the average inflow at the rotor disk, but this instrumentation is not yet used as standard equipment but rather for site assessment and for ad-hoc campaigns due to its still relatively high cost and complexity. Additionally, the performance of such instrumentation is severely dependent

on weather conditions.

To overcome such problems and provide with reliable rotor-effective information of the incoming flow, the concept of wind sensing is an attractive alternative. Indeed, by exploiting the rotor response, one can estimate the average inflow over the rotor disk area, avoiding point-wise measurements and mapping from different geographical locations. A very famous example of wind sensing consists in estimating the rotor-effective wind speed from the torque-balance equation [18]. By mapping the turbine torque/power response over the operating envelope of the machine, the equation is solved for the unknown wind speed once assuming that pitch, rotor speed and torque/power are measured at each instant of time.
The concept of the *rotor as an anemometer* was also introduced by Bottasso et al. [19], who suggested using multiple dynamic equilibrium equations, including tower and blade degrees of freedom, to estimate multiple wind states. This very complex approach, which requires knowledge of several wind turbine states, was later simplified just by mapping the relationship between the out and in-plane blade bending loads to yaw misalignment and vertical shear [20]. Notwithstanding the very promising first validation in the field [21], it was also shown that wind parameters not included in the modelling would negatively affect the results, calling therefore for a richer wind description.
A similar approach was presented by Simley and Pao [22], who related generator speed, fore-aft nacelle acceleration, pitch angle and the out of-plane moments to wind speed, vertical and horizontal shear. This approach nevertheless was only tested in synthetic non turbulent wind, and the effect of not modelled characteristics such as turbulence, yaw or upflow misalignment angles were not considered.
Another application of wind sensing is wake detection for wind farm control, where blade or fixed frame loads are used to estimate the vertical and horizontal shear, thus detecting the presence and location of an impinging wake. Some methodologies mirror the torque-balance equation approach: the out of-plane bending load is mapped over the turbine operating envelope to estimate the wind speed locally experienced by each blade once pitch angle, rotor speed and moments are measured at each instant of time [23–25]. This local wind speed information is then used to quantify the vertical and horizontal shear over the rotor disk. The approach of Cacciola et al. [26], on the other hand, is more similar to what proposed by Bottasso and Riboldi [20]: here the yawing and nodding moments in the fixed frame are directly linked to both shears with a linear model and are then used to estimate the position of the wake. Still, all these approaches do not provide with a comprehensive representation of the impinging inflow, since they do not model the effect of vertical and horizontal misalignment on the machine response.

Innovative contribution

In this work, the approach first proposed by Bottasso et al. [19] is expanded and further developed to relate the machine harmonic response to four wind parameters: vertical and horizontal shears, and vertical and horizontal wind misalignments. Along with the wind speed, these four states can provide with a full first order approximation of the wind field.
A simple either linear or non-linear model is used to relate the four wind states to the one per revolution (1P) of the out and in-plane blade root bending moments (**Paper I**). Indeed, these four parameters will mostly affect the 1P blade harmonics. For example, a vertical shear will change the velocity distribution over the rotor disk such that the blades will experience a minimum velocity in the lower part of the rotor and a maximum velocity at the rotor top. Similar effects will be caused by the misalignment angles and by the horizontal shear as well. Since these wind speed gradients are experienced by each blade once per rotor revolution, it follows that information about these wind parameters can be found in the 1P of the blade response.
Once a rich enough data set of measured loads and wind states is collected – either from synthetic, wind tunnel or field data – the model can be easily identified just by solving a least-squares problem

and then used online to estimate the wind parameters starting from the recorded blade loads. Since the mapping is identified through system identification, other than to generate the synthetic data if working in a simulated environment, there is no need for a finite element model of the turbine nor for sensitive turbine information. In addition, in **Paper II** the rotational symmetry of the rotor response is exploited to simplify the identification procedure to better fit field applications. In a nutshell, this procedure allows one to identify the model starting only from measurements of yaw misalignment and vertical shear, while still being able to then estimate all four parameters. To account for process and measurement noise, a non-deterministic estimation is proposed in **Paper IV**, whereas **Paper V** extends the model formulation to IPC controlled turbines.
The performance of the so called *wind observer* was tested in a simulated environment (**Paper I,II,IV,V**), considering a variety of different turbulent seeds and turbulence intensities, in the wind tunnel (**Paper II**), and in the field (**Paper III**). All the performed analysis confirm that this methodology is capable of estimating the instantaneous value of both shears with considerable accuracy, while the angle variations can be well followed in their mean value. The wind observer can therefore provide with reliable rotor-effective information about the incoming flow, real time and with virtually no additional cost: if load sensors are already installed, it consists in nothing else but a simple software upgrade. In addition, its computational cost is also considerably small: given one day of data sampled at 10 Hz, to estimate the inflow one requires about two minutes on a standard desktop computer, making therefore possible to run the software real time directly on the machine.

1.1.2 Rotor rebalancing

State of the art

The cost of operation and maintenance (O&M) is a significant driver for the cost of energy (CoE), especially when considering offshore installations, where costly on-site inspections can make up for 30% of the overall expenses [27]. Looking more in details at the specific systems, Wilkinson et al. [28] show that the power and rotor module account for almost 50% of the overall failure rate, with as most significant contributors the frequency converter, the generator and, especially, the pitch system, responsible for about 15% of the faults per year. This turbine system results to be the main contributor also for hour of downtime, being responsible for 20% of the overall yearly downtime [28]. Indeed, visual inspections are usually necessary for the detection and the correction of this type of faults, might they be a generic fault in the pitch system or a not correctly installed blade.
When a pitch offset is present among the blades, the aerodynamic, dynamic and gravitational loading experienced by the blades is not balanced. This can lead not only to a decrease in harvested power, but also to additional loading on the machine, significantly increasing rotor speed fluctuations, vibrations and also fatigue [29, 30]. To quantify which level of rotor asymmetry can constitute a problem, one should consider that certification guidelines require the verification of the effects of even relatively small pitch misalignments (typically ±0.3 for two blades; GL Standards, 2010, Sect. 4.3.4.1, pp. 4–20).

To address this issue, several strategies that analyse the turbine fixed frame response have been implemented. Indeed, if the loading among the blades is not balanced, additional harmonic components will appear in the fixed frame spectrum when compared to a balanced configuration. In fact, a balanced rotor acts like a filter, allowing for a transfer from the rotating to the fixed frame only of frequencies multiple of the number of blades. For example, the 1P experienced by the blades of a healthy rotor will not be transferred to the fixed frame: since each blade experiences the same 1P loading with a $\pm 2\pi/3$ phase shift, when summed up, these contribution perfectly cancel each other out. On the other hand, if an imbalance is present, one or more blades will experience a different 1P loading than the others, therefore not allowing for a compensation among blades. Of course, this does not only hold for 1P harmonics but more in general for frequencies not multiple of the number of

blades. Nevertheless, since the lower frequencies are generally the most energetic, the 1P component of a measurement in the fixed frame is the perfect candidate for imbalance detection.

Pierce and Slack [31] and Axelsson et al. [32], for example, very practically suggest to arbitrarily change the pitch settings to monitor the vibration and loading on the shaft and the yaw system. Since no mathematical formulation is presented, it is not possible to completely understand these methodologies and their limitations. A different approach is presented by Cacciola et al. [33], where system identification is used to train a simple classification neural network to estimate the pitch misalignment, its location and its root cause starting from fixed frame loads. This presents an innovative and interesting approach that, nevertheless, has the disadvantage of requiring a rich dataset for training, which should include different types, locations and magnitudes of faults.
Niebsch et al. [34] and Niebsch and Ramlau [35] proposed a method to simultaneously estimate both mass and aerodynamic imbalance effects from nacelle vibrational measurements. This methodology though uses a detailed finite element model of the machine, therefore significantly hindering its applicability. Another different approach was proposed by Kusnick et al. [36], where the blade misalignment estimation is performed by an ad hoc workflow using multiple measurements, including power output, blade loads and accelerations. Alternative approaches have also been developed to correct for rotor imbalances via the action of a turbine controller specifically targeting imbalance-induced vibrations [37–40]. Possible drawbacks are nevertheless the increase in control activity on the turbine, with consequent increase in duty cycle of the pitch system.

Innovative contribution

In this work, a new methodology is developed not only to detect a pitch imbalance, but also to remotely correct for it.
Starting from a measurement in the fixed frame, such as the fore-aft nacelle acceleration (**Paper VI**), the imbalance is detected when the one per revolution (1P) signal is higher than a given threshold. If access to the pitch system is granted, the correction algorithm can then be automatically implemented. This algorithm is based on a linear model relating the location and magnitude of the pitch offset to the chosen 1P measurement. In a nutshell, once the first 1P cosine and sine harmonics are recorded, $s_{(1)}$, the blades are arbitrarily further pitched of known offsets in order to measure a new and different imbalanced configuration, $s_{(2)}$. When these two data points are available, the model can be identified through system identification directly online, without the need for a finite element model of the machine nor a training data set. Once the model has been identified, it can be used to find the pitch offsets that would minimize the 1P signal and to pitch the blades accordingly, $s_{(3)}$. This method can also be applied iteratively, re-identifying the liner model from $s_{(2)}$ and $s_{(3)}$ if the desired 1P threshold is not met. An additional interesting advantage of this methodology is also that, since it aims at minimizing a generic 1P in the fixed frame, it could be also used to mitigate imbalances not caused by pitch faults. Comprehensive studies in a simulated environment (**Paper VI**) show the methodology to be effective and quite robust, being able to reduce the initial imbalance no matter the changes in wind speed, mean inflow or turbulence intensity. A first validation in the wind tunnel, presented in chapter 4.2, also gives a proof of concept of the algorithm.
Since this methodology is based on sensors that might already be installed on most machines, i.e. accelerometers in the fixed frame, it consists in nothing else but a software upgrade, representing a cheap and easy-to implement-solution that virtually avoids any downtime. Moreover, it also does not require any training nor sensitive turbine information, since it is based on online system identification, and it has a minimal computational cost. Indeed, once the measurements are available, a standard desktop computer needs about three seconds to both post process a 10-minute long 10 Hz signal and apply the algorithm.

1.2 Publications

This publication-based dissertation collects six publications, which are referred to in the text as (**Papers I-VI**). The list of publications is presented in § 1.2.1, whereas Fig. 1.2 gives an overview of the thesis structure in terms of both publications and content.

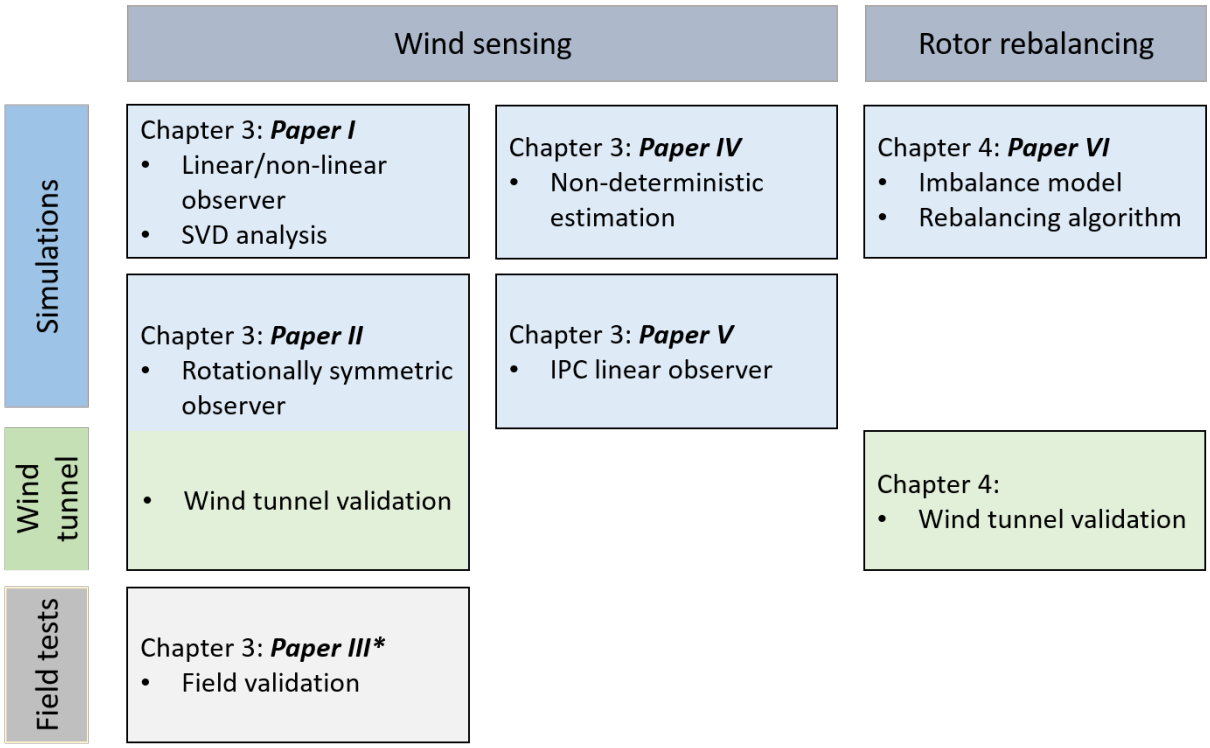

Figure 1.2: Schematic overview of the thesis structure in terms of publications and content; (·)*: paper in review.

The first set of papers (**Paper I-V**) presents the formulation and validation of the here developed wind sensing technology. **Paper I** introduces the so called *wind state observer*, discussing first the relationship between impinging inflow and turbine response, and then formulating both a linear and a non-linear model. A singular value decomposition (SVD) is performed to investigate the structural identifiability of the models, and the wind observer is validated in a comprehensive simulated environment. **Paper II** defines a new and simpler identification procedure exploiting the rotational symmetry in the turbine response. This allows to identify the wind observer even if only two of the four parameters (namely one angle and one shear) are known, while still being able to estimate all four. This new procedure is tested and successfully validated both in simulations and with wind tunnel tests. A further validation, based this time on field data, is presented in **Paper III**. Finally, **Paper IV** and **Paper V** present additional extensions of the method: **Paper IV** introduces the use of a Kalman Filter (KF) in the estimation process, to account for process and measurement noise, whereas **Paper V** extends the observer to IPC-controlled machines.

The problem of rotor rebalancing is addressed in **Paper VI**. Once again, the effect of a pitch imbalance on the turbine response is analysed first. Then, a linear model mapping rotor imbalance and fixed frame accelerations is identified and then used to automatically rebalance the rotor. This rebalancing algorithm is validated with a comprehensive analysis accounting for changes in wind speed, density, mean inflow, turbulence intensity and even noise. Finally, section 4.2 shows, as a first

proof of concept, the validation of the algorithm with a wind tunnel model.

1.2.1 List of publications

This section lists the publications collected in this dissertation. While most have already been published on peer-reviewed journals, **Paper III** and **Paper IV** are still in the review process. For each publication, the corresponding chapter not only includes the published paper, but also its summary and a description of the contribution of each author.

- **Paper I**: M. Bertelè, C. L. Bottasso, S. Cacciola, F. Daher Adegas, and S. Delport, "Wind inflow observation from load harmonics," *Wind Energy Science*, vol. 2, no. 2, pp. 615–640, 2017. doi: 10.5194/wes-2-615-2017.
- **Paper II**: M. Bertelè, C. L. Bottasso, and S. Cacciola, "Brief communication: Wind inflow observation from load harmonics – wind tunnel validation of the rotationally symmetric formulation", *Wind Energy Science*, vol. 4, no. 1, pp. 89–97, 2019. doi: 10.5194/wes-4-89-2019.
- **Paper III (in review)**: M. Bertelè, C. L. Bottasso and J. Schreiber, J., "Wind inflow observation from load harmonics: initial steps towards a field validation, *Wind Energ. Sci. Discuss.* [preprint],2020. doi: 0.5194/wes-2020-83.
- **Paper IV**: M. Bertelè, and C. L. Bottasso, "Non-deterministic wind observation from wind turbine loads," *Journal of Physics: Conference Series*, 1618 062022, 2020. doi: 10.1088/1742-6596/1618/6/062022.
- **Paper V**: M. Bertelè, C. L. Bottasso, and S. Cacciola, "Simultaneous estimation of wind shears and misalignments from rotor loads: formulation for ipc-controlled wind turbines", *Journal of Physics: Conference Series*, vol. 1037, p. 032007, 2018. doi: 10.1088/1742-6596/1037/3/032007.
- **Paper VI**: M. Bertelè, C. L. Bottasso, and S. Cacciola, "Automatic detection and correction of pitch misalignment in wind turbine rotors," *Wind Energy Science*, vol. 3, no. 2, pp. 791–803, 2018. doi: 10.5194/wes-3-791-2018.

CHAPTER 2

Methods

The work collected in this thesis comprises a variety of methods that have been developed and integrated to extract additional valuable information from the machine harmonic response. In this section, a brief overview of the methodology is summarized, whereas a detailed description can be found in the respective publications.

2.1 Wind field parametrization

To characterize the spatial dis-homogeneity of the incoming flow, four wind parameters have been chosen: a linear vertical and horizontal shear, κ_v and κ_h respectively, and a vertical (upflow) and horizontal (yaw) misalignment angle, here named χ and ϕ. Figure 2.1 gives a graphical overview of these wind parameters, defined in a nacelle-attached reference frame.

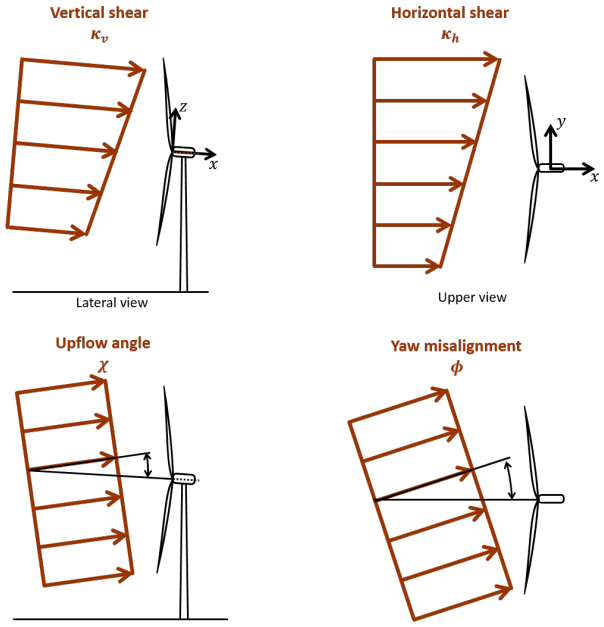

Figure 2.1: Schematic overview of wind parameters.

Although the definition of these so called *wind states* might slightly vary among the publications, i.e. in **Paper I**,**Paper V** and **Paper VI** the vertical shear is the exponential coefficient of a power-law profile, the two angles and shears represent a first approximation of the incoming flow together with the wind speed. Indeed, the wind speed V can be defined as a function of the vertical and horizontal coordinates, z and y respectively, as

$$V(y,z) = V_h\left(1 + \frac{z}{R}\kappa_v + \frac{y}{R}\kappa_h\right), \tag{2.1}$$

with V_h the wind speed at hub height and R the rotor radius. The components of the wind speed vector $\boldsymbol{V} = \{u, v, w\}^T$ are defined as a function of the wind parameters as follows

$$u(y,z) = V(y,z)\cos\phi\cos\chi \tag{2.2a}$$
$$v(y,z) = V(y,z)\sin\phi\cos\chi \tag{2.2b}$$
$$w(y,z) = V(y,z)\sin\chi. \tag{2.2c}$$

Looking at equation Eq. (2.1), one can clearly see the rotational symmetry of the rotor: the effect of a vertical linear shear on the wind inflow is the same as the effect of an equivalent horizontal shear, only with a $\pi/2$ phase shift. The same rotational symmetry holds for the misalignments, at least as long as no large nacelle uptilt angle is present. To overcome such issue, a change of variable can be performed

$$\tilde{v}(y,z) = \frac{v(0,0)}{V_h} = \sin\phi\cos\chi \tag{2.3a}$$
$$\tilde{w}(y,z) = \frac{w(0,0)}{V_h} = \sin\chi, \tag{2.3b}$$

and the wind field can be expressed as a function of the non-dimensional horizontal and vertical crossflow at the hub as

$$u(y,z) = V(y,z)\sqrt{1-\tilde{v}^2-\tilde{w}^2} \tag{2.4a}$$
$$v(y,z) = V(y,z)\tilde{v} \tag{2.4b}$$
$$w(y,z) = V(y,z)\tilde{w}. \tag{2.4c}$$

With this reformulation, one can clearly see that the effect of $\tilde{w}$ on w is the same as the effect of $\tilde{v}$ on v, only with a $\pi/2$ rotation. Finally, inverting Eq. (2.3) both wind misalignments can be easily derived from the newly defined variables

$$\chi = \arcsin(\tilde{w}) \tag{2.5a}$$
$$\phi = \arcsin\left(\tilde{v}/\cos\chi\right). \tag{2.5b}$$

2.2 Harmonic extraction

The response of a stable rotating system can, in general, be considered periodic. In the case of wind turbines, the loading on the machine can be analysed as function of the rotational speed Ω. Indeed, it is intuitive to visualize that any type of perturbation will be perceived by the turbine components once, (1P), twice, (2P) etc. per rotor revolution. For example, gravity will mostly affect the constant (0P) and 1P loading of each blade, while a vertically sheared flow will affect each blade mostly only once per revolution: each perturbation will leave a specific fingerprint in the harmonic response of the machine [20, 47].

Therefore, a generic machine load m can be expanded as a Fourier series as follows

$$m(\psi) = m_0 + \sum_{n=1}^{\infty}\left(m_{n_c}\cos(n\psi) + m_{n_s}\sin(n\psi)\right), \tag{2.6}$$

with ψ the azimuth angle, subscripts $(\cdot)_{n_c}$ and $(\cdot)_{n_s}$ the cosine and sine component of the nP harmonic, and m_0 the 0P constant amplitude.

As explained in details in the following sections, by analysing the harmonic response of different turbine measurements, one can obtain valuable information about the incoming inflow as well as the balancing of the rotor. Since the frequencies of interest are rotor speed-dependent, when extracting the harmonic components order tracking techniques [48–50] should be preferred to a simple Fast Fourier Transform (FFT) [51], where the nP peaks would be smeared over the spectrum if the rotor speed were not constant. In this work, the harmonic extraction is performed using two different techniques: a demodulation algorithm applied in the order domain (**Paper VI**) and the Coleman-Feingold transformation [52].

2.2.1 Harmonic demodulation

To extract the rotor speed-dependent harmonics, the signal is first transformed into the order domain. In a nutshell, the measurement points, which were initially evenly spaced in time, are resampled such that all entries are now equally spaced by shaft rotation: this allows to easily handle variations in rotational speed.

Sinusoidal nP waves are then fit onto the resampled signal, with a moving window whose length depends on the frequency range of interest. In the current case, the window was set to cover one complete rotor revolution. Finally, the nP cosine and sine amplitudes are computed in a least-squares sense. Considering a window containing N elements, from Eq. (2.6) one can write

$$\begin{Bmatrix} m_i \\ \vdots \\ m_N \end{Bmatrix} = \begin{bmatrix} 1 & \cos(n\psi_i) & \sin(n\psi_i) \\ & \ddots & \\ 1 & \cos(n\psi_N) & \sin(n\psi_N) \end{bmatrix} \begin{Bmatrix} m_0 \\ m_{n_c} \\ m_{n_s} \end{Bmatrix} = \boldsymbol{D} \begin{Bmatrix} m_0 \\ m_{n_c} \\ m_{n_s} \end{Bmatrix}, \tag{2.7}$$

and then invert the system to solve for the desired n-harmonic amplitudes

$$\begin{Bmatrix} m_0 \\ m_{n_c} \\ m_{n_s} \end{Bmatrix} = (D^T D)^{-1} D^T \begin{Bmatrix} m_i \\ \vdots \\ m_N \end{Bmatrix}. \tag{2.8}$$

2.2.2 Coleman-Feingold transformation

Another harmonic analysis technique is the Coleman-Feingold transformation [20,52,53], which allows to transform the individual blade measurements in a fixed reference frame. This multi-blade transformation has the advantage to have a small computational cost and to require no signal resampling, but can be applied only to rotors with 3 or more blades.

In this work, the Coleman transformation is used to extract the desired nP blade harmonics from the three available blade measurements as follows

$$\begin{Bmatrix} m_0 \\ m_{n_c} \\ m_{n_s} \end{Bmatrix} = \frac{2}{3} \begin{bmatrix} 1 & 1 & 1 \\ \cos(n\psi^{(1)}) & \cos(n\psi^{(2)}) & \cos(n\psi^{(3)}) \\ \sin(n\psi^{(1)}) & \sin(n\psi^{(2)}) & \sin(n\psi^{(3)}) \end{bmatrix} \begin{Bmatrix} m^{(1)} \\ m^{(2)} \\ m^{(3)} \end{Bmatrix}, \tag{2.9}$$

$m^{(i)}$ being the moment on the generic ith blade. This transformation has the effect of turning the nP harmonics into 0P, while either cancelling out the non-desired contributions or shifting them to a frequency multiple of the number of blades B. Therefore, the output of the transformation also needs to be low pass filtered with a cut-off frequency about or below the BP.

2.3 Wind sensing

In general, wind sensing refers to the possibility of estimating the ambient wind conditions using the turbine itself as a sensor. In this work, the wind parameters defined in Fig. 2.1 – vertical and horizontal shears and misalignments – will be estimated starting from the one per revolution harmonics of out and in-plane blade root bending moments.

2.3.1 Effect of a non-uniform inflow on the rotor harmonic response

To understand the effects of the wind states defined in Fig. 2.1 on the machine harmonic response, one can start with the analysis of the velocity triangle at the blade.
Figure 2.2 shows the velocity triangle and the angle of attack of a generic wing section: $V_\perp$ and $V_{//}$ represent the perpendicular and tangential velocity components, and a is the local induction factor. Let's now imagine a spatially dis-homogeneous wind field like, for example, a vertically sheared inflow. The presence of a vertical shear will affect $V_\perp$.
Moreover, whilst rotating, the ith blade will experience different incident wind speeds, with the maximum $V_\perp$ at the rotor top and a minimum in the lower part of the rotor. This periodic change in wind speed leads also to a periodic change in angle of attack, which in turn causes a periodic loading on the blades. Since this change in angle of attack will be mostly perceived by each blade once per rotor revolution, it follows that the 1P harmonics of the blade loads should carry some information about the wind states. Similar considerations can be made in the presence of a yaw misalignment, which will periodically affect the $V_{//}$ as $\Delta V_{//} = V\sin(\phi)$.

In addition to proving that the defined wind states periodically effect the blade loads, this very simple physical explanation also reveals that the blade loads are more sensitive to variations in wind shears than misalignments. Indeed, as also shown in the sketch, a variation in $V_\perp$ leads to a higher change in angle of attack than an equivalent variation in $V_{//}$. This physical characteristic of the system is also mirrored by the results of the following chapters, which show that the proposed wind sensing technology can estimate shears with more accuracy than misalignments.

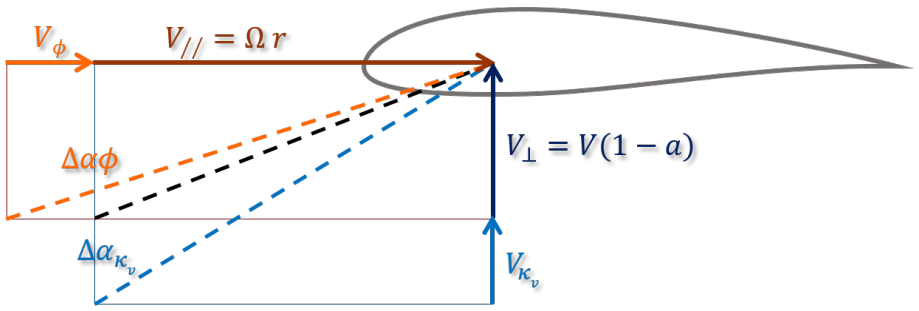

Figure 2.2: Effects of shear and misalignment changes on sectional angle of attack.

2.3.2 Wind observer formulation

To formulate the mapping between blade loads and wind states, we first need to define a wind turbine model expressed by a set of non-linear differential equations together with their output relations:

$$\boldsymbol{f}\big(\boldsymbol{x},\dot{\boldsymbol{x}},\boldsymbol{u}(\boldsymbol{\theta},V,\rho)\big)=\boldsymbol{0}, \tag{2.10a}$$

$$\boldsymbol{y}=\boldsymbol{g}\big(\boldsymbol{x},\dot{\boldsymbol{x}},\boldsymbol{u}(\boldsymbol{\theta},V,\rho)\big), \tag{2.10b}$$

where $\boldsymbol{x}$ is the state vector, $\boldsymbol{u}$ the input vector, $\boldsymbol{y}$ indicates the output vector (containing, in this case, the blade bending moments), and $\boldsymbol{\theta}$ is the wind state vector, collecting the four wind parameters as follows

$$\boldsymbol{\theta} = \{\tilde{v}, \kappa_v, \tilde{w}, \kappa_h\}^T. \tag{2.11}$$

Since the presence of a feedback controller is already modelled by $\boldsymbol{f}(\cdot)$, the input vector $\boldsymbol{u}$ includes only $\boldsymbol{\theta}$, V and the density ρ, i.e. the exogenous disturbances. As already mentioned in § 2.2, the response of the system converges to a periodic solution if the input $\boldsymbol{u}$ can be considered steady

$$\boldsymbol{x} = \boldsymbol{x}_0 + \sum_{n=1}^{\infty} \left(\boldsymbol{x}_{nc}\cos(n\psi) + \boldsymbol{x}_{ns}\sin(n\psi)\right). \tag{2.12}$$

Inserting (2.12) into (2.10a) and collecting all terms at the same frequency (a procedure termed *harmonic balance*), one can compute $\boldsymbol{x}_{nc}$ and $\boldsymbol{x}_{ns}$. Finally, the harmonics $\boldsymbol{x}_{nc}$ and $\boldsymbol{x}_{ns}$ can be inserted into the output Eq. (2.10b), yielding the desired relationship between load harmonics and wind parameters:

$$\boldsymbol{m} = \mathscr{M}(\boldsymbol{\theta}, V, \rho). \tag{2.13}$$

In the following, $\boldsymbol{m}$ will be defined as the vector collecting only the 1P harmonics of blade out and in-plane bending moments, m^{OP} and m^{IP} respectively, as follows

$$\boldsymbol{m} = \{m_{1_c}^{\mathrm{OP}}, m_{1_s}^{\mathrm{OP}}, m_{1_c}^{\mathrm{IP}}, m_{1_s}^{\mathrm{IP}}\}^T. \tag{2.14}$$

Indeed, as shown in **Paper I**, although higher harmonics still carry some information about the wind states, the effects of the wind parameters on higher frequencies is equal, if not smaller, than the effect caused by turbulent fluctuations. Therefore, higher order harmonics are not included in the proposed formulation.
This generic wind-load mapping will clearly depend on $\boldsymbol{\theta}$, V and ρ, whereas the dependency on parameters such as rotor speed or blade pitch angle is here not considered, since such parameters also depend on the ambient and operating conditions, according to the specific regulation strategies. While $\boldsymbol{\theta}$ represents the quantity to be estimated, V and ρ are scheduling parameters, which are known in a simulation environment and either measured or estimated [18, 22, 23, 54, 55] in the field.

The model of Eq. (2.13) represents a classical white box model, i.e. a model derived from analytical formulas relating the relevant parameters based on physical principles [56]. Other than the complexity of the derivation, another disadvantage of this approach is that any mismatch between model and reality might lead to considerable errors. To compensate for those, one could empirically correct the coefficients of Eq. (2.10) via system identification [57] starting from real measurements, formulating a grey box model [56]. In this work, a third approach is proposed: the wind-load mapping will be identified as a black box [56], relating therefore vector $\boldsymbol{m}$ and $\boldsymbol{\theta}$ bypassing any analytical formulas. The model identification can be performed starting from simulation data (**Paper I, II, IV, V**) - here both `CpLambda` [58] and `TurbSim` [59] are used as simulation tools - wind tunnel data (**Paper II**), or field data (**Paper III**). Although the black box model ignores any physics, a physical interpretation of its formulation and of its parameters will be also provided in the following sections.

Linear model

The mapping between wind states, Eq. (2.11), and 1P harmonic components of the blade root out and in-plane bending moments, Eq. (2.14), can be considered in first approximation linear. Indeed, as shown in **Paper I**, the considered harmonics tend to vary linearly with respect to the wind parameters, with only small non-linearities. The linear wind-load model can therefore be expressed as

$$\boldsymbol{m} = \boldsymbol{F}(V,\rho)\boldsymbol{\theta} + \boldsymbol{m}_0(V,\rho) = \boldsymbol{T}\bar{\boldsymbol{\theta}}, \tag{2.15}$$

with $\boldsymbol{F}$ and $\boldsymbol{m}_0$ the unknown model coefficients and $\bar{\boldsymbol{\theta}} = \{\boldsymbol{\theta}^T, 1\}^T$. As explained in details in **Paper I**, matrix $\boldsymbol{F}$ represents the derivative of the 1P cosine and sine moments with respect to the wind states, i.e. the effect the wind dis-homogeneity has on the machine response, whereas $\boldsymbol{m}_0$ represents the constant 1P loading due to gravity, independent from the wind parameters.
Moreover, one can note that the model is scheduled with respect to both V and ρ. While the dependency on ρ is linear and allows one to consider a simple linear correction rather than a real scheduling, the same does not hold for V since, as seen in **Paper I**, the machine behaviour considerably changes with the turbine operating region. Finally, particular attention has to be paid to the term $\boldsymbol{m}_0$. Indeed, this gravitational contribution can be expressed as

$$\boldsymbol{m}_0(V,\rho) = qA\boldsymbol{C}(V,\rho) + \boldsymbol{g}. \tag{2.16}$$

The first term represents the gravity-induced aerodynamic loading: if the blade bends under the effect of thrust, this deformation will cause a non-null lever arm of the gravity force with respect to the blade root, leading to a 1P loading. This term also needs to be scheduled with respect to V and ρ. Vector $\boldsymbol{g}$, on the other hand, represents the out and in-plane gravity-induced loads, caused for example by precone, prebent or uptilt: this term is independent from the inflow conditions. Therefore, before applying a linear correction for density, the blade loads should be also corrected for $\boldsymbol{g}$ (**Paper III**).

To identify the model coefficients, one needs to collect a rich enough data set of significant mean variations of wind parameters while recording the corresponding machine response. Collecting the N wind and load measurements in

$$\boldsymbol{\Theta} = \left[\bar{\boldsymbol{\theta}}_{(1)},\, \bar{\boldsymbol{\theta}}_{(2)},\, ...,\, \bar{\boldsymbol{\theta}}_{(N)}\right], \tag{2.17a}$$

$$\boldsymbol{M} = \left[\boldsymbol{m}_{(1)},\, \boldsymbol{m}_{(2)},\, ...,\, \boldsymbol{m}_{(N)}\right], \tag{2.17b}$$

one can rewrite the system of Eq. (2.15) as

$$\boldsymbol{M} = \boldsymbol{F}\boldsymbol{\Theta} + \boldsymbol{m}_0 = \boldsymbol{T}\boldsymbol{\Theta}, \tag{2.18}$$

and identify the model coefficients in a least-squares sense as

$$\boldsymbol{T} = \boldsymbol{M}\boldsymbol{\Theta}^T\left(\boldsymbol{\Theta}\boldsymbol{\Theta}^T\right)^{-1}. \tag{2.19}$$

Of course, the problem is well posed only if $\boldsymbol{\Theta}\boldsymbol{\Theta}^T$ is not singular: it is therefore fundamental to guarantee a rich enough identification dataset (**Paper I**).
Since the model is scheduled with respect to wind speed and density, the identification is performed for all the desired nodes. This can be done by performing steady simulations at different wind speeds and densities or, if starting from turbulent simulations/field data, by inserting piecewise shape functions centred in the desired nodes in Eq. (2.15) (**Paper III**). As already mentioned, given the linear dependency of the model on ρ, the identification only has to be performed for one chosen reference density, and a linear correction can then be applied.

Rotationally symmetric linear model

The rotationally symmetric formulation addresses the issue of identifying the model of Eq. (2.15) when a complete identification data set is not available. Indeed, if in a simulation environment this might not be a problem, the likelihood of measuring mean significant changes for all parameters when working with field data is not very high. Indeed, a complete description of the wind field as parametrized in

§ 2.1 can mostly be provided only by LiDARs or SoDARS [15, 17], which are not standard installed equipment, while met-mast and nacelle anemometers usually just provide with information about wind speed, wind direction and vertical shear. In addition, even if all wind states could be accurately measured within a field campaign, at a given test site the variations of horizontal shear (excluding possible waked conditions) and especially upflow angle can be considered minimal. Indeed, other than because of small wind direction-dependent orographic effects, such quantities can be considered in average constant at a given site.

To overcome this issue, the rotational symmetry of the rotor is exploited to reduce the number of unknown parameters and, with it, simplify the identification procedure (**Paper II**). Indeed, from Eq. (2.1), it is easy to see that the effect a linear vertical shear has on the wind field, and in turn on the loading, is the same as the effect of an equivalent horizontal shear, only with a $\pi/2$ delay. The same can be said for the vertical and horizontal crossflows, Eq. (2.4), and therefore for the misalignment angles. From the model perspective, this means that

$$\frac{\partial m_{1c}}{\partial \tilde{v}} = \frac{\partial m_{1s}}{\partial \tilde{w}}, \tag{2.20a}$$

$$\frac{\partial m_{1s}}{\partial \tilde{v}} = -\frac{\partial m_{1c}}{\partial \tilde{w}}, \tag{2.20b}$$

$$\frac{\partial m_{1c}}{\partial \kappa_h} = \frac{\partial m_{1s}}{\partial \kappa_v}, \tag{2.20c}$$

$$\frac{\partial m_{1s}}{\partial \kappa_h} = -\frac{\partial m_{1c}}{\partial \kappa_v}, \tag{2.20d}$$

thus reducing the number of unknown coefficients within matrix $\boldsymbol{F}$ from 16 to 8. Additionally, this also shows that if one were to measure only one angle and one shear, for example the yaw misalignment and the vertical shear, as it is usually the case within a field campaign, one could still identify the model of Eq. (2.15). From the identified yaw and vertical shear coefficients, one could then easily derive with Eq. (2.20) the coefficients for horizontal shear and upflow angle.

Non-linear model

In addition to the previously defined linear wind-load mapping, the possibility of a non-linear formulation was also investigated. Indeed, although **Paper I** shows that the out and in-plane 1P harmonics change almost linearly with the wind parameters, small non-linearity are also present.
The model structure remaining the same as Eq. (2.15), the non-linear model is defined as

$$\boldsymbol{m} = \boldsymbol{F}_{\mathrm{NL}}(V,\rho)\boldsymbol{\theta}_{\mathrm{NL}} + \boldsymbol{m}_{\mathrm{NL}_0}(V,\rho), \tag{2.21}$$

with $\boldsymbol{F}_{\mathrm{NL}}$ and $\boldsymbol{m}_{\mathrm{NL}_0}$ the unknown model coefficients and $\boldsymbol{\theta}_{\mathrm{NL}}$ the non-linear wind state vector.
The wind vector contains, in addition to the elements θ_i of $\boldsymbol{\theta}$, their non-linear combinations $\theta_{\mathrm{NL}\,j}$ up to a given order p, where

$$\theta_{\mathrm{NL}\,j} = \prod_i {\theta_i}^{\alpha_i} \quad \text{s.t.} \quad \sum_i \alpha_i \leq p. \tag{2.22}$$

In **Paper I**, non-linear combinations up to $p = 2$ where considered, leading to a wind state vector of 14 terms:

$$\boldsymbol{\theta}_{NL} = \{\tilde{v},\, \kappa_v,\, \tilde{w},\, \kappa_h,\, \tilde{v}\kappa_v,\, \tilde{v}\tilde{w},\, \tilde{v}\kappa_h, \kappa_v\tilde{w},\, \kappa_v\kappa_h,\, \tilde{w}\kappa_h,\, \tilde{v}^2, \kappa_v^2,\, \tilde{w}^2, \kappa_h^2\}^T. \tag{2.23}$$

Despite the good performance of this formulation in both turbulent and non turbulent conditions (**Paper I**), the linear model seems a better alternative for practical applications. Indeed, the higher the degree of non-linearity considered, the higher the number of unknown coefficients: for $p = 2$, the

initial 16 coefficients become 56. In addition, the rotational symmetry cannot be exploited to estimate cross terms such as $\tilde{v}\tilde{w}$, so that a complete dataset is necessary for the model identification. Therefore, **Papers II** to **V** will only focus on the linear formulation, whose performance is just slightly less accurate than the one of the non-linear model.

IPC-controlled machine model

As physically explained in § 2.3.1, the wind state parameters lead to a periodic change in sectional angle of attack and, with it, in the blade bending moments. This effect can nevertheless be mitigated by ad hoc control strategies implemented to reduce the loads on the machine.
In the case of Individual Pitch Control (IPC) [60–62], a PID controller computes the optimal pitch needed to reduce the loading in the fixed frame. Such pitch demand is then transformed to the rotating frame by the inverse of the Coleman transformation, resulting in a cyclic pitching that is then added to the desired collective, Fig 2.3. The frequency of the cyclic pitching is limited by the maximum pitch speed, but is in general further limited to the 1P to reduce duty cycles and because, to generate a 0P reduction of the loads in the fixed frame, one mainly needs to reduce the 1P moments in the rotating frame.

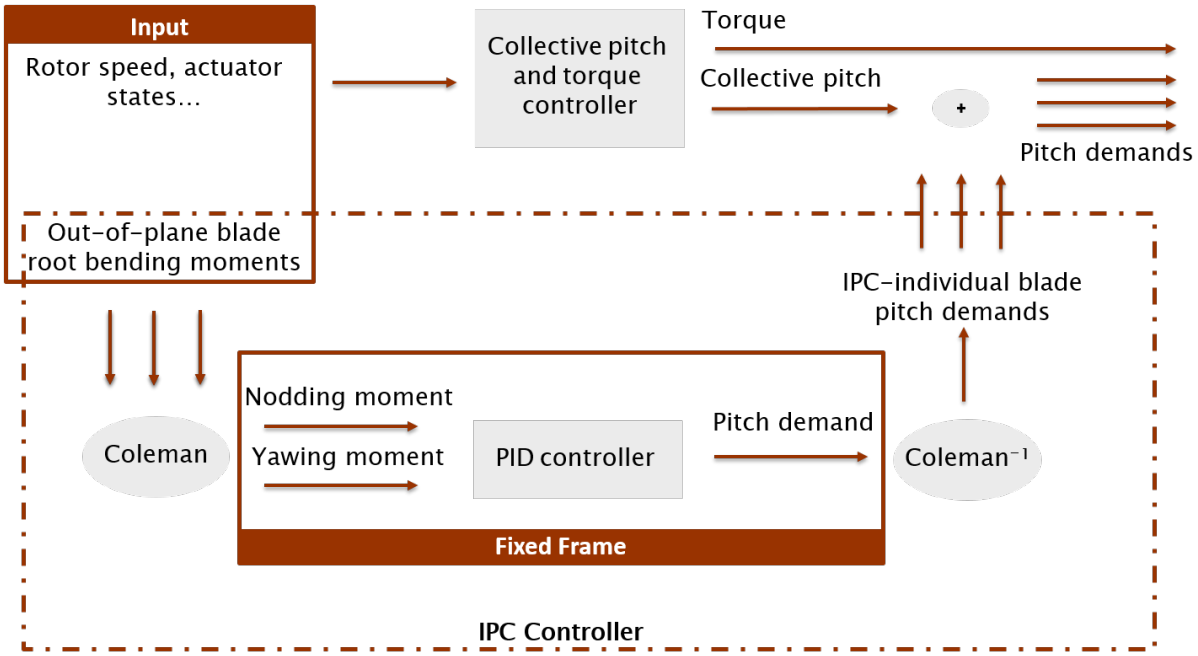

Figure 2.3: Schematic overview of the control system of an IPC-controlled machine.

Therefore, it follows that an IPC controller will flatten the effect wind perturbations have on the out of-plane moment, leading the wind observer of Eq. (2.15) to lose valuable information about the incoming flow. To overcome such problem, a new wind-load mapping was formulated taking into account also the machine pitch response (**Paper V**). Indeed, if the controller cyclically pitches the blades in response to wind perturbations, the information lost in the flattened load measurements can be found in the machine cyclic pitching.
The wind observer is therefore defined as

$$\boldsymbol{m} = \boldsymbol{F}(V,\rho)\boldsymbol{\theta} + \boldsymbol{G}(V,\rho)\boldsymbol{\beta} + \boldsymbol{m}_0(V,\rho), \tag{2.24}$$

with $\boldsymbol{\beta}$ the vector collecting the 1P cosine and sine pitch harmonics and $\boldsymbol{G}$ representing the controller action. To identify this new model, one has to collect a rich data set in which the IPC controller is turned on. Once the measurements are available, the identification procedure follows the previously described steps. Also in this case the rotational symmetry can be exploited to simplify the identification of the model coefficients collected in both $\boldsymbol{F}$ and $\boldsymbol{G}$.
Finally, one should also note that this wind observer can be installed on any turbine, no matter if the IPC controller is present, switched on or switched off. Indeed, once the IPC strategy has been identified with matrix $\boldsymbol{G}$, information on the controller status will be automatically provided by $\boldsymbol{\beta}$.

2.3.3 Wind estimation

The problem of computing an estimate $\boldsymbol{\theta}_{\mathrm{E}}$ of the wind state vector during operation given a measured load harmonic vector $\boldsymbol{m}_{\mathrm{M}}$ and, if needed, a measured pitch harmonic vector $\boldsymbol{\beta}_{\mathrm{M}}$, is considered next.

Deterministic estimation

Once the wind observer, in its different formulations, has been identified, it can be used to estimate the incoming flow from available turbine measurements.

Given the input-output model (2.13), a measured load $\boldsymbol{m}_{\mathrm{M}}$ can be expressed as

$$\boldsymbol{m}_{\mathrm{M}} = \mathscr{M}\left(\boldsymbol{\theta}, V, \rho\right) + \boldsymbol{r}, \tag{2.25}$$

where $\boldsymbol{r}$ is the measurement error with covariance $\boldsymbol{R} = \boldsymbol{E}\left[\boldsymbol{r}\boldsymbol{r}^T\right]$. The residual is assumed to be zero-mean, white and Gaussian. The residual is due not only to measurement noise, but also to all effects not captured by the model, such as sampling and discretization errors, not modelled non-linearities and turbulence-induced loads. This implies that the assumption of a zero-mean, white and gaussian noise can be far from real.

The generalized least-squares estimate of $\boldsymbol{\theta}$ given $\boldsymbol{m}_{\mathrm{M}}$ is

$$\boldsymbol{\theta}_{\mathrm{E}} = \arg\min_{\boldsymbol{\theta}} \Big(\big(\boldsymbol{m}_{\mathrm{M}} - \mathscr{M}\left(\boldsymbol{\theta}, V, \rho\right)\big)^T \boldsymbol{R}^{-1} \big(\boldsymbol{m}_{\mathrm{M}} - \mathscr{M}\left(\boldsymbol{\theta}, V, \rho\right)\big) \Big). \tag{2.26}$$

Consider now the linear model (2.15) and assume V and ρ to be known. The solution of problem (2.26) can be worked out analytically as

$$\boldsymbol{\theta}_{\mathrm{E}} = \left(\boldsymbol{F}(V,\rho)^T \boldsymbol{R}^{-1} \boldsymbol{F}(V,\rho)\right)^{-1} \boldsymbol{F}(V,\rho)^T \boldsymbol{R}^{-1} (\boldsymbol{m}_{\mathrm{M}} - \boldsymbol{m}_0(V,\rho)). \tag{2.27}$$

Vector $\boldsymbol{\theta}_{\mathrm{E}}$ is *structurally identifiable* (or *observable*) if matrix $\boldsymbol{F}(V,\rho)^T \boldsymbol{R}^{-1} \boldsymbol{F}(V,\rho)$ is non singular. The analysis of the structural identifiability of the proposed wind observer, performed through a SVD (**Paper I**), reveals the model to be identifiable; further details can be found also in § 2.3.4.
Similarly, if the IPC-formulation (2.24) were to be used, the analytical solution would be

$$\boldsymbol{\theta}_{\mathrm{E}} = \left(\boldsymbol{F}(V,\rho)^T \boldsymbol{R}^{-1} \boldsymbol{F}(V,\rho)\right)^{-1} \boldsymbol{F}(V,\rho)^T \boldsymbol{R}^{-1} (\boldsymbol{m}_{\mathrm{M}} - \boldsymbol{m}_0(V,\rho) - \boldsymbol{G}(V,\rho)). \tag{2.28}$$

For the non-linear model (2.21), the solution of problem (2.26) involves a non-linear unconstrained minimization, which was solved here starting from a suitable initial guess by the Levenberg-Marquardt method [63]. As multiple local solutions may characterize the non-linear problem, a global search algorithm or multiple starting points should be used for finding the optimum.

Non-deterministic estimation

The estimation procedure described so far is nevertheless completely deterministic: from given measured inputs, the model will output a determined solution. To account for both process and mostly measurement noise, **Paper IV** proposes to couple a Kalman Filter [64, 65] to the estimation procedure. Briefly, this implies that, at any time k, the estimated wind state vector will be

$$\boldsymbol{\theta}_{\mathrm{E}_k} = \boldsymbol{\theta}_{\mathrm{E}_{k-1}} + \hat{\boldsymbol{w}}_{k-1}, \tag{2.29}$$

with $\hat{\boldsymbol{w}}$ the process noise with covariance $\boldsymbol{Q}$, whereas the output equation of the filter writes

$$\boldsymbol{y}_k = \boldsymbol{m}_{\mathrm{M}} - \boldsymbol{m}_{\mathrm{obs}} + \hat{\boldsymbol{v}}_k. \tag{2.30}$$

Matrix $\hat{\boldsymbol{v}}_k$ represents the measurement noise, with covariance $\boldsymbol{P}$, whereas $\boldsymbol{m}_{\mathrm{obs}}$ represents the observed machine response, defined either with Eq. (2.15, 2.24) or Eq. (2.21). Note that the filter output $\boldsymbol{y}_k$ is set to zero to enforce Eq. (2.15, 2.21, 2.24).

2.3.4 Singular value decomposition analysis

As discussed in § 2.3.3, the estimation problem is structurally identifiable if matrix $\boldsymbol{F}(V,\rho)^T\boldsymbol{R}^{-1}\boldsymbol{F}(V,\rho)$ is non singular. To investigate this issue further, a Singular Value Decomposition (SVD) [66] analysis was performed on the wind observer of Eq (2.15) (**Paper I**).

Assuming a linear model, the real (unknown) wind state vector $\boldsymbol{\theta}_{\mathrm{R}}$ is related to the measured load vector $\boldsymbol{m}_{\mathrm{M}}$ as

$$\boldsymbol{m}_{\mathrm{M}} = \boldsymbol{F}\boldsymbol{\theta}_{\mathrm{R}} + \boldsymbol{m}_0 + \boldsymbol{r}. \tag{2.31}$$

Inserting (2.31) into (2.27), the estimation error $\boldsymbol{\epsilon}_\theta$ is readily derived as

$$\boldsymbol{\epsilon}_{\boldsymbol{\theta}} = \boldsymbol{\theta}_{\mathrm{E}} - \boldsymbol{\theta}_{\mathrm{R}} = \left(\boldsymbol{F}^T\boldsymbol{R}^{-1}\boldsymbol{F}\right)^{-1}\boldsymbol{F}^T\boldsymbol{R}^{-1}\boldsymbol{r}. \tag{2.32}$$

The estimate is *unbiased*, as in fact the expected value of the error $\boldsymbol{E}[\boldsymbol{\epsilon}_{\boldsymbol{\theta}}]$ is equal to zero when the residual is zero-mean. Additionally, the covariance of the estimation error $\mathrm{Cov}[\boldsymbol{\epsilon}_{\boldsymbol{\theta}}] = \mathscr{E}\left[\boldsymbol{\epsilon}_{\boldsymbol{\theta}}\boldsymbol{\epsilon}_{\boldsymbol{\theta}}^T\right]$ F [67] writes

$$\mathrm{Cov}[\boldsymbol{\epsilon}_{\boldsymbol{\theta}}] = \left(\boldsymbol{F}^T\boldsymbol{R}^{-1}\boldsymbol{F}\right)^{-1}. \tag{2.33}$$

This expression shows the interplay between noise $\boldsymbol{r}$ and sensitivity $\boldsymbol{F}$, captured by the term $\boldsymbol{R}^{-\frac{1}{2}}\boldsymbol{F}$: the higher the variance and/or the lower the sensitivity of the measurements with respect to the wind states, the worst the accuracy of the estimates.

The covariance $\mathrm{Cov}[\boldsymbol{\epsilon}_{\boldsymbol{\theta}}]$ expressed by Eq. (2.33) is typically fully populated, as the errors of the estimates are correlated. To ease the understanding of the estimation problem, the SVD [66] can be used to decouple the estimates. In fact, matrix $\boldsymbol{R}^{-\frac{1}{2}}\boldsymbol{F}$ can be factored as

$$\boldsymbol{R}^{-\frac{1}{2}}\boldsymbol{F} = \boldsymbol{U}\boldsymbol{\Sigma}\boldsymbol{V}^T, \tag{2.34}$$

where $\boldsymbol{U} \in \Re^{m\times m}$, $\boldsymbol{\Sigma} \in \Re^{m\times n}$ and $\boldsymbol{V} \in \Re^{n\times n}$, being m the number of measurements and n the number of wind state variables. Matrices $\boldsymbol{U}$ and $\boldsymbol{V}$ are orthonormal, i.e. $\boldsymbol{U}^T\boldsymbol{U} = \boldsymbol{U}\boldsymbol{U}^T = \boldsymbol{I}$ and $\boldsymbol{V}^T\boldsymbol{V} = \boldsymbol{V}\boldsymbol{V}^T = \boldsymbol{I}$, whereas $\boldsymbol{\Sigma} = \mathrm{diag}(\ldots, 1/\sigma_i, \ldots)$ is a diagonal matrix and σ_i the standard deviation. Inserting Eq. (2.34) into Eq. (2.33), the covariance of the estimation error can be expressed as

$$\mathrm{Cov}\left[\boldsymbol{V}^T\boldsymbol{\epsilon}_{\boldsymbol{\theta}}\right] = \boldsymbol{E}\left[\left(\boldsymbol{V}^T(\boldsymbol{\theta}_{\mathrm{E}} - \boldsymbol{\theta}_{\mathrm{R}})\right)\left(\boldsymbol{V}^T(\boldsymbol{\theta}_{\mathrm{E}} - \boldsymbol{\theta}_{\mathrm{R}})\right)^T\right] = \left(\boldsymbol{\Sigma}^T\boldsymbol{\Sigma}\right)^{-1} = \mathrm{diag}(\ldots, \sigma_i^2, \ldots). \tag{2.35}$$

This way, the problem is reformulated by the change of variables $\boldsymbol{\xi} = \boldsymbol{V}^T\boldsymbol{\theta}$, where $\boldsymbol{\xi}$ are statistically independent variables with diagonal covariance. This reformulation simplifies the interpretation of

the structural observability of the problem. In fact, the ith column of matrix $\boldsymbol{V}$ linearly combines the wind parameters, mapping them into a new parameter ξ_i with variance σ_i^2. Clearly, a high variance indicates a low level of identifiability of the associated linear combination of wind parameters.
Anticipating some of the results reported in **Paper I**, the SVD analysis revealed that both vertical and horizontal shears can be identified as independent parameters, whereas a coupling is present between the two misalignment angles: this means that an error in the estimation of one angle will propagate in the estimation of the other. Moreover, it was also shown that estimates of both shears have a smaller standard deviation than the estimates of the angles. These trends identified by the SVD analysis highlight, from a mathematical point of view, what was physically described in Fig. 2.2.

Exploiting the properties of the derived matrices even further, one can note that the analysis of $\boldsymbol{U}$ reveals on which linear combination of inflow parameters each load depends the most

$$\frac{\partial \boldsymbol{m}}{\partial \boldsymbol{\xi}} = \boldsymbol{R}^{\frac{1}{2}} \boldsymbol{U} \boldsymbol{\Sigma}. \tag{2.36}$$

A vertical shear predominately affects the cosine components of out and in-plane moments, whereas a horizontal shear affects mostly the sine components of these loads. The two misalignments, on the other hand, do not seem to have a predominant effect on any load components: all loads are affected by yaw and upflow angle, with a slightly higher sensitivity for the in-plane sine and cosine components, respectively. The results of this analysis show once again the $\pi/2$ symmetry between shears and between misalignments, further validating the hypothesis of rotational symmetry of § 2.3.2.

The SVD was here applied for simplicity to the linear model, but of course the same analysis can also be applied to the non-linear case, by linearizing Eq. (2.21) around a specific operating and wind condition and using $\boldsymbol{F} = \partial(\boldsymbol{F}_{\mathrm{NL}}\boldsymbol{\theta}_{\mathrm{NL}})/\partial\boldsymbol{\theta} = \boldsymbol{F}_{\mathrm{NL}}\partial\boldsymbol{\theta}_{\mathrm{NL}}/\partial\boldsymbol{\theta}$.

2.4 Rotor rebalancing

In this work, the rotor response is used to develop a methodology to address and correct for the problem of rotor imbalance, specifically caused by faults in the pitch system.
In details, the 1P harmonic components of accelerations measured in the fixed frame are used as detection parameter. Indeed, knowing that a balanced rotor acts as a filter, i.e. it allows for a transfer to the fixed frame only of frequencies multiple of the number of blades B, the presence of additional harmonics, such as a 1P, is a symptom of an imbalanced configuration.
Once the imbalance has been detected, a linear model relating machine response and pitch misalignment allows for an automatic correction of the imbalance, provided that access to the turbine pitch system is granted.

2.4.1 Effect of a rotor imbalance on the turbine harmonic response

As described in § 2.2, the wind turbine response is periodic and can be expanded in a Fourier series, Eq. (2.6). The generic shear force on the ith blade, for example, can be written as

$$t^{(i)} = {t_0}^{(i)} + \sum_{n=1}^{\infty} \left({t_{nc}}^{(i)} \cos(n\psi^{(i)}) + {t_{ns}}^{(i)} \sin(n\psi^{(i)}) \right). \tag{2.37}$$

Although any loading on the turbine can be expanded as a Fourier series, here the blade shear force is considered because the results reported in **Paper VI** are based on fore-aft accelerations measured on the main bearing, which derive from fluctuations of the thrust $t_{,F}$ in the fixed frame. Of course other measurements in the fixed frame, like for example yawing or nodding moments, could be considered as input for the rebalancing algorithm, but installing accelerometers is easier and more cost-effective than installing strain gages, especially if the installation has to be performed a posteriori.

If the rotor is balanced, the amplitude of the harmonic components will be the same on each blade

$$t_0 = {t_0}^{(i)} = {t_0}^{(j)}, \tag{2.38a}$$
$$t_{nc} = {t_{nc}}^{(i)} = {t_{nc}}^{(j)}, \tag{2.38b}$$
$$t_{ns} = {t_{ns}}^{(i)} = {t_{ns}}^{(j)}. \tag{2.38c}$$

On the other hand, in the presence of an imbalance the harmonic amplitudes of the kth (unbalanced) blade will differ from the other ones, and can be expressed as

$${t_0}^{(k)} = t_0 + \delta t_0, \tag{2.39a}$$
$${t_{nc}}^{(k)} = t_{nc} + \delta t_{nc}, \tag{2.39b}$$
$${t_{ns}}^{(k)} = t_{ns} + \delta t_{ns}. \tag{2.39c}$$

If now one were to compute the thrust force for a generic rotor by summing up the individual shear forces, Fig. 2.4, exploiting the properties of trigonometric functions one would obtain

$$t_{,F} = \sum_{i=1}^{B} t^{(i)}, \tag{2.40a}$$
$$= B t_0 + B \sum_{n=1}^{\infty} \left(t_{nBc} \cos(nB\psi^{(1)}) + t_{nBs} \sin(nB\psi^{(1)}) \right) + \delta t_0 + \sum_{n=1}^{\infty} \left(\delta t_{nc} \cos(n\psi^{(k)}) + \delta t_{ns} \sin(n\psi^{(k)}) \right). \tag{2.40b}$$

For simplicity, the Fourier series can be cropped to the lower frequencies and, grouping together the different harmonics (*harmonic balance*), the final expression for $t_{,F}$ is

$$t_{,F} = (B\,t_0 + \delta\,t_0)_{0\mathrm{P}} + \left(\delta\,t_{1\mathrm{c}}\cos\psi^{(k)} + \delta\,t_{1\mathrm{s}}\sin\psi^{k)}\right)_{1\mathrm{P}} + B\left(t_{B\mathrm{c}}\cos(B\psi^{(1)}) + t_{B\mathrm{s}}\sin(B\psi^{(1)})\right)_{B\mathrm{P}}. \tag{2.41}$$

If the rotor were balanced ($\delta\,t_0 = \delta\,t_{nc} = \delta\,t_{ns} = 0$), only harmonics multiple of the number of blades BP would be present. On the other hand, an imbalance generates additional harmonics that pollute the spectrum, and their phase is symptomatic of the imbalance location. Therefore, it follows that the 1P fixed frame harmonic, being one of the most energetic, is a perfect candidate to detect not only the presence of a rotor imbalance but also its location.

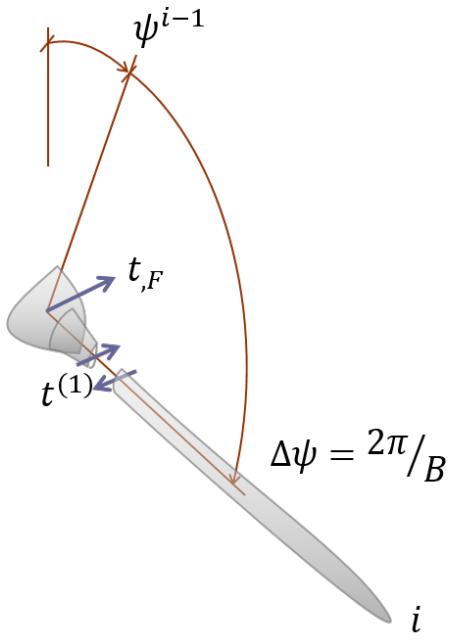

Figure 2.4: Thrust force $t_{,F}$ computed in terms of the shear forces $t^{(i)}$ of the B blades. One single blade is shown for clarity.

2.4.2 Linear imbalance model

In this work, the mapping between 1P fixed frame response and pitch misalignment, i.e. the difference between the desired collective and the actual pitch angle of the blade, is considered to be approximatively linear.
Indeed, computing the shear of the ith blade from a very simple one degree of freedom rigid body model of a flapping blade [68], one can see, in first approximation, the effects of a pitch misalignment on the 0P and 1P harmonics:

$$t_0^{(i)} = -\bar{t}\left(\frac{\Lambda}{2} - \frac{\beta^{(i)}}{3}\right), \tag{2.42a}$$

$$t_{1\mathrm{c}}{}^{(i)} = \bar{t}\left((\Lambda - \beta^{(i)})\bar{V} + \frac{\kappa_v}{3}\bar{U}\right), \tag{2.42b}$$

where $\bar{t} = \gamma J\Omega^2/(2R)$, $\gamma = \rho c C_{L,\alpha} R^4/J$ is the Lock number, ρ the air density, c the blade chord, $C_{L,\alpha}$ the lift slope, R the rotor radius, J the flapping moment of inertia, while $\Lambda = (1-a)V/(\Omega R)$ is the non-dimensional flow velocity at the rotor disk, a being the axial induction and Ω being the rotor

angular velocity. The terms $\bar{V}_0 = V_0/(\Omega R)$ represent the non-dimensional cross-flow, $\bar{U} = V/(\Omega R)$ the non-dimensional wind speed, κ_v the linear vertical wind shear, while β represents the blade pitch angle.

Assuming a pitch misalignment $\delta\beta$, the resulting imbalanced 0P and 1P harmonic amplitudes are:

$$\delta t_0 = \frac{\bar{t}}{3}\delta\beta, \tag{2.43a}$$

$$\delta t_{1c} = -\bar{t}\bar{V}\delta\beta. \tag{2.43b}$$

Although this analysis contemplates only the effects of cross-flow and vertical shear on the 1P harmonics, and although the model is based on one single degree of freedom and includes various simplifications [68], this derivation is useful to visualize that there is in principle a linear dependency between pitch misalignment and 1P harmonics of the blade shear forces, and, in turn, of the nacelle fore-aft accelerations. This linear approximation is also verified by the results of the following chapters, and holds also for fixed frame moments, such as yawing or nodding moments.

Model formulation

Based on the previous considerations, the 1P fixed frame response is related to the pitch misalignment via the following linear model

$$\boldsymbol{s} = \boldsymbol{C}(\boldsymbol{b} - \boldsymbol{b}_m), \tag{2.44a}$$

$$= \boldsymbol{C} + \boldsymbol{s}_m, \tag{2.44b}$$

with $\boldsymbol{s}$ the 1P fixed frame response, collecting the cosine and sine harmonics as follows: $\boldsymbol{s} = \{s_{1c}, s_{1s}\}^T$. Vector $\boldsymbol{s}$ is also scaled with respect to the dynamic pressure $q = 1/2\rho V^2$, in order to reduce the model dependency on the operating conditions.
Vector $\boldsymbol{b}$, defined as $\boldsymbol{b} = \{b^{(1)}, b^{(2)}, b^{(3)}\}^T$, represents the pitch adjustment that can be applied to each blade in order to correct for the individual pitch misalignments $\boldsymbol{b}_m$. Indeed, if one were able to apply a perfect pitch adjustment such that $\boldsymbol{b} = \boldsymbol{b}_m$, then no 1P harmonic would be measured in the fixed frame and $\boldsymbol{s} = 0$. On the other hand, before applying the rebalancing algorithm, $\boldsymbol{b} = 0$ and in the fixed frame one would measure a 1P equal to $\boldsymbol{s} = \boldsymbol{s}_m = -\boldsymbol{C}\boldsymbol{b}_m$.
Finally, $\boldsymbol{C}$ represents the matrix correlating pitch misalignment and machine response, and is defined as

$$\boldsymbol{C} = \begin{bmatrix} {c_c}^{(1)} & {c_c}^{(2)} & {c_c}^{(3)} \\ {c_s}^{(1)} & {c_s}^{(2)} & {c_s}^{(3)} \end{bmatrix}. \tag{2.45}$$

Since the rotor is radially symmetric, i.e. the effects of a pitch misalignment on the second blade will be the same as the those caused by an equivalent misalignment on the first blade, only with a $2\pi/3$ phase shift, one can write

$$\begin{Bmatrix} {c_c}^{(2)} \\ {c_s}^{(2)} \end{Bmatrix} = \begin{bmatrix} \cos(2\pi/3) & \sin(2\pi/3) \\ -\sin(2\pi/3) & \cos(2\pi/3) \end{bmatrix} \begin{Bmatrix} {c_c}^{(1)} \\ {c_s}^{(1)} \end{Bmatrix} = \bar{\boldsymbol{R}}\boldsymbol{c}. \tag{2.46}$$

Clearly, the same argument holds for the relationship between the response of blades two and three. Therefore, matrix $\boldsymbol{C}$ only depends on the two coefficients of vector $\boldsymbol{c}$, and can be written as

$$\boldsymbol{C} = \begin{bmatrix} \boldsymbol{c} & \bar{\boldsymbol{R}}\boldsymbol{c} & \bar{\boldsymbol{R}}^2\boldsymbol{c} \end{bmatrix}. \tag{2.47}$$

While $\boldsymbol{s}$ can be measured and $\boldsymbol{b}$ can be arbitrarily set or derived, $\boldsymbol{C}$ and $\boldsymbol{s}_m$ represent the unknown coefficient of the model that need to be identified.

Model identification

To identify the unknown model coefficients, one can conveniently rewrite the system of Eq. (2.44) as

$$\boldsymbol{s} = \boldsymbol{C}\boldsymbol{b} + \boldsymbol{s}_m, \tag{2.48a}$$

$$= \boldsymbol{B}\boldsymbol{c} + \boldsymbol{s}_m. \tag{2.48b}$$

so that the newly defined matrix $\boldsymbol{B}$ is a sole function of the pitch adjustment $\boldsymbol{b}$

$$\boldsymbol{B} = \begin{bmatrix} B_{11} & B_{12} \\ -B_{12} & B_{11} \end{bmatrix}, \tag{2.49}$$

where

$$B_{11} = b^{(1)} + \cos(2\pi/3)b^{(2)} + (\cos(2\pi/3)^2 - \sin(2\pi/3)^2)b^{(3)}, \tag{2.50a}$$

$$B_{12} = \sin(2\pi/3)b^{(2)} + 2\sin(2\pi/3)\cos(2\pi/3)b^{(3)}. \tag{2.50b}$$

With this reformulation, one can perform the model identification as follows:

- measure the initial 1P signal $\boldsymbol{s}_{(1)}$, before any pitch adjustment has been applied and therefore $\boldsymbol{b}_{(1)} = 0$;
- arbitrarily further pitch the blades, in order to create a second imbalanced configuration $\boldsymbol{s}_{(2)}$, with $\boldsymbol{b}_{(2)} \neq 0$.
  Note that to create a second configuration different from the initial one, $\sum_{i=1}^{3} \boldsymbol{b}^{(i)} = 0$: this also guarantees no change in collective and that $\boldsymbol{s}_{(1)}$ and $\boldsymbol{s}_{(2)}$ are measured at the same operative point.

Once the two measurements are available, one can finally invert the following system and solve for the model coefficients $\boldsymbol{c}$ and $\boldsymbol{s}_m$.

$$\begin{Bmatrix} \boldsymbol{s}_{(1)} \\ \boldsymbol{s}_{(2)} \end{Bmatrix} = \begin{bmatrix} \boldsymbol{B}_{(1)} & \boldsymbol{I} \\ \boldsymbol{B}_{(2)} & \boldsymbol{I} \end{bmatrix} \begin{Bmatrix} \boldsymbol{c} \\ \boldsymbol{s}_m \end{Bmatrix}. \tag{2.51}$$

2.4.3 Rotor rebalancing algorithm

Before applying the rebalancing algorithm, one should understand that the following methodology will have to suggest a pitch adjustment $\boldsymbol{b}$ so that $\sum_{i=1}^{3} b^{(i)} = 0$. Indeed, this *zero collective constraint* not only guarantees to be operating at a constant operative point, making the comparison between 1P amplitudes reasonable, but it also ensures that no collective rotation will be applied on the blades. A collective blade rotation, in fact, does not generate a 1P in the fixed frame: only misalignments among the blades do.
Therefore, the zero collective constraint is attached to the linear model of Eq. (2.44) as follows

$$\begin{Bmatrix} \boldsymbol{s} \\ 0 \end{Bmatrix} = \begin{bmatrix} \boldsymbol{C} \\ \mathbf{1} \end{bmatrix} \boldsymbol{b} + \begin{Bmatrix} \boldsymbol{s}_m \\ 0 \end{Bmatrix}, \tag{2.52}$$

where $\mathbf{1} = (1,1,1)$.

Since the goal of the algorithm is to minimize the measured 1P, to find the pitch adjustments that rebalances the rotor one has to solve the system for $\boldsymbol{b}$ after setting $\boldsymbol{s} = 0$

$$\boldsymbol{b} = -\begin{bmatrix} \boldsymbol{C} \\ \mathbf{1}^T \end{bmatrix}^{-1} \begin{Bmatrix} \boldsymbol{s}_m \\ 0 \end{Bmatrix}. \tag{2.53}$$

Once the pitch adjustment $\boldsymbol{b}$ has been computed, one can measure the residual 1P. If the vibrations are still too large, the method can be iteratively applied until the desired threshold is met. Figure 2.5 gives an overview of the algorithm logic, consisting of the following steps:

- first, the initial 1P $\boldsymbol{s}_{(1)}$ is measured;
- then, the blades are arbitrarily pitched of $\boldsymbol{b}_{(2)}$, so that a new $\boldsymbol{s}_{(2)}$ can be measured;
- the model is identified online with the measured $\boldsymbol{s}_{(1)}$ and $\boldsymbol{s}_{(2)}$;
- the identified model is used to compute the pitch adjustment $\boldsymbol{b}_{(3)}$ that minimizes the fixed frame 1P;
- the 1P in the rebalanced configuration, $\boldsymbol{s}_{(3)}$, is measured. If the desired threshold is not met, the model can be re-identified from $\boldsymbol{s}_{(2)}$ and $\boldsymbol{s}_{(3)}$, and then used to compute the new rebalancing pitch adjustment $\boldsymbol{b}_{(4)}$;
- the process is repeated until the desired 1P threshold is met.

This iterative procedure makes the algorithm very robust to disturbances. Indeed, it helps compensating for significant changes in operative conditions between steps, due for instance to changes in the incoming flow, as well as for possible non-linearities which cannot be modelled by the proposed formulation. Finally, as shown in the following chapters, the method tends to converge within two to three complete iterations of the algorithm, therefore not requiring a significant extra controller activity.

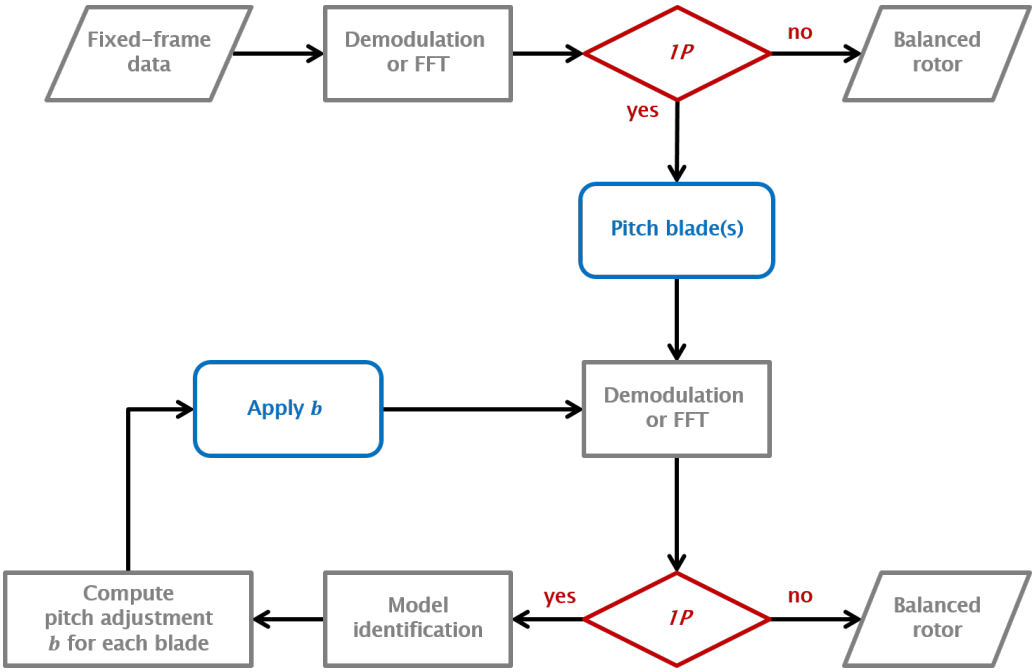

Figure 2.5: Graphical representation of the rotor rebalancing algorithm.

2.4.4 Rebalancing performance on different types of rotor imbalance

The methodology described so far was developed to detect and correct for rotor imbalances caused by a fault in the pitch system. A pitch misalignment angle b_m, i.e. the difference between the desired collective and the actual blade pitch angle, was introduced to simulate different possible faults: an offset in the zero-pitch angle due to an imprecise blade installation, a faulty sensor, a fault in the pitch actuator etc.

Nevertheless, since the method just aims at minimizing the 1P in the fixed frame, it will actually be able to reduce the fixed frame vibrations independently from their root cause. Indeed, no matter if the imbalance is due to ice accretion, soiling, mass variations or a combination of the above: the algorithm will compensate for the current imbalance with an ad hoc generated aerodynamic imbalance.
If the root cause for the imbalance does not strongly depend on the operative point, as in the case of a fault in the pitch system, the final pitch adjustment suggested by the algorithm will be able to constantly minimize the fixed frame vibrations.
On the other hand, if the imbalance strongly depends on the operative point, the algorithm will be able to minimize the 1P harmonics for the present configuration, but might have to be applied again, if needed, if the set point changes significantly. This might be the case if a significant mass imbalance were present, since a mass variation among the blades will lead to different gravitational and centrifugal forces, and the latter strongly depend on the rotor speed [34, 35].

CHAPTER 3

Wind sensing

3.1 Wind inflow observation from load harmonics (Paper I)

3.1.1 Summary

In this work, an already proposed wind sensing technology capable of estimating wind shears and misalignments from machine measured loads is further analysed and validated in a simulated environment.

Expanding on already published work [69], in this paper the spatial non-uniformity in the wind, parametrized with exponential vertical shear, linear horizontal shear and vertical and horizontal wind misalignments, is related to the cosine and sine harmonics of out and in-plane blade root bending moments via a linear and a non-linear model. Indeed, such a dis-homogeneous inflow causes a periodic loading on the machine: mapping this wind-load relationship will allow to estimate the wind parameters in a least-squares sense once the loads on the machine are measured.
Specifically, the one per revolution (1P) component was chosen as input for the mapping, since the effect the parametrized wind states have on higher harmonics is of the same order of magnitude as the effect of turbulent fluctuations. As a result, in realistic inflow conditions including higher harmonics would lead to significant errors.
In addition, a singular value decomposition analysis (SVD) [66] was performed to understand the correlation between parameters and to evaluate the theoretical performance of such observer. It was found that the effect of a vertically or horizontally sheared flow is mostly to be seen in the cosine or sine harmonics of the out of-plane moment, respectively. On the other hand, the misalignments mainly affect the in-plane loading and have a less significant effect on the blade moments than the shears. This can be intuitively visualized just by thinking about the velocity triangle: since a yaw angle would affect the tangential velocity component while a vertical shear the perpendicular one, to obtain the same change in angle of attack one would need a higher variation in misalignment than in shear. Based on these considerations, one could expect the observer to be more accurate in estimating shears than misalignments: this is also another finding of the SVD analysis.

The observer performance was tested simulating the behaviour of a 3 MW machine using a FEM aeroservoelastic simulator, `CpLambda` [58], and wind grids generated by `TurbSim` [59]. Both a linear and a non-linear model were identified from steady tests. Given the dependency of the loads on the operating condition, the models were scheduled with respect to the wind speed, whereas only a linear correction was suggested in case of density variations. A comprehensive analysis, considering wind speeds from 4 to 19 ms^{-1}, turbulence intensities (TI) from 0 to 20% and several turbulent seeds, shows that both the linear and non-linear observer follow the instantaneous values of the shears, while the misalignments can be estimated in their mean values. The standard deviation and mean absolute error in the estimation tend to increase with wind speed and TI, showing a slightly higher accuracy for the non-linear model. It was also proven that changes in the mean yaw misalignment can be followed.

Finally, a lifetime performance assessment of the wind observer was performed using the wind speed and TI distribution measured on the offshore test site FINO1 [70]. Based on 4 years of data, the results show that the observer is expected to estimate the yaw misalignment with an error of 2 deg 95% of the times, and a vertical shear with an error of 0.022. Such results prove very promising both for turbine and wind farm control, also considering that the described wind sensing technology exploits measurements already available on the machine and therefore consists in nothing more than a software upgrade.

3.1.2 Contribution

This paper is the result of the common effort of more authors. In details, Bertelè implemented the proposed observer, while taking care of the simulation pre and post-processing, while Cacciola worked on the lifetime performance assessment. Bottasso and Cacciola guided and supervised the whole work. Finally, all authors further developed the concept and contributed to the writing of this paper.

3.1.3 Reference

M. Bertelè, C. L. Bottasso, S. Cacciola, F. Daher Adegas, and S. Delport, “Wind inflow observation from load harmonics,” *Wind Energy Science*, vol. 2, no. 2, pp. 615–640, 2017. doi: 10.5194/wes-2-615-2017.

3.2 Wind inflow observation from load harmonics – wind tunnel validation of the rotationally symmetric formulation (Paper II)

3.2.1 Summary

In this work, the wind sensing technology capable of estimating wind shears and misalignments from the machine response was further developed and simplified to address field tests requirements. This new formulation was thoroughly validated both with simulations and wind tunnel experiments.

Starting from already published work [41, 69], in this paper the spatial non-uniformity in the wind, here parametrized with a linear vertical and horizontal shear and a vertical and horizontal wind misalignment, was related via a linear model to the one per revolution (1P) cosine and sine harmonics of the out of and in-plane blade root bending moments. Indeed, since a spatially non uniform wind leads to periodic loading, a linear mapping can be identified between wind parameters and 1P blade moments so that, once the turbine loads are measured, the wind states can be estimated from the machine response in a least-squares sense.
To identify a model depending on four parameters, i.e. the four wind states, one requires a comprehensive set of tests in which all parameters experience sensitive variations in their mean value. This might not often be the case if field data are used: the vertical misalignment, for example, tends to be constant for a given test site. To overcome such problem, a new identification procedure that exploits the rotational symmetry of the rotor is presented. Indeed, it is intuitive to visualize that the effect a vertically sheared flow has on the blade loads is the same as the effect of a horizontally sheared one, only with a $\pi/2$ phase shift; the same holding for the wind misalignments. Therefore, as long as the training data set includes sensitive changes in one angle and one shear the identification can be performed: the coefficients related to the missing parameters can be easily derived through rotor symmetry.

To validate this new identification procedure, the performance of the so called rotationally symmetric observer was compared to the one of the already validated linear model. Several tests were run simulating the behaviour of a 3 MW horizontal axis machine with the aeroservoelastic FEM simulator `CpLambda` [58] starting from inflows provided by `TurbSim` [59]. Steady tests were used to identify both models and to schedule them with respect to the wind speed, in order to account for the dependency of the loads on the operating condition. Comparing both the standard deviation and mean absolute error in the parameter observations for wind speeds between 4 to 15 ms^{-1}, turbulence intensities (TI) from 2 to 16% and more turbulent seeds, no significant difference can be noted between the two models. The estimation accuracy tends to decrease with wind speed and TI, and the maximum expected error in yaw and vertical shear estimation is, for both models, smaller than 2.5 deg and 14e-03 respectively. Finally, this wind observer, and with it its rotor symmetric formulation, was also tested for the first time in the wind tunnel. An aeroelastically scaled wind turbine model, with 2 m rotor diameter, 1.8 m hub height and strain gages at the root of each blade, was placed in the test section of the Politecnico di Milano [71]. Two different vertical shears and turbulent intensities, 3.8 and 8.5 % TI, were simulated and measured with hot wire probes. The rotationally symmetric observer was identified starting from 30% of the available tests, including wind speeds in both regions II and III, and only changes in vertical shear and yaw misalignment: the coefficients of the remaining parameters were derived through rotor symmetry. Changes in horizontal misalignment were also performed and were included only in the validation set. Given the accuracy in the inflow estimation, these wind tunnel experiments not only validate the proposed technology, but also this more field test-friendly identification procedure. Moreover, the performance accuracy is in accordance with the synthetic data, leading to a maximum mean error, for 8.5 % TI, of 1 deg and 7e-3 in the estimation of angles and shears, respectively.

3.2.2 Contribution

This paper is the result of the common effort of more authors. In details, Bertelè implemented the proposed observer, while taking care of the simulation pre and post-processing. Bottasso and Cacciola guided and supervised the whole work. Finally, all authors further developed the concept and contributed to the writing of this paper.

3.2.3 Reference

M. Bertelè, C. L. Bottasso, and S. Cacciola, "Brief communication: Wind inflow observation from load harmonics – wind tunnel validation of the rotationally symmetric formulation", *Wind Energy Science*, vol. 4, no. 1, pp. 89–97, 2019. doi: 10.5194/wes-4-89-2019.

3.3 Wind inflow observation from load harmonics: initial steps towards a field validation (Paper III)

3.3.1 Summary

In this paper, a first field validation of the already described wind sensing technology capable of estimating wind shears and misalignments from the rotor loads was performed.

The one per revolution (1P) out and in-plane blade root bending loads of a 3.5 MW machine, with 92 m hub height and 114.9 m rotor diameter, were related to the wind inflow via a linear model. Indeed, given that any spatial dis-homogeneity in the wind, here parametrized with linear vertical and horizontal shears and misalignments, causes a periodic loading on the machine, by mapping this wind-load response one might estimate in a least-squares sense the wind states starting from measured loads [41, 42, 69].

Information about the impinging inflow was provided by a nearby met-mast, measuring wind speed and wind direction, and by another wind observer [25], capable of estimating vertical and horizontal shears also starting from rotor loads. Indeed, while the met-mast can provide with a reference for the turbine yaw misalignment, which is nevertheless still point-wise and not rotor-effective, the met-mast derived vertical shear might not be representative of the full rotor shear, since the met-mast reaches only up to hub height. Therefore, the observer described in [25], whose successful validation was performed within the same test campaign, is here used as reference for both shears. No information about the vertical misalignment was provided: the rotational symmetry of the rotor was exploited to derive the upflow coefficients [42]. The linear model, identified from 15% of the available data, was also scheduled with respect to the wind speed, computed via the torque balance equation, and a density correction was also implemented to account for the model dependency on the operating conditions.

The results obtained over about 40 days of data show that the observer can very well follow the instantaneous variation in shears and the mean values of yaw misalignment. Indeed, with respect to the met-mast reference, the maximum mean absolute error is about 0.06 and 3 deg respectively. The performance does not seem to be significantly affected by turbulence or density variations, whereas the incoming wind direction plays a role in the vertical shear estimation. The fact that the minimum estimation error is obtained when turbine and mast are aligned proves once again that the met-mast, not co-located with the turbine and providing only point-wise measurement of the lower half the rotor, might not be an exact ground truth. Nevertheless, despite the not exact reference provided by the mast, the very convincing performance of the observer suggests that its implementation is possible even in a standard turbine-mast set up.

3.3.2 Contribution

This paper is the result of the common effort of more authors. In details, Bertelè implemented the proposed observer, while taking care of the simulation pre and post-processing. Schreiber also took part in the post-processing, while Bottasso guided and supervised the whole work. Finally, all authors further developed the concept and contributed to the writing of this paper.

3.3.3 Reference

M. Bertelè, C. L. Bottasso and J. Schreiber, J., “Wind inflow observation from load harmonics: initial steps towards a field validation, *Wind Energ. Sci. Discuss.* [preprint],2020. doi: 0.5194/wes-2020-83.

3.4 Non-deterministic wind observation from wind turbine loads (Paper IV)

3.4.1 Summary

In this work, the already proposed wind sensing technology capable of estimating wind shears and misalignments from the turbine response is further developed into a non-deterministic formulation.

Building on already published work [41,42,69], the wind spatial dis-homogeneity, here parametrized as linear vertical and horizontal shears, as well as vertical and horizontal misalignments, is linked to the one per revolution (1P) out and in-plane blade root bending moments through a linear model. Indeed, such a non-uniform wind field will cause a periodic loading in the machine response: by mapping this wind-load relation one can then estimate in a least-squares sense the wind parameters once the blade loads are measured. So far, this wind observer model was deterministically formulated: in this work, a Kalman Filter (KF) [64,65] is employed to account for both process and measurement noise.

To evaluate the increase in performance of this new non-deterministic formulation with respect to the deterministic one, the behaviour of a 3 MW machine was simulated with a FEM aeroservoelastic tool, `CpLambda` [58], under uniform and turbulent inflows provided by `TurbSim` [59]. Both a linear and rotationally symmetric linear model were identified and then scheduled with respect to the wind speed, in order to account for the load dependency on the operating condition. In a nutshell, the rotationally symmetric model differs from the linear one only in the identification procedure [42]. While the linear model is identified from measurements of all four parameters, the symmetric model assumes only two, for example vertical shear and yaw misalignment, to be measurable: the coefficients of the missing wind states can then be mathematically derived after identification exploiting the rotor symmetry. This can be particularly important when working with field data, where variations in upflow angle are not very likely to occur at a given test site.
Several tests performed with wind speeds ranging from 7 to 17 ms^{-1}, turbulence intensities from 5 to 12% and different turbulent seeds prove the the non-deterministic formulation can significantly increase the accuracy of angle estimations, while no significant improvement can be noted for the shears. Indeed, applying a KF to both the linear and rotationally symmetric model, for higher wind speeds and turbulence the mean absolute error can decrease from 4 to about 2 deg. Moreover, one can once again note that there is no difference in performance between linear and symmetric model, suggesting that the identification procedure can indeed be simplified for field test applications without worsening the estimation accuracy.

3.4.2 Contribution

This paper is the result of the common effort of more authors. In details, Bertelè implemented the proposed observer, while taking care of the simulation pre and post-processing. Bottasso guided and supervised the whole work. Finally, both authors further developed the concept and contributed to the writing of this paper.

3.4.3 Reference

M. Bertelè, and C. L. Bottasso, "Non-deterministic wind observation from wind turbine loads," *Journal of Physics: Conference Series*, 1618 062022, 2020. doi: 10.1088/1742-6596/1618/6/062022.

3.5 Simultaneous estimation of wind shears and misalignments from rotor loads: formulation for IPC-controlled wind turbines (Paper V)

3.5.1 Summary

In this work, the already proposed wind sensing technology capable of estimating wind shears and misalignments from the turbine response is extended to IPC-controlled machines.

Following previously published work [41, 69], in this paper the spatial non-uniformity in the wind, here parametrized with vertical exponential shear, linear horizontal shear, vertical and horizontal misalignments, is related via a linear model to the one per revolution (1P) cosine and sine harmonics of the pitch angle and of the out and in-plane blade root bending moments. Indeed, a non-uniform wind will cause a periodic loading on the blades which, in the case of an IPC-controlled machine, will be counteracted by a sinusoidal pitching. An IPC-controller aims, in fact, at minimizing the loading on the turbine by periodically changing the angle of attack of each blade depending on its individual azimuthal position [60–62]. It follows therefore that, although the controller will tend to flatten the effect a wind dis-homogeneity has on the blade loads, information about the impinging inflow can be derived by the action of the controller itself.

This newly developed formulation was tested on a 3 MW machine simulated with a FEM aeroservoelastic tool, `CpLambda` [58], using turbulent and non turbulent grids provided by `TurbSim` [59]. The linear wind-turbine response mapping was identified from steady simulations with and without IPC-controller, scheduled with respect to the wind speed to consider the dependency on the operating condition and then finally used to estimate the wind parameters in a least-squares sense. Several turbulent tests in region II 1/2 and III, with wind speeds ranging from 11 to 15 ms^{-1} and turbulence intensities (TI) from 5 to 10%, were run with and IPC-controller to assess the observer performance. The accuracy of the estimates is in line with the results of previous publications, showing a maximum mean absolute error at 11 ms^{-1} of about 2.5 deg and 5e-2 in the estimates of angles and shears, respectively. Similar tests were also run with a simple collective controller to simulate operating conditions were the IPC-controller is switched off: accurate estimates of both shears and angles could still be obtained. This newly proposed formulation is therefore fit to be installed both on IPC and collective-controlled machines and, since it exploits sensors that might already be installed on the turbine, it consists in nothing more than a software upgrade.

3.5.2 Contribution

This paper is the result of the common effort of more authors. In details, Bertelè implemented the proposed observer, while taking care of the simulation pre and post-processing. Bottasso and Cacciola guided and supervised the whole work. Finally, all authors further developed the concept and contributed to the writing of this paper.

3.5.3 Reference

M. Bertelè, C. L. Bottasso, and S. Cacciola, “Simultaneous estimation of wind shears and misalignments from rotor loads: formulation for ipc-controlled wind turbines”, *Journal of Physics: Conference Series*, vol. 1037, p. 032007, 2018. doi: 10.1088/1742-6596/1037/3/032007.

CHAPTER 4

Rotor rebalancing

4.1 Automatic detection and correction of pitch misalignment in wind turbine rotors (Paper VI)

4.1.1 Summary

In this work, a novel algorithm to first detect and then correct for pitch imbalances is developed. The advantage of such methodology consists in relying only on load/acceleration sensors installed on the machine fixed frame, and in the fact that the detected imbalance can be automatically corrected for during operation if access to the control system is granted, avoiding therefore any machine downtime.

The algorithm is based on a linear model relating the one per revolution (1P) of a fixed frame measurement, in this case fore-aft accelerations of the main bearing, to a pitch misalignment. This model can be easily identified in the field. First, the current 1P measurement is recorded, $s_{(1)}$. Then, after intentionally applying an additional misalignment by pitching two or more blades, a second 1P signal is recorded, $s_{(2)}$. With these two signals, the model can be easily identified and immediately used to derived the pitch offsets that need to be applied in order to minimize the 1P measured on the fixed frame, i.e. to rebalance the rotor. The new 1P measured after rebalancing, $s_{(3)}$, can be used along with $s_{(2)}$ to re-identify the model and further reduce the 1P, if needed. Indeed, the iterative application of the algorithm can compensate for possible non-linearities. Finally, to account for changes in the inflow within the algorithm steps, the recorded 1P is scaled with the dynamic pressure.

To evaluate the performance of the algorithm, the behaviour of a 3 MW machine was simulated with `CpLambda` [58] using turbulent wind grids computed by `TurbSim` [59]. First, the linearity of the imbalance-machine response was proven, showing also that the imbalance leaves a specific fingerprint in the 1P according to its location. Moreover, the algorithm itself proved to be very robust: although run while varying wind speed, density, turbulence intensity, crossflow and vertical shear within the steps, the methodology was always able to minimize if not perfectly correct for the pitch imbalance within a few iterations. The effect of signal noise or error in the wind speed measurement was also considered, showing that even for very low signal to noise ratio the method is still capable of reducing the rotor imbalance.

4.1.2 Contribution

This paper is the result of the common effort of more authors. In details, Bertelè implemented the algorithm, while taking care of the simulation pre and post-processing. Bottasso and Cacciola guided and supervised the whole work. Finally, all authors further developed the concept and contributed to the writing of this paper.

4.1.3 Reference

M. Bertelè, C. L. Bottasso, and S. Cacciola, "Automatic detection and correction of pitch misalignment in wind turbine rotors," *Wind Energy Science*, vol. 3, no. 2, pp. 791–803, 2018. doi: 10.5194/wes-3-791-2018.

4.2 Validation on a scaled wind turbine model

As a proof of concept, the rebalancing algorithm was tested on a scaled wind turbine model, named in the following G1 [72].

4.2.1 Scaled wind turbine model

The G1 [72] is a three-bladed horizontal axis machine, with a 1.1 m rotor diameter and rated rotor speed of 850 rpm. Each blade, composed by a layer of unidirectional carbon fiber, is equipped with its own pitch encoder and motor, allowing therefore for individual blade pitching. Four strain gages, installed on small bridges connected to the shaft, measure the shaft torsional and bending loads, while their power supply and conditioning is provided by three miniaturized electronic boards on the hub. The conversion of the electrical signal from the rotating to the fixed frame and vice versa is given by a through-bore 12-channels slip ring. A torque meter is also present to measure the torque, along with an optical encoder to measure the rotor azimuth. Additional strain gages are placed at the tower base. The motor, located in the rear part of the nacelle, is operated as a generator thanks to a servocontroller. A yaw motor and a yaw brake are also present, granting the possibility of yawing the machine with respect to the wind during the experiments.
Given its small dimensions, low-Reynolds airfoils are used to compensate for low-Reynolds effects. Overall, the maximum power coefficient of this machine is approximately 0.42 at a tip speed ratio $\lambda \in [7,8]$ and a pitch angle $\beta \in [-2,0]$ deg.

4.2.2 Linearity

To verify also outside of a simulated environment the linearity of the imbalance-turbine response model, the G1 was used in motor mode at 400 rpm. Specifically, the blades were individually pitched one at a time to add a pitch misalignment angle $\boldsymbol{b}_m \in [-3,3]$ deg, and the signal harmonics were extracted as described in §2.2.1. Figure 4.1 shows the 1P cosine and sine harmonics of the nodding moment on the shaft as a function of the added pitch misalignment on each blade.

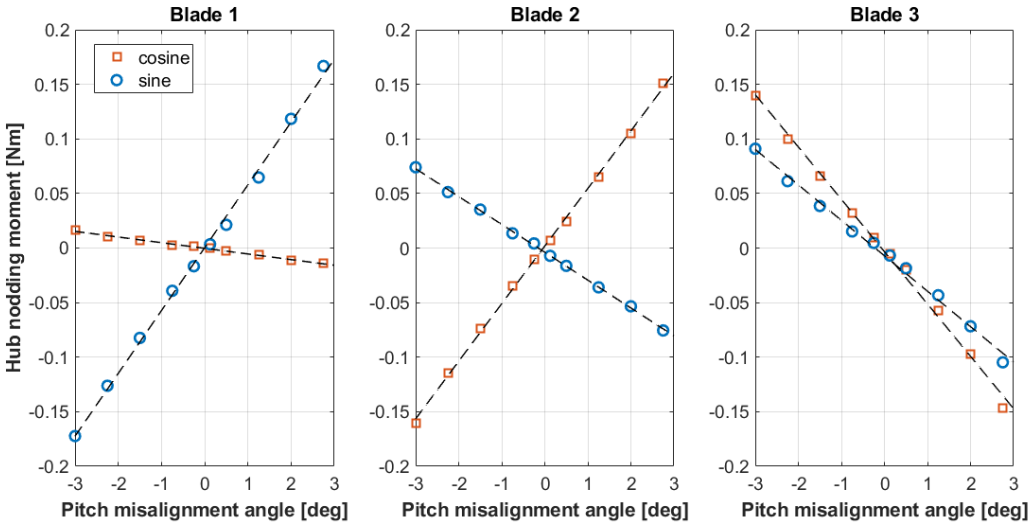

Figure 4.1: Cosine (squares) and sine (circles) 1P components of the shaft nodding moment as functions of pitch misalignment.

One can clearly note that the results mirror those obtained in a simulated environment (**Paper VI**): both cosine and sine harmonics appear to be linearly dependent on the degree of misalignment, with their minima very close to the origin. Moreover, one can also note that the slope of the sine and cosine components differ from plot to plot. This proves that the location of the imbalance leaves a unique fingerprint in the machine response, allowing one to estimate not only the magnitude of the imbalance but also the faulty blade/blades. Additional tests were also performed at different rotational speeds. The results, not reported here for the sake of brevity, prove to be consistent with the linear approximation.

4.2.3 Rotor rebalancing

The algorithm presented in **Paper VI** was also applied to the G1 model. Indeed, after noticing unusual vibrations, the imbalance-turbine response was once more characterized at 400 rpm, leading to the results shown in Fig 4.2

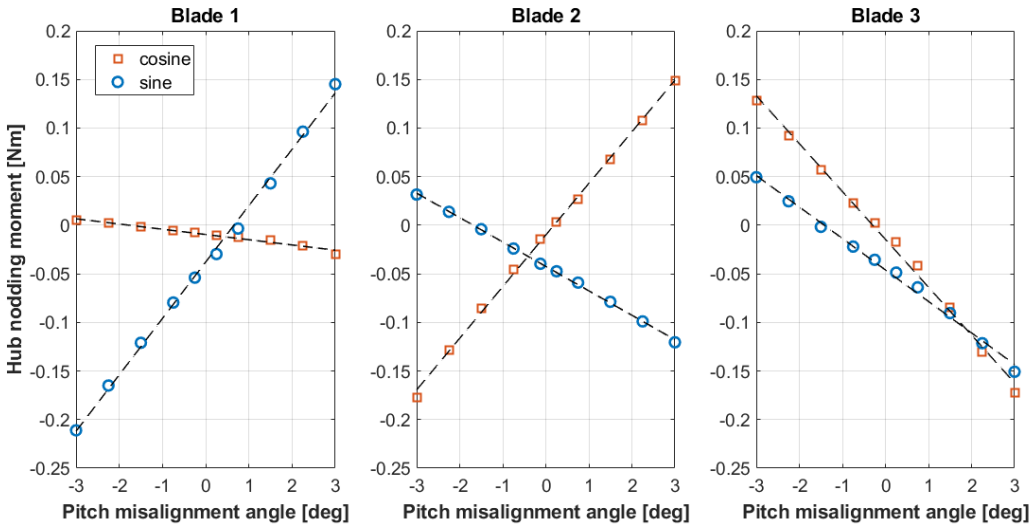

Figure 4.2: Cosine (squares) and sine (circles) 1P components of the shaft nodding moment as functions of pitch misalignment.

While the linear approximation still holds, one can also note that the crossing between sine and cosine harmonics is not placed at the origin, meaning that even when no apparent pitch misalignment is present, a 1P is still present in the fixed frame: this suggests a mass and/or pitch imbalances. Indeed, the G1 was disassembled and reassembled between this experiment and the one presented in § 4.1, so that the tests were actually run on two virtually different machines.

To reduce the vibrations, the rebalancing algorithm was applied on the G1 running in motor mode, using the 1P nodding moment as detection parameter. Figure 4.3 shows the 1P variation from the initial imbalanced configuration for each step. In addition, the pitch misalignment applied to each blade is also reported, along with the absolute residual pitch misalignment ϵ, defined as

$$\epsilon = max(\boldsymbol{b}_m - \boldsymbol{b}) - min(\boldsymbol{b}_m - \boldsymbol{b}). \tag{4.1}$$

The method is capable of rebalancing the rotor after only three blade movements, i.e. two complete iterations of the algorithm. Specifically, blade two and blade three were further pitched of 0.7 and -0.7

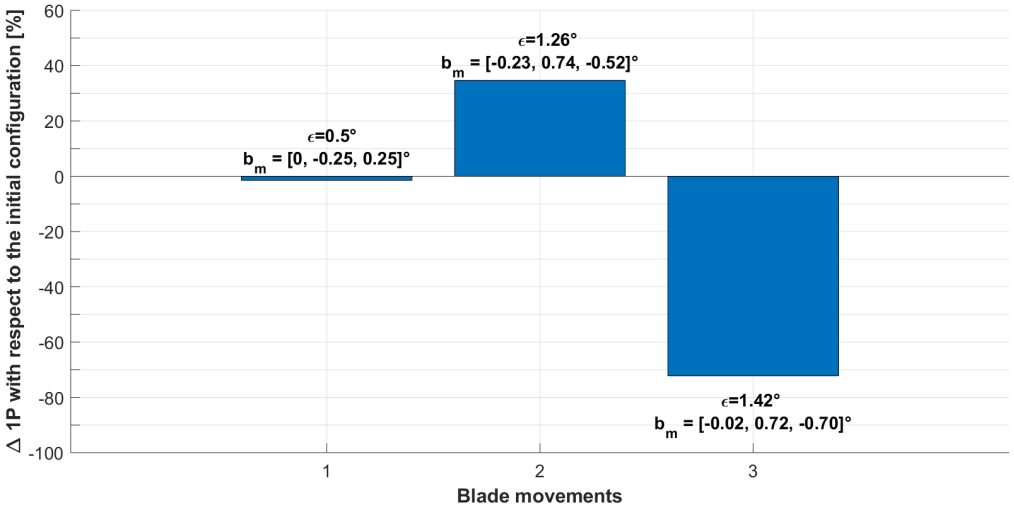

Figure 4.3: Reduction of the 1P nodding moment with respect to the initial configuration.

deg respectively, achieving an overall reduction of 70% in the 1P of the nodding moment.

Although the complete rebalancing procedure was performed only once on the scaled turbine, this test can serve as proof of concept of the algorithm. Indeed, the results mirror what extensively observed in a simulated environment (**Paper VI**): they validate the linearity of the imbalance-response model and the ability of the algorithm to reduce the 1P loads in the fixed frame.

CHAPTER 5

Discussion and conclusions

Within this dissertation, the turbine harmonic response was analysed and successfully exploited to develop new methodologies aiming at correcting for rotor imbalances but also at estimating the inflow impinging on the rotor disk.
Nowadays, turbines are equipped with a wide variety of sensors, such as strain gages, accelerometers etc. Even though they are thought of and installed to perform a very specific task (load monitoring, component monitoring etc.), the measurements they collect could carry additional valuable information also for other applications. Indeed, no matter the type, sensors just measure the turbine response during operation: if one is able to identify the relation between harmonic response and problem at hand, this already available information can be exploited for numerous different applications, with no additional hardware cost.

Among all the possible applications, this dissertation focused on two main research topics: wind sensing and rotor rebalancing. As a result, two new methodologies were developed. The first is capable of estimating the incoming inflow, parametrized with both vertical and horizontal shears and misalignments, starting from the one per revolution (1P) measured blade bending loads. The second can first detect and then remotely correct for a rotor imbalance, here simulated as a fault in the pitch system, starting from the 1P harmonics of accelerations in the fixed frame.
Both technologies exploit already available turbine measurements, meaning that they consist of nothing else than a software upgrade, with also a minimal computational cost. In fact, even if blade load sensors and accelerometers are not already planned for during manufacturing, they can be installed a posteriori as part of standard condition monitoring systems [9–12].
Moreover, both methods were validated with extensive simulations but also with data from a scaled wind turbine model and, in the case of the wind sensing technology, also in the field. The consistency in the performance of both methods, no matter if tested with synthetic or real data, further adds to the value of this work.
Based on the results collected in this dissertation, the following conclusions can be drawn.

5.1 Wind sensing

It is possible to exploit the rotor response to estimate the flow impinging on the rotor disk.
Indeed, a spatially dis-homogeneous inflow will lead to periodic changes in the angle of attack and, in turn, in the blade loads. Therefore, the out and in-plane blade root bending moments were chosen as input of this wind sensing technology. The non-uniformity in the wind, on the other hand, was parametrized by four wind states – vertical and horizontal shears and vertical and horizontal misalignments – in order to provide, along with the wind speed, a full first order approximation of the wind field. So far, no other wind sensing approach considered such a rich wind parametrization. While some authors included only vertical and horizontal shears [22, 24–26], others only considered vertical shear and yaw misalignment [19, 20, 23]. Bottasso and Riboldi also proved that the effect of wind parameters

not included in the modelling would negatively affect the results [23].

Both a linear and a non-linear model were formulated to relate the chosen four parameters to 1P harmonics of the blade root bending moments. Higher order harmonics were not considered, since their sensitivity to turbulent fluctuations is comparable to their sensitivity to the four wind states. As direct consequence, one can also assume that once the model has been identified for a turbine, it should also be directly applicable to a different turbine of the same type. Indeed, it is reasonable to assume that the response of different installations of the same turbine should not significantly differ at least in the lowest frequencies, although this still remains to be verified.

The models can be identified as a black box [56] once load and wind state measurements are available, bypassing the need for a turbine model or any sensitive turbine information. Moreover, an even simpler identification procedure was developed to ease the identification for field applications, where usually only measurements of the yaw misalignment and of the vertical shear are available. Since the effect that a vertical shear has on the blade loads is the same as the effect of a horizontal shear only with a $\pi/2$ phase shift – the same holding for the misalignments – this rotational symmetry can be used to reduce the model coefficients. In a nutshell, one only needs measurements of the vertical shear and the yaw misalignment to identify the model: once the missing coefficients are derived using the rotor symmetry, all four parameters can be estimated. After the model has been identified, the wind states can be estimated online from wind turbine measurements in a least square sense. A Kalman Filter was also used in the estimation to account for process and measurement noise [64, 65].

In addition, the proposed wind-load mapping was also adapted to the case of IPC-controlled turbines. Since the IPC controller will flatten the effect of the wind states on the machine loads, an additional input parameter was added to the model. Indeed, to reduce the machine loading the IPC controller will apply a cyclic pitching to each blade, according to its azimuthal position [60–62]. Therefore, the new wind-turbine response model relates the four wind states to both 1P blade bending moments and 1P blade pitch, since the information lost in the load measurements can be found in the cyclic pitching of the blades.

This so called *wind observer*, in its different formulations, was extensively tested in a simulation environment, considering different mean inflows, turbulence intensities (TI) and seeds, proving capable of accurately estimating the instantaneous value of the shears and of accurately following the mean values of the misalignment angles. Tests in the wind tunnel, performed also with different TIs, confirm the synthetic results, also proving that the rotational symmetry can be exploited to identify the wind observer. Finally, a first validation with field data was also performed. Despite the limits of the available dataset – the lack of a rotor-effective reference for all wind states – the observer proved once again capable of estimating the fast shear fluctuations, while following the mean trends of the yaw misalignment over a wide range of different operative conditions.

5.1.1 Discussion and outlooks

As a next step, an ad hoc field campaign could be planned to further validate the performance of the wind observer. Since this observer estimates the rotor-effective inflow from rotor loads, it follows that it should be first trained and then validated starting from rotor-effective inflow measurements, such as those provided for example by LiDARs [15, 17]. In the results presented within this thesis though, such data is not available, and the nevertheless promising validation had to be performed starting from met-mast measurements. The lack of a reference for the rotor-effective inflow in the field constitutes of course a possible drawback of this method, which can nevertheless be addressed and partially

coped with by exploiting several point-wise measurements of the wind parameters, if available, or alternatively, by training the observer with an accurate model of the machine.

When working with field data, one should also account for possible sensor issues such as miscalibrations and drift but also for other phenomena such as soiling or ageing, whose effect on the observer accuracy still remains to be investigated. This might become considerably relevant when, once the model has been identified for a turbine, it is used on other installations of the same type.

A validation in the field could also identify additional phenomena that might affect the observer accuracy. For example, if applied to large rotors, a first order approximation of the impinging inflow might not suffice. Indeed, parameters such as the horizontal wind misalignment might vary with height, leading to significant wind veer [73]. Also the vertical shear profile might be not properly represented either by a linear or exponential approximation [74]. To capture also these characteristics, the current observer implementation needs to be further developed considering the effects of these specific wind parameters on the machine harmonic response.
Further development will also be required to apply this methodology to floating machines. Indeed, off-shore turbines are exposed to additional motions with respect to on-shore installations, leading to additional loading and extra apparent wind speed components. The overall machine harmonic response needs therefore to be analysed, in order to clearly distinguish the fingerprint of the wind from that of other effects.

So far, the wind-load response was mapped with a simple analytical model, either linear or non-linear. Although very simple and accurate, these analytical mappings could be also substituted with more complex solutions, like the ones provided, for example, by artificial neural networks. Indeed, given their more complex formulation, such machine learning techniques could be able to capture additional useful information missed by simple analytical models, in turn increasing the observer accuracy. They could also be able to handle information lying in higher order harmonics, being able to separate the contribution due to the wind states from the one due to turbulent fluctuations. This might allow for a richer description of the impinging inflow, so that maybe additional parameters such as veer could also be estimated.
It would also be interesting to verify if neural networks could model the relationship between turbine response and each single wind state independently. A current limitation of the wind observer proposed within this thesis is that to identify the wind-turbine mapping one requires measurement of at least two wind states. If neural networks could completely separate the effect of each single wind parameter on the machine response, then one could theoretically estimate the desired wind state without requiring any measurements of the others. If possible, this would further simplify the identification procedure and would constitute an additional advantage especially for field applications.

Finally, a field test campaign could also be used to validate the observer, in its different formulations, as a valuable tool for wind farm control. The rotor effective estimate of the yaw misalignment could be used to realign the machine to the wind. It would be interesting to understand whether driving the yaw motor with a rotor-effective measurement rather than a point-wise one, for example provided by a nacelle anemometer, could lead to an increase in power production. But the estimate of the turbine yaw misalignment could also be used to implement wake redirection strategies: after detecting the presence of a wake by looking at the estimate for the horizontal shear, the wake could be redirected by yawing the upstream turbine. Also the estimate of the vertical shear could be used for wind farm control. Indeed, together with information about the ambient turbulence intensity, it could be used to derive the level of atmospheric stability and, with it, the wake recovery rate.

But the information provided by this wind observer could be extended also to other applications. Once the turbine is equipped with blade load measurements, it automatically turns into a wind sensor. This means that it can be used to characterize the inflow at a given test site, for power curve verification, but also to create a turbine digital twin. Indeed, one could feed to the simulation model of the turbine, i.e. its digital twin, the actual inflow impinging on that turbine rotor disk. This opens a wide range of possibilities for prediction, maintenance, and fatigue and residual lifetime assessment.

5.2 Rotor rebalancing

It is possible to exploit the rotor response to first detect and then automatically remotely correct for a rotor imbalance.
Indeed, any type of imbalance in the rotating frame – either caused by a fault in the pitch system, ice accretion or mass variations among the blades – will generate additional harmonics in the fixed frame. Therefore, by detecting a significant 1P in either fixed frame moments or accelerations, one can automatically detect a rotor imbalance. In this work, the signal used as detection parameter was the fore-aft acceleration measured on the main bearing. On turbines, acceleration sensors are often used for vibration monitoring and, if not already present, are relatively easy to install.

A linear model was formulated to map the 1P fixed frame response to the rotor imbalance, here simulated by applying an offset to one or more blades with respect to the desired pitch angle. While other methodologies require a finite element model of the turbine [34–36] or a comprehensive training data set [33], the coefficients of this model can be identified as a black box [56] through simple system identification once two imbalance configurations are available. In a nutshell, to identify the model one just needs to record a 1P measurement and then arbitrarily further pitch the blades to collect the second one. This simple identification constitutes a significant advantage for the methodology, making it very easy to implement. To account for possible wind speed changes between measurements, the 1P signal is also scaled by the dynamic pressure.

After the model has been identified, it can be used to automatically and, most importantly, remotely rebalance the rotor once access to the pitch system is granted. Indeed, the model is used to find the combination of pitch offsets that needs to be applied to the blades in order to minimize the measured 1P. The procedure can also be iteratively repeated, if the desired 1P threshold is not met. Therefore, while other methodologies strongly rely on a continuous controller action [38–40] to minimize 1P vibrations, causing increased duty cycle and fatigue in pitch actuators, the presented algorithm engages the controller only for few iterations.

The linearity of the turbine-imbalance model was proved in a simulation environment. It was also shown that the turbine harmonic response is unique depending on the imbalance location: the model can therefore be used not only to estimate the gravity of the imbalance but also its location. Extensive simulations, including a wide range of wind conditions, different TI, turbulence seeds and different noise levels, proved the robustness of the algorithm, which is capable of significantly reducing the initial imbalance within two to three complete iterations.
Moreover, the methodology was also tested on a scaled wind turbine model where measurements of the shaft moments were available. Again, the linearity of the turbine-response model was demonstrated along with the dependency of the response on the imbalance location. Finally, the rebalancing procedure was also tested, leading to a significant 1P reduction after only two iterations.

5.2.1 Discussion and outlooks

Future steps for this methodology could be a validation in the field. Specific tests could be designed to purposely misalign one or more blades, both to validate the linearity of the imbalance-turbine response but also to verify, in a controlled environment, the performance of the algorithm.

Further studies could also investigate the effect of different types of imbalances. Indeed, although the algorithm was thought of to correct for a pitch imbalance, it is actually designed to reduce a 1P in the fixed frame, irrespective of its root cause. If on one hand this can represent an advantage, since it is possible to remotely reduce virtually all types of dangerous vibrations, it might also constitute a disadvantage. For example, in the case of a mass imbalance, the algorithm will generate an aerodynamic imbalance that compensates the original mass imbalance. While this will reduce vibrations in the fixed frame, it could also negatively affect the power performance of the turbine, depending on the severity of the initial problem. To address this issue, one could consider further investigating the response of the machine to identify additional inputs that could carry useful information about the type of imbalance present. For example, it is reasonable to assume that a mass imbalance will have a smaller effect on the produced power than a pitch imbalance, as well as the latter will affect power production less than an imbalance due to ice accretion [33]. Such information might help in distinguishing the origin of the imbalance problem, although this might require knowledge of sensitive turbine information.

In addition, the effectiveness of the methodology still remains to be quantified in the case the imbalance strongly depends on the operative conditions. Considering again the case of a mass imbalance, which strongly depends on the rotational speed, as already mentioned the algorithm would derive the optimal pitch setting to minimize vibrations. Nevertheless, with changing operating conditions, the effect of a mass imbalance might significantly change, depending on the severity of the problem. Therefore, the final rebalanced configuration might also have to be derived again for different operative points. Nevertheless, possible additional iterations would not constitute a considerable disadvantage, given the very low computational cost of the method and its fast convergence rate.

Overall, this newly developed methodology could lead to significant reductions in operation and maintenance costs. If accelerometers are already installed as part of a standard condition monitoring system, no additional hardware is necessary for its implementation, so that it actually consists in a software upgrade, with also a very small computational cost. Most importantly, since it allows to correct for imbalances remotely, costly on-site inspections can be virtually avoided: this constitutes a very significant advantage, especially in a future headed towards more off-shore installations.

[1] United Nations, "7. d paris agreement." [Online]. Available: https://treaties.un.org/Pages/ViewDetails.aspx?src=TREATY&mtdsg_no=XXVII-7-d&chapter=

[2] Wind Europe, "Wind energy in europe in 2018: Trends and statistics."

[3] Intergovernmental Panel on Climate Change, "Summary for policymakers," in *Climate Change 2013*, I. P. o. C. Change, Ed. Cambridge: Cambridge University Press, 2014, pp. 1–30. ISBN 9781107415324

[4] Global Wind Energy Council, "Global wind report 2019."

[5] Wind Europe, "Wind energy in europe in 2019: Trends and statistics."

[6] International Energy Agency, "World energy outlook 2019."

[7] International Energy Agency, "Key world energy statistics 2019."

[8] H. Saruhan, S. Sandemir, A. Çiçek, and I. Uygur, "Vibration analysis of rolling element bearings defects," *Journal of Applied Research and Technology*, vol. 12, no. 3, pp. 384–395, 2014. doi: 10.1016/S1665-6423(14)71620-7

[9] clockworkX GmbH, "Smart monitoring of wind turbine main bearings (mb)." [Online]. Available: https://clockworkx.de/wp-content/uploads/2020/05/clockworkX_Case_Study.pdf

[10] Bachmann electronic GmbH, "Bachmann electronic gmbh | hardware und installation," 05/06/2020. [Online]. Available: https://www.bachmann.info/produkte/condition-monitoring-system/hardware-und-installation/

[11] Wind-Consult GmbH, "Lasten – wind-consult, messinstitut für windenergie," 05/06/2020. [Online]. Available: https://www.wind-consult.de/lasten/

[12] fos4X GmbH, "retrox | fos4x," 03/04/2020. [Online]. Available: https://fos4x.com/en/solutions/retrox/

[13] Á. Jiménez, A. Crespo, and E. Migoya, "Application of a les technique to characterize the wake deflection of a wind turbine in yaw," *Wind Energy*, vol. 13, no. 6, pp. 559–572, 2010. doi: 10.1002/we.380

[14] P. A. Fleming, P. M. Gebraad, S. Lee, J.-W. van Wingerden, K. Johnson, M. Churchfield, J. Michalakes, P. Spalart, and P. Moriarty, "Evaluating techniques for redirecting turbine wakes using sowfa," *Renewable Energy*, vol. 70, pp. 211–218, 2014. doi: 10.1016/j.renene.2014.02.015

[15] A. I. Carswell, "Lidar measurements of the atmosphere," *Canadian Journal of Physics*, vol. 61, no. 2, pp. 378–395, 1983. doi: 10.1139/p83-049

[16] S. Vogt and P. Thomas, "Sodar — a useful remote sounder to measure wind and turbulence," *Journal of Wind Engineering and Industrial Aerodynamics*, vol. 54-55, pp. 163–172, 1995. doi: 10.1016/0167-6105(94)00039-G

[17] S. Lang and E. McKeogh, "Lidar and sodar measurements of wind speed and direction in upland terrain for wind energy purposes," *Remote Sensing*, vol. 3, no. 9, pp. 1871–1901, 2011. doi: 10.3390/rs3091871

[18] M. N. Soltani, T. Knudsen, M. Svenstrup, R. Wisniewski, P. Brath, R. Ortega, and K. Johnson, "Estimation of rotor effective wind speed: A comparison," *IEEE Transactions on Control Systems Technology*, vol. 21, no. 4, pp. 1155–1167, 2013. doi: 10.1109/TCST.2013.2260751

[19] C. L. Bottasso, A. Croce, and C. Riboldi, "Spatial estimation of wind states from the aeroelastic response of a wind turbine," in *The Science of Making Torque from Wind 2010*.

[20] C. L. Bottasso and C. Riboldi, "Estimation of wind misalignment and vertical shear from blade loads," *Renewable Energy*, vol. 62, pp. 293–302, 2014. doi: 10.1016/j.renene.2013.07.021

[21] C. L. Bottasso and C. Riboldi, "Validation of a wind misalignment observer using field test data," *Renewable Energy*, vol. 74, pp. 298–306, 2015. doi: 10.1016/j.renene.2014.07.048

[22] E. Simley and L. Y. Pao, "Evaluation of a wind speed estimator for effective hub-height and shear components," *Wind Energy*, vol. 19, no. 1, pp. 167–184, 2016. doi: 10.1002/we.1817

[23] C. L. Bottasso, S. Cacciola, and J. Schreiber, "A wake detector for wind farm control," *Journal of Physics: Conference Series*, vol. 625, p. 012007, 2015. doi: 10.1088/1742-6596/625/1/012007

[24] C. L. Bottasso, S. Cacciola, and J. Schreiber, "Local wind speed estimation, with application to wake impingement detection," *Renewable Energy*, vol. 116, pp. 155–168, 2018. doi: 10.1016/j.renene.2017.09.044

[25] J. Schreiber, C. L. Bottasso, and M. Bertelè, *Field testing of a local wind inflow estimator and wake detector*, 2020.

[26] S. Cacciola, M. Bertelè, J. Schreiber, and C. L. Bottasso, "Wake center position tracking using downstream wind turbine hub loads," *Journal of Physics: Conference Series*, vol. 753, p. 032036, 2016. doi: 10.1088/1742-6596/753/3/032036

[27] M. I. Blanco, "The economics of wind energy," *Renewable and Sustainable Energy Reviews*, vol. 13, no. 6-7, pp. 1372–1382, 2009. doi: 10.1016/j.rser.2008.09.004

[28] M. Wilkinson, B. Hendriks, F. Spinato, and K. Harman, E. Gomez, H. Bulacio, J. Roca, P. J. Tavner, Y. Feng, and H. Long, Ed. *Methodology and results of the Reliawind reliability field study*, 2010.

[29] R. W. Hyers, J. G. McGowan, K. L. Sullivan, J. F. Manwell, and B. C. Syrett, "Condition monitoring and prognosis of utility scale wind turbines," *Energy Materials*, vol. 1, no. 3, pp. 187–203, 2006. doi: 10.1179/174892406X163397

[30] A. Kusiak and A. Verma, "A data-driven approach for monitoring blade pitch faults in wind turbines," *Sustainable Energy, IEEE Transactions on*, 2010. doi: 10.1109/TSTE.2010.2066585

[31] K. G. Pierce, and R. P. Slack, "Methods and apparatus for balancing a rotor: Us patent," Patent 0 035 136, 2009.

[32] U. Axelsson, M. Bjork, and C. Haag, "Method for balancing a wind turbine: Us patent," Patent 8 683 688 B2, 2014.

[33] S. Cacciola, I. M. Agud, and C. L. Bottasso, "Detection of rotor imbalance, including root cause, severity and location," *Journal of Physics: Conference Series*, vol. 753, p. 072003, 2016. doi: 10.1088/1742-6596/753/7/072003

[34] J. Niebsch, R. Ramlau, and T. T. Nguyen, "Mass and aerodynamic imbalance estimates of wind turbines," *Energies*, vol. 3, no. 4, pp. 696–710, 2010. doi: 10.3390/en3040696

[35] J. Niebsch and R. Ramlau, "Simultaneous estimation of mass and aerodynamic rotor imbalances for wind turbines," *Journal of Mathematics in Industry*, vol. 4, no. 1, p. 12, 2014. doi: 10.1186/2190-5983-4-12

[36] J. Kusnick, D. E. Adams, and D. T. Griffith, "Wind turbine rotor imbalance detection using nacelle and blade measurements," *Wind Energy*, vol. 18, no. 2, pp. 267–276, 2015. doi: 10.1002/we.1696

[37] S. Kanev, and T. G. Engelen, Ed., *Exploring the limits in individual pitch control*, 2009.

[38] V. Petrović, M. Jelavić, and M. Baotić, "Advanced control algorithms for reduction of wind turbine structural loads," *Renewable Energy*, vol. 76, pp. 418–431, 2015. doi: 10.1016/j.renene.2014.11.051

[39] S. Cacciola and C. E. Riboldi, "Equalizing aerodynamic blade loads through individual pitch control via multiblade multilag transformation," *Journal of Solar Energy Engineering*, vol. 139, no. 6, 2017. doi: 10.1115/1.4037744

[40] S. Cacciola, C. E. Riboldi, and A. Croce, "A new decentralized pitch control scheme for wind turbines * *paper prepared for ifac open invited session: Wind turbine and wind farm control: Control challenges and solutions," *IFAC-PapersOnLine*, vol. 50, no. 1, pp. 9908–9913, 2017. doi: 10.1016/j.ifacol.2017.08.1627

[41] M. Bertelè, C. L. Bottasso, S. Cacciola, F. Daher Adegas, and S. Delport, "Wind inflow observation from load harmonics," *Wind Energy Science*, vol. 2, no. 2, pp. 615–640, 2017. doi: 10.5194/wes-2-615-2017

[42] M. Bertelè, C. L. Bottasso, and S. Cacciola, "Brief communication: Wind inflow observation from load harmonics – wind tunnel validation of the rotationally symmetric formulation", *Wind Energy Science*, vol. 4, no. 1, pp. 89–97, 2019. doi: 10.5194/wes-4-89-2019

[43] M. Bertelè, and C. L. Bottasso, "Non-deterministic wind observation from wind turbine loads," *Journal of Physics: Conference Series*, 1618 062022, 2020. doi: 10.1088/1742-6596/1618/6/062022

[44] M. Bertelè, C. L. Bottasso and J. Schreiber, J., "Wind inflow observation from load harmonics: initial steps towards a field validation, *Wind Energ. Sci. Discuss.* [preprint],2020. doi: 0.5194/wes-2020-83

[45] M. Bertelè, C. L. Bottasso, and S. Cacciola, "Simultaneous estimation of wind shears and misalignments from rotor loads: formulation for ipc-controlled wind turbines", *Journal of Physics: Conference Series*, vol. 1037, p. 032007, 2018. doi: 10.1088/1742-6596/1037/3/032007

[46] M. Bertelè, C. L. Bottasso, and S. Cacciola, "Automatic detection and correction of pitch misalignment in wind turbine rotors," *Wind Energy Science*, vol. 3, no. 2, pp. 791–803, 2018. doi: 10.5194/wes-3-791-2018

[47] D. M. Eggleston and F. S. Stoddard, *Wind turbine engineering design*. New York: Van Nostrand Rehinold Company, 1987. ISBN 0442221959

[48] R. Potter and M. Gribler, "Computed order tracking obsoletes older methods," in *SAE Technical Paper Series*, ser. SAE Technical Paper Series. SAE International400 Commonwealth Drive, Warrendale, PA, United States, 1989. doi: 10.4271/891131

[49] R. Potter, "A new order tracking method for rotating machinery," *Sound and Vibration*, vol. 24, pp. 30–34, 1990.

[50] E. D. S. Munck, and K. R. Fyfe, "Computed order tracking applied to vibration analysis of rotating machinery," *Canadian Acoustics*, vol. 19, pp. 57–58, 1991.

[51] K. R. Rao, J. J. Hwang, and D. N. Kim, *Fast Fourier transform: Algorithms and applications*. Dordrecht etc: Springer, 2010. ISBN 978-1-4020-6628-3

[52] R. P. Coleman and A. M. Feingold, "Theory of self-excited mechanical oscillations of helicopter rotors with hinged blades: Technical report."

[53] M. H. Hansen, "Modal dynamics of structures with bladed isotropic rotors and its complexity for two-bladed rotors," *Wind Energy Science*, vol. 1, no. 2, pp. 271–296, 2016. doi: 10.5194/wes-1-271-2016

[54] X. Ma, N. K. Poulsen, and H. Bindner, "Estimation of wind speed in connection to wind turbine," *Procededings for ASTED International Conference on Control*, pp. 105–109, 1997.

[55] C. L. Bottasso, A. Croce, Y. Nam, and C. Riboldi, "Power curve tracking in the presence of a tip speed constraint," *Renewable Energy*, vol. 40, no. 1, pp. 1–12, 2012. doi: 10.1016/j.renene.2011.07.045

[56] L. Ljung, "Perspectives on system identification," *Annual Reviews in Control*, vol. 34, no. 1, pp. 1–12, 2010. doi: 10.1016/j.arcontrol.2009.12.001

[57] R. V. Jategaonkar, *Flight vehicle system identification: A time-domain methodology*, second edition ed., ser. Progress in astronautics and aeronautics. Reston, VA: American Institute of Aeronautics and Astronautics, Inc, 2015, vol. volume 245. ISBN 978-1-62410-278-3

[58] C. L. Bottasso and A. Croce, "Cp-lambda: user's manual."

[59] B. Jonkman and L. Kilcher, "Turbsim users guide: version 1.06.00."

[60] E. A. Bossanyi, "Individual blade pitch control for load reduction," *Wind Energy*, vol. 6, no. 2, pp. 119–128, 2003. doi: 10.1002/we.76

[61] E. A. Bossanyi, "Wind turbine control for load reduction," *Wind Energy*, vol. 6, no. 3, pp. 229–244, 2003. doi: 10.1002/we.95

[62] E. A. Bossanyi, "Further load reductions with individual pitch control," *Wind Energy*, vol. 8, no. 4, pp. 481–485, 2005. doi: 10.1002/we.166

[63] J. J. Moré, "The levenberg-marquardt algorithm: Implementation and theory," in *Numerical analysis*, ser. Lecture Notes in Mathematics, G. A. Watson, Ed. Berlin: Springer, 1978, vol. 630, pp. 105–116. ISBN 978-3-540-08538-6

[64] R. E. Kalman, "A new approach to linear filtering and prediction problems," *Journal of Basic Engineering*, vol. 82, no. 1, pp. 35–45, 1960. doi: 10.1115/1.3662552

[65] R. E. Kalman and R. S. Bucy, "New results in linear filtering and prediction theory," *Journal of Basic Engineering*, vol. 83, no. 1, pp. 95–108, 1961. doi: 10.1115/1.3658902

[66] G. H. Golub and C. F. Van Loan, *Matrix Computations*, 4th ed. Baltimore: John Hopkins University press, 2013. ISBN 9781421407944

[67] H. Cramer, *Mathematical methods of statistics*. Princeton: Princeton University Press, 1999. ISBN 0691005478

[68] J. F. Manwell, J. G. McGowan, and A. L. Rogers, *Wind energy explained: Theory, design and application*, 2nd ed. Chichester: Wiley, 2009. ISBN 9780470015001

[69] S. Cacciola, M. Bertelè, and C. L. Bottasso, "Simultaneous observation of wind shears and misalignments from rotor loads," *Journal of Physics: Conference Series*, vol. 753, p. 052002, 2016. doi: 10.1088/1742-6596/753/5/052002

[70] FINO, "Fino 1-2-3 – forschungsplattformen in nord- und ostsee: Nr. 1." [Online]. Available: http://www.fino1.de/en/

[71] C. L. Bottasso, F. Campagnolo, and V. Petrović, "Wind tunnel testing of scaled wind turbine models: Beyond aerodynamics," *Journal of Wind Engineering and Industrial Aerodynamics*, vol. 127, pp. 11–28, 2014. doi: 10.1016/j.jweia.2014.01.009

[72] F. Campagnolo, V. Petrović, J. Schreiber, E. M. Nanos, A. Croce, and C. L. Bottasso, "Wind tunnel testing of a closed-loop wake deflection controller for wind farm power maximization," *Journal of Physics: Conference Series*, vol. 753, p. 032006, 2016. doi: 10.1088/1742-6596/753/3/032006

[73] M. Bromm, A. Rott, H. Beck, L. Vollmer, G. Steinfeld, and M. Kühn, "Field investigation on the influence of yaw misalignment on the propagation of wind turbine wakes," *Wind Energy*, vol. 21, no. 11, pp. 1011–1028, 2018. doi: 10.1002/we.2210

[74] P. Murphy, J. K. Lundquist, and P. Fleming, "How wind speed shear and directional veer affect the power production of a megawatt-scale operational wind turbine", *Wind Energy Science*, vol. 5, no. 3, pp. 1169–1190, 2020. doi: 10.5194/wes-5-1169-2020

Appendices

APPENDIX **A**

Included publications

A.1 Paper I: Wind inflow observation from load harmonics

Reference: M. Bertelè, C. L. Bottasso, S. Cacciola, F. Daher Adegas, and S. Delport, "Wind inflow observation from load harmonics," *Wind Energy Science*, vol. 2, no. 2, pp. 615–640, 2017. doi: 10.5194/wes-2-615-2017.

Wind Energ. Sci., 2, 615–640, 2017
https://doi.org/10.5194/wes-2-615-2017

eawe european academy of wind energy
Open Access
WIND ENERGY SCIENCE

Wind inflow observation from load harmonics

Marta Bertelè[1], Carlo L. Bottasso[1,2], Stefano Cacciola[2], Fabiano Daher Adegas[3], and Sara Delport[3]

[1]Wind Energy Institute, Technische Universität München, 85748 Garching bei München, Germany
[2]Dipartimento di Scienze e Tecnologie Aerospaziali, Politecnico di Milano, 20156 Milan, Italy
[3]GE Global Research, 85748 Garching bei München, Germany

Correspondence: Carlo L. Bottasso (carlo.bottasso@tum.de)

Received: 16 May 2017 – Discussion started: 20 June 2017
Revised: 23 September 2017 – Accepted: 2 October 2017 – Published: 19 December 2017

Abstract. The wind field leaves its fingerprint on the rotor response. This fact can be exploited by using the rotor as a sensor: by looking at the rotor response, in the present case in terms of blade loads, one may infer the wind characteristics. This paper describes a wind state observer that estimates four wind parameters, namely the vertical and horizontal shears and the yaw and upflow misalignment angles, from out-of-plane and in-plane blade bending moments. The resulting observer provides on-rotor wind inflow characteristics that can be exploited for wind turbine and wind farm control. The proposed formulation is evaluated through extensive numerical simulations in turbulent and nonturbulent wind conditions using a high-fidelity aeroservoelastic model of a multi-MW wind turbine.

1 Introduction

The wind blowing over a wind turbine rotor leaves its own specific fingerprint on the machine response. If this information is rich enough and if the wind turbine response can be measured (for example in terms of loads), then one may think of turning the rotor into a wind sensor and use it to infer the wind inflow.

Measurements of the rotor inflow during operation are attractive for a number of reasons, as they may find a wide range of applications. For example, information on the wind speed at the rotor disk is typically useful for wind turbine control, as controller behavior is often scheduled as a function of wind speed. In addition, knowledge of the wind direction with respect to the rotor is necessary not only to maximize energy harvesting, but also because operating with excessive misalignment increases loading. Wake redirection strategies (Fleming et al., 2014; Jimenez et al., 2010) deliberately point the rotor away from the wind with the goal of deflecting the wake and reducing its interaction with downstream machines. This is a control strategy that also requires good knowledge of the wind direction in order to be implemented. Upflow can change significantly in complex terrain applications and, if known, it can be used to reduce loading. The presence of an impinging wake, shed from an upstream wind turbine, may result in high horizontally sheared flow at the rotor disk. Turbulence intensity (TI) and vertical shear may give indications of the characteristics of the atmosphere, which is information that can be used to optimize wind turbine and wind farm control behavior. More generally, by turning each wind turbine into a wind sensor capable of measuring the local inflow characteristics, one may build a more complete picture of the wind flow within a power plant and provide information that may possibly have a variety of uses.

Unfortunately, high-quality information on wind inflow is generally difficult to obtain. Onboard wind turbines, wind speed is typically measured by cup or sonic anemometers, while direction is provided by wind vanes. These sensors invariably suffer from a number of disturbances, such as the presence of the nacelle, blade passing and wake-induced flow deformation. Although most of these effects can be mitigated by the use of calibrated transfer functions, filtering and ad hoc processing of the raw measurements, all these sensors provide only local information at the specific point in the flow where they are installed. For control applications, it is clear that rotor-equivalent information is generally more appropriate than local data because what determines the overall rotor response is what is felt by the whole rotor rather

than what takes place at a specific point. Additionally, certain wind characteristics can only be defined over a rotor disk and do not have pointwise equivalents, for example shears. Met masts, being equipped with multiple wind sensors away from the rotor, do not suffer from some of these issues. However, the problem of mapping the information from a met mast to the rotor disk of a wind turbine is generally very difficult to solve, and it will clearly always be prone to possibly severe inaccuracies. With lidar (light detection and ranging), laser-based sensing technology is rapidly becoming a game changer, and other remote sensing solutions are also very promising. While their potential is clearly very real and will probably have a deep impact on wind energy technology, these devices are still not in widespread use, mostly because of cost, reliability, availability and lifetime issues.

In this scenario, wind sensing by using the rotor response seems to offer an attractive alternative. In fact, any wind property estimated from the rotor response will be nonlocal and rotor effective in contrast to local sensors. In addition, this approach provides measurements directly at the rotor disk, avoiding the need for mapping flow characteristics from one point to another.

The rotor-effective wind speed estimator (Van der Hooft and Engelen, 2004; Soltani et al., 2013) is one of the first examples of the use of the rotor response for estimating wind characteristics. In this case, the idea is to use the dynamic torque balance equation: based on a map of the aerodynamic torque (or power) of the rotor over the operating envelope of the machine, one may solve this equation in terms of the unknown wind speed, assuming that the other operational parameters (rotor speed, pitch setting, electrical torque) are measured at each instant in time.

This idea was first generalized by Bottasso et al. (2010), who introduced the concept of the rotor as an anemometer. Instead of using the single torque balance, additional equations for the dynamic equilibrium of the machine were used, including the tower and blade degrees of freedom. As multiple equations are now available, multiple wind states can be estimated in addition to wind speed. Although attractive, the need to estimate some wind turbine states resulted in a fairly complicated formulation.

A much simpler approach was developed later in Bottasso and Riboldi (2014), where the idea was not to use the equations of dynamic equilibrium, but rather to consider the steady-state response of the machine. Specifically, the approach exploited the fact that steady wind conditions are associated with a periodic response of the wind turbine. Therefore, a load–wind model was derived linking the harmonics of the blade out- and in-plane bending moments at the rotor frequency (noted $1\times$ Rev, i.e., once per revolution) with the wind vertical shear and yaw misalignment. A simple blade flapping model was used to derive and justify the structure of the model, while, for accuracy, its actual coefficients were obtained through identification from a higher-fidelity aeroservoelastic model of the wind turbine or directly from field tests. A validation of the observer using field data was described in Bottasso and Riboldi (2015) using the Control Advanced Research Turbine (CART3) (Fleming et al., 2011; Bossanyi et al., 2009). The results indicated a significantly higher correlation of the observer results with respect to a met mast, assumed as ground truth, than for the onboard nacelle anemometer and wind vane. Notwithstanding these very promising results, the same study also showed a marked sensitivity of the results on the wind upflow angle, indicating the probable need for a richer description of the wind field.

Following the idea described in Bottasso et al. (2010), an estimator based on a linearized wind turbine model was proposed in Simley and Pao (2014). The formulation used generator speed, fore–aft nacelle acceleration and collective cosine and sine components of the blade out-of-plane bending moments to estimate, with a Kalman filter, the equivalent wind speed together with the linear vertical and horizontal shears. That study demonstrated the performance of the formulation using nonturbulent wind fields that were exactly parameterized by the assumed wind states. However, the effects of unmodeled wind characteristics (for example, turbulence and yaw or upflow misalignments) were not considered.

The concept of the wind turbine as a wind sensor was recently extended to the detection of wake impingement in Bottasso et al. (2015, 2018) and Cacciola et al. (2016a), where loads are used to detect if and where a wake shed by an upstream wind turbine interferes with the rotor.

Motivated by the very promising validation results both in simulations and in the field, the present paper extends and improves the formulation of Bottasso and Riboldi (2014) and Cacciola et al. (2016b) with the goal of addressing some of their weaknesses.

First, extensive numerical experiments have shown that the load–wind model on which the estimator is based must consider at least four wind states instead of two, i.e., the two yaw misalignment and upflow angles as well as the two horizontal and vertical shears. These four states, together with the mean rotor-equivalent speed, represent the lowest-order full approximation of the wind inflow at the rotor disk: the two angles give the orientation of the mean wind vector with the rotor axis, while mean speed and the two shears describe a tilted planar (or mixed linear–exponential, depending on the type of shears considered) inflow. All of these states leave significant signatures in the low-frequency response of the rotor. Therefore, failure to include one of them in the model will invariably create inaccuracies in the others.

Second, the paper shows that the estimators of these four states should be limited to the use of the $1\times$ Rev response. In fact, although $2\times$ Rev harmonics are indeed excited by the four states, these same harmonics are also very significantly excited by turbulence, i.e., by higher-order wind states (describing a nonplanar inflow distribution over the rotor disk). As it is not possible to distinguish the part of the $2\times$ Rev response caused by the four wind states from the part caused by

turbulence, inclusion of this higher-order response will result in significant pollution of the estimates.

Third, the paper compares both a linear and a nonlinear (quadratic) load–wind model. Both models are scheduled with respect to wind speed in order to account for the different characteristics of a wind turbine in its wind speed operating range. Numerical experiments show that the two are very similar in performance, with a small improvement in accuracy for the nonlinear model over the linear one.

Fourth, experience has shown that angles (yaw misalignment and upflow) are significantly more difficult to estimate than shears. The paper explains the reason for this behavior from two different perspectives. From a mathematical point of view, an a priori analysis based on the singular value decomposition (SVD) demonstrates that angles have a lower level of observability than shears, implying that any small error or perturbation (in the model, in the measurements, in the numerical solution, etc.) will be significantly amplified during the model inversion necessary for the estimation of the wind states. From a physical point of view, this is also easily explained in terms of the sensitivity of angle of attack changes at the blade section to wind state changes. As angles of attack (and hence loads) change less in response to angle changes than to shear changes, angles are harder to estimate than shears when looking at rotor loads.

Finally, the paper demonstrates the performance of the estimator through extensive numerical simulations performed with a high-fidelity aeroservoelastic model of a multi-MW wind turbine. The numerical results illustrate the excellent ability of the proposed formulation to follow rapid fluctuations in shears. The same results also show very interesting behavior of the angle estimators. In fact, although angle estimates are indeed generally polluted by oscillations that depend on turbulence level, their mean errors are significantly low. An analysis that considers the probability distributions of wind speed and turbulence intensity at a given site shows that the expected average inaccuracy of the angle estimates is remarkably low, i.e., less than 1 degree. This means that angles, although apparently oscillatory on short time horizons, can be followed quite precisely in their mean value changes.

The paper is organized according to the following plan. Section 2 presents the formulation of the observer, first introducing load–wind models that relate wind states and blade harmonics, then describing the identification of the model parameters with a system identification approach and finally inverting the model to give wind states when loads are measured. A first set of simulations is used to motivate the limitation of the load vector to the $1\times$ Rev harmonics. To this end, the simulation environment is briefly introduced together with the aeroservoelastic mathematical model of a wind turbine, which is used throughout the entire work to support all numerical experiments. Section 3 is devoted to an a priori observability analysis of the wind parameters using the SVD followed by a concise summary of the expected observer behavior given in Sect. 3.2. The results of extensive testing of the proposed method in nonturbulent and turbulent wind conditions are given in Sect. 4. Finally, Sect. 5 completes the paper by listing the main conclusions and suggesting possible further improvements to the methodology.

2 Formulation

2.1 Wind anisotropy and its parameterization

The development of the proposed wind inflow observer is inspired by the idea of using the wind turbine as an anemometer. In this sense, wind is not only the source of energy to be harvested, but also one of the principal factors affecting the wind turbine response. Specifically, the present observer is based on the lowest load harmonics. Although other response indicators could be used in principle, for example accelerations, loads are considered in this work because they are now often measured onboard modern large wind turbines for enabling load feedback control, and load sensors will probably be standard equipment available on most future machines.

In order to understand the connection between blade loads and wind characteristics, consider two different constant-in-time wind fields. A first wind field is axially symmetric with respect to the rotation axis of the wind turbine rotor, while the second is not in magnitude or direction. In the second – anisotropic – case, differences in speed and/or direction over the rotor disk may be due to wind shears (both vertical and horizontal) and/or misalignments with the wind direction (due to both yawed flow and upflow caused by rotor uptilt, terrain orography, etc.). In the axially symmetric case, the angle of attack experienced by the blade sections during their azimuthal travel over the rotor disk will be constant; hence, the resulting aerodynamic loads will also be constant. In the non-axially symmetric case, any anisotropy in the wind will cause periodic fluctuations in the angle of attack at the blade sections and hence periodic loads. The amplitude and phase of such loads will depend on the wind field at the rotor disk and on the aeroelastic characteristics of the rotor blades. Therefore, the amplitude and phase of the periodic loads carry information on the wind anisotropy at the rotor disk. This fact can be readily verified with simplified mathematical models of a rotating blade in an anisotropic wind field, for example the classical flapping and lagging blade model developed in Eggleston and Stoddard (1987). Using such a model, Bottasso and Riboldi (2014) suggested a linear structure for a blade-response-based observer of cross-flow and vertical shear.

In this work, the wind field anisotropy is parameterized using four variables (termed wind states in the following): the vertical shear exponent κ_v, horizontal linear shear κ_h and the two angles ϕ and χ measuring the yaw misalignment and upflow, respectively. These quantities are collected in the wind state vector $\boldsymbol{\theta}$, defined as

$$\boldsymbol{\theta} = (\phi,\, \kappa_\mathrm{v},\, \chi,\, \kappa_\mathrm{h})^T. \tag{1}$$

More complex wind distributions over the rotor disk might be modeled using higher-order terms. However, such local fluctuations would manifest themselves in higher Rev harmonics, complicating the estimation process.

The wind states are defined with respect to a nacelle-attached frame of reference with origin at the hub made of three mutually orthogonal unit vectors $\boldsymbol{x}$, $\boldsymbol{y}$ and $\boldsymbol{z}$. The $\boldsymbol{x}$ vector is parallel to the rotor axis and pointing downwind and $\boldsymbol{z}$ points upward in the vertical plane, while $\boldsymbol{y}$ is defined according to the right-hand rule. The wind vector $\overrightarrow{\boldsymbol{V}}$ is expressed in terms of its components in the nacelle frame as $\boldsymbol{V} = (u, v, w)^T$. The wind speed at the rotor disk $W(y,z) = |\boldsymbol{V}|$ is readily computed as

$$W(y,z) = V\left(\left(\frac{H+z}{H}\right)^{\kappa_v} + \frac{y}{R}\kappa_h\right), \tag{2}$$

where V is the wind speed at hub height H, while R is the rotor radius. The three wind velocity vector components are then expressed as

$$u(y,z) = W(y,z)\cos(\phi)\cos(\chi), \tag{3a}$$
$$v(y,z) = W(y,z)\sin(\phi)\cos(\chi), \tag{3b}$$
$$w(y,z) = W(y,z)\sin(\chi). \tag{3c}$$

Note that because of the definition of the nacelle-attached reference frame $(\boldsymbol{x}, \boldsymbol{y}, \boldsymbol{z})$, a horizontal wind results in an upflow equal to the negative of the nacelle uptilt angle. This is useful for separating the effects of gravitational loads from aerodynamic ones, as shown later. To ease the interpretation of the results, all computed wind states reported in the numerical examples of the rest of this paper were mapped to a frame of reference similar to the nacelle-attached one, but with an $\boldsymbol{x}$ unit vector that is horizontal with respect to the ground instead of being aligned with the rotor axis. Figure 1 illustrates the meaning of the four wind states.

Two different wind fields are considered in the following. In the fully parameterized case, the wind field is completely defined at each instant in time by V and $\boldsymbol{\theta}$. A more realistic wind field is generated using the Kaimal turbulent wind model implemented in the open-source code `TurbSim` (Jonkman and Kilcher, 2012). In the latter case, the wind field can be considered the superposition of a fully parameterized wind with turbulent fluctuations possessing specific space–time characteristics. Given a wind turbine operating in a turbulent wind field, the goal of the proposed observer is to estimate online a wind state $\boldsymbol{\theta}$ that approximates the turbulent wind at each instant in time.

2.2 Blade load harmonics

Under the effects of a steady anisotropic wind, the response of a stable wind turbine converges to a periodic motion. In such a regime, a generic blade load m can be expanded in Fourier series as

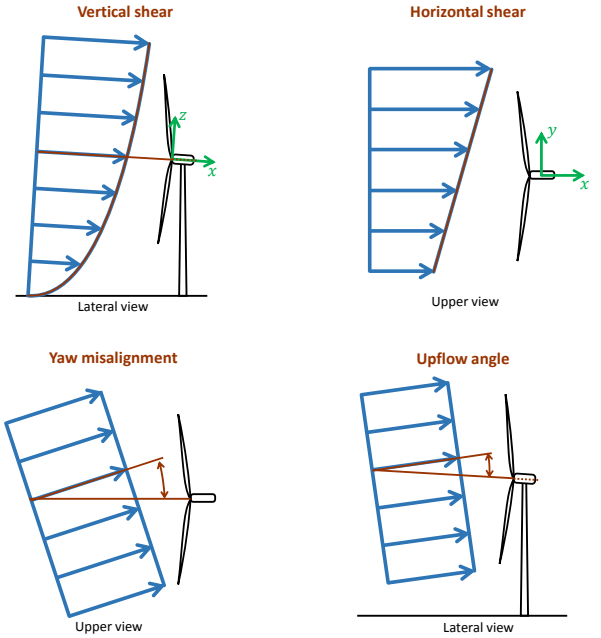

Figure 1. Definition of the four wind states used for parameterizing the wind field over the rotor disk.

$$m(\psi) = m_0 + \sum_{n=1}^{\infty}\left(m_{nc}\cos(n\psi) + m_{ns}\sin(n\psi)\right), \tag{4}$$

where ψ is the azimuth angle, the subscripts $(\cdot)_{nc}$ and $(\cdot)_{ns}$ refer to the $n\times$ Rev cosine and sine components, respectively, and m_0 is the 0th harmonic constant amplitude. The signal harmonics can be computed by demodulating the blade load $m(\psi)$ or, for rotors with at least three blades, by using the Coleman–Feingold (or multi-blade coordinate) transformation (Coleman and Feingold, 1958; Bottasso and Riboldi, 2014). By using the latter method, harmonics at the $n\times$ Rev frequency can be computed as

$$\begin{Bmatrix} m_{nc} \\ m_{ns} \end{Bmatrix} = \frac{2}{3}\begin{bmatrix} \cos(n\psi_{(1)}) & \cos(n\psi_{(2)}) & \cos(n\psi_{(3)}) \\ \sin(n\psi_{(1)}) & \sin(n\psi_{(2)}) & \sin(n\psi_{(3)}) \end{bmatrix} \begin{Bmatrix} m_{(1)} \\ m_{(2)} \\ m_{(3)} \end{Bmatrix}, \tag{5}$$

where $m_{(i)}$ and $\psi_{(i)}$ are the ith blade moment and azimuth angle, respectively. Similar relationships also exist for a higher number of blades but not for a smaller number. It can be shown that harmonics at the $i\times$ Rev are thus transformed into $0\times$ Rev components, whereas the other harmonics are either canceled out or transformed into multiples of the number B of blades. This implies that it is always necessary to filter around and above the $B\times$ Rev frequency after having applied the Coleman transformation. Adaptive filtering can

be used to follow rotor speed changes caused by variations in the wind speed.

Both out-of-plane (superscript $(\cdot)^{\mathrm{OP}}$) and in-plane (superscript $(\cdot)^{\mathrm{IP}}$) blade bending harmonic components up to a desired Rev frequency are considered and collected in a vector $\boldsymbol{m}$, defined as

$$\boldsymbol{m} = \left(m_{1\mathrm{c}}{}^{\mathrm{OP}}, m_{1\mathrm{s}}{}^{\mathrm{OP}}, m_{1\mathrm{c}}{}^{\mathrm{IP}}, m_{1\mathrm{s}}{}^{\mathrm{IP}}, m_{2\mathrm{c}}{}^{\mathrm{OP}}, m_{2\mathrm{s}}{}^{\mathrm{OP}}, m_{2\mathrm{c}}{}^{\mathrm{IP}}, m_{2\mathrm{s}}{}^{\mathrm{IP}}, \ldots\right)^T. \quad (6)$$

2.3 Wind state observer

2.3.1 Modeling of the load–wind relationship

The formulation of a wind state observer necessitates a model expressing the dependency of the loads on the wind conditions, in particular of the load harmonics $\boldsymbol{m}$ on the wind state vector $\boldsymbol{\theta}$. To this end, first consider a wind turbine model expressed by a set of nonlinear differential equations together with their output relations:

$$\boldsymbol{f}\left(\boldsymbol{x}, \dot{\boldsymbol{x}}, \boldsymbol{u}(\boldsymbol{\theta}, V, \varrho)\right) = \boldsymbol{0}, \quad (7a)$$

$$\boldsymbol{y} = \boldsymbol{g}\left(\boldsymbol{x}, \dot{\boldsymbol{x}}, \boldsymbol{u}(\boldsymbol{\theta}, V, \varrho)\right), \quad (7b)$$

where $\boldsymbol{x}$ is the state vector, $\boldsymbol{u}$ is the input vector and $\boldsymbol{y} = (m^{\mathrm{OP}}, m^{\mathrm{IP}})^T$ indicates the output vector (in this case, containing the out- and in-plane components of the blade bending moment m). The input vector only includes the exogenous disturbance represented by the wind parameters $\boldsymbol{\theta}$, the wind speed V and the air density ϱ because the presence of a feedback controller (usually in the form of a pitch-torque controller) can be considered to be included in the definition of the system model $\boldsymbol{f}(\cdot)$.

Under a steady input $\boldsymbol{u}$, the response of the system (Eq. 7a) in terms of its states converges to a periodic solution, which can be described through a truncated Fourier expansion as

$$\boldsymbol{x} = \boldsymbol{x}_0 + \sum_{n=1}^{N} \left(\boldsymbol{x}_{n\mathrm{c}} \cos(n\psi) + \boldsymbol{x}_{n\mathrm{s}} \sin(n\psi)\right). \quad (8)$$

By inserting Eq. (8) into Eq. (7a) and collecting all terms at the same frequency (a procedure termed harmonic balance), one can compute $\boldsymbol{x}_{n\mathrm{c}}$ and $\boldsymbol{x}_{n\mathrm{s}}$, which will clearly depend on $\boldsymbol{\theta}$, V and ϱ. Finally, the harmonics $\boldsymbol{x}_{n\mathrm{c}}$ and $\boldsymbol{x}_{n\mathrm{s}}$ can be inserted into the output Eq. (7b), yielding the desired relationship between load harmonics and wind parameters:

$$\boldsymbol{m} = \boldsymbol{\mathcal{M}}(\boldsymbol{\theta}, V, \varrho). \quad (9)$$

An example of this derivation for a simplified flapping blade model can be found in Bottasso and Riboldi (2014). In principle, the resulting input–output relationship should also include the dependency on other parameters, such as blade pitch and rotor speed, as shown for example in Simley and Pao (2014). However, all these quantities depend in turn on the environmental and operating conditions according to the particular regulation strategy adopted by the onboard controller. Therefore, in this work the model is assumed to depend only on $\boldsymbol{\theta}$, V and ϱ. Vector $\boldsymbol{\theta}$ is to be estimated with the proposed observer, while V, which is a scheduling parameter for the model, can either be measured or observed using a rotor-equivalent wind speed estimator (Soltani et al., 2013; Simley and Pao, 2014; Bottasso et al., 2015, 2018).

This approach leads to a white box model, i.e., a model using analytical formulas to express relationships among the relevant variables based on physical principles (Ljung, 2010). The use of white box models may suffer from inaccuracies. Any mismatch between model (Eq. 7) and reality will inevitably pollute the input–output relationship (Eq. 9). To address this problem, one may calibrate some of the parameters of the model (Eq. 7) based on available measurements. This procedure is carried out using parameter identification techniques (Jategaonkar, 2015) and leads to a gray box model, defined as a white box model in which some parameters are taken as unknown (Ljung, 2010).

In this paper, a third approach is used, which is entirely based on system identification. In this case, the desired input–output relationship between loads and wind states is considered as a black box (Ljung, 2010). In this case, the model does not contain any physics-based formulas, but it is designed to be capable of parameterizing the desired functional dependency in a general and flexible way. This is typically done through a set of assumed bases and associated free parameters (Ljung, 2010), which are then identified directly from measurements of $\boldsymbol{m}$ and $\boldsymbol{\theta}$. This way, the need for an analytical model is bypassed completely. The advantage of avoiding the use of a white or gray model is paid in terms of the need for a set of measurements that is rich and complete enough to enable the identification of the relationship of interest. Also note that although we use a black box approach, which by definition is blind to the physics, we bring specific knowledge on the nature of the problem through the definition of the output vector in terms of load harmonics.

The data set for the identification of the black box model can be obtained either by simulation or by measurements performed in the field. The former approach, which is also the one that was used for the present work, is relatively simple because in a simulation environment one can readily measure all necessary quantities (loads and wind states). In contrast to this simplicity, it is clear that any mismatch between the simulation model and reality will affect the quality of the identified input–output model. While this is in principle a possible drawback, one should not forget that the present approach only uses the very lowest harmonics (typically only the $1\times$ Rev) of the response. State-of-the-art aeroservoelastic codes used for the design and certification of wind turbines are typically quite accurate in this frequency range. An additional remark on this modeling approach is in order: it is clear that identifying a black box model based on the outputs of a simulation is in a sense akin to the extraction of a white box model from the simulation model itself. However, given the level of complexity of modern comprehensive aeroservoelastic codes, the direct extraction of the necessary input–output relationship through the manipulation of the underly-

ing equations is hardly feasible in practice, especially when working with legacy codes.

Another possible approach is to use field measurements. In this case the machine should be equipped with load sensors, a met mast and a lidar or other flow sensors to measure wind states. Each of these techniques implies its own hypothesis (e.g., frozen turbulence in the case of flow measurements performed away from the rotor disk), each is limited by its own specific inherent accuracy and each is affected by errors and disturbances. While this approach is certainly possible and was in fact successfully demonstrated in Bottasso and Riboldi (2014), it was not pursued further in the present work.

2.3.2 Linear model

Inspired by Eq. (9), a linear input–output model can be expressed as

$$\boldsymbol{m} = \mathbf{F}(V,\varrho)\boldsymbol{\theta} + \boldsymbol{m}_0(V,\varrho), \tag{10a}$$

$$= \mathbf{T}\overline{\boldsymbol{\theta}}, \tag{10b}$$

where $\mathbf{F}$ and $\boldsymbol{m}_0$ are the model coefficients, while $\mathbf{T}(V,\varrho) = [\mathbf{F}(V,\varrho),\ \boldsymbol{m}_0(V,\varrho)]$ and $\overline{\boldsymbol{\theta}} = (\boldsymbol{\theta}^T,\ 1)^T$.

Matrix $\mathbf{F}$ is the sensitivity of the harmonics with respect to the wind states and depends on the operating condition of the machine through the wind speed V and the air density ϱ. Vector $\boldsymbol{m}_0$ is a term accounting for gravity-induced loads. In fact, when $\boldsymbol{\theta} = 0$, the wind field is a constant-over-the-rotor-disk flow parallel to the rotor axis, which only causes a $0\times$ Rev load response and therefore does not contribute to $\boldsymbol{m}$. Similarly, inertial effects due to the rotor spinning with an angular velocity Ω also generate only $0\times$ Rev loads, and hence do not contribute to Eq. (10). Vector $\boldsymbol{m}_0$ can be expressed as

$$\boldsymbol{m}_0 = \boldsymbol{g} + q\,A\boldsymbol{c}(V,\varrho). \tag{11}$$

The first term, $\boldsymbol{g}$, accounts for in-plane and out-of-plane gravity-induced loads, the latter being caused by blade precone, prebend and rotor uptilt. The second term, $q\,A\boldsymbol{c}$, is a gravity-induced load due to the rotor deformation caused by aerodynamic loads, which can therefore be nondimensionalized accordingly. For the same reasons noted above, this term also generally depends on V and ϱ.

Separating the effects of gravity from aerodynamic-induced loads allows for the correction of air density changes. This is important in practice because density, being dependent on temperature, undergoes significant fluctuations in the field, thereby affecting load measurements. The split of gravity-induced terms into constant and aerodynamically caused terms is also important, as it highlights the variability of the latter term with the operating condition.

The unknown matrix of coefficients $\mathbf{T}$ can be computed by collecting multiple observations for the moments $\boldsymbol{m}^{(i)}$ and inputs $\overline{\boldsymbol{\theta}}^{(i)}$, where $(\cdot)^{(i)}$ indicates the ith of N_{exp} available observations. By grouping the measurements into the matrices

$$\mathbf{M} = \left[\ \boldsymbol{m}^{(1)},\ \boldsymbol{m}^{(2)},\ \ldots,\ \boldsymbol{m}^{(N_{\text{exp}})}\ \right], \tag{12a}$$

$$\boldsymbol{\Theta} = \left[\ \overline{\boldsymbol{\theta}}^{(1)},\ \overline{\boldsymbol{\theta}}^{(2)},\ \ldots,\ \overline{\boldsymbol{\theta}}^{(N_{\text{exp}})}\ \right], \tag{12b}$$

the input–output relationship (10) can be written collectively for all observations as

$$\mathbf{M} = \mathbf{T}\boldsymbol{\Theta}. \tag{13}$$

Finally, matrix $\mathbf{T}$ is readily estimated in a least-squares sense as

$$\mathbf{T} = \mathbf{M}\boldsymbol{\Theta}^T\left(\boldsymbol{\Theta}\,\boldsymbol{\Theta}^T\right)^{-1}. \tag{14}$$

The problem is solvable if and only if matrix $\boldsymbol{\Theta}$ has a full rank. In this sense, the condition number of matrix $\boldsymbol{\Theta}\,\boldsymbol{\Theta}^T$ gives an indication of the identifiability of a model given a set of measurements. If the condition number is excessively high, then the problem is ill posed and the data set has to be enriched and/or modified.

As previously noted, the input–output model should be scheduled in terms of the wind speed V and air density ϱ, as the model coefficients depend on the operating condition of the machine. To this end, a piecewise linear scheduled model can be expressed as

$$\begin{aligned}\boldsymbol{m} &= \sum_{k=1}^{N_{\text{node}_V}}\sum_{w=1}^{N_{\text{node}_\varrho}} \mathbf{F}_{k,w}n_{k,w}(V,\varrho)\boldsymbol{\theta} + \boldsymbol{m}_{0k,w}n_{k,w}(V,\varrho)\\ &= \sum_{k=1}^{N_{\text{node}_V}}\sum_{w=1}^{N_{\text{node}_\varrho}} \mathbf{T}_{k,w}n_{k,w}(V,\varrho)\overline{\boldsymbol{\theta}},\end{aligned} \tag{15}$$

where the wind speed and air density ranges have been discretized by introducing N_{node_V} wind speed nodes and N_{node_ϱ} density nodes, while $\mathbf{F}_{k,w}$ and $\boldsymbol{m}_{0k,w}$ are the model coefficient nodal matrices grouped together as $\mathbf{T}_{k,w} = [\mathbf{F}_{k,w}\,\boldsymbol{m}_{0k,w}]$. Finally, two-dimensional shape functions are noted $n_{k,w}(V,\varrho)$. The scheduled model (Eq. 15) can be written in a more compact form as

$$\boldsymbol{m} = \widehat{\mathbf{T}}\widehat{\boldsymbol{\theta}}(V,\varrho) \tag{16}$$

where $\widehat{\boldsymbol{\theta}}(V,\varrho) = \widehat{\mathbf{N}}(V,\varrho)\overline{\boldsymbol{\theta}}$ and

$$\widehat{\mathbf{T}} = \left[\mathbf{T}_{1,1},\ \mathbf{T}_{1,2},\ \ldots,\ \mathbf{T}_{k,w},\ \ldots,\ \mathbf{T}_{N_{\text{node}_V},N_{\text{node}_\varrho}}\right], \tag{17a}$$

$$\widehat{\mathbf{N}} = \Big[n_{1,1}(V,\varrho)\mathbf{I},\ n_{1,2}(V,\varrho)\mathbf{I},\ \ldots,\ n_{k,w}(V,\varrho)\mathbf{I},\ \ldots,\ n_{N_{\text{node}_V},N_{\text{node}_\varrho}}(V,\varrho)\mathbf{I}\Big]^T, \tag{17b}$$

where $\mathbf{I}$ is an identity matrix of suitable dimensions.

Samples of the wind states and associated loads are now collected at N_{exp} different operating conditions, each corresponding to its own wind speed $V^{(i)}$ and air density $\varrho^{(i)}$. The

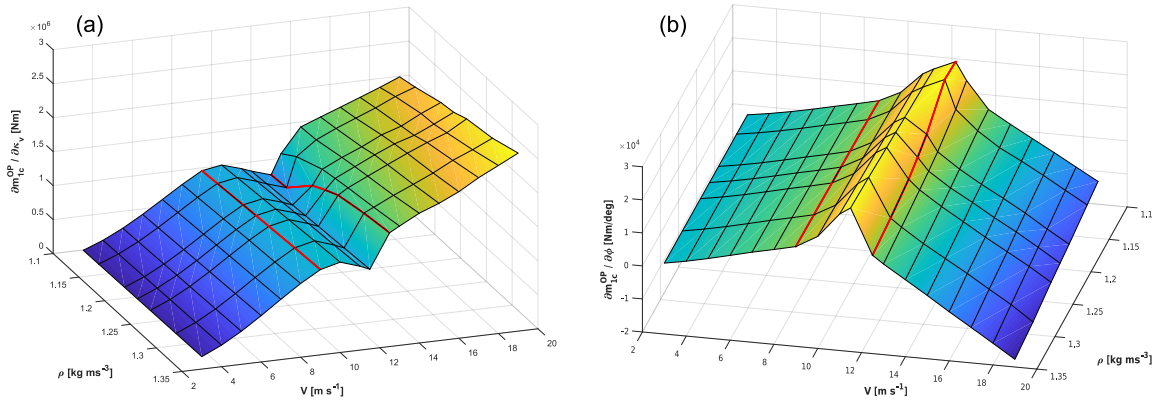

Figure 2. Behavior of two load sensitivities as functions of wind speed V and air density ϱ: sensitivity of out-of-plane $1\times$ Rev cosine moment with respect to vertical shear κ_v **(a)** and yaw misalignment ϕ **(b)**. The boundaries between regions II, II$\frac{1}{2}$ and III are indicated by red solid lines. The color indicates the value of the function, i.e., the elevation of the plot.

ith load vector and wind state vector are notated as $\boldsymbol{m}^{(i)}$ and $\widehat{\boldsymbol{\theta}}(V^{(i)}, \varrho^{(i)})$, respectively. Both loads and wind states are collected into matrices as

$$\widehat{\mathbf{M}} = \left[\boldsymbol{m}^{(1)},\ \boldsymbol{m}^{(2)},\ \ldots,\ \boldsymbol{m}^{(N_\mathrm{exp})} \right], \tag{18a}$$

$$\widehat{\boldsymbol{\Theta}} = \left[\widehat{\boldsymbol{\theta}}(V^{(1)}, \varrho^{(1)}),\ \widehat{\boldsymbol{\theta}}(V^{(2)}, \varrho^{(2)}),\ \ldots,\ \widehat{\boldsymbol{\theta}}(V^{(N_\mathrm{exp})}, \varrho^{(N_\mathrm{exp})}) \right], \tag{18b}$$

leading to the overall system

$$\widehat{\mathbf{M}} = \widehat{\mathbf{T}}\widehat{\boldsymbol{\Theta}}. \tag{19}$$

Finally, the matrix of unknown coefficients $\widehat{\mathbf{T}}$ is computed in a least-squares sense as

$$\widehat{\mathbf{T}} = \widehat{\mathbf{M}}\widehat{\boldsymbol{\Theta}}^T \left(\widehat{\boldsymbol{\Theta}}\,\widehat{\boldsymbol{\Theta}}^T \right)^{-1}. \tag{20}$$

The problem is well posed if the solving least-squares matrix, $\widehat{\boldsymbol{\Theta}}\,\widehat{\boldsymbol{\Theta}}^T$, is non-singular. One must clearly ensure that samples adequately cover all wind speed intervals in order to ensure the identifiability of all nodal matrices $\mathbf{F}_{k,w}$ and $\boldsymbol{m}_{0k,w}$.

An example of the typical behavior of the model coefficients is given in Fig. 2 for the wind turbine described later in this paper. The figure reports $\partial {m_1}_\mathrm{c}{}^\mathrm{OP}/\partial\kappa_\mathrm{v}$ (Fig. 2a) and $\partial {m_1}_\mathrm{c}{}^\mathrm{OP}/\partial\phi$ (Fig. 2b) as functions of V and ϱ. There is distinctly different behavior with respect to the wind speed of the load sensitivities in regions II (partial load) and III (full load). The rapid changes in the transition region II$\frac{1}{2}$ call for a suitable refinement of the node spacing in this regime. In general, the situation with respect to density is simpler, with small departures from linear behavior only in the transition region.

2.3.3 Nonlinear model

The assumption of linearity in the input–output relationship (Eq. 9) might lead to inaccuracies. To correct for these potential effects while limiting model complexity, a model with an assumed degree of nonlinearity is formulated as

$$\boldsymbol{m} = \mathbf{F}_\mathrm{NL}\boldsymbol{\theta}_\mathrm{NL} + \boldsymbol{m}_{\mathrm{NL}_0}. \tag{21}$$

The nonlinear wind state vector $\boldsymbol{\theta}_\mathrm{NL}$ contains, in addition to the elements of $\boldsymbol{\theta}$, their nonlinear combinations $\theta_{\mathrm{NL}\,j}$ up to a given order p, where

$$\theta_{\mathrm{NL}\,j} = \prod_i \theta_i{}^{\alpha_i} \quad \text{s.t.} \quad \sum_i \alpha_i \le p; \tag{22}$$

θ_i is the ith element of the linear wind state vector $\boldsymbol{\theta}$. For $p = 2$, which is the case considered here, the nonlinear wind state vector contains 14 terms:

$$\boldsymbol{\theta}_\mathrm{NL} = (\phi,\ \kappa_\mathrm{v},\ \chi,\ \kappa_\mathrm{h},\ \phi\kappa_\mathrm{v},\ \phi\chi,\ \phi\kappa_\mathrm{h},\ \kappa_\mathrm{v}\chi,\ \kappa_\mathrm{v}\kappa_\mathrm{h},\ \chi\kappa_\mathrm{h},\ \phi^2,\ \kappa_\mathrm{v}{}^2,\ \chi^2,\ \kappa_\mathrm{h}^2)^T. \tag{23}$$

As the nonlinear model (Eq. 21) is linear in the unknown coefficients $\mathbf{F}_\mathrm{NL}$ and $\boldsymbol{m}_{\mathrm{NL}_0}$, its identification is formally identical to that of the linear model for both the unscheduled and the scheduled cases. However, as more coefficients are present, one has to check that the data set is complete enough to guarantee that the problem is well posed.

2.3.4 Wind turbine simulation model

In this work, an aeroservoelastic simulation model is used to represent the dynamic behavior of a wind turbine in all different scenarios of interest. The model represents a horizontal axis wind turbine with a rotor of 93 m diameter with an uptilt of 4.5°, a hub height of 80 m and a rated power of 3 MW. The

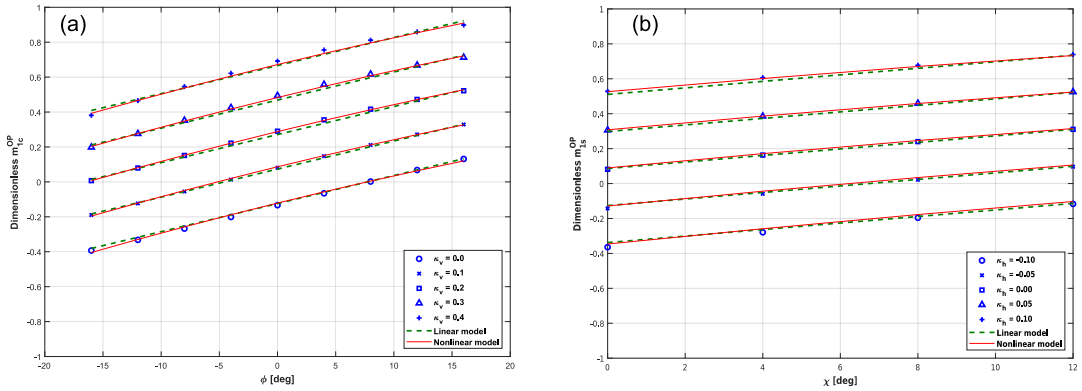

Figure 3. Comparison between measured and predicted harmonics for the linear model (dashed thick lines) and the nonlinear model of order 2 (solid thin lines). Normalized 1× Rev cosine **(a)** and sine **(b)** out-of-plane moment components are shown for different wind state variables.

wind speeds at cut-in (V_{CI}), rated power (V_{RP}) and cut-out (V_{CO}) are respectively equal to 3, 12.5 and 25 m s^{-1}. A rather wide transition region II$\frac{1}{2}$ extends from 9 to 12.5 m s^{-1}. The cut-in rotor speed is equal to 5.2 RPM, whereas the rated rotor speed is equal to 15 RPM. Both side–side and fore–aft tower frequencies f_{tower} are equal to 0.3 Hz. The first blade flapwise frequency f_{flap} varies between 0.9 Hz at cut-in and 1 Hz at rated rotor speed. Finally, the first blade edgewise mode f_{edge} is at around 1.5 Hz.

The aeroservoelastic model of the machine is developed using the finite-element multi-body code `Cp-Lambda` (Bauchau et al., 2003; Bottasso and Croce, 2006). The model includes flexible blades, a tower and a drivetrain implemented with geometrically exact nonlinear beam models (Bauchau, 2011). Rotor-speed-dependent mechanical losses are considered within the drivetrain generator model, and compliant foundations are used to connect the tower base to the ground. The aerodynamics are rendered through the classical blade element momentum theory (BEM) and consider hub and tip losses, dynamic stall and unsteady corrections. The model is completed by an active pitch torque controller implemented as a speed-scheduled linear quadratic regulator (LQR) (Bottasso et al., 2012; Riboldi, 2012). Additionally, the pitch and torque actuators are modeled as second- and first-order systems, respectively. Finally, the model is subjected to wind time histories generated by the code `TurbSim` (Jonkman and Kilcher, 2012).

2.3.5 Load–wind relationship in steady conditions

To test the performance of the linear and nonlinear models, the wind turbine was simulated in a variety of different operating conditions. Fully parameterized steady winds were generated at $N_{node_V} = 10$ speeds $V = \{3, 4, 5, 6, 7, 8, 9, 11, 15, 19\}$ m s^{-1}, where for each different wind speed all 900 possible combinations of the following wind parameters were considered:

$$\phi = \{-16, -12, -8, -4, 0, 4, 8, 12, 16\} \text{ deg}, \quad (24a)$$

$$\kappa_v = \{0.0, 0.1, 0.2, 0.3, 0.4\}, \quad (24b)$$

$$\chi = \{0, 4, 8, 12\} \text{ deg}, \quad (24c)$$

$$\kappa_h = \{-0.1, -0.05, 0.0, 0.05, 0.1\}, \quad (24d)$$

resulting in $N_{exp} = 9000$ available observations. Loads were measured on the aeroelastic model in a blade-attached reference frame located at the root of each blade, thereby simulating the presence of strain gages measuring flapwise and edgewise bending moment components, which were then transformed into out- and in-plane rotor components by using the blade pitch angle. Next, the out- and in-plane loads were decomposed into their harmonics at the 1× Rev and 2× Rev with the Coleman transformation and used together with the corresponding wind states to identify the linear and nonlinear models used throughout this work.

From the full range of tests performed, Fig. 3 shows two representative examples at a wind speed of 7 m s^{-1}, illustrating the match between the measurements obtained on the wind turbine simulation model (taken as ground truth) and the outputs of the identified models. The ground truth is reported with markers, the linear model with dashed lines and the nonlinear model with solid lines. Figure 3a shows $m_{1c}{}^{OP}$ as a function of ϕ for different values of κ_v and for $\kappa_h = 0.0$ and $\chi = 4°$. Figure 3b shows $m_{1s}{}^{OP}$ as a function of χ for different values of κ_h and for $\kappa_v = 0.0$ and $\phi = 0°$. Both moments are nondimensionalized with respect to their own maximum absolute values.

The figure shows that both models are capable of capturing the relevant behavior of the harmonics with respect to wind states. The relationships appear to be linear, with only very minor nonlinearities. These analyses also graphically illustrate the sensitivity of the loads with respect to the wind parameters. As expected, even though all parameters have a certain effect on all loads, cosine harmonics are mainly influenced by the couple $\{\phi, \kappa_v\}$, whereas sine harmonics are

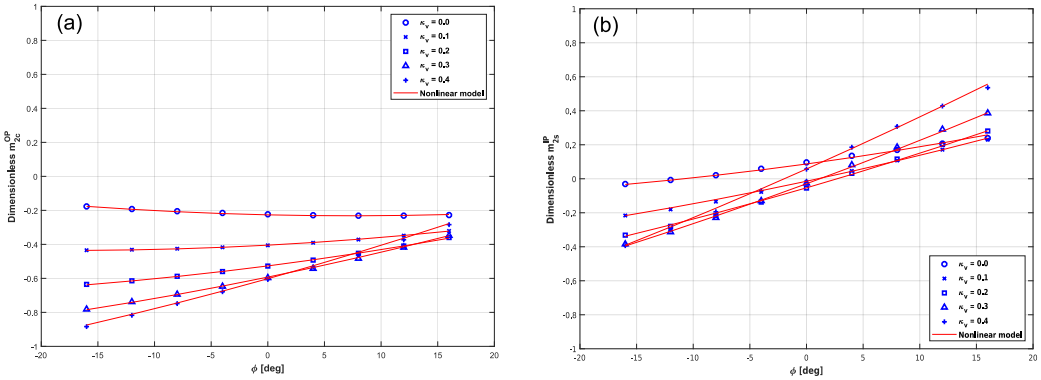

Figure 4. Comparison between measured and predicted harmonics for the nonlinear model of order 2 (solid thin lines). Normalized out-of-plane 2× Rev cosine **(a)** and in-plane 2× Rev sine **(b)** are shown for different wind state variables.

influenced by $\{\chi, \kappa_h\}$. Similar considerations can be derived for the in-plane harmonics, which are not shown here for the sake of brevity.

In contrast, the 2× Rev harmonics have markedly different behavior, as shown in Fig. 4. The plots report the nondimensional out-of-plane 2× Rev cosine term (Fig. 4a) and the in-plane 2× Rev sine term (Fig. 4b) as functions of ϕ and for varying κ_v, with $\kappa_h = 0.0$ and $\chi = 4°$. Given the clear nonlinearity of the relationships, only the nonlinear model is able to capture the correct trends of these higher harmonics with respect to the wind states.

2.3.6 Choosing the number of harmonics

The previous analysis performed in steady wind conditions showed that the 1× Rev harmonics exhibit largely linear behavior with respect to the wind states, while the 2× Revs exhibit marked nonlinearities. In order to understand the behavior of the models in more realistic conditions, simulations were conducted in turbulent winds. In particular, it is necessary to establish whether the unsteadiness in the excitation provided by a turbulent wind is compatible with the steady-state harmonic models considered herein. In addition, as previously noted, a turbulent wind field cannot generally be exactly represented by the reduced set of wind states.

To investigate these effects, a 10 min simulation was performed at a 5 m s^{-1} mean wind speed with a TI equal to 20 % and null mean yaw misalignment, upflow and vertical and horizontal shears. At each instant in time, values of the wind parameters were computed from the wind grid generated with `TurbSim` (Jonkman and Kilcher, 2012) by fitting in a least-squares sense Eqs. (2) and (3). Blade load harmonics were extracted from the simulated outputs using the Coleman transformation and filtered with a low-pass sixth-order Butterworth filter with a cut-out frequency of 0.14 Hz in order to remove the remaining 3× Rev harmonic content in the Coleman-transformed moments. Figure 5 shows a comparison of the harmonics extracted from the simulation (shown as a thick blue solid line and again assumed to represent the ground truth) with those predicted by the second-order nonlinear model (shown as a thin red solid line) fed with the wind parameters computed from the wind grid. Figure 5a shows moment ${m_{1c}}^{IP}$, while Fig. 5b shows moment ${m_{2c}}^{OP}$.

By looking at Fig. 5a, it appears that there is an excellent match between the predictions and measurements for the in-plane 1× Rev cosine harmonic. The small delay between the two signals is due to the filter used for removing higher frequencies. Both the linear and nonlinear models yield similarly accurate results for the sine and out-of-plane components, which are not reported here for brevity. These results show that 1× Rev harmonics are primarily influenced by the wind states used here for parameterizing the wind field, with only small disturbances caused by turbulent fluctuations and blade dynamic effects. In this sense, 1× Rev harmonics are good candidates for feeding a wind state observer.

In contrast, Fig. 5b shows completely different behavior of the measurements and predictions for the 2× Rev components in turbulent conditions. It should be remarked that, as previously illustrated in Fig. 4, the model is perfectly capable of capturing these higher harmonics with good accuracy in steady wind conditions. The reason for the very poor results in the turbulent case is that small-scale turbulent fluctuations in the wind field cause 2× Rev harmonics that are comparable to, if not larger than, those caused by the wind states used for the parameterization. Therefore, although 2× Rev harmonics carry information on the wind states, this information cannot be separated from the pollution brought by the smaller-scale wind field fluctuations. In this sense, 2× Rev harmonics are not good candidates for the observation of wind states. Based on these results, the vector of blade harmonics is limited in the rest of this work to 1× Revs and simply defined as

$$\boldsymbol{m} = \left({m_{1c}}^{OP}, {m_{1s}}^{OP}, {m_{1c}}^{IP}, {m_{1s}}^{IP}\right)^T. \quad (25)$$

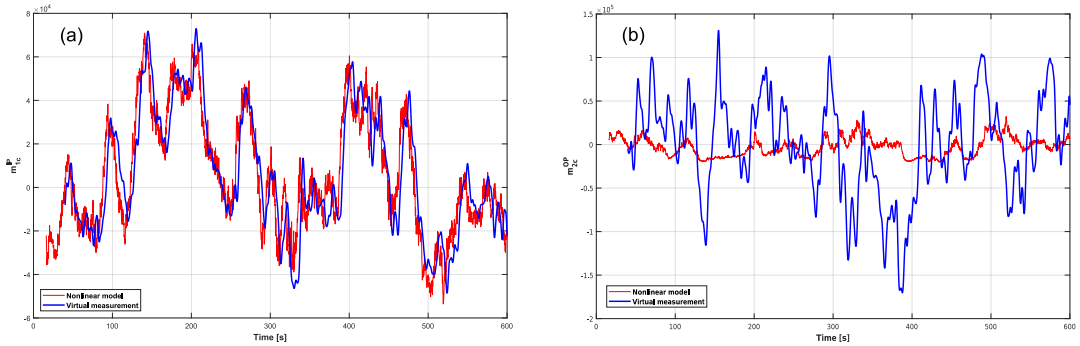

Figure 5. Comparison in turbulent wind conditions between measured harmonics (thick solid line) and harmonics predicted with a second-order nonlinear model (thin solid line). **(a)** In-plane 1× Rev cosine component; **(b)** out-of-plane 2× Rev cosine component.

2.3.7 Wind state estimation

The problem of computing an estimate $\boldsymbol{\theta}_{\mathbf{E}}$ of the wind state vector given a load harmonic vector $\boldsymbol{m}_{\mathrm{M}}$ is considered next. Given the input–output model (Eq. 9), a measured load $\boldsymbol{m}_{\mathrm{M}}$ can be expressed as

$$\boldsymbol{m}_{\mathrm{M}} = \boldsymbol{\mathcal{M}}(\boldsymbol{\theta}, V, \varrho) + \boldsymbol{r}, \tag{26}$$

where $\boldsymbol{r}$ is the measurement error with covariance $\mathbf{R} = \mathbf{E}\left[\boldsymbol{r}\boldsymbol{r}^T\right]$. The residual is assumed to be zero-mean, white and Gaussian. The residual is due not only to measurement noise, but also to all effects not captured by the model, such as sampling and discretization errors, unmodeled nonlinearities and turbulence-induced loads. This implies that the assumption of a zero-mean, white and Gaussian noise might be far from real.

The generalized least-squares estimate of $\boldsymbol{\theta}$ given $\boldsymbol{m}_{\mathrm{M}}$ is

$$\boldsymbol{\theta}_{\mathbf{E}} = \arg\min_{\theta} \Big(\big(\boldsymbol{m}_{\mathrm{M}} - \boldsymbol{\mathcal{M}}(\boldsymbol{\theta}, V, \varrho)\big)^T \mathbf{R}^{-1} \big(\boldsymbol{m}_{\mathrm{M}} - \boldsymbol{\mathcal{M}}(\boldsymbol{\theta}, V, \varrho)\big) \Big). \tag{27}$$

Consider the linear model (Eq. 10a) and assume V to be known. The solution to the problem in Eq. (27) can be worked out analytically as

$$\boldsymbol{\theta}_{\mathbf{E}} = \Big(\mathbf{F}(V)^T \mathbf{R}^{-1} \mathbf{F}(V)\Big)^{-1} \mathbf{F}(V)^T \mathbf{R}^{-1} (\boldsymbol{m}_{\mathrm{M}} - \boldsymbol{m}_0). \tag{28}$$

Vector $\boldsymbol{\theta}_{\mathbf{E}}$ is structurally identifiable (or observable) if matrix $\mathbf{F}(V)^T \mathbf{R}^{-1} \mathbf{F}(V)$ is non-singular. The structural identifiability analysis, which reveals when the estimation problem is well posed and to what degree of accuracy it can be solved, will be analyzed in Sect. 3.

For the nonlinear model (Eq. 21), the solution to the problem (Eq. 27) involves a nonlinear unconstrained minimization, which was solved here starting from a suitable initial guess by using the Levenberg–Marquardt method (More, 1977). As multiple local solutions may characterize the nonlinear problem, a global search algorithm or multiple starting points should be used to find the optimum. Here again, one must verify observability, as discussed later in Sect. 3.

The estimator (Eq. 27) was first characterized in steady wind conditions, and the results of this analysis are shown next. All plots are arranged in a similar way: any estimated wind state variable is plotted on the y axis as a function of its corresponding ground truth quantity, which is reported on the x axis. A black thin solid line indicates the bisector of the plot, representing a perfect match between the two quantities. Estimates are plotted using markers and thick solid lines for different wind conditions. Clearly, any deviation from the bisector directly indicates an estimation error.

Figure 6 shows an excerpt of the results obtained with the linear model for different wind conditions at $5\,\mathrm{m\,s^{-1}}$. The estimates appear to be of good accuracy for all wind state variables, although some small errors affect the two angles. The reason for this behavior can be traced back to mild nonlinearities clearly not captured by the linear model that affect angles to a greater extent than shears. Among the wind parameters, the upflow seems to be the least accurate, while the horizontal shear appears as the most precise. Similar results not shown here were obtained for different wind speeds and flow conditions.

The match improves with the use of the nonlinear model, as reported in Fig. 7. The plots show that all quantities appear to be well captured, with a clear improvement in the quality of the results.

3 A priori observability analysis

The observability of the wind parameters is analyzed next. As one can easily imagine, the level of accuracy of the estimates strongly depends on the sensitivity of the moments with respect to the to-be-estimated parameters and the noise in the measurements.

Assuming a linear model, the real (unknown) wind state vector $\boldsymbol{\theta}_{\mathrm{R}}$ is related to the measured load vector $\boldsymbol{m}_{\mathrm{M}}$ as

$$\boldsymbol{m}_{\mathrm{M}} = \mathbf{F}\boldsymbol{\theta}_{\mathrm{R}} + \boldsymbol{m}_0 + \boldsymbol{r}. \tag{29}$$

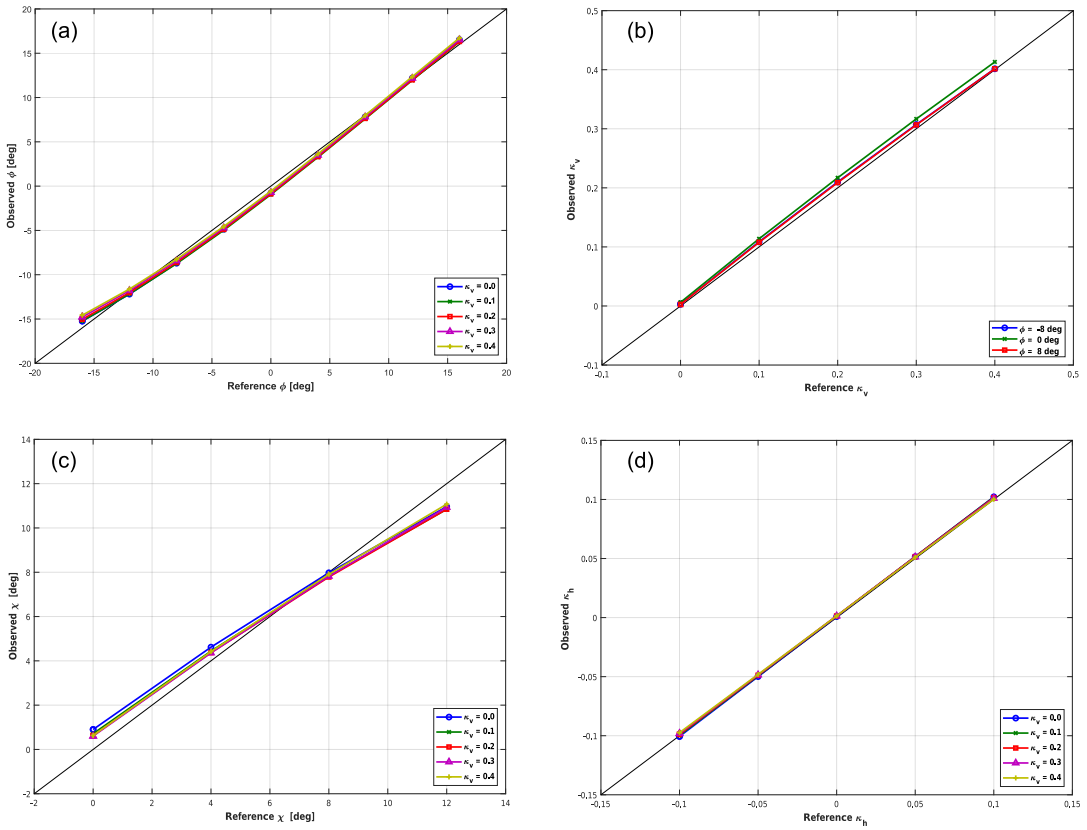

Figure 6. Wind states observed using the linear model for different steady inflow conditions at 5 m s^{-1}: yaw misalignment ϕ at $\chi = 8°$ and $\kappa_h = -0.1$ **(a)**, vertical shear κ_v at $\chi = 8°$ and $\kappa_h = -0.1$ **(b)**, upflow angle χ at $\phi = -8°$ and $\kappa_h = -0.1$ **(c)**, horizontal shear κ_h at $\chi = 8°$ and $\phi = -8°$ **(d)**.

By inserting Eq. (29) into Eq. (28), the estimation error $\boldsymbol{\epsilon}_\theta$ is readily derived as

$$\boldsymbol{\epsilon}_{\boldsymbol{\theta}} = \boldsymbol{\theta}_\mathrm{E} - \boldsymbol{\theta}_\mathrm{R} = \left(\mathbf{F}^T\mathbf{R}^{-1}\mathbf{F}\right)^{-1}\mathbf{F}^T\mathbf{R}^{-1}\boldsymbol{r}. \tag{30}$$

The estimate is unbiased because the expected value of the error $\mathbf{E}[\boldsymbol{\epsilon}_{\boldsymbol{\theta}}]$ is equal to zero when the residual is zero-mean. Additionally, the covariance of the estimation error $\mathrm{Cov}[\boldsymbol{\epsilon}_{\boldsymbol{\theta}}] = \mathcal{E}\left[\boldsymbol{\epsilon}_{\boldsymbol{\theta}}\boldsymbol{\epsilon}_{\boldsymbol{\theta}}{}^T\right]$ (Crámer, 1946) is written as

$$\mathrm{Cov}\left[\boldsymbol{\epsilon}_{\boldsymbol{\theta}}\right] = \left(\mathbf{F}^T\mathbf{R}^{-1}\mathbf{F}\right)^{-1}. \tag{31}$$

This expression shows the interplay between noise $\boldsymbol{r}$ and sensitivity $\mathbf{F}$ captured by the term $\mathbf{R}^{-\frac{1}{2}}\mathbf{F}$: the higher the variance and/or the lower the sensitivity of the measurements with respect to the wind states, the worse the accuracy of the estimates.

The covariance $\mathrm{Cov}[\boldsymbol{\epsilon}_{\boldsymbol{\theta}}]$ expressed by Eq. (31) is typically fully populated, as the errors of the estimates are correlated. To ease the understanding of the estimation problem, the SVD (Golub and van Loan, 1996) can be used to decouple the estimates. In fact, matrix $\mathbf{R}^{-\frac{1}{2}}\mathbf{F}$ can be factored as

$$\mathbf{R}^{-\frac{1}{2}}\mathbf{F} = \mathbf{U}\boldsymbol{\Sigma}\mathbf{V}^T, \tag{32}$$

with $\mathbf{U} \in \Re^{m\times m}$, $\boldsymbol{\Sigma} \in \Re^{m\times n}$ and $\mathbf{V} \in \Re^{n\times n}$, where m is the number of measurements and n is the number of wind state variables. Matrices $\mathbf{U}$ and $\mathbf{V}$ are orthonormal, i.e., $\mathbf{U}^T\mathbf{U} = \mathbf{U}\mathbf{U}^T = \mathbf{I}$ and $\mathbf{V}^T\mathbf{V} = \mathbf{V}\mathbf{V}^T = \mathbf{I}$, whereas $\boldsymbol{\Sigma} = \mathrm{diag}(\ldots, 1/\sigma_i, \ldots)$ is a diagonal matrix and σ_i is the standard deviation. By inserting Eq. (32) into Eq. (31), the covariance of the estimation error can be expressed as

$$\begin{aligned}\mathrm{Cov}\left[\mathbf{V}^T\boldsymbol{\epsilon}_\theta\right] &= \boldsymbol{E}\left[\left(\mathbf{V}^T\left(\boldsymbol{\theta}_\mathrm{E} - \boldsymbol{\theta}_\mathbf{R}\right)\right)\left(\mathbf{V}^T\left(\boldsymbol{\theta}_\mathrm{E} - \boldsymbol{\theta}_\mathbf{R}\right)\right)^T\right] \\ &= \left(\boldsymbol{\Sigma}^T\boldsymbol{\Sigma}\right)^{-1} = \mathrm{diag}(\ldots, {\sigma_i}^2, \ldots).\end{aligned} \tag{33}$$

This way, the problem is reformulated by the change in variables $\boldsymbol{\xi} = \mathbf{V}^T\boldsymbol{\theta}$, where $\boldsymbol{\xi}$ variables are statistically independent with diagonal covariance. This reformulation simplifies the interpretation of the structural observability of the problem. In fact, the ith column of matrix $\mathbf{V}$ linearly combines the wind parameters by mapping them into a new parameter

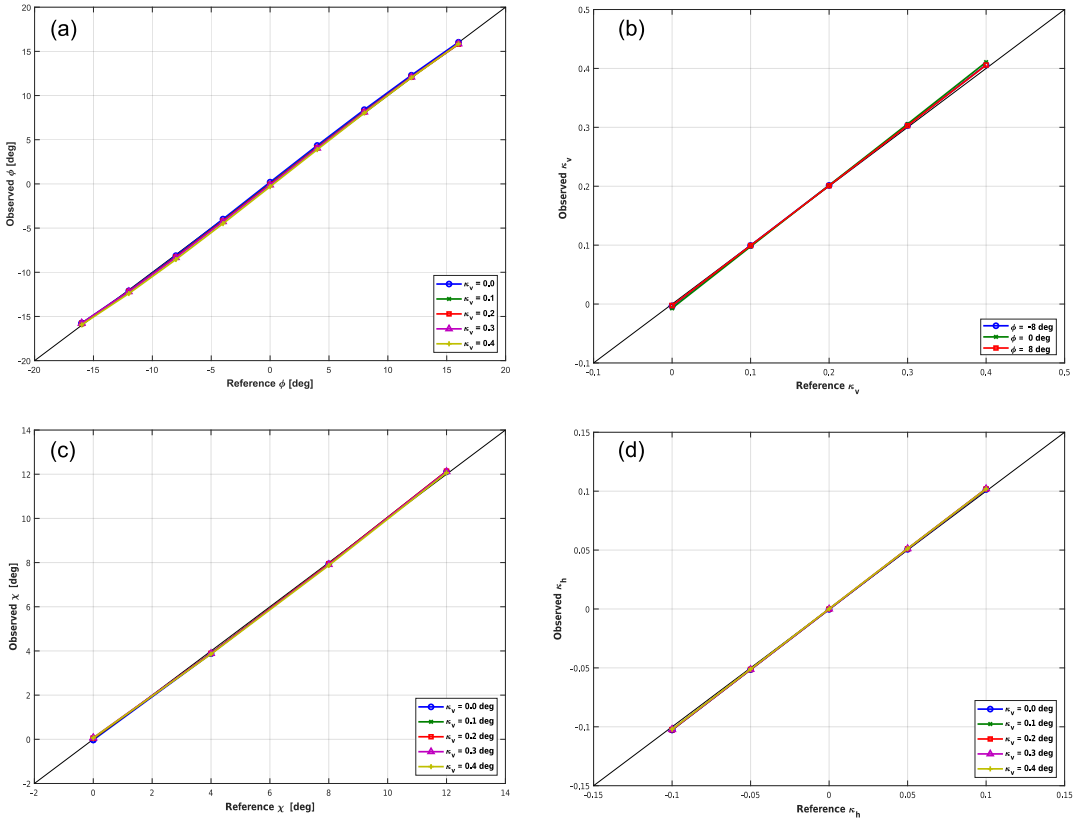

Figure 7. Wind state observed with the nonlinear model for different steady inflow conditions at 5 m s^{-1}: yaw misalignment ϕ at $\chi = 8°$ and $\kappa_h = -0.1$ **(a)**, vertical shear κ_v at $\chi = 8°$ and $\kappa_h = -0.1$ **(b)**, upflow angle χ at $\phi = -8°$ and $\kappa_h = -0.1$ **(c)**, horizontal shear κ_h at $\chi = 8°$ and $\phi = -8°$ **(d)**.

ξ_i with variance ${\sigma_i}^2$. Clearly, a high variance indicates a low level of identifiability of the associated linear combination of wind parameters.

This analysis also provides information on the dependence of loads on wind states. In fact, one can easily show that

$$\frac{\partial \boldsymbol{m}}{\partial \boldsymbol{\xi}} = \mathbf{R}^{\frac{1}{2}}\mathbf{U}\boldsymbol{\Sigma}. \tag{34}$$

Therefore, the analysis of $\mathbf{U}$ reveals the linear combination of inflow parameters on which each load depends the most.

The same analysis can be applied to the nonlinear case by linearizing Eq. (21) around a specific operating and wind condition and using $\mathbf{F} = \partial(\boldsymbol{F}_{\mathbf{NL}}\theta_{\mathrm{NL}})/\partial\boldsymbol{\theta} = \boldsymbol{F}_{\mathbf{NL}}\partial\theta_{\mathrm{NL}}/\partial\boldsymbol{\theta}$.

3.1 Results of the a priori analysis

The a priori analysis was applied to the identified input–output model. Three different values of the noise covariance $\mathbf{R}$ were considered. In the first two cases, all measures were assumed to be uncorrelated and affected by the same noise level, i.e., $\mathbf{R} = \gamma^2\mathbf{I}$, where γ is a positive real number. In the first case, γ was set to $0.01m_{\min}$, with $m_{\min}$ being the minimum of the load amplitude maxima. In the second case, γ was set to $0.01m_{\max}$, with $m_{\max}$ being the maximum of the load amplitude maxima. In the third case, the noise covariance was computed using Eq. (26):

$$\begin{aligned}\mathbf{R}_\epsilon &= \frac{1}{N_{\mathrm{exp}}}\sum_{i=1}^{N_{\mathrm{exp}}} \boldsymbol{r}_i {\boldsymbol{r}_i}^T \\ &= \frac{1}{N_{\mathrm{exp}}}\sum_{i=1}^{N_{\mathrm{exp}}} (\boldsymbol{m}_{\mathrm{M}i} - \boldsymbol{\mathcal{M}}_i(\boldsymbol{\theta}, V, \varrho)) \\ &(\boldsymbol{m}_{\mathrm{M}i} - \boldsymbol{\mathcal{M}}_i(\boldsymbol{\theta}, V, \varrho))^T,\end{aligned} \tag{35}$$

where $\boldsymbol{m}_{\mathrm{M}i}$ values are loads measured on the simulation model and $\boldsymbol{\mathcal{M}}_i(\boldsymbol{\theta}, V, \varrho)$ represents those given by the observation model.

For the first case, matrices $\mathbf{V}$ and $\mathbf{U}$ were computed at a wind speed of 5 m s^{-1} to obtain

$$\mathbf{V} = \begin{bmatrix} \sim 0 & \sim 0 & \mathbf{0.55} & \mathbf{0.83} \\ \sim 0 & \mathbf{\sim 1} & \sim 0 & \sim 0 \\ \sim 0 & \sim 0 & \mathbf{0.83} & \mathbf{0.55} \\ \mathbf{\sim 1} & \sim 0 & \sim 0 & \sim 0 \end{bmatrix},$$

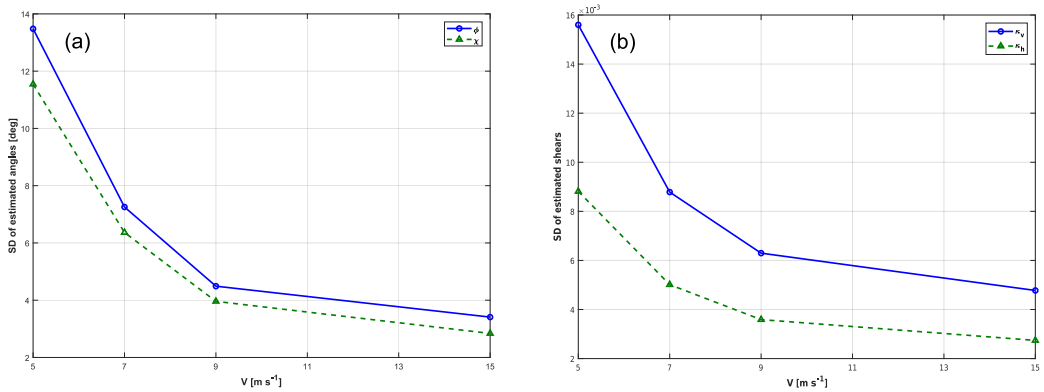

Figure 8. Expected standard deviation of the wind state estimates as a function of wind speed. **(a)** Standard deviations for angles ϕ and χ; **(b)** standard deviations for shears κ_v and κ_h.

$$\mathbf{U} = \begin{bmatrix} 0.11 & 0.97 & 0.14 & 0.18 \\ -0.97 & 0.11 & 0.18 & -0.14 \\ 0.03 & 0.22 & -0.60 & -0.77 \\ -0.23 & 0.02 & -0.77 & 0.60 \end{bmatrix}, \tag{36}$$

where ~ 0 and ~ 1 indicate a number approximately equal to 0 and to 1, respectively. To interpret these results, remember that the wind state vector is defined as $\boldsymbol{\theta} = (\phi, \kappa_v, \chi, \kappa_h)^T$, whereas the load vector is defined as $\boldsymbol{m} = \left(m_{1c}{}^{OP}, m_{1s}{}^{OP} m_{1c}{}^{IP}, m_{1s}{}^{IP}\right)^T$.

The first and second columns of $\mathbf{U}$ are related to the horizontal and vertical shears, respectively. Since their maximum entries approach 1, both parameters can be independently identified. However, a coupling between the two angles can be seen in the third and fourth columns: an error in the estimation of one angle will propagate and affect the estimate of the other. Similar $\mathbf{V}$ matrices leading to the same conclusions were computed at different wind speeds and different noise levels γ^2.

To interpret matrix $\mathbf{U}$, consider that rows are associated with entries of the load vector, whereas columns are associated with entries of the wind state vector. The first column of $\mathbf{U}$ shows that the horizontal shear mostly affects the sine components of both out- and in-plane moments. Similarly, the second column shows that the vertical shear mostly affects the cosine components of the loads. In contrast, the third and fourth columns, associated with the angles, do not indicate a predominant effect on some load components. In fact, all loads are affected by both upflow and yaw misalignment, with the in-plane harmonics exhibiting higher sensitivity.

As a side observation, also note the symmetry between the couples $\{\phi, \kappa_v\}$ and $\{\chi, \kappa_h\}$, which is an effect of the nearly 90° symmetry in the definition of the wind parameters and in the response of the machine (see Fig. 1). In other words, for the same horizontal or vertical shear the rotor response will be the same but shifted by 90°. Similarly, for the same upflow and misalignment angles, the rotor response will be the same with a 90° shift. This symmetry in the behavior of the rotor can be exploited to simplify the identification problem, as shown in Cacciola et al. (2016a).

Table 1. Expected variance of wind state estimates based on the a priori analysis.

Standard deviations	$0.01\,m_{\min}$	$0.01\,m_{\max}$	$\mathbf{R}_\epsilon$
σ_ϕ[deg]	0.95	26.0	2.5
σ_{κ_v}	1.1×10^{-3}	3.0×10^{-2}	6.5×10^{-2}
σ_χ[deg]	0.81	22.3	1.5
σ_{κ_h}	6.2×10^{-4}	1.7×10^{-2}	2.3×10^{-2}

Table 1 reports the expected variances of the wind state estimation errors for the three considered noise variances. It appears that, as expected, higher noise levels are associated with higher variances of the estimates. In addition, the variance of the angles appears to be significantly higher than that of the shears. In fact, angle variances approach and exceed tens of degrees for the higher noise levels, indicating that instantaneous estimates of these wind states are probably impractical. However, longer-term observation could be possible with time filtering, as discussed and shown later.

Finally, Fig. 8 shows the standard deviation (SD) of the wind parameter estimates with respect to the wind speed, computed assuming $\mathbf{R} = \gamma \mathbf{I}$ with $\gamma = 0.01(m_{\min} + m_{\max})/2$. The plot shows a marked improvement in the quality of the estimates with wind speed.

Similar results not shown here for the sake of brevity were obtained with the nonlinear model.

3.2 Expected observer behavior

Given the behavior of the linear and nonlinear observers and the results of the SVD-based a priori observability analysis, the following conclusions can be made.

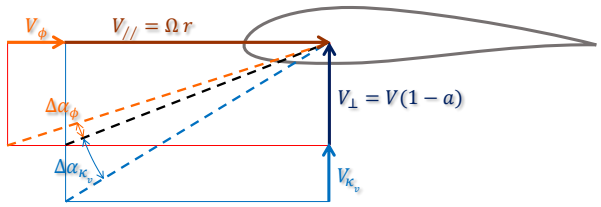

Figure 9. Effects of shear and misalignment changes on sectional angle of attack.

- In general, it should be possible to estimate both shears with satisfactory precision, as their errors are moderate even for significant measurement noise levels.
- It is expected that the estimation of both yaw misalignment and upflow angle will be more significantly affected by measurement noise. Because of this, the estimation of these angles should be accompanied by a suitable filtering action in order to remove fast fluctuations. This also implies that these angles can only be estimated on longer time horizons than in the case of shears.
- The observation accuracy should increase with increasing wind speed.
- The nonlinear model appears to be more accurate than the linear model for the estimation of yaw misalignment and upflow angles. However, shears also seem to be captured well by the linear model.

The different expected accuracy in the estimation of shears and angles can be given an even more intuitive explanation. Consider the blade section depicted in Fig. 9. The relative airflow velocity vector can be decomposed into the component $V_\perp = (1-a)V$ perpendicular to the rotor disk plane, where a is the local induction factor and the one $V_{//} = \Omega r$ parallel to it, with r being the section radial position.

A change in shear will be seen by the blade section mainly as a change in $V_\perp$. However, a change in misalignment will induce a change mainly in $V_{//}$. The figure shows that two equal velocity perturbations, $\Delta V = V_{\kappa_v} = V\sin(\phi)$ perpendicular and parallel to the rotor plane, respectively, will induce different changes in the sectional angle of attack. In particular, the change due to perpendicular (shear-caused) variation is larger than that due to parallel (misalignment-caused) variation.

This is also easily shown by considering that the inflow angle is $\tan\zeta = V_\perp/V_{//}$. Hence, for a perturbation ΔV due to shear variation, the inflow changes as $\tan\zeta = (V_\perp + \Delta V)/V_{//}$. In contrast, for a perturbation ΔV due to misalignment variation, the inflow changes as $\tan\zeta = V_\perp/(V_{//} + \Delta V)$. For typical values of $V_\perp$ and $V_{//}$, Fig. 10 shows the behavior of $\tan\zeta$ as a function of ΔV. As clearly shown by the plot, for a same perturbation ΔV (for example, $1\,\mathrm{m\,s^{-1}}$, as shown in the figure), the ensuing change in inflow angle is larger when the perturbation is due to a change in shear than when it is due to a change in misalignment. This implies similarly larger variation in the sectional angle of attack and hence in the loads. In conclusion, one may expect that the rotor response will be more sensitive to variations in shear than in misalignment when these two different phenomena produce velocity perturbations of the same magnitude. Due to the rotational symmetry of the problem, the same conclusions clearly hold true for variation in horizontal shear or for variation in the vertical upflow angle.

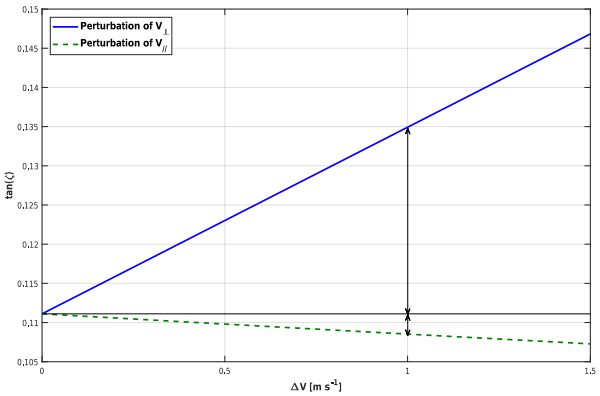

Figure 10. Variation in the inflow angle ζ at a blade section as a function of a perturbation ΔV in a direction either perpendicular (solid line) or parallel (dashed line) to the rotor plane.

4 Results

After having verified in the previous sections that blade load harmonics carry enough information to infer wind states in steady conditions, attention is now turned to the dynamic problem. The nonturbulent case is considered first by using fully parameterized wind fields with variable-in-time wind states. Next, the turbulent case is considered by using wind fields modeled by the Kaimal method for different constant mean wind states. Finally, turbulent conditions with variable-in-time mean quantities are considered.

4.1 Nonturbulent case with fully parameterized wind fields

Ideal nonturbulent and fully parameterized wind fields with time-varying wind states were generated according to Eq. (3) by independently varying angles ϕ and χ as well as shears κ_v and κ_h. Here and in the following examples, load harmonics were extracted from the simulated wind turbine response by using the Coleman transformation followed by filtering with an eighth-order Butterworth filter with a cut-out frequency equal to $0.35\,f_{\mathrm{tower}} = 0.105\,\mathrm{Hz}$ to remove load oscillations at the tower frequency. Finally, inflow conditions were es-

timated with the proposed observer and compared with the real ones.

Figure 11a and b show the results obtained at 4 and $9\,\mathrm{m\,s^{-1}}$, respectively, using the linear and nonlinear models. The agreement is generally good as all parameters are well observed by both models. The observed states are affected by a delay of about 7 s, primarily due to the effects of the filter. There are minor differences between the linear and the nonlinear models, which are not large enough to allow any conclusions to be drawn.

4.2 Turbulent case

Different turbulent wind fields were generated using the `TurbSim` software according to the Kaimal model. The corresponding inflow conditions, in terms of hub-height wind speed V and wind states $\boldsymbol{\theta}$, were then computed by fitting at each instant in time the wind state parameterization (Eq. 1) to the turbulent wind grid over the complete rotor disk. The wind parameters obtained this way were then used as reference quantities to verify the accuracy of the estimated ones.

As wind states are inferred from blade loads, which in turn depend on the wind conditions at the location occupied by each single blade at each time instant, an alternative way of computing the reference wind conditions was also used. In this second implementation, wind parameters were computed by fitting the wind state parameterization expressed by Eqs. (2) and (3) not over the complete rotor disk, but only to its portion occupied at that time instant by the three blades. Spanwise weighting was also used on account of the nonuniform power extraction characteristics of rotors (Soltani et al., 2013). As the two methods do not yield significantly different reference wind states, only the results obtained with the first approach are reported in the following.

Figures 12 and 13 report the results obtained at 7 and $19\,\mathrm{m\,s^{-1}}$, which respectively belong to regions II and III. Figures 12a and 13a show the results for a TI equal to 2 %, and Figs. 12b and 13b show the 12 % TI case.

These results suggest several possible considerations.

First, the estimates of both shears κ_v and κ_h appear to have generally high accuracy: their mean values and their rapid oscillations are well captured by both the linear and nonlinear models. Here again, the results are affected by a 7 s delay induced by the filter. For the lower wind speeds and turbulence intensities, the linear and nonlinear observers exhibit very similar behavior. However, differences appear at $19\,\mathrm{m\,s^{-1}}$ and 12 % TI, as shown by Fig. 13b. In fact, between second 250 and second 350 of the simulation, the estimation of the vertical shear provided by the linear model is affected by large errors, whereas the nonlinear observer results still remain acceptable.

The good behavior of the shear estimates suggests the possible use of a faster filter in order to reduce the estimation delay. For example, the delay can be reduced to only 4 s by using a filter cut-out frequency of 0.17 Hz, which corresponds to 1.2 times the rotor frequency at $5\,\mathrm{m\,s^{-1}}$.

An estimation of the angles ϕ and χ does not prove to be as accurate as the estimation of the shears, as fully expected based on the a priori observability study. Mean values are well captured, especially by the nonlinear model, but fluctuations are missed by both observers.

The general lower quality of the estimates for the angles was previously explained by the a priori analysis, and it is clearly illustrated a posteriori by the simulation results shown here. Various sources of error may ultimately be responsible for the oscillations in the estimates shown by the plots, including unmodeled dynamics, rapid pitch motions or variable rotor speed. It is interesting to recall that the steady model (Eq. 9) appeared capable of capturing the behavior of the $1\times$ Rev loads in turbulent conditions, as clearly illustrated by the results shown in Fig. 5a. Notwithstanding this apparently more than satisfactory behavior when used to simulate loads given wind states, the inversion of the model to yield wind states given loads appears to be more problematic. In fact, because of the generally lower level of observability of the angles with respect to the shears (see Sect. 3), errors propagate throughout the solution at a high rate for wind misalignment and upflow, in turn generating fast fluctuations of the estimates.

It should also be remarked that an additional source of uncertainty is the ground truth. In fact, the presence of turbulent eddies in the flow implies that the wind field cannot be exactly parameterized by the assumed wind states. Hence, the reference quantities plotted here should also be considered only as indicative proxies of the actual wind states.

The observation errors were further analyzed from a statistical standpoint by generating five different 10 min turbulent wind field realizations and computing means and standard deviations. To eliminate the effects of the delay caused by the filter, which would have prevented any instantaneous comparison between the reference and observed quantities, reference wind states were processed with the same filter used for the moment harmonics.

Figure 14 shows the behavior of the standard deviation of the estimation error for the four wind states as functions of the wind speed and for different TI levels. The curves labeled "TI = 0 %" refer to the nonturbulent fully parameterized conditions already described in Sect. 4.1. Since similar behavior characterizes the results of both observers, only those obtained with the nonlinear model are shown here to avoid cluttering the figure.

As expected, the standard deviation increases with the TI level. Moreover, in regions II and II$\frac{1}{2}$, accuracy tends to increase for increasing wind speed, as similarly predicted by the a priori observability analysis. The opposite happens in region III, where oscillations in the results are more significant and strongly affect the estimates. This behavior is particularly visible in the estimation of the angles, as shown in Fig. 14a and c.

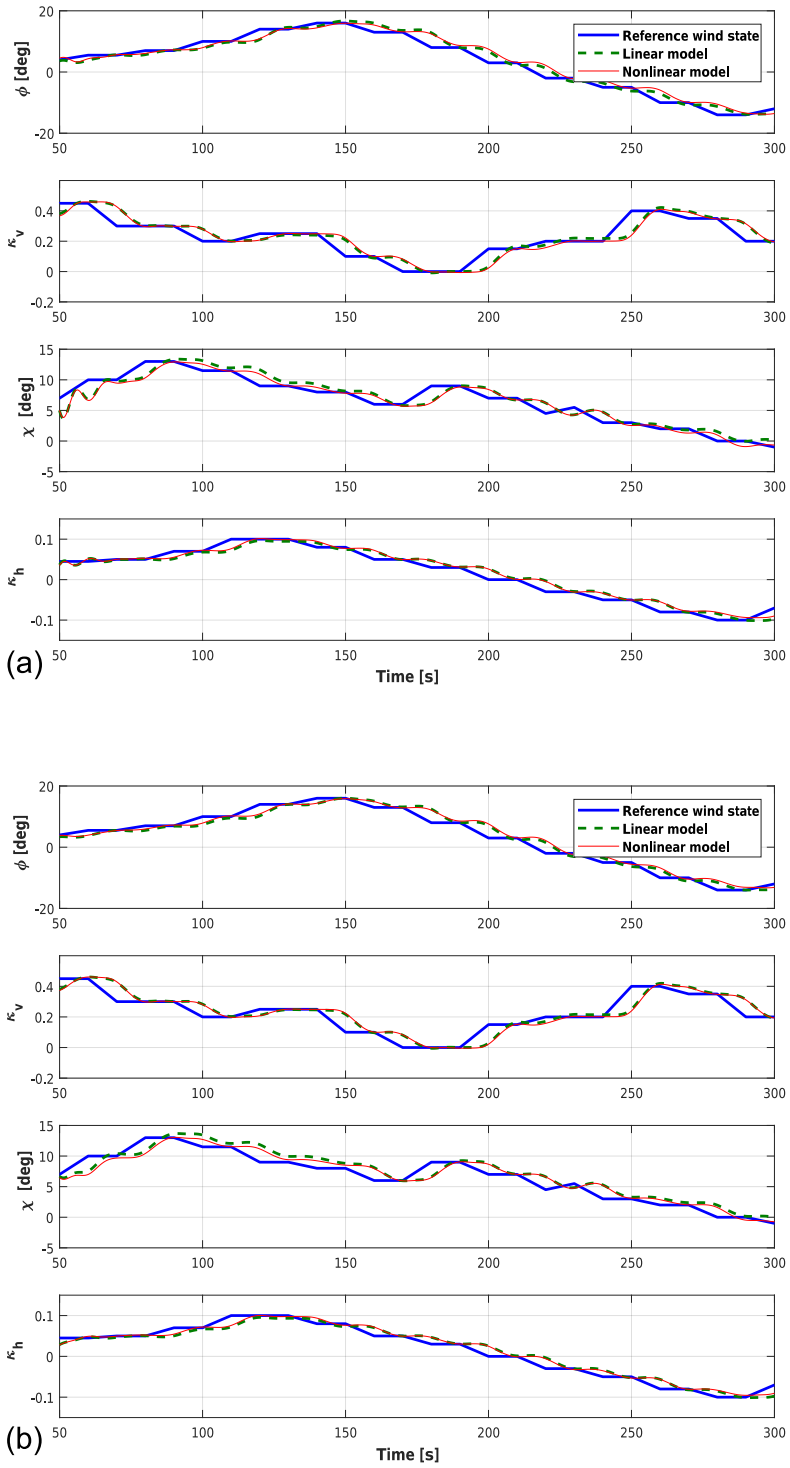

Figure 11. Wind state observations in nonturbulent wind conditions with variable wind parameters at 4 **(a)** and 9 m s^{-1} **(b)**. Solid thick blue lines: real wind parameters; dashed thick green lines: observations by the linear model; solid thin red lines: observations by the nonlinear model.

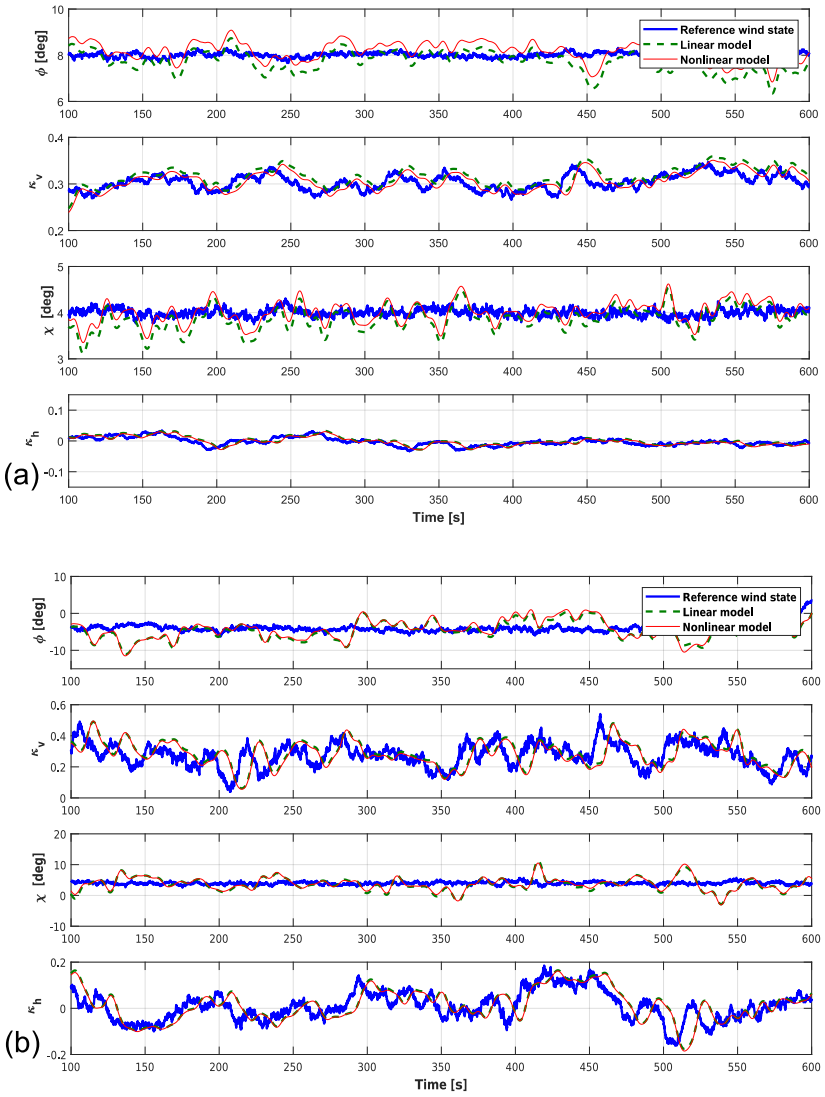

Figure 12. Wind state observations in turbulent wind conditions at $7\,\mathrm{m\,s^{-1}}$ for a TI equal to 2 **(a)** and 12 % **(b)**. Solid thick blue lines: reference wind parameters; dashed thick green lines: observations by the linear model; solid thin red lines: observations by the nonlinear model.

Shear errors also remain low at very high TI levels, as illustrated by Fig. 14b and d, indicating that fast, good-quality shear estimates are possible. In fact, for example, the standard deviation of κ_v at $7\,\mathrm{m\,s^{-1}}$ and 20 % TI is circa 0.055, which means that about 95 % of the observer samples have an instantaneous error lower than 0.11.

The evaluation of the observer performance for the angles deserves special attention. Looking at the yaw misalignment in Fig. 14a for regions II, II$\frac{1}{2}$ and the low region III up to $15\,\mathrm{m\,s^{-1}}$, the instantaneous error remains within acceptable bounds for turbulence intensities lower than 5 %. In fact, σ_ϕ is lower than 1.5°, which implies that estimates are affected by an error lower than 3° 95 % of the time. On the contrary, the estimation error standard deviation may reach 3, 4 or even 6° for the higher turbulence intensities of 12, 16 and 20 %. The maximum error deviation is obtained at $19\,\mathrm{m\,s^{-1}}$ for a TI of 12 %. The same considerations can be derived for the estimation of the upflow angle.

Figure 15 reports the mean observation errors with respect to the wind speed for both the linear and nonlinear observers. Not unexpectedly, the estimation of the shears is characterized by almost negligible error means. More surprisingly, however, even the mean errors of the angles are quite low for all conditions, although a mild reduction of accuracy can be observed for increasing wind speeds. In addition, as previously noted, the nonlinear observer appears to be slightly

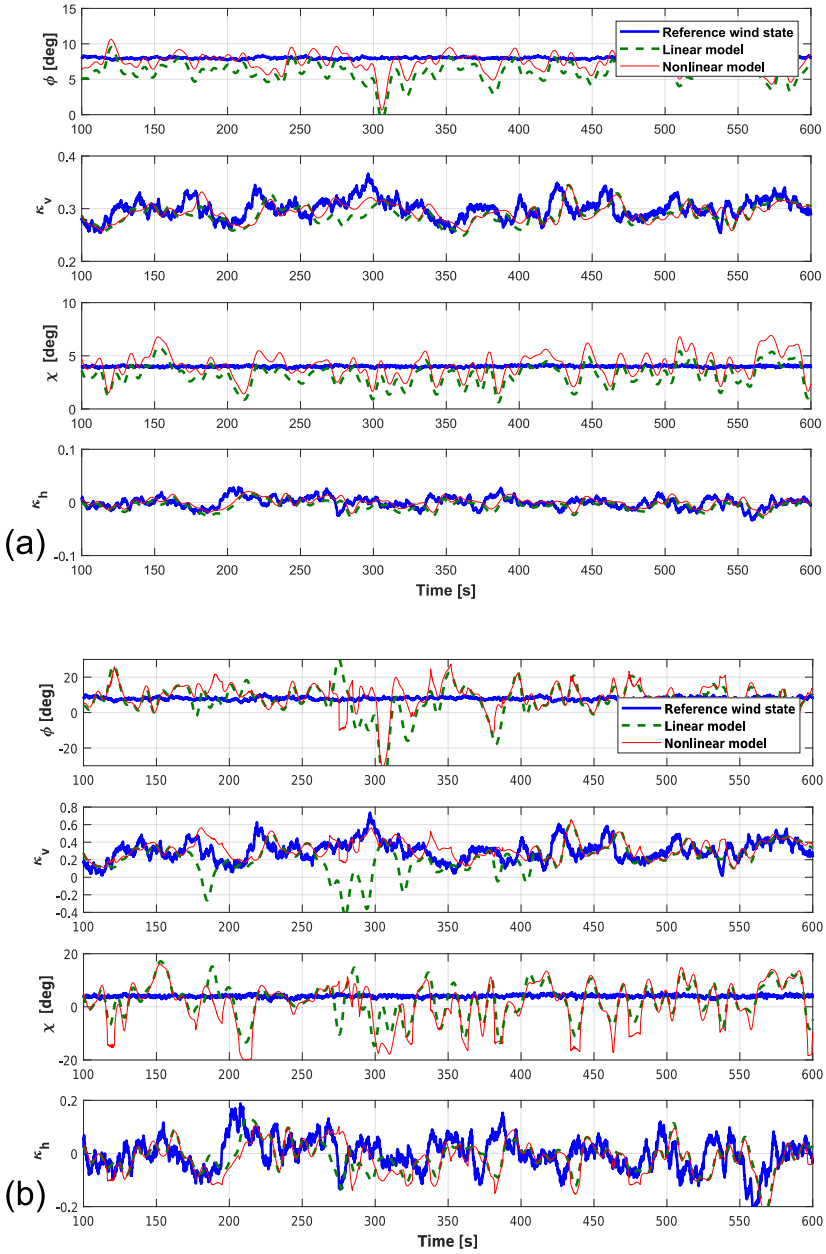

Figure 13. Wind state observations in turbulent wind conditions at 19 m s^{-1} for a TI equal to 2 **(a)** and 12 % **(b)**. Solid thick blue lines: reference wind parameters; dashed thick green lines: observations by the linear model; solid thin red lines: observations by the nonlinear model.

more accurate than the linear one. As a final remark, it was found that the error means are not significantly influenced by TI. Hence, the TI-dependent curves were not displayed in Fig. 15 to avoid cluttering the plot.

4.2.1 Evaluation of lifetime performance

The previous examples have shown that observed angles are typically affected by spurious oscillations for the reasons explained by the a priori analysis. The same examples, however, have also shown that mean values are typically well captured and that the amplitude of oscillations is related to TI. This seems to indicate that fast accurate observations

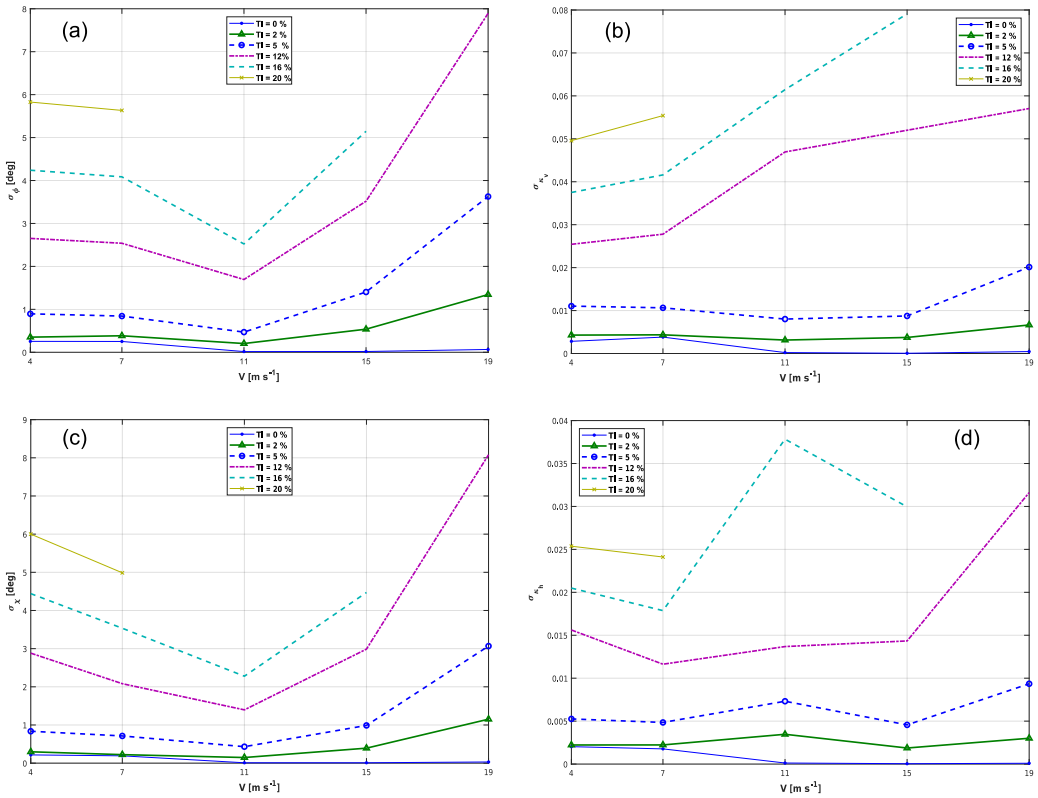

Figure 14. Standard deviation of the estimation error of yaw misalignment **(a)**, vertical shear **(b)**, upflow angle **(c)** and horizontal shear **(d)** as functions of wind speed for varying TI levels. All curves refer to the nonlinear observer results.

of angles are generally not possible, while observations on longer time windows might still be relatively accurate. By simple inspection of the temporal responses, it is, however, not easy to get a clear idea of the actual precision of the observers in turbulent conditions. In order to provide a more meaningful indication of the observer accuracy, the "lifetime" standard deviation of the observed states is evaluated in this section. This is computed by weighting the results at each wind speed and TI with the corresponding probability distributions at a given site. To this end, measurements taken at the offshore platform FINO1 (FINO, 2017) from September 2003 to August 2007 were considered. In fact, given the standard deviation of the observation error as a function of TI and wind speed (given in Fig. 14) and the wind statistics of a specific site, one can evaluate the observer performance when applied to the wind turbine used in the present study if it were located at that site.

Figure 16 shows some statistical metrics of the wind at an altitude over the water line of 80 m, which corresponds to the hub height of the wind turbine considered in the present study. The TI percentiles at 90 m were extracted from Fig. 2 of Türk and Eimeis (2010) and mapped to the current hub height by scaling with a factor equal to 1.028 according to Fig. 5.21 of Emeis (2013), which reports the variation in TI as a function of hub height.

Next, a shifted Weibull probability density function (PDF) $\mathcal{W}_\tau$ was fitted to the TI for each wind speed. The PDF is defined as

$$\mathcal{W}_\tau(\tau, V) = \begin{cases} \frac{\alpha(V)}{\beta(V)}\left(\frac{(\tau-\tau_{\min}(V))}{\beta(V)}\right)^{\alpha(V)-1} \mathrm{e}^{-\left(\frac{(\tau-\tau_{\min}(V))}{\beta(V)}\right)^{\alpha(V)}}, & \tau \geq \tau_{\min}(V), \\ 0, & \tau < \tau_{\min}(V), \end{cases} \quad (37)$$

while its associated cumulative distribution function (CDF) is written as

$$\mathfrak{W}_\tau(\tau, V) = \begin{cases} 1 - \mathrm{e}^{-\left(\frac{(\tau-\tau_{\min})}{\beta(V)}\right)^{\alpha(V)}}, & \tau \geq \tau_{\min}(V), \\ 0, & \tau < \tau_{\min}(V), \end{cases} \quad (38)$$

where τ is the TI level, $\tau_{\min}(V)$ is its minimum value and $\alpha(V)$ and $\beta(V)$ are the shape and scale parameters, respectively, of the probability density function. Figure 17 represents the Weibull PDF and CDF at 9 m s^{-1}.

Given the probability density function of the observation error $\mathcal{P}_\epsilon$, the TI PDF $\mathcal{W}_\tau$ and the wind speed PDF $\mathcal{W}_V$, the

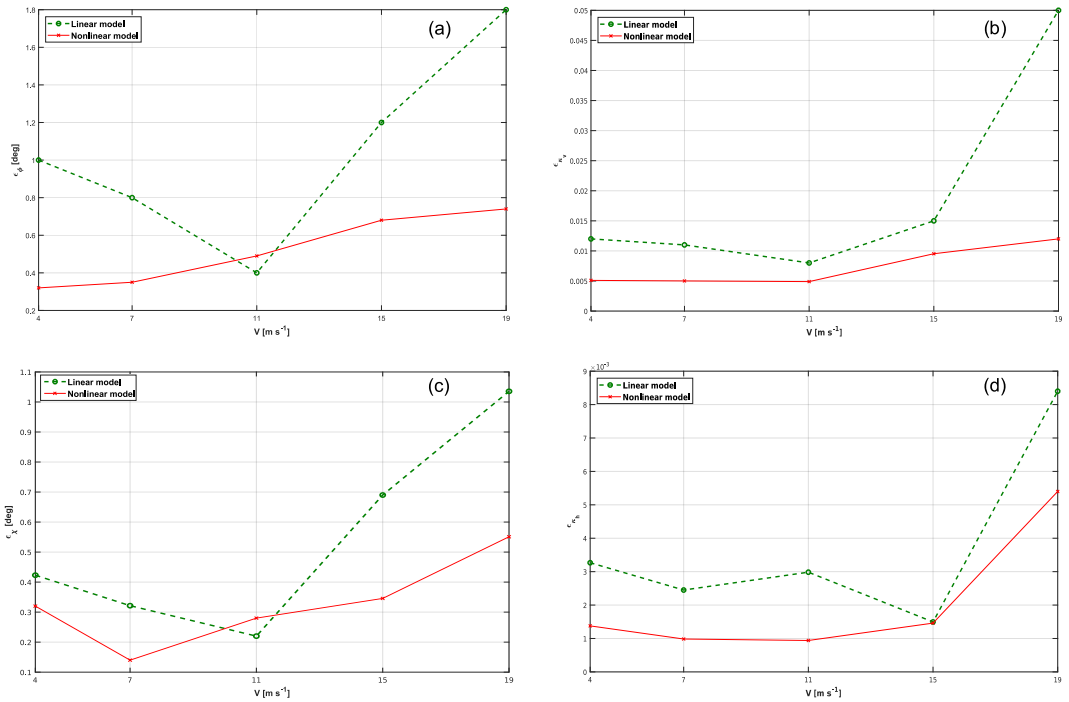

Figure 15. Mean estimation error of yaw misalignment **(a)**, vertical shear **(b)**, upflow angle **(c)** and horizontal shear **(d)** with respect to wind speed.

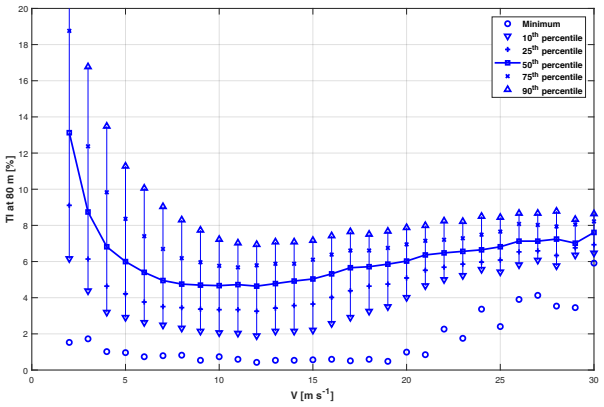

Figure 16. Minimum value, 10th, 25th, 50th, 75th and 90th TI percentiles as functions of wind speed at 80 m above the water line at FINO1 from September 2003 to August 2007. Data taken from Türk and Eimeis (2010).

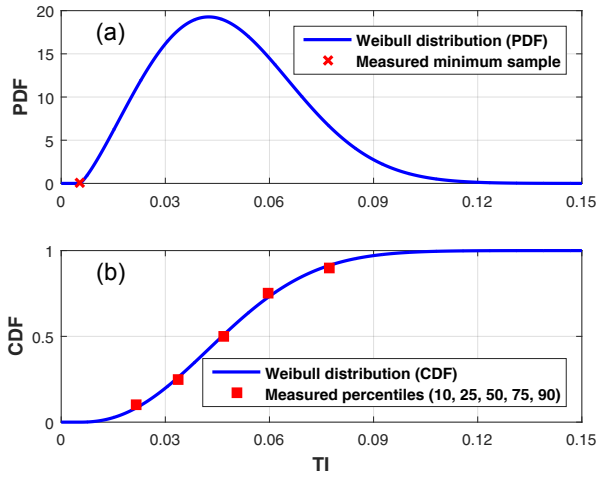

Figure 17. TI PDF **(a)** and CDF **(b)** at 9 m s^{-1}.

lifetime standard deviation σ_{LT} can be readily computed as

$$\sigma_{\mathrm{LT}} = \frac{1}{\int_{V_{\mathrm{CI}}}^{V_{\mathrm{CO}}} \mathcal{W}_V(V)\mathrm{d}V} \int_{V_{\mathrm{CI}}}^{V_{\mathrm{CO}}} \mathcal{W}_V(V) \left(\int_0^{+\infty} \mathcal{W}_\tau(V,\tau) \left(\int_{-\infty}^{+\infty} \epsilon \mathcal{P}_\epsilon(V,\tau,\epsilon)\mathrm{d}\epsilon \right) \mathrm{d}\tau \right) \mathrm{d}V, \quad (39)$$

where the innermost integral represents the wind-speed-specific and TI-specific standard deviation of the observation error, $\sigma(V,\tau)$, which was previously computed and reported in Fig. 14. This quantity is then weighted by the probability of each wind speed and TI values to occur at this specific site, as given in Fig. 16.

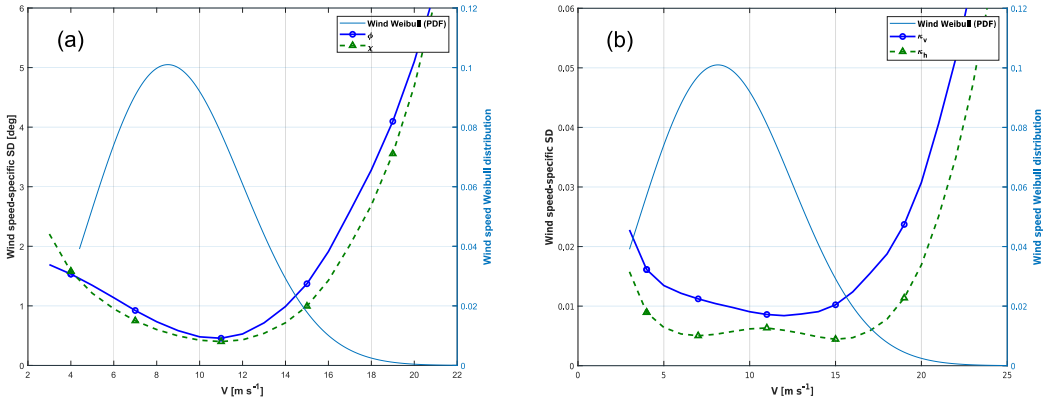

Figure 18. Wind-speed-specific standard deviation of the observation error for angles ϕ and χ **(a)** and for shears κ_v and κ_h **(b)**. The wind Weibull distribution is characterized by shape and scale parameters equal to 2.5 and 10, respectively.

Table 2. Lifetime standard deviation and 2σ bounds of the estimation error for the wind parameters.

Wind parameter	ϕ [deg]	κ_v	χ [deg]	κ_h
σ_{LT}	0.97	0.011	0.84	0.006
$2\sigma_{LT}$	1.94	0.022	1.68	0.012

Figure 18 shows the wind-speed-specific standard deviations for the yaw misalignment and upflow errors (Fig. 18a) and for the shear errors (Fig. 18b) as well as the wind Weibull distribution at FINO1 as functions of wind speed. The picture clearly illustrates the fact that for both angles and shears, errors are quite limited for the more probable wind speeds.

Finally, the lifetime standard deviations are reported in Table 2. From this point of view, the results are clearly quite satisfactory not only for shears, but also for angles. In fact, although fluctuations pollute the instantaneous observation of these quantities, their long-term metrics are well captured.

4.2.2 Following mean changes in yaw misalignment

The fact that the mean estimation errors of the angles, especially for yaw misalignment, are limited suggests the use of a moving average in order to lower the error standard deviation. This way one may capture the slower variations in the means while filtering out the faster oscillations. The resulting estimates can be used for slower control actions, for example yaw control, or for the slow scale monitoring of parameters of interest.

To test whether it is indeed possible to follow changes in the mean, large changes in yaw misalignment were simulated. Turbulent wind fields were generated with `TurbSim` and gradually rotated to generate mean wind direction changes from -4 to $4°$ in about 20 s. The observed yaw misalignment was filtered with a moving average of variable window length on account of the mean wind speed. The results of the observations at $7\,\mathrm{m\,s^{-1}}$ for different turbulence levels with and without moving average are shown in Fig. 19.

For the very low TI levels shown in Fig. 19a, both the mean and instantaneous values of yaw misalignment can be sufficiently well captured even without the use of a filter. With increasing turbulence, spurious oscillations of the estimates mask the mean wind direction change. However, it appears that the use of a moving average is capable of eliminating the faster fluctuations, revealing the presence of a change in wind direction. Clearly, higher values of turbulence require longer filtering windows with consequently longer time delays. This delayed detection is, however, compatible with the usually rather slow and conservative approach used for yaw control in which the actual realignment of the machine is performed only when a wind direction change of some significant entity has been observed for a sufficiently long window of time, usually many tens of seconds.

As a final remark, the nonlinear observer appears to perform slightly better than the linear one, as it is more easily visible for low turbulence conditions.

5 Conclusions

This paper has presented a method to estimate the wind inflow at the rotor disk of an operating wind turbine. The proposed method uses the low-frequency response of the wind turbine limited to the $1\times$ Rev harmonics to infer four wind states representing two misalignment angles and two shears. The rotor response is measured by load sensors, which are becoming standard equipment on many modern wind turbines. When such sensors are available, the proposed method does not require any additional hardware and amounts to a simple software upgrade.

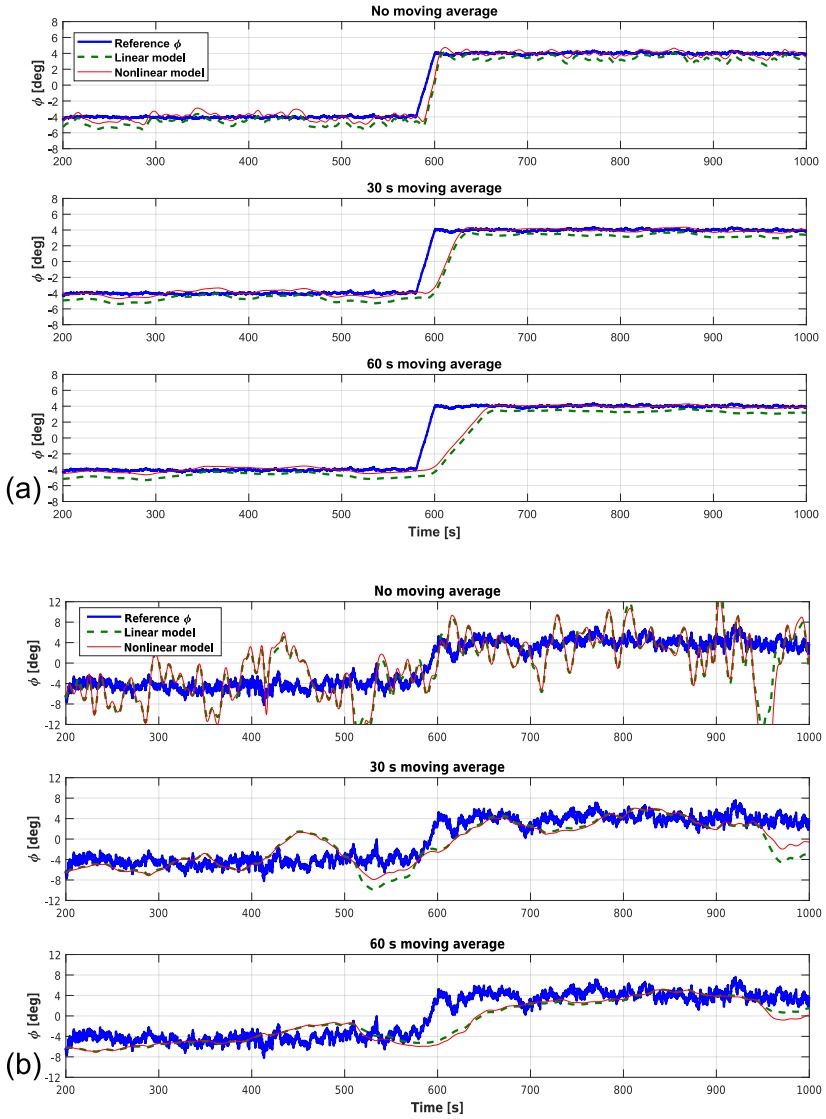

Figure 19. Yaw misalignment for an 8° change in wind direction at 7 m s^{-1} with 2 % **(a)** and 20 % **(b)** TI. Solid thick blue lines: real yaw misalignment; dashed thick green lines: estimate by the linear model; solid thin red lines: estimate by the nonlinear model.

An input–output model was formulated to represent the relationship between wind states and load harmonics. The model was treated as a black box with unknown coefficients estimated by using the simulated response of a wind turbine implemented in a high-fidelity aeroservoelastic model. The input–output relationship was then inverted in a least-squares sense in order to provide estimates of the wind states when fed with measured load harmonics. The statistical properties of the model and, in turn, the observability of the wind states were analyzed using the SVD. This a priori analysis highlighted the different nature of the problem of estimating shears and angles, the former being characterized by a higher level of observability than the latter. Finally, the proposed observer was analyzed in a wide range of operating conditions in turbulent wind fields with different characteristics.

From the results of the present study, the following conclusions can be made.

- The behavior of the blade out-of-plane and in-plane load harmonics at 1× Rev are captured well in both steady and turbulent conditions by a linear or second-order nonlinear function of the wind states.

- It is not advisable to include in the model harmonics that are higher than 1× Rev. In fact, although 2× Rev components are indeed correlated with wind states, they are also strongly affected by turbulence. In addition, if one

uses a simulation model for the estimation or synthesis of the load–wind model, it is expected that such a model will better capture the $1\times$ Rev response than the higher harmonics. Therefore, limiting load inputs to the $1\times$ Rev components helps ensure higher accuracy of the load–wind model and hence of the estimates.

- Wind states can be estimated from $1\times$ Rev blade harmonics, as these quantities carry enough informational content for the model to be invertible.
- An a priori observability analysis shows that the accuracy of the shears is generally superior to that of the angles. This is not because of a limit to the present specific formulation, but it is due to the intrinsic sensitivity of angle of attack changes to wind state changes, which is different for angles and shears.
- Extensive simulations in turbulent conditions have shown that the mean value of the estimation error is generally significantly low for all states. For example, the mean yaw error is about 0.5° independently of wind speed and TI, whereas the vertical shear error is about 0.01.
- Standard deviations of the shears are generally very low even for high TI levels, implying that the observer is capable of following fast shear fluctuations with good precision.
- Standard deviations for angles are significantly higher due to their overall lower observability. In general, angle estimates are polluted by rapid spurious oscillations due to the amplification of errors through the inverted estimation model. This implies that one cannot generally follow rapid variations in the angles, and only observations on longer timescales are possible.
- Although polluted by fluctuations, on average even the angle estimates are of good quality thanks to their small mean errors.
- An analysis, conducted by taking into account the probability distributions of both wind speed and TI at the offshore FINO1 platform in the German Bight, has shown that the expected standard deviation of the estimation error in the angles is below 1°, which appears to be a very interesting result.
- It was shown that, by filtering the estimated yaw misalignment with a moving average, one may track with good accuracy significant mean changes in the wind direction even for very high TI, indicating the possible use of this estimate to drive the wind turbine yaw control system.

The proposed formulation should be extended to consider the possible presence of an individual pitch control (IPC) strategy. This can be done by also including in the load–wind model the presence of a term depending on pitch load harmonics. As these quantities are known, they represent further inputs that do not change the overall approach, although the model will have additional coefficients that need to be identified. This extension of the formulation has already been tested, and it will be described in a forthcoming publication.

Data availability. Data can be obtained upon request from the authors (carlo.bottasso@tum.de.).

Appendix: Nomenclature

f	Frequency
m	Generic blade moment
n_k	Piecewise linear shape function
p	Order of the nonlinear model
q	Dynamic pressure
t	Time
B	Number of blades
H	Hub height
N_{obs}	Number of experiments for model identification
N_{nodes}	Number of nodes for wind speed scheduling
R	Rotor radius
V	Wind speed
V_{CI}	Cut-in wind speed
V_{CO}	Cut-out wind speed
V_{RP}	Rated wind speed
$\mathfrak{R}$	Real number set
$\mathfrak{W}$	Weibull cumulative distribution function
$\mathcal{P}_\epsilon$	Probability density function of the observation error
$\mathcal{V}$	Variance
$\mathcal{W}$	Weibull probability density function
$\boldsymbol{m}$	Vector of moment harmonics
$\boldsymbol{r}$	Measurement error
$\boldsymbol{u}$	Input vector
$\boldsymbol{x}$	State vector
$\boldsymbol{y}$	Output vector
$\mathbf{1}$	Unitary vector
$\mathbf{I}$	Identity matrix
$\mathbf{R}$	Measurement error covariance matrix
$\mathbf{U}$	Matrix of left singular vectors
$\mathbf{V}$	Matrix of right singular vectors
$\mathbf{X}$	Demodulation matrix
$\boldsymbol{\mathcal{M}}$	Steady-state relation between load harmonics and wind state vector
$\mathbf{E}[\cdot]$	Expected value
$\text{Cov}[\cdot]$	Covariance
α	Shape parameter of the Weibull distribution
β	Scale parameter of the Weibull distribution
ϱ	Air density
χ	Upflow angle
κ_{v}	Vertical shear
κ_{h}	Horizontal shear
ϕ	Yaw misalignment angle
ψ	Azimuth angle
σ	Standard deviation
τ	Turbulence intensity level
ζ	Blade section inflow angle
Ω	Rotor angular velocity

$\boldsymbol{\epsilon}_\theta$	Wind state observation error
$\boldsymbol{\xi}$	Vector of statistically independent wind state variables, $\mathbf{V}^T\boldsymbol{\theta}$
$\boldsymbol{\theta}$	Wind state vector
$\boldsymbol{\Sigma}$	Rectangular matrix of singular values
$\dot{(\cdot)}$	Time derivative, i.e., $\mathrm{d}\cdot/\mathrm{d}t$
$(\cdot)^{(i)}$	Quantity related to the ith experiment
$(\cdot)_{(j)}$	Quantity related to the jth blade
$(\cdot)_k$	Nodal quantity at the kth node
$(\cdot)_{n\mathrm{c}}$	$n\times$ Rev cosine amplitude
$(\cdot)_{n\mathrm{s}}$	$n\times$ Rev sine amplitude
$(\cdot)_{\mathrm{E}}$	Estimated quantity
$(\cdot)^{\mathrm{IP}}$	In-plane quantity
$(\cdot)_{\mathrm{M}}$	Measured quantity
$(\cdot)_{\mathrm{NL}}$	Nonlinear term
$(\cdot)^{\mathrm{OP}}$	Out-of-plane quantity
$(\cdot)_{\mathrm{R}}$	Real quantity
$(\cdot)^{\mathrm{T}}$	Transpose
BEM	Blade element momentum
CDF	Cumulative distribution function
IPC	Individual pitch control
Lidar	Light detection and ranging
PDF	Probability density function
SD	Standard deviation
SVD	Singular value decomposition
TI	Turbulence intensity
TSR	Tip speed ratio

Competing interests. The authors declare that they have no conflict of interest.

This work was supported by the German Research Foundation (DFG) and the Technische Universität München within the funding program Open Access Publishing.

Edited by: Sandrine Aubrun
Reviewed by: two anonymous referees

References

Bauchau, O. A.: Flexible Multibody Dynamics, Solid Mechanics and its Applications, Springer, Dordrecht, Heidelberg, London, New York, 2011.

Bauchau, O. A., Bottasso, C. L., and Trainelli, L.: Robust integration schemes for flexible multibody systems, Comput. Method. Appl. M., 192, 395–420, https://doi.org/10.1016/S0045-7825(02)00519-4, 2003.

Bossanyi, E., Fleming, P. A., and Wright, A. D.: Controller field tests on the NREL CART3 turbine, Technical Report 11593/BR/09, National Renewable Energy Laboratory, Golden, CO, USA, 2009.

Bottasso, C. L. and Croce, A.: Cp-Lambda: user's manual, Technical Report, Dipartimento di Ingegneria Aerospaziale, Politecnico di Milano, Milano, Italy, 2006.

Bottasso, C. L. and Riboldi, C. E. D.: Estimation of wind misalignment and vertical shear from blade loads, Renew. Energ., 62, 293–302, https://doi.org/10.1016/j.renene.2013.07.021, 2014.

Bottasso, C. L. and Riboldi, C. E. D.: Validation of a wind misalignment observer using field test data, Renew. Energ., 74, 298–306, https://doi.org/10.1016/j.renene.2014.07.048, 2015.

Bottasso, C. L., Croce, A., and Riboldi, C. E. D.: Spatial estimation of wind states from the aeroelastic response of a wind turbine, The Science of Making Torque from Wind (TORQUE 2010), Heraklion, Crete, Greece, 28–30 June 2010, 2010.

Bottasso, C. L., Croce, A., Nam, Y., and Riboldi, C. E. D.: Power curve tracking in the presence of a tip speed constraint, Renew. Energ., 40, 1–12, https://doi.org/10.1016/j.renene.2011.07.045, 2012.

Bottasso, C. L., Cacciola, S., and Schreiber, J.: A wake detector for wind farm control, J. Phys. Conf. Ser., 625, 012007-1–8, https://doi.org/10.1088/1742-6596/625/1/012007, 2015.

Bottasso, C. L., Cacciola, S., and Schreiber, J.: Local wind speed estimation, with application to wake impingement detection, Renew. Energ., 116, 155–168, https://doi.org/10.1016/j.renene.2017.09.044, 2018.

Cacciola, S., Bertelè, M., Schreiber, J. and Bottasso, C. L.: Wake center position tracking using downstream wind turbine hub loads, J. Phys. Conf. Ser., 753, 032036-1–6, https://doi.org/10.1088/1742-6596/753/3/032036, 2016a.

Cacciola, S., Bertelè, M., and Bottasso, C. L.: Simultaneous observation of wind shears and misalignments from rotor loads, J. Phys. Conf. Ser., 753, 052002-1–8, https://doi.org/10.1088/1742-6596/753/5/052002, 2016b.

Coleman, R. P. and Feingold, A. M.: Theory of self-excited mechanical oscillations of helicopter rotors with hinged blades, Technical Report, NACA TN 1351, 1958.

Cramér, H.: Mathematical Methods of Statistics, Princeton University Press, Princeton, NJ, USA, 1946.

Eggleston, D. M. and Stoddard, F. S.: Wind Turbine Engineering Design, Van Nostrand Reinhold, New York, USA, 1987.

Emeis, S.: Wind Energy Meteorology – Atmospheric Physics for Wind Power Generation, Springer-Verlag, Berlin, Heidelberg, Germany, 2013.

FINO: FINO 1-2-3 – Forschungsplattformen in Nord- und Ostsee Nr. 1, available at: http://www.fino1.de/en/, last access: 13 November 2017.

Fleming, P. A., Wright, A. D., Fingersh, L. J., and van Wingerden, J. W.: Resonant vibrations resulting from the re-engineering of a constant-speed 2-bladed turbine to a variable-speed 3-bladed turbine, Proceedings of the 49th AIAA Aerospace Sciences Meeting, Orlando, FL, USA, 2011.

Fleming, P. A., Gebraad, P. M. O., Lee, S., van Wingerden, J. W., Johnson, K., Churcheld, M., Michalakes, J., Spalart, P., and Moriarty, P.: Evaluating techniques for redirecting turbine wakes using SOWFA, Renew. Energ., 70, 211–218, https://doi.org/10.1016/j.renene.2014.02.015, 2014.

Golub, G. H. and van Loan, C. F.: Matrix Computations, Johns Hopkins University Press, Baltimore, MD, USA, 1996.

Jategaonkar, R. V.: Flight Vehicle System Identification: a Time Domain Methodology, AIAA, Progress in Astronautics and Aeronautics, Reston, VA, USA, 2nd edn., 2015.

Jimenez, A., Crespo, A., and Migoya, E.: Application of a LES technique to characterize the wake detection of a wind turbine in yaw, Wind Energy, 13, 559–572, https://doi.org/10.1002/we.380, 2010.

Jonkman, B. J. and Kilcher, L.: TurbSim user's guide: version 1.06.00, NREL Technical report, 2012.

Ljung, L.: Perspectives on system identification, Annu. Rev. Control, 34, 1–12, 2010.

Moré, J. J.: The Levenberg–Marquardt algorithm: implementation and theory, Numerical Analysis: Proceedings of the Biennial Conference Held at Dundee, 28 June–1 July 1977, Springer, Berlin Heidelberg, Germany, Lect. Notes Math., 630, 105–116, https://doi.org/10.1007/BFb0067700, 1978.

Riboldi, C. E. D.: Advanced control laws for variable-speed wind turbines and supporting enabling technologies, PhD thesis, Politecnico di Milano, Milano, Italy, 2012.

Simley, E. and Pao, L. Y.: Evaluation of a wind speed estimator for effective hub-height and shear components, Wind Energy, 19, 167–184, https://doi.org/10.1002/we.1817, 2014.

Soltani, M. N., Knudsen, T., Svenstrup, M., Wisniewski, R., Brath, P., Ortega, R., and Johnson, K.: Estimation of rotor effective wind speed: a comparison, IEEE T. Contr. Syst. T., 21, 1155–1167, https://doi.org/10.1109/TCST.2013.2260751, 2013.

Türk, M. and Eimeis, S.: The dependence of offshore turbulence intensity on wind speed, J. Wind Eng. Ind. Aerod., 98, 466–471, https://doi.org/10.1016/j.jweia.2010.02.005, 2010.

Van der Hooft, E. L. and Engelen, T.: Estimated wind speed feed forward control for wind turbine operation optimisation, European Wind Energy Conference & Exhibition (EWEC 2004), London, UK, 22–25 November 2004.

A.2 Paper II: Wind inflow observation from load harmonics – wind tunnel validation of the rotationally symmetric formulation

Reference: M. Bertelè, C. L. Bottasso, and S. Cacciola, "Brief communication: Wind inflow observation from load harmonics – wind tunnel validation of the rotationally symmetric formulation", *Wind Energy Science*, vol. 4, no. 1, pp. 89–97, 2019. doi: 10.5194/wes-4-89-2019.

Wind Energ. Sci., 4, 89–97, 2019
https://doi.org/10.5194/wes-4-89-2019

eawe european academy of wind energy
Open Access
WIND ENERGY SCIENCE

Brief communication: Wind inflow observation from load harmonics – wind tunnel validation of the rotationally symmetric formulation

Marta Bertelè[1], Carlo L. Bottasso[1], and Stefano Cacciola[2]

[1]Wind Energy Institute, Technische Universität München, Garching bei München 85748, Germany
[2]Dipartimento di Scienze e Tecnologie Aerospaziali, Politecnico di Milano, Milano 20156, Italy

Correspondence: Carlo L. Bottasso (carlo.bottasso@tum.de)

Received: 14 September 2018 – Discussion started: 28 September 2018
Revised: 6 December 2018 – Accepted: 7 January 2019 – Published: 29 January 2019

Abstract. The present paper further develops and experimentally validates the previously published idea of estimating the wind inflow at a turbine rotor disk from the machine response. A linear model is formulated that relates one per revolution (1P) harmonics of the in- and out-of-plane blade root bending moments to four wind parameters, representing vertical and horizontal shears and misalignment angles. Improving on this concept, the present work exploits the rotationally symmetric behavior of the rotor in the formulation of the load-wind model. In a nutshell, this means that the effects on the loads of the vertical shear and misalignment are the same as those of the horizontal quantities, simply shifted by $\pi/2$. This results in a simpler identification of the model, which needs a reduced set of observations. The performance of the proposed method is first tested in a simulation environment and then validated with an experimental data set obtained with an aeroelastically scaled turbine model in a boundary layer wind tunnel.

1 Introduction

The ability to control a system is often intimately linked to the awareness of the surrounding environment. For a wind turbine, the environment is represented by the wind inflow, which is characterized by speed, direction, shears, veer, turbulence intensity, presence of impinging wakes, etc. Such parameters have a profound effect on the response of a single wind turbine as well as on clusters of interacting machines within a power plant. Better awareness of the wind environment can be translated into better turbine-level and plant-level operation and control.

The current standard equipment mounted on board wind turbines for the measurement of the wind inflow is composed of one or more anemometers and wind vanes, typically located at hub height, either on the nacelle or on the spinner. Even when properly calibrated, all such devices suffer from one inherent unavoidable limitation: they provide measurements at the single point in space where they are located. As such, they are necessarily blind to all wind characteristics that imply wind variations across the rotor disk. Alternative sensors are represented by lidars, which are, however, not yet routinely installed on board wind turbines because of cost, availability, reliability, effects due to weather conditions and lifetime issues. In this sense, current wind turbines have only a very limited awareness of the environment in which they operate.

The concept of the "rotor as a sensor" was developed to address the limitations of current wind measurement devices. The idea is conceptually very simple: changes in the wind inflow produce changes in the wind turbine response. If the wind-response map is known, one can then measure the response (for example, in the form of loads and/or accelerations) and estimate the inflow by inverting the map.

Various formulations have been proposed for this concept (Bottasso et al., 2010; Bottasso and Riboldi, 2014; Simley and Pao, 2014; Bottasso and Riboldi, 2015). In this paper we improve on the work described by Cacciola et al. (2016a) and Bertelè et al. (2017, 2018). The approach parameterizes the inflow in terms of four quantities: vertical and horizon-

tal shears and misalignment angles. The wind-response map relates these four wind states to the 1P in- and out-of-plane blade root bending moments. Both linear and quadratic maps were considered in Bertelè et al. (2017), with a marginally better accuracy for the latter. System identification was used to find the model coefficients from simulations performed with an aeroservoelastic model in a variety of wind conditions, spanning the range of interest of the four wind states. Results indicate a better accuracy of the shears than the angles, although the latter are still well captured in their mean values.

Despite the more than promising results reported in Bertelè et al. (2017), the identification of the model relating wind states to load harmonics can be cumbersome. In fact, a data set is required that covers a desired range of the four wind states. While this is not a major issue in a simulation environment where one can generate all desired wind conditions, an identification based on field test data might not be easy or even possible. In fact, some wind parameters might not change much at a given site, e.g. upflow angle and horizontal shear. This would clearly be a major hurdle, as a model only knows what is in the data used for training it.

To address this issue, the present work exploits the rotationally symmetric behavior of the rotor. In fact, the effect caused by a horizontal shear on the rotor response is the same as that caused by a vertical shear, only shifted by $\pi/2$. Similarly, the effect of a vertical upflow angle is the same of a horizontal yaw misalignment, again shifted by $\pi/2$. This means that one can collect data sets containing the desired changes in vertical shears and yaw misalignments, and identify a model that is also capable of representing the same range of horizontal shears and upflow angles.

The paper is organized as follows. Section 2 first introduces the wind parameterization and the wind-load map, and then uses the rotational symmetry of the rotor to eliminate some of the model coefficients from the identification problem unknowns. Section 3 compares the results of the new formulation to the original one first by simulations – conducted with an aeroservoelastic model – and then experimentally – using a scaled turbine in a wind tunnel. Finally, the work is closed by Sect. 4, where conclusions are drawn.

2 Formulation

2.1 Wind parameterization and rotational symmetry

The wind inflow is characterized in terms of four so-called wind states, which are defined as the vertical (upflow) and horizontal (yaw) misalignment angles χ and ϕ, respectively, and the vertical and horizontal linear shears κ_v and κ_h, respectively. These quantities should be regarded as rotor-equivalent fits of the actual spatial distribution of the wind impinging on the rotor disk at a certain instant of time.

The wind states are defined with respect to a nacelle-attached reference frame ($\boldsymbol{x}$, $\boldsymbol{y}$, $\boldsymbol{z}$) centered at the hub as shown in Fig. 1: unit vector $\boldsymbol{x}$ is aligned with the rotor axis and faces downwind, $\boldsymbol{z}$ points upward in the vertical plane, while $\boldsymbol{y}$ is defined according to the right-hand rule. The components of the wind vector in the nacelle-attached frame of reference are noted $\boldsymbol{V} = \{u, v, w\}^\mathrm{T}$ and they write

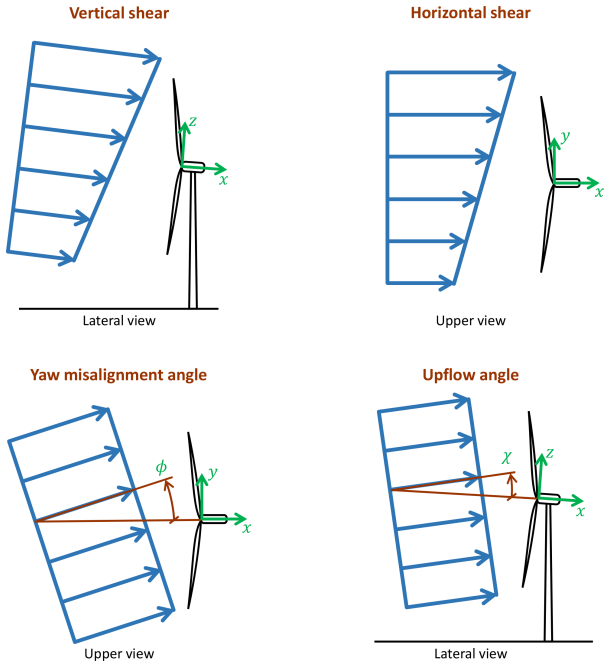

Figure 1. Definition of the four wind states used for parameterizing the wind field over the rotor disk.

$$u(y,z) = W(y,z)\cos(\phi)\cos(\chi), \tag{1a}$$
$$v(y,z) = W(y,z)\sin(\phi)\cos(\chi), \tag{1b}$$
$$w(y,z) = W(y,z)\sin(\chi), \tag{1c}$$

where $W(y,z)$ is a linearly sheared wind field

$$W(y,z) = V_\mathrm{H}\left(1 + \frac{z}{R}\kappa_\mathrm{v} + \frac{y}{R}\kappa_\mathrm{h}\right), \tag{2}$$

V_H being the wind speed at hub height, and R the rotor radius. According to this definition, the yaw misalignment and upflow angles are positive when the wind blows from the left and the lower part of the rotor, respectively, when looking upstream.

Notice that the formulation of Cacciola et al. (2016a) used a horizontal reference frame with respect to the terrain, while in the present case the frame is aligned with the rotor axis. Together with the assumed linearity of both shears, this is necessary in order to exploit the rotational symmetry of the rotor response. Hence, if the rotor is uptilted, one will have to transform the nacelle-frame wind components into a frame aligned with the ground if necessary.

Looking at Eq. (2), it appears that the effect of the vertical shear κ_v on the velocity distribution is the same of the

one caused by the horizontal shear κ_h, when rotated by $\pi/2$. On the other hand, looking at Eq. (1a–c), the effect of the angles ϕ and χ is more complex. To eliminate this problem, the rotor-in-plane wind velocity components can be expressed in terms of the new variables

$$\widetilde{v} = \frac{v(0,0)}{V_H} = \sin(\phi)\cos(\chi), \tag{3a}$$

$$\widetilde{w} = \frac{w(0,0)}{V_H} = \sin(\chi), \tag{3b}$$

which, respectively, represent the nondimensional horizontal and vertical wind cross flows at the hub. This change of variables results in

$$u(y,z) = W(y,z)\sqrt{1-\widetilde{v}^2-\widetilde{w}^2}, \tag{4a}$$

$$v(y,z) = W(y,z)\widetilde{v}, \tag{4b}$$

$$w(y,z) = W(y,z)\widetilde{w}. \tag{4c}$$

With this reformulation, the effect of $\widetilde{v}$ on v is the same as the effect of $\widetilde{w}$ on w, when rotated by $\pi/2$. Given $\widetilde{v}$ and $\widetilde{w}$, the misalignment angle ϕ and upflow χ can be readily recovered by inverting their respective definitions (Eq. 3a–b):

$$\chi = \arcsin(\widetilde{w}), \tag{5a}$$

$$\phi = \arcsin(\widetilde{v}/\cos\chi), \tag{5b}$$

although for small angles the difference between the two sets of variables will be negligible.

2.2 Wind observer formulation

In this work, the linear model of Cacciola et al. (2016a) and Bertelè et al. (2017) is used to relate inflow conditions and machine response. The model writes

$$\begin{aligned}\boldsymbol{m} &= \mathbf{F}(V,\varrho)\boldsymbol{\theta} + \boldsymbol{m}_0(V,\varrho)\\ &= \left[\mathbf{F}(V,\varrho)\ \boldsymbol{m}_0(V,\varrho)\right]\begin{bmatrix}\boldsymbol{\theta}\\ 1\end{bmatrix} = \mathbf{T}\,\overline{\boldsymbol{\theta}},\end{aligned} \tag{6}$$

where $\boldsymbol{m}$ is the load vector, $\boldsymbol{\theta} = \{\widetilde{v}\ \kappa_v\ \widetilde{w}\ \kappa_h\}^T$ is the wind state vector, while $\mathbf{F}$ and $\boldsymbol{m}_0$ represent the model coefficients, scheduled with respect to wind speed V and air density ϱ. The load vector is defined as

$$\boldsymbol{m} = \left\{m_{1c}^{OP},\ m_{1s}^{OP},\ m_{1c}^{IP},\ m_{1s}^{IP}\right\}^T, \tag{7}$$

where m indicates the blade bending moment, subscripts $(\cdot)_{1s}$ and $(\cdot)_{1c}$, respectively, indicate sine and cosine harmonics, while superscripts $(\cdot)^{OP}$ and $(\cdot)^{IP}$, respectively, out- and in-plane components. The load harmonics are readily computed via the Coleman and Feingold transformation (Coleman and Feingold, 1958) once three measured blade loads are available. For simplicity and brevity, the present paper only considers a linear wind-response map. However, nonlinearities in the map can be readily included, as shown by Bertelè et al. (2017).

To identify the model coefficients $\mathbf{T}$, one should collect a rich enough data set for which both wind states $\boldsymbol{\theta}$ and associated blade loads $\boldsymbol{m}$ are known. Stacking side by side the ith wind and load vectors into matrices $\boldsymbol{\Theta}$ and $\mathbf{M}$, one gets

$$\mathbf{M} = \mathbf{T}\boldsymbol{\Theta}. \tag{8}$$

Finally, the model coefficients are readily identified as

$$\mathbf{T} = \mathbf{M}\boldsymbol{\Theta}^T(\boldsymbol{\Theta}\boldsymbol{\Theta}^T)^{-1}. \tag{9}$$

The invertibility of the system is discussed in Bertelè et al. (2017).

Once the model expressed by Eq. (6) has been identified, it can be used to express the dependency of given measured loads $\boldsymbol{m}_M$ on the wind states,

$$\boldsymbol{m}_M = \mathbf{F}\boldsymbol{\theta} + \boldsymbol{m}_0 + \boldsymbol{r}, \tag{10}$$

where $\boldsymbol{r}$ is the measurement error, and the dependency on V and ϱ has been dropped for a simpler notation. The least squares estimate of the wind states $\boldsymbol{\theta}_E$ is then readily obtained as

$$\boldsymbol{\theta}_E = \left(\mathbf{F}^T\mathbf{R}^{-1}\mathbf{F}\right)^{-1}\mathbf{F}^T\mathbf{R}^{-1}(\boldsymbol{m}_M - \boldsymbol{m}_0), \tag{11}$$

where $\mathbf{R} = \mathbf{E}[\boldsymbol{r}\boldsymbol{r}^T]$ is the covariance weighting matrix. Given $\boldsymbol{\theta}_E$, the misalignment and upflow angles can be recovered by using Eq. (5).

2.3 Rotational symmetry

By considering the rotational symmetry of the rotor, the number of unknown coefficients in $\mathbf{F}$ can be reduced. Indeed, a vertical shear will cause the same response of an equivalent horizontal shear, simply shifted by an azimuthal delay of $\pi/2$. The same consideration holds for the vertical and horizontal cross flows. This rotational symmetry is reflected in the derivatives of the loads with respect to the wind states, i.e., in the coefficients of matrix $\mathbf{F}$. By a rotation of $\pi/2$, the load component m_{1c} becomes m_{1s}, while the load component m_{1s} becomes $-m_{1c}$. As a result, the following conditions apply between pairs of model coefficients:

$$\frac{\partial m_{1c}}{\partial \widetilde{v}} = \frac{\partial m_{1s}}{\partial \widetilde{w}}, \tag{12a}$$

$$\frac{\partial m_{1s}}{\partial \widetilde{v}} = -\frac{\partial m_{1c}}{\partial \widetilde{w}}, \tag{12b}$$

$$\frac{\partial m_{1c}}{\partial \kappa_h} = \frac{\partial m_{1s}}{\partial \kappa_v}, \tag{12c}$$

$$\frac{\partial m_{1s}}{\partial \kappa_h} = -\frac{\partial m_{1c}}{\partial \kappa_v}. \tag{12d}$$

These conditions apply to both the out- and the in-plane components.

The term $\boldsymbol{m}_0$ in Eq. (6) represents the effects of gravity on the loads (Bertelè et al., 2017). Since this term is nonsymmetric, no reduction of these coefficients is possible in this case.

The advantage of this approach is not only in the reduced number of unknown model coefficients, but, most importantly, in the reduced datapoints necessary for identification. In fact, by eliminating the coefficients of horizontal shear and upflow angle, one can use tests in which only yaw misalignment angle and vertical shear are changing. Therefore, since the model is linear and depends on two parameters, a minimum of only three operating conditions is required for identification.

3 Results

3.1 Verification in a simulation environment

The proposed method was first tested by numerical simulations, using the model of a horizontal-axis three-bladed 3 MW wind turbine. The machine has a rotor diameter of 93 m; a hub height of 80 m; 4.5° of nacelle uptilt; and cut-in, rated and cut-out speeds equal to 3, 12.5 and 25 m s^{-1}, respectively. A transition region $II\,1/2$ connects the partial- and full-load regimes, extending between 9 and 12.5 m s^{-1}. The machine response was simulated by the aeroservoelastic multibody software `Cp-Lambda` (Bauchau et al., 2003; Bottasso and Croce, 2006), which is based on a geometrically exact finite element formulation. The model includes flexible blades, tower and drive train, and compliant foundations. The collective pitch and torque controller is implemented according to Riboldi (2012) and Bottasso et al. (2012), while generator and pitch actuators are modeled as first- and second-order dynamical systems, respectively. The aerodynamic rotor model is based on blade element momentum theory (BEM), augmented by classical tip and root losses, unsteady aerodynamics and dynamic stall models. Turbulent wind time histories were generated with the `TurbSim` code (Jonkman and Kilcher, 2012) in accordance with the Kaimal model, at the nodes of a square grid overlapping the rotor disk. "Ground truth" values of the wind states – to be used for assessing the quality of observed quantities – were obtained by fitting the instantaneous wind field at the grid nodes to the rotor swept area.

Turbulent simulations were run for a duration of 10 min, according to standard practice. The 1P harmonics were computed by the Coleman and Feingold transformation (Coleman and Feingold, 1958), using in- and out-of-plane bending moment components measured by strain gauges placed at the root of each blade. The resulting signal was finally cleaned with a low-pass filter; on-line adaption of the filter parameters was used to account for changes in rotational speed due to turbulent wind fluctuations.

Two observation models were identified. The first is the linear formulation of Bertelè et al. (2017), which does not exploit the rotational symmetry of the rotor, while the second is the linear rotationally symmetric formulation of the present paper. In the first case, the model was identified from nonturbulent wind cases corresponding to all combinations of the following wind parameters:

$$\phi = [0 \;\; 16]^\circ, \tag{13a}$$
$$\kappa_\mathrm{v} = [0.06 \;\; 0.18], \tag{13b}$$
$$\chi = [4.5 \;\; 16.5]^\circ, \tag{13c}$$
$$\kappa_\mathrm{h} = [0 \;\; -0.1]. \tag{13d}$$

A separate identification was performed for each wind speed, considering the values $V = [3\ 4\ 5\ 6\ 7\ 8\ 9\ 11\ 15\ 19]\,\mathrm{m\,s^{-1}}$. A second model was obtained by exploiting symmetry and linearity. Accordingly, the identification set was reduced to the following wind parameter combinations:

$$\phi = [0\ 16]^\circ, \tag{14a}$$
$$\kappa_\mathrm{v} = [0.06 \;\; 0.18], \tag{14b}$$
$$\chi = 4.5^\circ, \tag{14c}$$
$$\kappa_\mathrm{h} = 0, \tag{14d}$$

therefore assuming both upflow χ and horizontal shear κ_h to be constant. Notice that the upflow angle is set to 4.5°, which corresponds to the rotor uptilt.

The two models were then tested and compared in turbulent wind conditions. Three different combinations of inflow angles and shears (not included in the identification set) were considered, each using four different turbulent realizations, for a total of 12 tests performed at each given wind speed and turbulence intensity (TI). Figures 2 and 3 show, respectively, the mean (over 10 min and over all turbulent seeds) absolute error ϵ and standard deviation σ as functions of wind speed, for two different levels of TI, equal to 5 % and 12 %. The results of the reference full model are shown using solid lines, while the ones of the rotationally symmetric formulation using dashed lines. The two formulations appear to be characterized by a very similar performance. Actually, notwithstanding its reduced identification set, the symmetric method obtains marginally better results. As expected, TI has a negative effect on the quality of the estimates. In addition, as already noticed in Bertelè et al. (2017), angle estimates appear to be less precise than shear estimates. Nonetheless, for 12 % TI at 15 m s^{-1}, the yaw misalignment mean error is about 2.5°. This appears to be a good result when compared to the typical accuracy of nacelle-mounted anemometers.

3.2 Verification with a scaled model in a wind tunnel

Next, the proposed formulation was tested using an aeroelastically scaled wind turbine operated in a boundary layer wind tunnel. The scaled model represents a three-bladed horizontal-axis wind turbine with a hub height of about 1.8 m, a rotor diameter of 2 m and a rated wind speed of

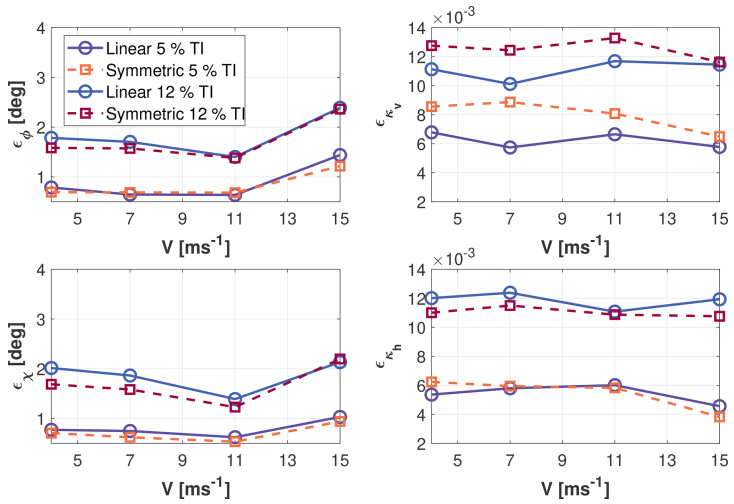

Figure 2. Mean absolute error ϵ of the four wind states vs. wind speed for 5 % and 12 % turbulence intensity (TI) levels. Nonsymmetric model: solid lines; symmetric model: dashed lines.

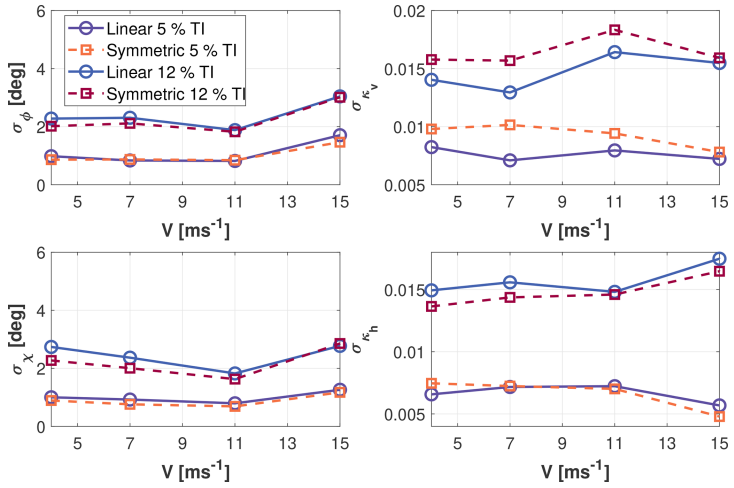

Figure 3. Standard deviation σ of the four wind states vs. wind speed for 5 % and 12 % turbulence intensity (TI) levels. Nonsymmetric model: solid lines; symmetric model: dashed lines.

6 m s^{-1} (Bottasso et al., 2014). The turbine design preserves the tip speed ratio, Lock number, and placement of the lowest tower and rotor nondimensional frequencies of the reference machine, resulting in a scaled model of realistic aeroelastic behavior (Bottasso et al., 2014). Each of the flexible scaled blades is equipped with strain gauges at the blade roots, which measure the flapwise and edgewise bending moments, while an optical incremental encoder is used to measure the blade azimuthal position.

Tests were performed in the boundary layer test section of the wind tunnel of Politecnico di Milano (Bottasso et al., 2014). Two different boundary layer conditions, characterized by different mean vertical shears and TI levels, were obtained by the use of suitable turbulence generators at the chamber inlet and roughness elements placed on the floor. Such inflow conditions were then accurately mapped over the rotor swept area with triple hot-wire probes, providing a reference mean inflow that can be considered the "ground truth". The lower turbulence condition was characterized by a TI of 3.8 % and a linear vertical shear of 0.03, while the higher turbulence case by a TI of 8.5 % and a linear vertical shear of 0.12.

For various wind speeds, several tests were performed for different combinations of yaw misalignment, vertical shear and upflow angle as reported in Table 1. Changes in mean vertical shear were obtained by changing the wind tunnel boundary layer conditions. Changes in mean misalignment angle were realized by yawing the turbine model with re-

Table 1. Test matrix for the wind tunnel experiments. Symbol "×" marks the identification set; "○" marks the validation set.

Experiments conducted with an upflow angle $\chi = 6°$									
		Misalignment angle ϕ (°)							
Wind speed V ($m\,s^{-1}$)	Vertical shear κ_v	20	15	10	6	0	−6	−10	−15	−18
5	0.03 and 0.12	×		○		×	○			○
5.5	0.03 and 0.12	×		○		×	○			○
6	0.03 and 0.12		×	○	○	×	○	○	○	
7	0.03 and 0.12		×	○	○	×	○	○	○	
7.5	0.03 and 0.12		×		○	×	○		○	
Experiments conducted with upflow angles $\chi = 0$ and 12°									
		Misalignment angle ϕ (°)							
Wind speed V ($m\,s^{-1}$)	Vertical shear κ_v	20	15	10	6	0	−6	−10	−15	−18
5.5	0.03 and 0.12				○	○	○			

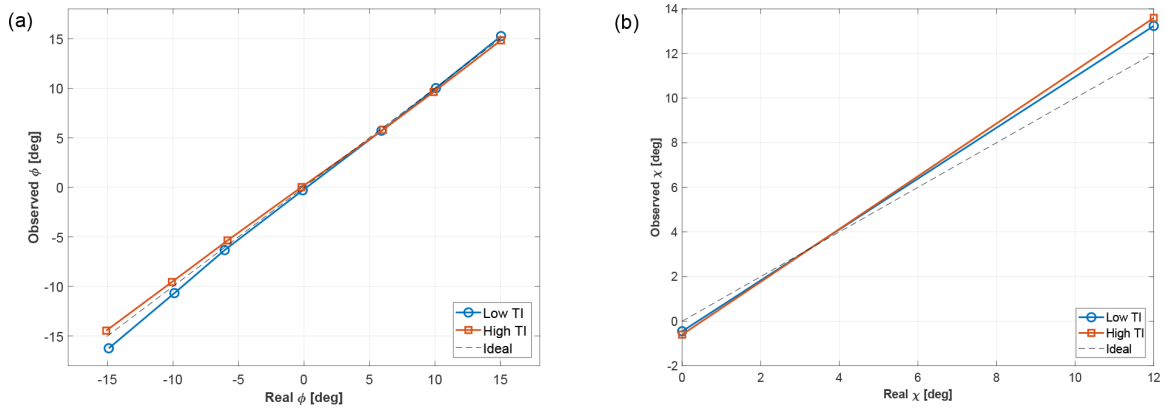

Figure 4. Wind states observed for different steady inflow conditions: yaw misalignment ϕ at $\chi = 6°$ and $\kappa_h = 0$ at a wind speed of $7\,m\,s^{-1}$ (**a**), upflow angle χ at $\phi = 6°$ and $\kappa_h = 0$ at a wind speed of $5.5\,m\,s^{-1}$ (**b**).

spect to the wind. To create different upflow angles, the wind turbine tower foot was installed on a tiltable ramp. By changing the ramp angle, the turbine can be pitched by ±6°. As the rotor has an uptilt angle of 6° with respect to the tower, the use of the ramp allows one to obtain upflow angles between 0 and 12°. Finally, the horizontal shear for all tests can be considered null, as the flow in the wind tunnel is essentially uniform in the lateral direction.

A total number of 174 different conditions were tested. The entire set of experiments was then divided into two subsets. The first one was used for identifying the observer model, and it contains two combinations of vertical shear and misalignment angle per wind speed, with an upflow of 6°; these test points are indicated with "×" symbols in Table 1. The second subset was instead used for validating the observer performance. This second subset contains all the other experiments, indicated with "○" symbols in Table 1. Notice that the second set of experiments correspond to upflow angles of 0 and 12°, values that are not contained in the identification set. This is possible thanks to the symmetry of the rotor: the information contained in the identification set on the effect of the misalignment angle is used to infer the effect of the upflow, although no operating points at different upflows are used during training.

To validate the performance of the observer, the machine response during each test was averaged over a time window of 180 s in order to estimate the corresponding mean inflow parameters. The length of the time window is dictated in this case not only by the need to average out turbulent fluctuations, but also by the dynamic characteristics of this particular closed-return wind tunnel. Figure 4 shows an excerpt of the results obtained at a wind speed of $7\,m\,s^{-1}$ (Fig. 4a), which corresponds to the beginning of the full load region, and a speed of $5.5\,m\,s^{-1}$ (Fig. 4b), which corresponds to the end of the partial load region. In each panel, the reference (true) wind parameter is shown on the x axis, while

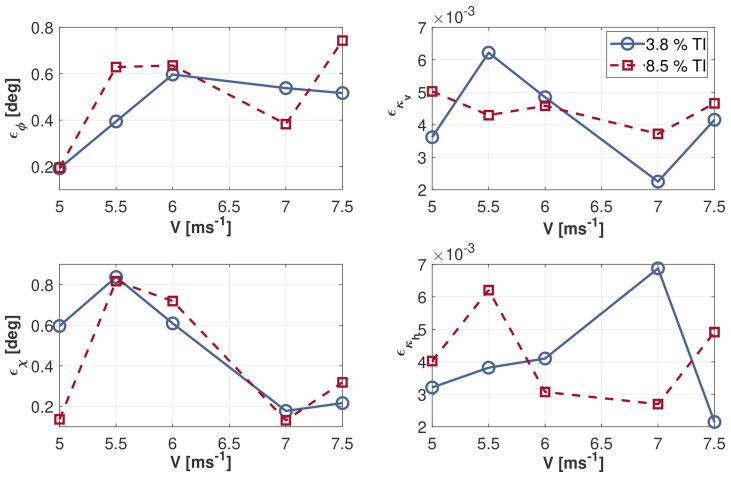

Figure 5. Mean absolute error ϵ of the four wind states vs. wind speed for 3.8 % and 8.5 % turbulence intensity (TI) levels.

the corresponding observed quantity is given on the y axis. It follows that an ideal match would be represented by the bisector of the quadrant. The yaw misalignment estimation (Fig. 4a) appears to be quite accurate and has a maximum error of less than 1.3°. Better accuracy can be achieved for high positive yaw angles; this is to be expected, since such conditions are included in the identification set (cf. Table 1). Even the upflow estimation (Fig. 4b) appears to be quite accurate, with a maximum error of about 1.5°. Note that the accuracy in the upflow estimation validates the assumption of rotational symmetry of the parameters, as no upflow changes were present in the data set used for identifying the load-wind model (again, cf. Table 1). Indeed, the model coefficients related to this parameter were obtained using the symmetry conditions given by Eq. (12a–d).

Finally, to better understand the performance of the observer, mean inflow parameters were estimated and compared to the respective ground truth for each test not included in the identification set. For each wind speed, such mean errors were averaged over the number of tests and reported in Fig. 5. Here again, results appear to be significantly accurate; in fact, for both turbulence levels, a maximum mean error smaller than 1° is observed in the angle estimates, while the error in the shear estimates is less than 6×10^{-3}.

Comparing the experimental results with the numerical ones in the low TI cases (equal to 3.8 % and 5 %, respectively), one should notice that the mean estimation errors present the same range of accuracy, as one can appreciate by comparing Fig. 5 with Fig. 2. This can be considered an additional proof of the general applicability of the method, since these results were obtained with two different models applied to two very different machines, using numerical and experimental data sets.

4 Conclusions

Following the work presented in Cacciola et al. (2016a) and Bertelè et al. (2017), this paper has further developed and experimentally validated a method to estimate the inflow at the rotor disk. Specifically, a linear model was formulated to estimate four wind parameters: the vertical and horizontal shears, and the vertical and horizontal wind misalignments. Improving on the previous publications, the rotationally symmetric behavior of the rotor was exploited in order to simplify the model identification procedure, by reducing the number of necessary measured operating conditions.

The performance of the proposed rotationally symmetric model was tested both in simulation and with an aeroelastically scaled wind turbine model in a boundary layer wind tunnel. Results indicate no significant difference in the accuracy of the new rotationally symmetric formulation with respect to the original one, even if the number of tests required for identification is significantly decreased. The expected mean error in the angle estimation is less than 1 and 2.5° for low and high TI levels, respectively. An even higher accuracy can be obtained for the estimation of shears. Moreover, the experimental results are well in line with the ones obtained by numerical simulations.

Data availability. Data can be provided upon request. Please contact the corresponding author Carlo L. Bottasso (carlo.bottasso@tum.de).

Appendix A: Nomenclature

m	Generic blade moment
$\boldsymbol{m}$	Vector of moment harmonics
R	Rotor radius
V	Wind speed
$\boldsymbol{V}$	Wind vector
$\widetilde{v}$	Non-dimensional horizontal cross flow at the hub
$\widetilde{w}$	Non-dimensional vertical cross flow at the hub
ϱ	Air density
ϕ	Yaw misalignment angle
χ	Upflow angle
κ_{v}	Vertical shear
κ_{h}	Horizontal shear
ϵ	Mean error
σ	Standard deviation
$\boldsymbol{\theta}$	Wind state vector
$(\cdot)^{\mathrm{T}}$	Transpose
$(\cdot)_{\mathrm{E}}$	Estimated quantity
$(\cdot)^{\mathrm{OP}}$	Out-of-plane quantity
$(\cdot)^{\mathrm{IP}}$	In-plane quantity
$(\cdot)_{1\mathrm{c}}$	1P cosine amplitude
$(\cdot)_{1\mathrm{s}}$	1P sine amplitude
BEM	Blade element momentum
Lidar	Light detection and ranging
TI	Turbulence intensity
1P	Once per revolution

Author contributions. All authors equally contributed to this work.

Competing interests. The authors declare that they have no conflict of interest.

Acknowledgements. This work has been partially supported by the CL-Windcon project, which receives funding from the European Union Horizon 2020 research and innovation program under grant agreement No. 727477.

This work was supported by the German Research Foundation (DFG) and the Technical University of Munich (TUM) in the framework of the Open Access Publishing Program.

Edited by: Sandrine Aubrun
Reviewed by: two anonymous referees

References

Bauchau, O. A., Bottasso, C. L., and Trainelli, L.: Robust integration schemes for flexible multibody systems, Comput. Method. Appl. M., 192, 395–420, https://doi.org/10.1016/S0045-7825(02)00519-4, 2003.

Bertelè, M., Bottasso, C. L., Cacciola, S., Daher Adegas, F., and Delport, S.: Wind inflow observation from load harmonics, Wind Energ. Sci., 2, 615–640, https://doi.org/10.5194/wes-2-615-2017, 2017.

Bertelè, M., Bottasso, C. L., and Cacciola, S.: Simultaneous estimation of wind shears and misalignments from rotor loads: formulation for IPC-controlled wind turbines, J. Phys. Conf. Ser., 1037, 032007, https://doi.org/10.1088/1742-6596/1037/3/032007, 2018.

Bottasso, C. L. and Croce, A.: Cp-Lambda: user's manual, Technical Report, Dipartimento di Ingegneria Aerospaziale, Politecnico di Milano, Milano, Italy, 2006.

Bottasso, C. L. and Riboldi, C. E. D.: Estimation of wind misalignment and vertical shear from blade loads, Renew. Energ., 62, 293–302, https://doi.org/10.1016/j.renene.2013.07.021, 2014.

Bottasso, C. L. and Riboldi, C. E. D.: Validation of a wind misalignment observer using field test data, Renew. Energ., 74, 298–306, https://doi.org/10.1016/j.renene.2014.07.048, 2015.

Bottasso, C. L., Croce, A., and Riboldi, C. E. D.: Spatial estimation of wind states from the aeroelastic response of a wind turbine, The Science of Making Torque from Wind (TORQUE 2010) 28–30 June 2010, Heraklion, Crete, Greece, 2010.

Bottasso, C. L., Croce, A., Nam, Y., and Riboldi, C. E. D.: Power curve tracking in the presence of a tip speed constraint, Renew. Energ., 40, 1–12, https://doi.org/10.1016/j.renene.2011.07.045, 2012.

Bottasso, C. L., Campagnolo, F., and Petrovic`: Wind tunnel testing of scaled wind turbine models: beyond aerodynamics, J. Wind. Eng. Ind. Aerod., 127, 11–28, https://doi.org/10.1016/j.jweia.2014.01.009, 2014.

Bottasso, C. L., Cacciola, S., and Schreiber, J.: A wake detector for wind farm control, J. Phys. Conf. Ser., 625, 012007, https://doi.org/10.1088/1742-6596/625/1/012007, 2015.

Bottasso, C. L., Cacciola, S., and Schreiber, J.: Local wind speed estimation, with application to wake impingement detection, Renew. Energ., 116, 155–168, 2018.

Cacciola, S., Bertelè, M., and Bottasso, C. L.: Simultaneous observation of wind shears and misalignments from rotor loads, J. Phys. Conf. Ser., 753, 052002, https://doi.org/10.1088/1742-6596/753/5/052002, 2016a.

Cacciola, S., Bertelè, M., Schreiber, J., and Bottasso, C. L.: Wake center position tracking using downstream wind turbine hub loads, J. Phys. Conf. Ser., 753, 032036-1–6, https://doi.org/10.1088/1742-6596/753/3/032036, 2016b.

Coleman, R. P. and Feingold, A. M.: Theory of self-excited mechanical oscillations of helicopter rotors with hinged blades, Technical Report, NACA TN 1351, 1958.

Jonkman, B. J. and Kilcher, L.: TurbSim user's guide: version 1.06.00, NREL Technical report, 2012.

Riboldi, C. E. D.: Advanced control laws for variable-speed wind turbines and supporting enabling technologies, PhD thesis, Politecnico di Milano, Milano, Italy, 2012.

Simley, E. and Pao, L. Y.: Evaluation of a wind speed estimator for effective hub-height and shear components, Wind Energy, 19, 167–184, https://doi.org/10.1002/we.1817, 2014.

A.3 Paper III: Wind inflow observation from load harmonics: initial steps towards a field validation

Reference: M. Bertelè, C. L. Bottasso and J. Schreiber, J., "Wind inflow observation from load harmonics: initial steps towards a field validation, *Wind Energ. Sci. Discuss.* [preprint],2020. doi: 0.5194/wes-2020-83.

https://doi.org/10.5194/wes-2020-83
Preprint. Discussion started: 9 July 2020

eawe european academy of wind energy
Open Access WIND ENERGY SCIENCE DISCUSSIONS

Wind inflow observation from load harmonics: initial steps towards a field validation

Marta Bertelè[1], Carlo L. Bottasso[1], and Johannes Schreiber[1]
[1]Wind Energy Institute, Technische Universität München, Garching bei München, D-85748 Germany
Correspondence to: C.L. Bottasso (carlo.bottasso@tum.de)

Abstract.

A previously published wind sensing method is applied to an experimental dataset obtained on a 3.5 MW turbine and a nearby hub-tall met-mast. The method uses blade load harmonics to estimate rotor-equivalent shears and wind directions at the rotor disk. A second independent method is used to extend the met-mast-measured shear above hub height to cover the entire rotor disk.

Although the experimental setup falls short of providing a real validation of the method, it still allows for a realistic practical demonstration of some of its main features. The method appears to be robust to turbulent fluctuations and air density changes. Results indicate a good quality of the estimated shear, both in terms of 10-min averages and of resolved time histories, and a reasonable accuracy in the estimation of the yaw misalignment.

1 Introduction

This paper presents a first attempt at the field validation of a wind sensing method based on load harmonics.

Wind sensing refers to the general concept of using the response of the turbine to estimate characteristics of the inflow, which can be done in several different ways (Bottasso et al., 2010; Bottasso and Riboldi, 2014; Simley and Pao, 2016; Bottasso and Riboldi, 2015; Bertelè et al., 2017; Bottasso et al., 2018; Schreiber et al., 2020). Information on the inflow can support a variety of applications, including turbine and farm-level control, lifetime assessment and fatigue consumption estimation, power and wind forecasting, and others (Schreiber et al., 2020). In wind sensing, the rotor response is typically measured in the form of blade loads. If blade load sensors are already available, for example for load-mitigating control, wind sensing is a way of augmenting the value of load sensors, by providing an extra set of uses to the data that they already collect.

The method based on load harmonics was first proposed by Bottasso and Riboldi (2014), and then further elaborated and improved by Bottasso and Riboldi (2015); Cacciola et al. (2016a); Bertelè et al. (2017, 2018, 2019). In a nutshell, this method is based on the fact that some characteristics of the inflow (horizontal and vertical shear, lateral and vertical misalignment angles) generate a specific response of the rotor at the 1P (once per revolution) frequency. This is a very desirable feature, because:

- The 1P frequency is strongly dominated by these "deterministic" characteristics of the wind, and much less so by turbulent fluctuations (Bertelè et al., 2017);

https://doi.org/10.5194/wes-2020-83
Preprint. Discussion started: 9 July 2020

eawe european academy of wind energy
Open Access WIND ENERGY SCIENCE DISCUSSIONS

- Low frequencies are easier to measure than higher frequencies, as they require slower sampling rates (typically around one second for capturing the 1P of a wind turbine);
- There should be limited variability in such low frequencies among different installations of a same wind turbine type;
- The lower spectrum of the response of a wind turbine should be reasonably well captured by existing simulation tools used for design and certification.

The load-harmonic method requires a training dataset consisting of measured rotor loads and corresponding measured wind characteristics. The dataset can be based on experimental measurements, or be generated synthetically using a simulation model; these two approaches were respectively termed model-free and model-based in Bottasso and Riboldi (2014). Here we consider the former approach; indeed, a model might not always be available, for example in cases when wind sensing is applied to a turbine without the support of the manufacturer. Even when a model is available, it might not have been fully validated, so that a purely data-driven approach has a significant appeal. Thanks to the rotational symmetry of the rotor (Bertelè et al., 2019), the measured wind conditions that are necessary for training can be limited to the vertical shear and the horizontal (or yaw) misalignment; based on these quantities, the effects caused by horizontal shear and vertical (upflow) misalignment can be reconstructed. After training, the method can estimate the four wind parameters online during turbine operation simply from measured rotor loads.

It is envisioned that, in a practical application of the model-free harmonic-based method, the training phase would be a one-off activity performed at a test site equipped with a met-mast or other wind measuring devices such as lidars or sodars (Carswell, 1983; Vogt and Thomas, 1995; Lang and McKeogh, 2011). Indeed, hub-tall met-masts are routinely used during certification (IEC, 2017), and could be employed for the additional purpose of training the observer. After training, the method could be used on other installations of that same turbine type at normal production sites without necessitating of met-masts or other devices.

Goal of this paper is to present the application of the load-harmonic estimator to field test data collected at a test site on a 3.5 MW wind turbine and a nearby met-mast (Schreiber et al., 2020; Bertelè and Bottasso, 2020). This experimental setup is a realistic representation of the scenario outlined above, where a hub-tall met-mast is located in close proximity of a wind turbine for certification purposes. From this point of view, the present dataset provides opportunities not only for a first —partial— field demonstration of the method, but also for addressing some important practical implementational aspects.

Specifically, the vertical shear requires special attention. In fact, a hub-tall met-mast with more than one anemometer can only measure the wind shear over the lower part of the rotor disk; on the other hand, the load-harmonic observer estimates a rotor-equivalent shear (i.e. a shear over the entire rotor disk area). For large modern rotors, half-rotor or full-rotor shears are not necessarily equal (Murphy et al., 2019; Schreiber et al., 2020). Therefore, a way is needed to extend the measurement of the inflow above the met-mast, possibly without resorting to extra wind-scanning equipment to reduce cost and complexity. This problem is solved here using yet another wind sensing method (Bottasso et al., 2018; Schreiber et al., 2016, 2020). This second approach uses blade loads to estimate the average local speed over sectors of the rotor disk; from these sector-equivalent wind speeds, one can then estimate shears, including a vertical shear defined over just the lower half of the rotor.

https://doi.org/10.5194/wes-2020-83
Preprint. Discussion started: 9 July 2020

eawe european academy of wind energy
Open Access WIND ENERGY SCIENCE DISCUSSIONS

The sector-effective speed and load-harmonic observers have distinct characteristics, which make them somewhat complementary and applicable to different scenarios. In fact, the sector-effective observer does not need to be trained with data before it can be used, which is particularly useful in the case considered here, but can only reconstruct shears and not wind directions (Schreiber et al., 2020). On the contrary, the load-harmonic observer can reconstruct both shears and directions but needs to be trained from data, which is a potential complication. A three-step procedure is developed and demonstrated here, where the two observers are used in synergy:

1. The lower-half-rotor shear measured by the sector-equivalent speed method is tuned and validated with respect to the met-mast reference;

2. The full-rotor shear is computed using the validated sector-equivalent speed method, extending the measurement of the inflow above the met-mast;

3. This rotor-equivalent shear is finally used for training the harmonic-based estimator.

Although the present setup allows for a first demonstration of this procedure, it also presents some limitations that hinder a real and complete validation of the method. First, the extension of the shear above the met-mast is performed through the same rotor loads that are also used by the harmonic-based estimator. Clearly, a completely independent measurement of the inflow up to the tip of the rotor would be preferable for validation purposes. Second, the present met-mast only includes a wind vane at hub height. This is a point-wise measurement, whereas the one provided by the observer —being obtained through the response of the rotor— is a rotor-effective quantity. Here again, it would be desirable to train and verify the method with an independently-derived rotor-equivalent quantity. Third, a met-mast cannot really provide a true and absolute ground truth, as it measures the flow away from the rotor disk (two and half diameters away, in the present case). When the wind is not directly aligned with turbine and mast, the wind shear and direction may be slightly different, on account of wind spatial variability, orographic and vegetation-induced effects. These differences are indeed visible to some extent in the present dataset. Even when wind, mast and turbine are aligned, the two measurements are not co-located and therefore not necessarily identical. Clearly, a more precise characterization of the effective inflow experienced by the rotor disk would be desirable for validation purposes.

Although the present study clearly falls short of a true validation of the harmonic-based formulation of wind sensing, it still provides for an interesting and —in the authors' opinion— very promising insight into some of its characteristics.

The paper is organized as follows. Section 2 describes the overall methodology, including a brief review of the harmonic-based estimator in §2.2 and a description of the test site and the measurement of the inflow characteristics in §2.3. The analysis of the wind observer performance is presented in Section 3, while Section 4 concludes the paper.

https://doi.org/10.5194/wes-2020-83
Preprint. Discussion started: 9 July 2020

eawe european academy of wind energy
Open Access WIND ENERGY SCIENCE DISCUSSIONS

2 Methods

2.1 Wind parametrization

The wind inflow is described by four parameters: the vertical linear shear κ_v, the horizontal linear shear κ_h, the vertical wind misalignment angle (or upflow) χ, and the horizontal (or yaw) misalignment angle ϕ. These quantities are illustrated in Fig. 1.

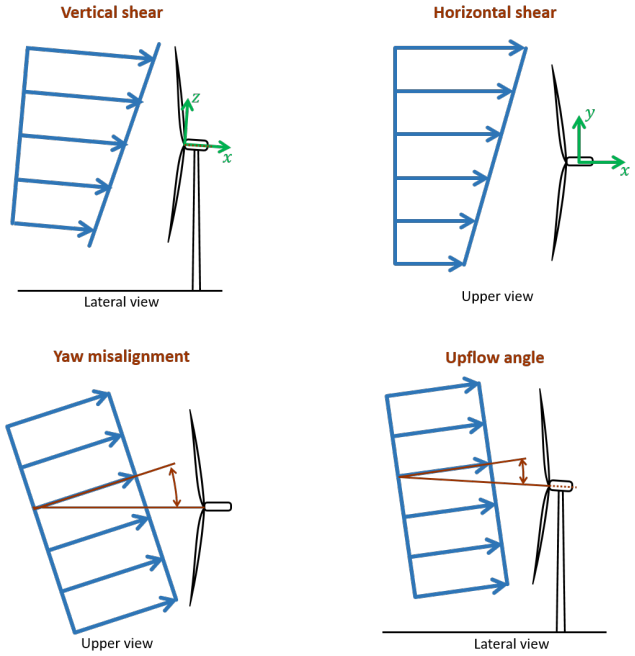

Figure 1. Definition of the four wind states used for parameterizing the wind field over the rotor disk.

A linearly sheared wind speed W at the rotor disk is defined as

$$W(y,z) = V_h \left(1 + \frac{y}{R}\kappa_h + \frac{z}{R}\kappa_v\right), \tag{1}$$

where V_h is the hub-height speed, and R the rotor radius. With reference to Fig. 1, the wind velocity vector components u, v and w along the x, y and z axes, respectively, of a hub-centered nacelle-attached frame write

$$u(y,z) = W(y,z)\sqrt{1-\tilde{v}^2-\tilde{w}^2}, \tag{2a}$$

$$v(y,z) = W(y,z)\tilde{v}, \tag{2b}$$

$$w(y,z) = W(y,z)\tilde{w}, \tag{2c}$$

https://doi.org/10.5194/wes-2020-83
Preprint. Discussion started: 9 July 2020

eawe european academy of wind energy
Open Access WIND ENERGY SCIENCE DISCUSSIONS

where $\tilde{v}$ and $\tilde{w}$ are defined as

$$\tilde{v} = \frac{v(0,0)}{V_h} = \sin\phi\cos\chi, \tag{3a}$$

$$\tilde{w} = \frac{w(0,0)}{V_h} = \sin\chi. \tag{3b}$$

For notational simplicity, the four wind parameters are grouped together in the wind state vector $\boldsymbol{\theta} = \{\tilde{v},\ \kappa_v,\ \tilde{w}, \kappa_h\}^T$. Given $\boldsymbol{\theta}$, the misalignment angles can be readily computed by inverting Eqs. (3) to get $\chi = \arcsin\tilde{w}$ and $\phi = \arcsin\tilde{v}/\cos\chi$.

2.2 Wind observer formulation

The relationship between wind states and rotor loads is assumed in the form

$$\boldsymbol{m} = \boldsymbol{F}(V,\rho)\boldsymbol{\theta} + \boldsymbol{m}_0(V,\rho) = [\boldsymbol{F}(V,\rho)\ \boldsymbol{m}_0(V,\rho)] \begin{bmatrix} \boldsymbol{\theta} \\ 1 \end{bmatrix} = \boldsymbol{T}\,\overline{\boldsymbol{\theta}}, \tag{4}$$

where $\boldsymbol{F}$ and $\boldsymbol{m}_0$ are model coefficients that depend on wind speed V and air density ρ. The dependency on wind speed is taken into account by discretizing the wind speed range in nodal values and linearly interpolating the model based on the current wind speed, while density is accounted for as explained in §2.2.1. The load vector $\boldsymbol{m}$ is defined as

$$\boldsymbol{m} = \left\{m_{1\mathrm{c}}^{\mathrm{OP}},\ m_{1\mathrm{s}}^{\mathrm{OP}},\ m_{1\mathrm{c}}^{\mathrm{IP}},\ m_{1\mathrm{s}}^{\mathrm{IP}}\right\}^T, \tag{5}$$

where m indicates the blade bending moment, subscripts $(\cdot)_{1\mathrm{s}}$ and $(\cdot)_{1\mathrm{c}}$ respectively indicate 1P sine and cosine harmonic amplitudes, while superscripts $(\cdot)^{\mathrm{OP}}$ and $(\cdot)^{\mathrm{IP}}$ indicate out- and in-plane load components, respectively. Harmonic components are obtained from measured blade loads using the Coleman transformation (Coleman and Feingold, 1958), followed by low pass filtering.

The model coefficients $\boldsymbol{F}$ are not all independent, because of the rotational symmetry of the rotor (Bertelè et al., 2019). In a nutshell, the effects on loads caused by the horizontal shear are the same as the ones caused by the vertical shear after a rotation of $\pi/2$; the same holds true for the wind misalignment angles. This not only reduces the number of unknowns, but also eases the identification of the model. In fact, whereas vertical shear changes naturally over a significant range (for example, because of diurnal fluctuations), horizontal shear does not (except in waked conditions). Similarly, whereas yaw misalignment changes significantly in normal operation because of the inability of the yaw system to immediately and exactly track wind direction fluctuations, upflow changes little (except that for orographic wind-direction-dependent effects). Therefore, a complete model can be identified simply from variable vertical shear and horizontal misalignment, because the effects of the other two wind states are obtained by the symmetry of the coefficients.

The model coefficients $\boldsymbol{T}$ are identified by stacking side by side measured wind states $\boldsymbol{\theta}$ into a matrix $\boldsymbol{\Theta} = [\overline{\boldsymbol{\theta}}_1, \ldots, \overline{\boldsymbol{\theta}}_N]$, while the corresponding measured blade loads $\boldsymbol{m}$ are stacked into matrix $\boldsymbol{M} = [\boldsymbol{m}_1, \ldots, \boldsymbol{m}_N]$, obtaining

$$\boldsymbol{M} = \boldsymbol{T}\boldsymbol{\Theta}. \tag{6}$$

https://doi.org/10.5194/wes-2020-83
Preprint. Discussion started: 9 July 2020

eawe european academy of wind energy
Open Access WIND ENERGY SCIENCE DISCUSSIONS

The model coefficients are then computed by least squares as

$$\boldsymbol{T} = \boldsymbol{M}\boldsymbol{\Theta}^T(\boldsymbol{\Theta}\boldsymbol{\Theta}^T)^{-1}. \tag{7}$$

Given the model coefficients, the estimated wind states $\boldsymbol{\theta}_{\mathrm{E}}$ are computed online from the measured loads $\boldsymbol{m}_{\mathrm{M}}$ as

$$\boldsymbol{\theta}_{\mathrm{E}} = \left(\boldsymbol{F}^T\boldsymbol{Q}^{-1}\boldsymbol{F}\right)^{-1}\boldsymbol{F}^T\boldsymbol{Q}^{-1}(\boldsymbol{m}_{\mathrm{M}} - \boldsymbol{m}_0), \tag{8}$$

where $\boldsymbol{Q}$ is the co-variance weighting matrix.

2.2.1 Density correction

Aerodynamic loads can be written as

$$m_{\mathrm{A}} = qAC, \tag{9}$$

where $q = 1/2\rho V^2$ is the dynamic pressure, A the rotor disk area and C a non-dimensional coefficient. A correction for density can be simply obtained as

$$m_{\mathrm{A}_{\mathrm{ref}}} = m_{\mathrm{A}_{\mathrm{i}}}\frac{\rho_{\mathrm{ref}}}{\rho_i}, \tag{10}$$

where ρ_{ref} is a reference density, and ρ_i the density corresponding to measurement $m_{\mathrm{A}_{\mathrm{i}}}$.

However, blade load sensors measure not only aerodynamic loads but also the effects of inertia and gravity, which do not depend on air density. Inertial loads for a rotor spinning at constant rotor speed do not generate 1P harmonics, and hence do not appear in Eq. (4). On the other hand, gravitational terms generate 1P loads represented by the non-homogeneous term $\boldsymbol{m}_0$ in that same equation. According to Bertelè et al. (2017), this term can be written as

$$\boldsymbol{m}_0 = qA\boldsymbol{C} + \boldsymbol{g}. \tag{11}$$

The first term is a gravity-induced load due to the rotor deformation caused by aerodynamic loads; for example, if the blade bends under the push of thrust, the resulting deformation generates a non-null moment arm for gravity with respect to the blade root where the load sensor is located, resulting in a 1P load. This term is proportional to dynamic pressure and can be corrected for density. The second term $\boldsymbol{g}$ accounts for in-plane and out-of-plane gravity-induced loads, the latter being caused by blade precone, prebend and rotor uptilt. This term does not depend on density, and hence it should be eliminated by the equations before a density correction can be applied. To this end, the model coefficients of Eq. (4) were identified for a very low wind speed, just above cut-in. Here the effects caused by $qA\boldsymbol{C}$ are negligible, and hence $\boldsymbol{g} \approx \boldsymbol{m}_0$. Having first identified the gravity term $\boldsymbol{g}$ and then having eliminated it from model (4), each measured load was finally corrected for density using Eq. (10).

2.3 Wind parametrization in the field

Before wind states can be estimated at run time from measured loads using Eq. (8), the model coefficients must be identified through the simultaneous measurements of wind states and associated loads using Eq. (7). This section presents a practical

https://doi.org/10.5194/wes-2020-83
Preprint. Discussion started: 9 July 2020

eawe european academy of wind energy
Open Access WIND ENERGY SCIENCE DISCUSSIONS

method to perform this task, based on the use of a standard IEC-compliant (IEC, 2017) hub-tall met-mast. A similar procedure could be used to identify the observer for a specific wind turbine type. Having obtained the model coefficients, one should be able to use the same observer for other installations of that same wind turbine type. Although there is yet no direct demonstration of this assertion, it seems reasonable to assume that wind turbines of the same model will have a similar 1P response to shears and misalignment angles. Additionally, Bottasso and Riboldi (2015) showed that the method is fairly robust to changes in some of the wind turbine parameters that may vary among different installations of a same wind turbine type, including changes in the stiffness of foundations, orographic effects, imbalance due to pitch misalignment, miscalibration of the load sensors and changes in airfoil lift and drag due to soiling/erosion.

2.3.1 Test site

Figure 2 shows a panoramic view of the test site (Bromm et al., 2018), which is located in Germany a few kilometers inland from the Baltic Sea and characterized by gentle hills, open fields and forests. Data was measured between October 19 and November 29, 2017 on a 3.5 MW eno114 turbine designed and produced by eno energy systems GmbH. The turbine (labelled WT1 in the figure) has a 92 m hub height and a rotor radius of 114.9 m.

A met-mast is situated at about 2.5 diameters (D) from the turbine. Wind direction was measured at a height above ground of 89.3 m with a Thies GmbH wind vane, while wind speed measurements were obtained with three cup anemometers produced from the same company and located at 89.3 m, 91.5 m and at the lower tip of the rotor (about 34 m).

A second turbine (labelled WT2) is also present on site, and its wake affects the met-mast and WT1 for easterly and south-easterly winds. Similarly, the wake of WT1 affects the met-mast for northern wind directions. All these conditions were discarded from the training dataset, in addition to all other situations when WT1 was not in a normal power production state. A forest of 15-20 m tall trees is located 300 m east of WT1; as only wind directions $\Gamma \in [180, 340]$ deg were considered in this work, this high roughness area was never in the inflow direction. On the other hand, the town of Brusow is located about 1 km to the west of the site, and its effects on the inflow are unknown. A test campaign conducted at the same site in the period July-November of the previous year revealed an almost equal distribution of unstable, neutral and stable conditions, as measured by an eddy covariance station (Bromm et al., 2018).

Synchronized turbine and blade load data was sampled at 10 Hz on WT1. Blades 1 and 3 were equipped with strain gages, installed in close proximity of the blade roots and measuring both flapwise and edgewise bending components. The load on blade 2 was computed as the mean of the measurements of blades 1 and 3, shifted by $\pm\pi/3$. In general, sensors deployed in the field cannot be assumed to be always exactly calibrated, and they may suffer from a variety of issues that affect the quality of the measurements that they provide. To address this problem, it is useful to devise simple and practical ways to correct the measurements, even when the root cause of the problem is unknown. Here, consistent mismatches between the long-term mean readings of the two blade load sensors were observed; this problem was eliminated by scaling the measurements as $\overline{m}_1(1+s) = \overline{m}_3(1-s)$, with $s = 0.0274$. Additionally, the azimuth signal was corrected to account for sensor bias and dynamic effects, as explained in Schreiber et al. (2020). The turbine on-board wind vane was not used here, because these

https://doi.org/10.5194/wes-2020-83
Preprint. Discussion started: 9 July 2020

eawe european academy of wind energy
Open Access WIND ENERGY SCIENCE DISCUSSIONS

sensors typically require a careful calibration to correct for nacelle and rotor effects. The yaw encoder signal was also corrected for an apparent inconsistency of its readings, as explained later in this section.

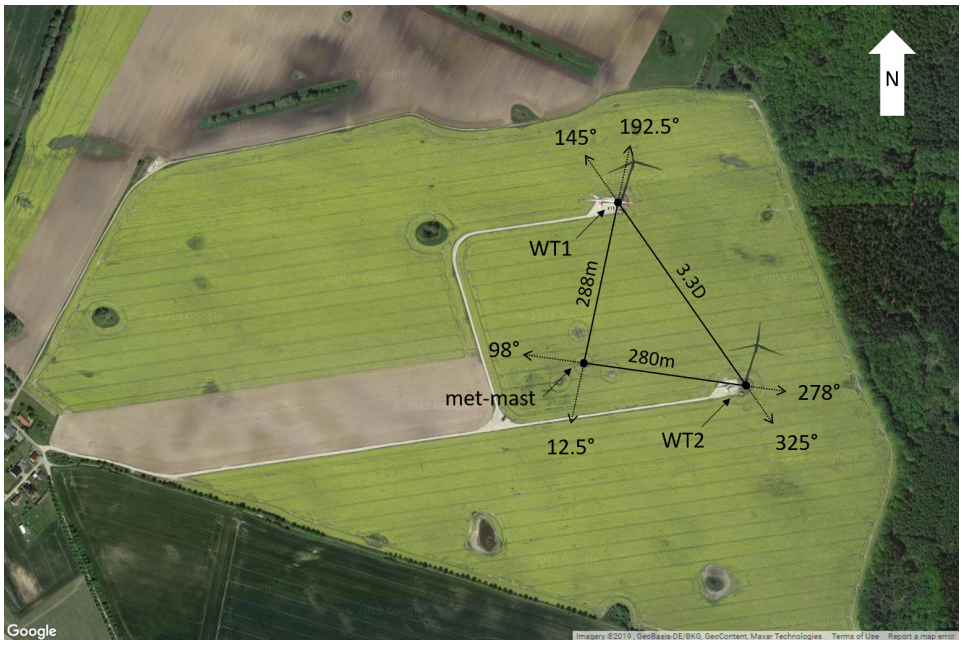

Figure 2. Satellite view of the test site, including waking directions and distances. WT1 indicates the turbine used for the present analysis (© Google Maps).

2.3.2 Wind shears

The met-mast present at the test site reaches only up to hub height; this is also the typical case of IEC-compliant met-masts used for certification (IEC, 2017). The three anemometers at 34, 89 and 92 m can be used to estimate the shear over the lower half of the rotor, which however in general differs from the shear computed over the whole rotor height.

To address this issue, the sector-effective wind speed (SEWS) estimation method described in Schreiber et al. (2020) was employed. In a nutshell, the blades are used as local speed sensors that, scanning the rotor disk, provide average speeds over four rotor quadrants. By using the two lateral and the lower quadrants, the shear over the lower part of the rotor disk can be computed. This quantity is validated with respect to the shear measured by the met-mast, assumed as a ground truth. Then, having verified a good correlation between the measured and estimated shears over the lower part of the rotor, the average speeds for all four quadrants are used to calculate the wind shear over the whole rotor disk. A brief overview of the SEWS estimator is reported next, and the interested reader is referred to Schreiber et al. (2020) for further details.

https://doi.org/10.5194/wes-2020-83
Preprint. Discussion started: 9 July 2020

eawe european academy of wind energy
Open Access WIND ENERGY SCIENCE DISCUSSIONS

The rotor cone coefficient is defined as

$$C_m\left(\beta,\lambda,q,\psi_i\right)=\frac{m_i}{0.5\rho A R V^2}, \tag{12}$$

where β is the pitch angle, $\lambda=\Omega R/V$ the tip speed ratio and Ω the rotor speed, m_i the out-of-plane bending load of the ith blade and ψ_i its azimuthal position. Coefficient C_m was computed here with the aeroelastic code FAST (Jonkman and Jonkman, 2018). Inverting Eq. (12), a look-up table (LUT) is generated that returns the blade-effective wind speed V_i given measured blade pitch angle, rotor speed, azimuthal blade position, bending moment and density:

$$V_i=\mathrm{LUT}_{C_m}\left(\beta,\Omega,\psi,m_i,\frac{\rho}{\rho_{\mathrm{ref}}}\right). \tag{13}$$

This way each individual blade is turned into a local wind speed sensor, which scans the rotor disk. Since this local measurement is noisy, the rotor disk is divided into sectors of area A_{S}, and a sector-equivalent wind speed is computed as

$$V_{\mathrm{S}}=\int_{A_{\mathrm{S}}} V_i(\psi_i)\,\mathrm{d}A_{\mathrm{S}}. \tag{14}$$

Here the four sectors shown in Fig. 3 were used. This yields four measurements of the local speed at the rotor disk, located at $2/3\,R$ above, below and to the sides of the hub center (Bottasso et al., 2018).

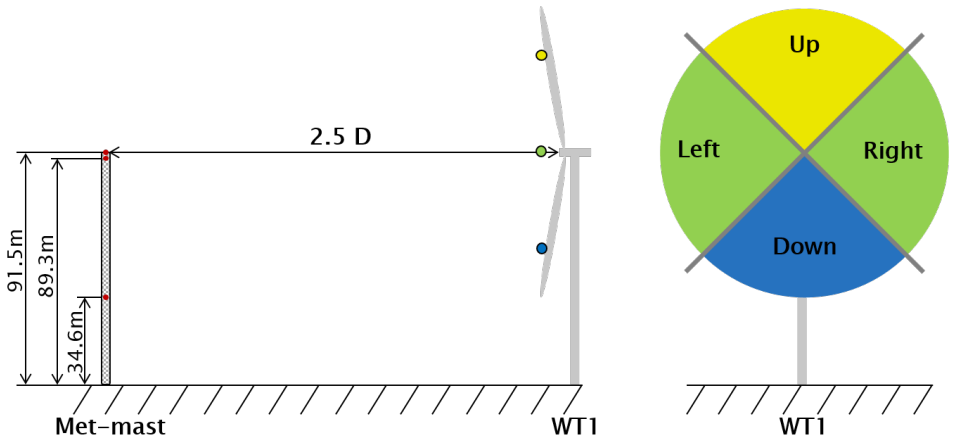

Figure 3. Definition of the four rotor sectors and their relative position with respect to the met-mast. Right: view looking downstream.

The rotor-effective horizontal linear shear can be computed inserting the sector-effective wind speeds in Eq. (1) to get

$$\kappa_h=\frac{3}{2}\frac{V_{\mathrm{S,left}}-V_{\mathrm{S,right}}}{V_{\mathrm{S,left}}+V_{\mathrm{S,right}}}. \tag{15}$$

For a more coherent comparison of the linear vertical shears estimated by the met-mast and by the sector-effective speeds, it is useful to first fit a power law to the respective wind speed measurements, as they are obtained at different heights above

https://doi.org/10.5194/wes-2020-83
Preprint. Discussion started: 9 July 2020

eawe european academy of wind energy
Open Access WIND ENERGY SCIENCE DISCUSSIONS

ground. The power law profile is defined as

$$V(z)_{\mathrm{PL}} = V_{\mathrm{ref}} \left(\frac{z+H}{H} \right)^{\alpha}, \tag{16}$$

where H is the height of the hub, V_{ref} the wind speed at that point, and α the power law exponent. Given n measurements V_i at z_i, the parameters of the power law are computed by the following best fit:

$$(V_{\mathrm{ref}}, \alpha) = \arg \min_{V_{\mathrm{ref}}, \alpha} \sum_{i=1}^{n} \left(V_{\mathrm{PL}}(z_i) - V_i \right)^2. \tag{17}$$

Notice that two measurements at two different heights are sufficient to estimate the power law. Having solved the fitting problem (17), the linear shear κ_v between heights z_A and z_B is computed as

$$\kappa_v = \frac{R(V_{\mathrm{PL}}(z_A) - V_{\mathrm{PL}}(z_B))}{z_A V_{\mathrm{PL}}(z_B) - z_B V_{\mathrm{PL}}(z_A)}. \tag{18}$$

The left plot of Fig. 4 shows the correlation between 10-min averages of the vertical shears obtained by the met-mast and by the sector-effective wind speeds on the lower half of the rotor. Only wind directions between 170 and 220 deg are considered, where the turbine and met-mast are aligned. The power law for the met-mast was obtained by using all three speed measurements, although the two at 89.3 and 91.5 m above ground are almost coincident. For the sector-effective estimator the power law was obtained by using the two measurements $(V_{\mathrm{S,left}} + V_{\mathrm{S,right}})/2$ at $z = 0$, and $V_{\mathrm{S,down}}$ at $z = -2/3\,R$. For both cases, the lower-half-rotor linear shear was computed from Eq. (18) using $z_A = 0$ and $z_B = -R$ and the corresponding fitted power law. The figure shows that there is a good correlation between the two lower-half-rotor shears, resulting in a Pearson's coefficient of 0.906. However, the figure also shows that the linear fit (red dashed line) has a different slope than the ideal match (black solid line). The results presented later in Section 3 were corrected to account for this error.

For the same data points, the right plot of Fig. 4 shows the correlation between the vertical shears obtained by the met-mast and by the sector-effective estimator over the complete rotor. Here again the power law for the met-mast was obtained by using all three speed measurements. For the sector-effective estimator the power law was obtained by using the three measurements $V_{\mathrm{S,up}}$ at $z = 2/3\,R$, $(V_{\mathrm{S,left}} + V_{\mathrm{S,right}})/2$ at $z = 0$, and $V_{\mathrm{S,down}}$ at $z = -2/3\,R$. For both cases, the full-rotor linear shear was computed from Eq. (18) using $z_A = R$ and $z_B = -R$ and the corresponding power laws. It should be noted that, since the height of the top anemometer reaches only up to hub height, for the met-mast the calculation of the full rotor shear implies a considerable extrapolation outside of the available measurements.

Comparison of the right and left plots of Fig. 4 shows that in the full-rotor case there is a lower correlation between the met-mast and the SEWS observer than in the lower-half rotor case. This indicates that the shear changes over the height of the rotor disk. In addition, as expected for a typical power law where the profile gradient increases with height, the lower-half-shear coefficient is typically higher than the full-rotor one.

Based on these results, it appears that the rotor-effective shear used for identifying the model of §2.2 would require a tall met-mast or other wind measurement devices such as lidars or sodars capable of scanning the inflow reaching the top of the rotor. Here —as such a tall mast was not available— an alternative approach was used: the sector-equivalent wind speed method was used to virtually extend the met-mast measurements to the required height. Based on the good correlation shown by the

https://doi.org/10.5194/wes-2020-83
Preprint. Discussion started: 9 July 2020

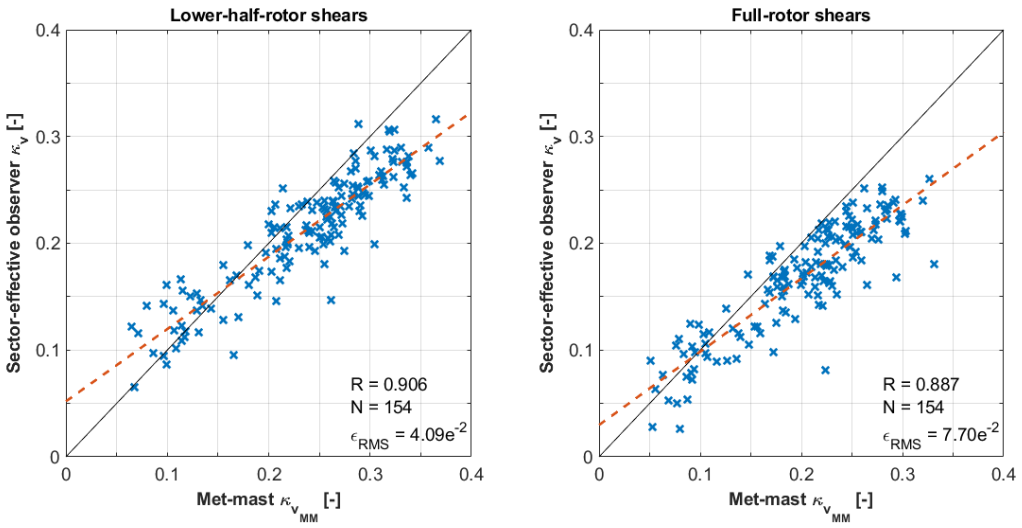

Figure 4. Correlation between 10-min averages of the vertical linear shears measured with the met-mast and the sector-effective observer. Left: lower-half rotor shears; right: full-rotor shears. Red dashed line: linear best fit; black dashed line: ideal match; R: Pearson's correlation coefficient; N: number of data points; ϵ_{RMS}: root mean square error.

left plot of Fig. 4 for the lower-half-rotor shear, it was concluded that the two lateral and the lower sector-equivalent speeds are sufficiently accurate for the purpose of estimating shears. Since the top sector speed is based on exactly the same calculation procedure as the other ones, all four speeds were then used to estimate the full-rotor shear, which in turn was used as reference for the identification of the model of §2.2.

Unfortunately a similar validation cannot be performed for the horizontal shear with the present met-mast, because of the lack of multiple lateral measurements. However, the horizontal shear is based on the same sector-equivalent wind speeds that estimate the vertical shear with good accuracy, so that there is no reason to believe that Eq. (15) should not provide a similarly good-quality estimate. Additionally, the horizontal shear based on the two lateral sector-effective wind speeds was shown in Schreiber et al. (2020) to track the movement of an impinging wake with remarkable accuracy.

2.3.3 Wind misalignment angles

The met-mast is equipped with a single wind vane measuring the wind direction Γ at hub height. Unfortunately, this means that only a point-wise measurement is available, instead of the rotor-equivalent one that would be ideally necessary for the training of the load-harmonic method of §2.2. This is a limit of the current setup and of the present attempt at validating the approach. Nonetheless, a pragmatic choice was made here to filter the wind vane signal with a moving average to remove the faster fluctuations, and to use this signal as a proxy for the rotor-effective horizontal wind direction. The misalignment angle between turbine and wind was obtained by subtracting the absolute yaw angle of the nacelle from the met-mast-measured

https://doi.org/10.5194/wes-2020-83
Preprint. Discussion started: 9 July 2020

eawe european academy of wind energy
Open Access WIND ENERGY SCIENCE DISCUSSIONS

wind direction. The result was shifted in time on account of the distance between turbine and met-mast, the time delay being computed from the average wind speed.

The top plot of Fig. 5 shows 10-min averages of the resulting met-mast yaw misalignment angle Φ_{MM}, plotted as a function of wind direction Γ. The clear trend visible in the plot is probably due to a miscalibration of the nacelle yaw encoder. Indeed, Bromm et al. (2018) also noticed a non-constant offset when comparing the turbine SCADA orientation with the one provided by a temporarily installed GPS system. This trend was removed using the first ten days of data, excluding waked directions, obtaining the bottom plot of Fig. 5.

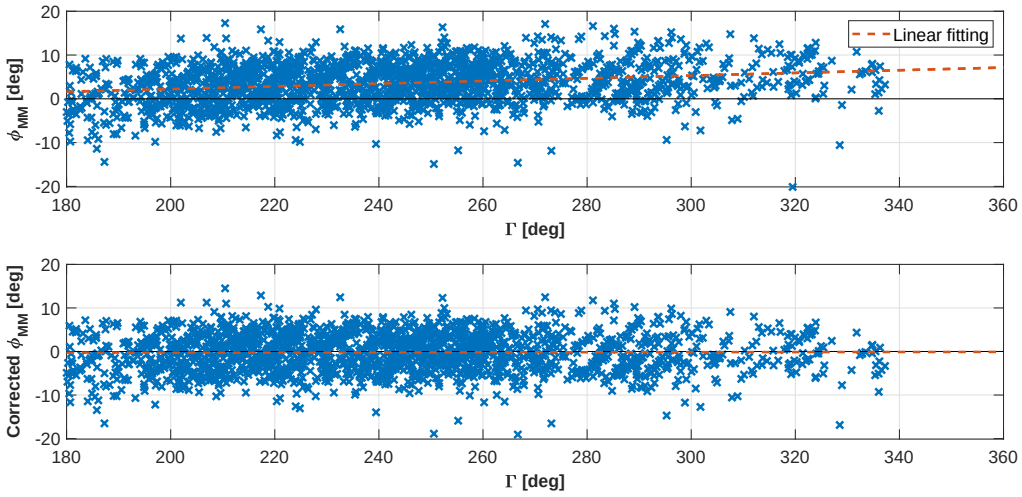

Figure 5. 10-min averages of met-mast horizontal wind misalignment angle ϕ_{MM} vs. wind direction at the met-mast Γ, before (top) and after (bottom) correction for yaw encoder error.

As the current setup does not provide for measurements of the upflow, the rotational symmetry of the rotor was used to compute the relevant model coefficients.

2.3.4 Wind speed and density

Since the load-wind model expressed by Eq. (4) depends on the operating conditions, a rotor-effective wind speed was computed with the torque balance equation (Ma et al., 1995; Van der Hooft and Engelen, 2004; Soltani et al., 2013; Schreiber et al., 2020) and used as scheduling parameter of the wind observer. Figure 6 shows an excellent correlation for the 10-min averages of the computed rotor-effective wind speed and the met-mast hub-height speed. Density was obtained from the ideal gas law based on temperature, since no additional information was available, and was used to rescale the load measurements.

https://doi.org/10.5194/wes-2020-83
Preprint. Discussion started: 9 July 2020

eawe european academy of wind energy
Open Access WIND ENERGY SCIENCE DISCUSSIONS

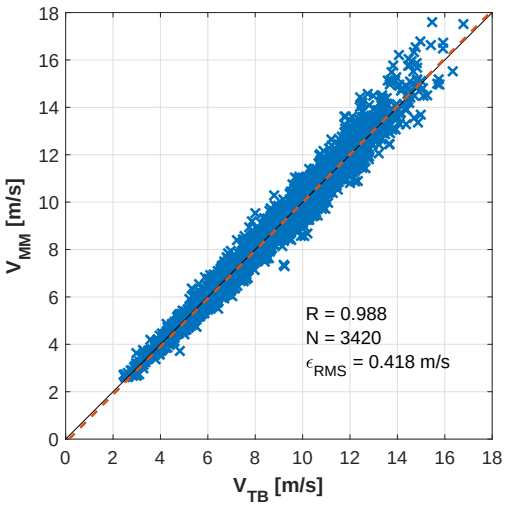

Figure 6. Correlation between 10-min averages of met-mast hub-height wind speed V_{MM} and rotor-effective wind speed V_{TB} estimated with the torque balance equation. Red dashed line: linear best fit; black dashed line: ideal match; R: Pearson's correlation coefficient; N: number of data points available; ϵ_{RMS}: root mean square error.

3 Results

3.1 Model identification

The observer coefficients were identified with Eq. (7) using the horizontal and vertical shears obtained from the sector-effective wind speeds, and the yaw misalignment angle computed from the met-mast wind vane and the nacelle yaw encoder, corrected according to Fig. 5. The upflow model coefficients were obtained from the rotational symmetry of the rotor behavior. The model coefficients were scheduled as functions of the rotor-effective wind speed computed from the torque balance equation, and load measurements were corrected for density.

The model was identified based on 10-min averages. The wind speed nodes of the linear parameter varying model (4) were defined as $V = [4,\ 5,\ 6.5,\ 8,\ 9,\ 10,\ 12,\ 13.5]$ m/s, while the reference density was set to 1.238 kg/m^3. Table 1 shows the range covered by each parameter within the training dataset.

About 15% of the available data was used for identification, leaving about 370 hours of measurements for validation. In the following, the performance of the harmonic observer is evaluated solely based on the validation dataset.

A similar identification was also performed using the same training set, but using instantaneous 10 Hz measurements instead of 10-min averages. As this led to a small decrease in model performance, it was concluded that some time averaging may be beneficial as it probably alleviates the effects of possible outliers.

https://doi.org/10.5194/wes-2020-83
Preprint. Discussion started: 9 July 2020

eawe european academy of wind energy
Open Access WIND ENERGY SCIENCE DISCUSSIONS

Table 1. Minimum and maximum values of rotor effective wind speed, turbulence intensity (TI), density, yaw misalignment, vertical and horizontal shear within the training dataset.

	V [m/s]	TI [%]	ρ [kg/m^3]	ϕ_{MM} [deg]	κ_v [-]	κ_h [-]
min	3.89	1.15	1.221	-12.66	-0.045	-0.053
max	13.68	11.06	1.256	8.28	0.242	0.087

3.2 Wind observer performance

Figure 7 gives an overview of the model performance in terms of correlations between 10-min averages of reference and observed parameters, using the validation sub-set for wind speeds above 8 m/s. For each parameter, one per subplot, the reference state is shown on the x axis, whereas the observed one on the y axis. For the shears, the Pearson's correlation coefficients (R) is above 0.9, and the root mean square (RMS) error ϵ_{RMS} is of the order of 10^{-3}. The yaw misalignment angle is less accurate, possibly because the reference is point-wise whereas the estimate is rotor-effective. Indeed, investigations at the same site with a more complete setup including a lidar profiler reported significant veer at the inflow (Bromm et al., 2018). However, with a correlation coefficient of 0.85 and an ϵ_{RMS} of 1.9 deg, the matching is still good.

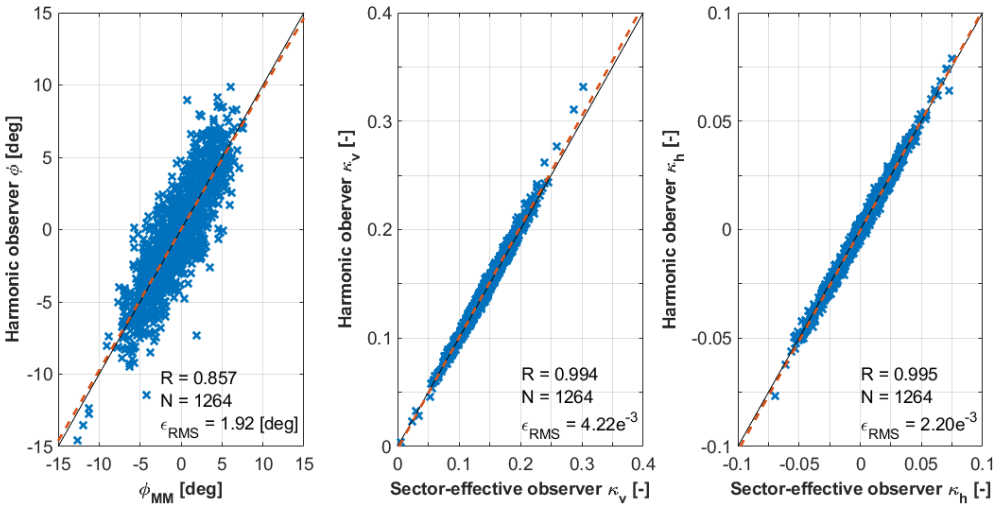

Figure 7. Correlation of 10-min averages between estimated parameters (y axis) and their reference quantities (x axis) for $V \geq 8$ m/s. From left to right: yaw misalignment angle, vertical linear shear, horizontal linear shear. Red dashed line: linear best fit; black dashed line: ideal match; R: Pearson's correlation coefficient; N: number of data points; ϵ_{RMS}: root mean square error.

It is very interesting to observe that, although the model was trained only with 10-min averages, it is still able to provide for time-resolved estimates of the parameters. To illustrate this fact, Fig. 8 reports a 10 Hz time history of the vertical shears from

https://doi.org/10.5194/wes-2020-83
Preprint. Discussion started: 9 July 2020

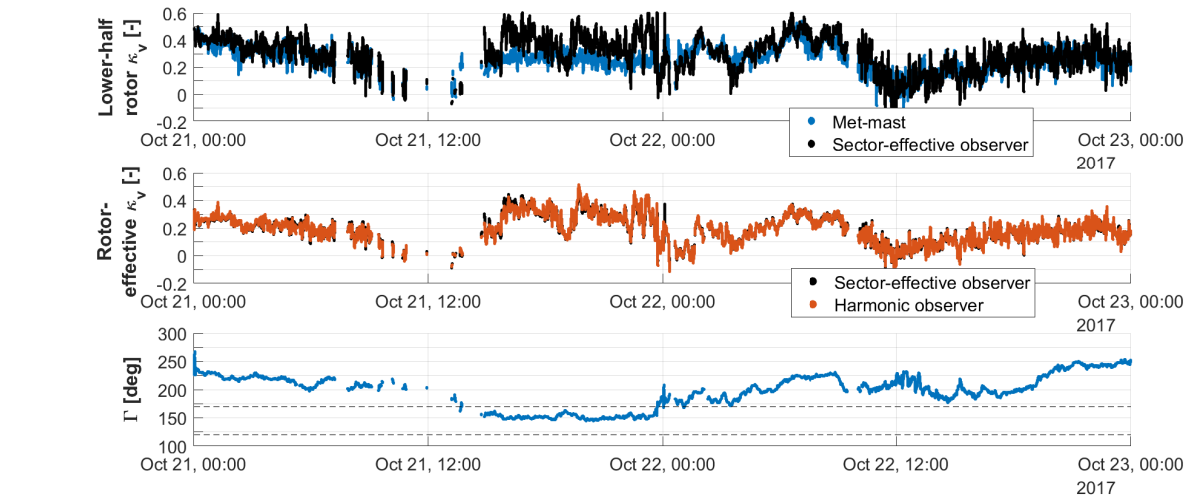

Figure 8. Time history of vertical shears at 10 Hz. From top to bottom: lower-half-rotor shear from the met-mast (blue) and the sector-effective observer (black); full-rotor-equivalent shear using Eq. (8) (red) and reference from the sector-effective observer (black); wind direction measured at the met-mast, with WT1 in the wake of WT2 between 120 and 170 deg (dashed horizontal lines).

To provide for a more complete statistical characterization of the observer performance, the 10-min data points were binned for the various relevant parameters. For each bin, the mean absolute error (MAE) between the estimated θ_{E} and reference θ_{R} wind parameter was computed as $\epsilon = 1/N \sum_i^N |\boldsymbol{\theta}_{\mathrm{R}_i} - \boldsymbol{\theta}_{\mathrm{E}_i}|$.

Figure 9 shows the MAE ϵ for yaw misalignment (top left), vertical and horizontal shear (top and bottom right, respectively), plotted as functions of binned wind speed, for various binned turbulence intensity (TI) levels. The number of available hours of data is reported in the bottom left histogram of the figure, to help determine the statistical significance of the results. Looking

https://doi.org/10.5194/wes-2020-83
Preprint. Discussion started: 9 July 2020

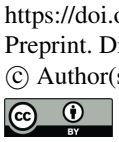

eawe european academy of wind energy
Open Access WIND ENERGY SCIENCE DISCUSSIONS

at the yaw angle results, it appears that the maximum error is about 3 deg and that accuracy tends to increase for higher wind speeds. Moreover, TI appears to play only a small effect on the results. The error in the vertical shear includes the error between the met-mast and the sector-effective observer of §2.3.2. Even in this case the error is small, and effects of TI are present but relatively mild. The figure also reports the horizontal shear, whose error —although very small— might not be very indicative, as no reference value was available from the met-mast for this quantity.

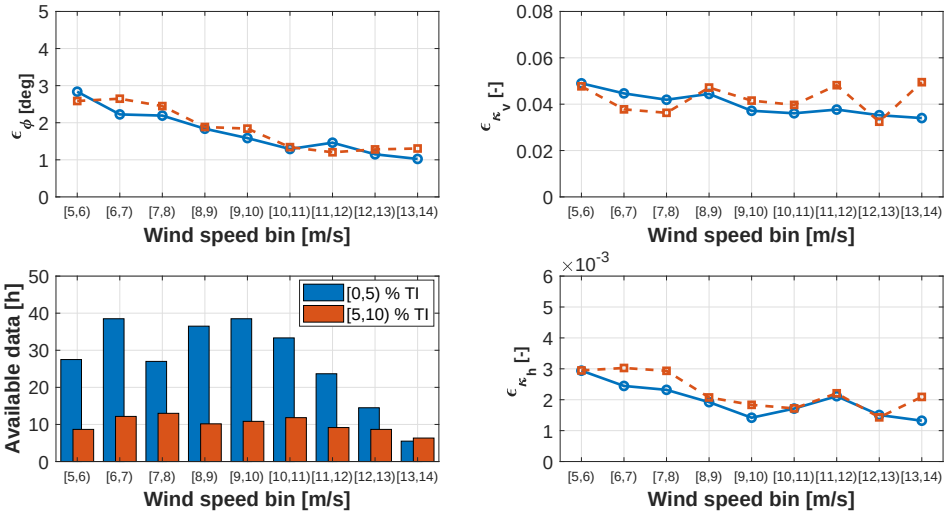

Figure 9. MAE ϵ vs. binned rotor-effective wind speed, for binned TI. Top left: yaw misalignment; top right: vertical shear; bottom right: horizontal shear; bottom left: hours of available data.

Figure 10 reports the results for varying binned air density. The plots show that the density correction of §2.2.1 is not perfect, probably because of an only approximate identification of the gravity term in Eq. (11).

Finally, Fig. 11 reports the results for varying wind direction. Looking at the vertical shear, the best results are obtained for wind directions between 170 and 210 deg, when turbine and met-mast are aligned, whereas the error increases significantly for other wind directions. When turbine and met-mast are not aligned, the two can be subjected to slightly different inflows, on account of orographic and vegetation-induced effects. This indicates once again that, as noted earlier on, the information provided by the reference met-mast cannot be regarded as an absolute ground truth. The yaw misalignment angle seems to be less influenced by these local effects, which might induce stronger local changes in shear than in direction at this particular site.

https://doi.org/10.5194/wes-2020-83
Preprint. Discussion started: 9 July 2020

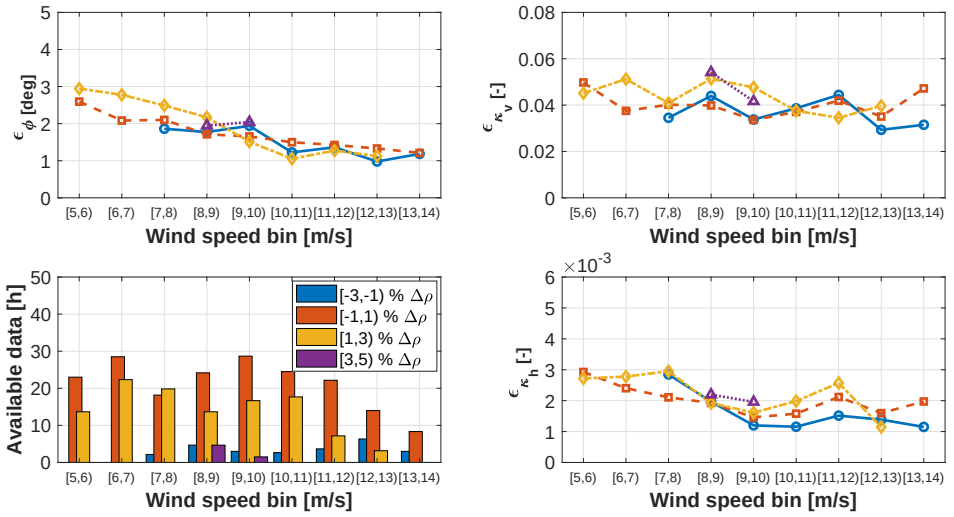

Figure 10. MAE ϵ vs. binned rotor-effective wind speed, for binned density change $\Delta\rho$ wrt. standard air. Top left: yaw misalignment; top right: vertical shear; bottom right: horizontal shear; bottom left: hours of available data.

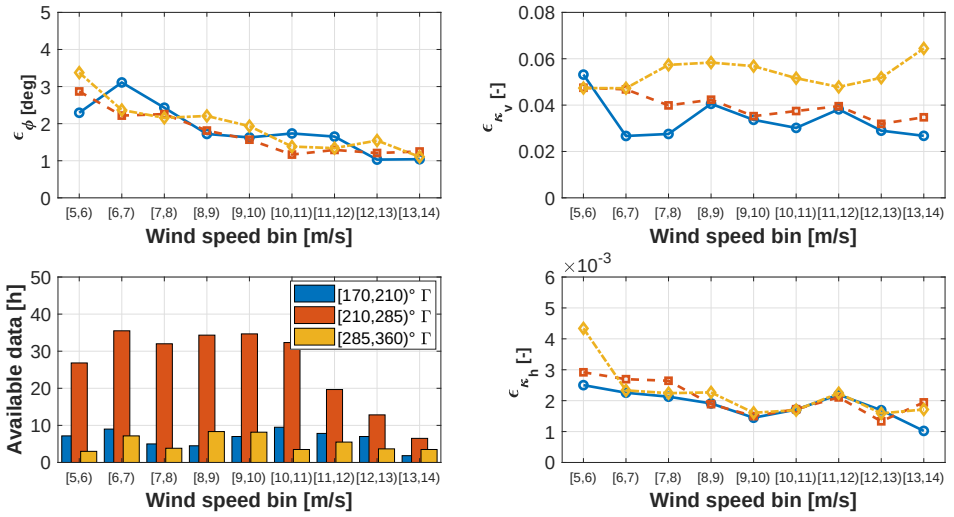

Figure 11. MAE ϵ vs. binned rotor-effective wind speed, for binned wind direction Γ. Top left: yaw misalignment; top right: vertical shear; bottom right: horizontal shear; bottom left: hours of available data.

https://doi.org/10.5194/wes-2020-83
Preprint. Discussion started: 9 July 2020

eawe european academy of wind energy
Open Access WIND ENERGY SCIENCE DISCUSSIONS

4 Conclusions

This paper has presented the application of a previously published harmonic-based wind sensing method to an experimental dataset. The setup at the test site is not complete enough to provide for a true field validation of the method. However, it is representative of a practical scenario where, by using a hub-tall certification met-mast, the method is trained for a given turbine model, before being deployed on assets of that same type at other production sites. After having explained the methodology and described the test site, the paper has also formulated a new method to extend the shear measured by a hub-tall mast to the tip of the rotor, in order to compute a full-rotor shear.

Based on the results analyzed herein, and notwithstanding the limits of the present dataset, the following conclusions can be drawn:

- There is a good correlation between met-mast and estimated lower-half rotor shears;
- There is an excellent correlation between the full-rotor shear extended above the mast and the one estimated by harmonic loads;
- Training with 10-min data improves the quality of the estimates with respect to the case where a much larger set of higher-sampling-frequency data points are used.
- Notwithstanding a training based on 10-min averages, the quality of the correlation between estimates and references does not only apply to 10-min quantities, but it also extends to time-resolved 10 Hz signals. In this sense, the observer seems capable of following relatively fast changes in shear. This might be useful for certain application scenarios, as for example the tracking of horizontal shears induced by wake interactions.
- There is a non-negligible effect of wind-mast-turbine non-exact alignment. In this sense, the actual quality of the correlation might be even better than what appears from the results shown here. This is in fact an intrinsic limit of field testing, where an exact ground truth is in general difficult if not impossible to obtain. Realistic simulations and wind tunnel studies as the ones reported in Bertelè et al. (2017, 2018, 2019) —where the ground truth is known— may help in this sense.
- Yaw misalignment is also estimated with reasonable quality, although the results here are less conclusive due to the fact that the met-mast reference is a point-wise measurement that might not fully represent rotor-effective conditions.
- There is only a modest effect of TI, which supports the hypothesis that 1P harmonics are mostly driven by “deterministic” wind characteristics and less affected by turbulent fluctuations.
- Notwithstanding the complicated effect of gravity on harmonic load components, its presence can be eliminated with enough accuracy to allow for a reasonably precise density correction.

A continuation of this work would greatly benefit from access to a more complete dataset, without the limits discussed above. Multiple, independent rotor-effective measurements of the inflow in very close proximity of the rotor disk would be

https://doi.org/10.5194/wes-2020-83
Preprint. Discussion started: 9 July 2020

eawe european academy of wind energy
Open Access WIND ENERGY SCIENCE DISCUSSIONS

necessary to establish an effective ground truth. This would allow for a better characterization of the accuracy of this method, and to study the effects induced by training with a standard hub-tall mast. A remaining open point is the demonstration that the method can indeed be trained on a turbine and, then, applied to another machine of that same model at another site; although this seems to be a very reasonable assumption, the evidence that this is indeed possible is lacking. Finally, it remains to be shown that the method does not need to be re-trained for an aging turbine. Here again, based also on the reassuring results already reported by Bottasso and Riboldi (2015), it is difficult to believe that 1P loads might change over time to the point of affecting the estimates, although a field proof of this assertion is clearly missing at this point in time.

Acknowledgements. The authors express their gratitude to Stefan Bockholt and Alexander Gerds of eno energy systems GmbH, who granted access to the measurement data and turbine model, and to Marijn van Dooren, Anantha Sekar and Martin Kühn of ForWind Oldenburg, who shared insight on the data. This work has been supported by the CompactWind II project (FKZ: 0325492G), which receives funding from the German Federal Ministry for Economic Affairs and Energy (BMWi).

Nomenclature

A	Rotor area
C_m	Cone coefficient
H	Height of the hub above ground
m	Blade bending moment
$\boldsymbol{m}$	Vector of moment harmonics
N	Number of available data points
q	Dynamic pressure
R	Rotor radius or Pearson's coefficient
$\boldsymbol{Q}$	Covariance matrix
V	Wind speed
V_h	Wind speed at hub height
V_S	Sector-effective wind speed
V_{TB}	Torque-balance rotor-effective wind speed
$\tilde{v}$	Non-dimensional tangential cross flow at hub height
$\tilde{w}$	Non-dimensional vertical cross flow at hub height
x, y, z	Hub-centered nacelle-attached axes
β	Pitch angle
Γ	Wind direction
ϵ	Mean absolute error
$\boldsymbol{\theta}$	Wind state vector

https://doi.org/10.5194/wes-2020-83
Preprint. Discussion started: 9 July 2020

eawe european academy of wind energy
Open Access WIND ENERGY SCIENCE DISCUSSIONS

κ_h	Horizontal shear
κ_v	Vertical shear
λ	Tip speed ratio
ρ	Air density
ϕ	Yaw misalignment angle
χ	Upflow angle
ψ	Azimuth angle
Ω	Rotor speed
$(\cdot)^T$	Transpose
$(\cdot)^{\mathrm{IP}}$	In-plane component
$(\cdot)^{\mathrm{OP}}$	Out-of-plane component
$(\cdot)_{\mathrm{1c}}$	1P cosine amplitude
$(\cdot)_{\mathrm{1s}}$	1P sine amplitude
$(\cdot)_{\mathrm{E}}$	Estimated quantity
$(\cdot)_{\mathrm{MM}}$	Met-mast measurement
$(\cdot)_{\mathrm{ref}}$	Reference quantity
$(\cdot)_{\mathrm{RMS}}$	Root mean square
1P	Once per revolution
MAE	Mean absolute error
Lidar	Light detection and ranging
LUT	Look-up table
RMS	Root mean square
SEWS	Sector-effective wind speed
Sodar	Sound detection and ranging
TI	Turbulence intensity
WT	Wind turbine

https://doi.org/10.5194/wes-2020-83
Preprint. Discussion started: 9 July 2020

eawe european academy of wind energy
Open Access WIND ENERGY SCIENCE DISCUSSIONS

References

Bertelè, M., Bottasso, C.L., Cacciola, S., Daher Adegas, F. and Delport, S.: Wind inflow observation from load harmonics, Wind Energ. Sci., 2, 615–640, doi:10.5194/wes-2-615-2017, 2017.

Bertelè, M., Bottasso, C.L., Cacciola, S.: Simultaneous estimation of wind shears and misalignments from rotor loads: formulation for IPC-controlled wind turbines, J. Phys. Conf. Ser., 1037 032007, doi:10.1088/1742-6596/1037/3/032007, 2018.

Bertelè, M., Bottasso, C.L. and Cacciola, S.: Wind inflow observation from load harmonics: wind tunnel validation of the rotationally symmetric formulation, Wind Energ. Sci., doi:10.5194/wes-2018-61, 2019.

Bertelè, M., Bottasso, C.L.: Initial results from the field testing of the "rotor as a sensor" concept, J. Phys. Conf. Ser., 1452 012074, doi:10.1088/1742-6596/1452/1/012074, 2020.

Bottasso, C.L. and Riboldi, C.E.D.: Estimation of wind misalignment and vertical shear from blade loads,Renew. Energ., 62, 293–302, doi:10.1016/j.renene.2013.07.021, 2014.

Bottasso, C.L. and Riboldi, C.E.D.: Validation of a wind misalignment observer using field test data, Renew. Energ., 74, 298–306, doi:10.1016/j.renene.2014.07.048, 2015.

Bottasso, C.L., Cacciola, S. and Schreiber, J.: Local wind speed estimation, with application to wake impingement detection, Renew. Energ., 116, 155–168, doi:10.1016/j.renene.2017.09.044, 2018.

Bottasso, C.L., Croce, A. and Riboldi, C.E.D.: Spatial estimation of wind states from the aeroelastic response of a wind turbine, The Science of Making Torque from Wind (TORQUE 2010), Heraklion, Crete, Greece, 28–30 June 2010.

Bromm, M., Rott, A., Beck, H., Vollmer, L., Steinfeld, G. and Kühn, M.: Field investigation on the influence of yaw misalignment on the propagation of wind turbine wakes, Wind Energy, 21, 1011–1028, doi:10.1002/we.2210, 2018.

Cacciola, S., Bertelè, M., Bottasso, C.L.: Simultaneous observation of wind shears and misalignments from rotor loads, J. Phys. Conf. Ser., 753(5),052002-1-8, doi:10.1088/1742-6596/753/5/052002, 2016.

Carswell, A.: Lidar measurements of the atmosphere, Canadian Journal of Physics, 6(2), 378–395, doi:10.1139/p83-049, 1983.

Coleman, R.P. and Feingold, A.M.: Theory of self-excited mechanical oscillations of helicopter rotors with hinged blades, Technical Report, NACA TN 1351, 1958.

Lang, S. and McKeogh, E.: LIDAR and SODAR Measurements of Wind Speed and Direction in Upland Terrain for Wind Energy Purposes, Remote Sensing, 3, 1871–1901, doi:10.3390/rs3091871, 2011.

International Electrotechnical Commission: DV IEC 61400-12-1, Technical Report, IEC, 2017.

Jonkman, J. and Jonkman, B.: FAST v7, https://nwtc.nrel.gov/FAST7, 2018.

Ma, X., Poulsen, N. and Bindner, H.: Estimation of Wind Speed in Connection to a Wind Turbine, Technical Report, Informatics and Mathematical Modelling, Technical University of Denmark, 1995.

Murphy, P., Lundquist, J. K., and Fleming, P.: How wind speed shear and directional veer affect the power production of a megawatt-scale operational wind turbine, doi:10.5194/wes-2019-86, 2019.

Schreiber, J., Cacciola, S., Campagnolo, F., Petrovic´, V., Mourembles, D., and Bottasso, C. L.: Wind shear estimation and wake detection by rotor loads — First wind tunnel verification, Journal of Physics: Conference Series, 753, 032 027, doi:10.1088/1742-6596/753/3/032027, 2016.

Schreiber, J., Bertelè, M., and Bottasso, C.L.: Field testing of a local wind inflow estimator and wake detector, Wind Energ. Sci. Disc., doi:10.5194/wes-2020-48, 2020.

https://doi.org/10.5194/wes-2020-83
Preprint. Discussion started: 9 July 2020

Simley, E. and Pao, L.Y.: Evaluation of a wind speed estimator for effective hub-height and shear components, Wind Energy, 19(1), 167–184, doi:10.1002/we.1817, 2016.

Soltani, M., Knudsen, T., Svenstrup, M., Wisniewski, R., Brath, P., Ortega, R. and Johnson, K.: Estimation of rotor effective wind speed: a comparison, IEEE Trans. Control Syst. Technol. 21 (4) 1155e1167, doi:10.1109/tcst.2013.2260751, 2013.

Van der Hooft, E. L. and Engelen, T.: Estimated wind speed feed forward control for wind turbine operation optimisation, European Wind Energy Conference & Exhibition (EWEC 2004), London, UK, 22–25 November 2004.

Vogt, S. and Thomas, P.: SODAR — A useful remote sounder to measure wind and turbulence, Journal of Wind Engineering and Industrial Aerodynamics, 54–55, 163–172, doi:10.1016/0167-6105(94)00039-G, 1995.

A.4 Paper IV: Non-deterministic wind observation from wind turbine loads

Reference: M. Bertelè, and C. L. Bottasso, "Non-deterministic wind observation from wind turbine loads," *Journal of Physics: Conference Series*, 1618 062022, 2020. doi: 10.1088/1742-6596/1618/6/062022.

Non-deterministic wind observation from wind turbine loads

M. Bertelè[1] **and C.L. Bottasso**[1]

[1] Wind Energy Institute, Technische Universität München, Garching bei München, Germany

E-mail: {marta.bertele, carlo.bottasso}@tum.de

Abstract. In this work, the wind sensing technology that exploits the turbine rotor as an anemometer is further developed into a non-deterministic formulation. First, an inflow-turbine response map is identified, which relates out and in-plane blade root bending moments to both vertical and horizontal shears and misalignments. Then, this linear model is used with and without a Kalman filter to estimate online the wind field at the rotor disk once blade loads are measured. A comprehensive simulation study, including different wind speeds and turbulence intensity levels, was performed to evaluate the accuracy of the new non-deterministic formulation. The results show that introducing a Kalman filter in the estimation process allows for a significant improvement in the angle estimates with respect to the deterministic formulation, with no considerable additional computational cost.

1. Introduction

Reliable and accurate measurements of the inflow conditions at the rotor disk are of significant importance both at the single turbine level as well as within a wind farm. To realign the rotor to the wind, decreasing in turn fatigue loads and increasing the harvested power, one must be aware of the horizontal wind direction. Such information is particularly valuable for wind farm control strategies as well, where one could also make use of the estimate of the impinging horizontal shear for wake detection. The wake recovery rate could be inferred from the level of stability of the atmosphere, which is strongly linked to the vertical shear exponent, but also information about the vertical wind direction could prove useful to characterize the flow in complex terrain.

To measure the wind inflow in the field, commonly used devices are nacelle anemometers and met-mast towers. While the first ones provide with a pointwise measurement of the wind speed and horizontal wind misalignment at the nacelle, the latter can also provide information about the vertical shear, since they are normally equipped with more measurement points over the height. Still, this information is representative of an inflow not co-located with the turbine, whereas the nacelle measurements have to be corrected for blade passing and interference with the nacelle. To characterize the free stream at the rotor disk as well as to measure also the vertical wind direction and the horizontal shear, one might use LiDARs, which are nevertheless still relatively costly and susceptible to weather conditions.

To overcome such issues and to ensure that inflow measurements are actually rotor-effective, i.e. measured at the rotor disk and over the rotor disk area, references [7, 2] have proposed to turn the rotor itself into an anemometer. Indeed, in [7, 2] the turbine response is linked to the spatial dis-homogeneity in the wind via a model so that, once the model itself has been

identified from either field data or simulations, it can be inverted and used to estimate the inflow conditions given measured loads. Such methodology with its different formulations has been validated with comprehensive simulations [7, 2, 3], in the wind tunnel [4] and using field measurements [1].

The wind observer formulation proposed so far is nevertheless completely deterministic, not allowing therefore for any process or measurement noise. To include such effects and improve the robustness and accuracy of the methodology, in this work a Kalman filter is used in the estimation process. Section 2 will first introduce the wind-load mapping with its deterministic and non-deterministic estimation procedure. Then, section 3 will provide a comparison of the overall performance of both methodologies.

2. Methodology

2.1. Wind field parametrization

In this work, the wind inflow is parametrized by four states: vertical and horizontal wind direction, χ and ϕ respectively, and vertical and horizontal linear wind shears, κ_v and κ_h, (shown in Fig. 1). Along with the wind speed, this rotor-effective parameters represent a full first order description of the inflow at the rotor disk. Indeed, the wind field is defined as

$$V(y,z) = V_h \left(1 + \frac{z}{R}\kappa_v + \frac{y}{R}\kappa_h\right), \tag{1}$$

where V_h is the wind speed at hub height and R is the rotor radius. The three wind velocity components are therefore

$$u(y,z) = V(y,z)\cos\phi\cos\chi, \tag{2a}$$
$$v(y,z) = V(y,z)\sin\phi\cos\chi, \tag{2b}$$
$$w(y,z) = V(y,z)\sin\chi. \tag{2c}$$

From Eq. (1), one can easily note the rotational symmetry between vertical and horizontal shear: the effect of a given horizontal shear on the inflow is the same as the one caused by an equivalent vertical shear, only shifted by $\pi/2$ [4]. To better visualize the rotational symmetry characterizing the wind directions, one can define new variables representing the non dimensional horizontal and vertical cross flow at hub height

$$\tilde{v} = \frac{v(0,0)}{V_h} = \sin\phi\cos\chi, \tag{3a}$$
$$\tilde{w} = \frac{w(0,0)}{V_h} = \sin\chi, \tag{3b}$$

and rewrite the problem in terms of the wind state vector $\boldsymbol{\theta} = \{\tilde{v}, \kappa_v, \tilde{w}, \kappa_h\}$. Such reformulation can be later exploited for a simpler identification of the model.

2.2. Winds state observer

Since any spatial dis-homogeneity in the wind will cause a periodic response on a stable system, as described in [7, 2, 3, 4], one can identify a mapping relating the non-uniform inflow to the one per revolution (1P) harmonics of the blade in and out of-plane bending moments, noted IP and OP respectively. The harmonic amplitudes can be readily extracted with the Coleman transformation [8] and grouped into vector $\boldsymbol{m} = \{{m_{1c}}^{\mathrm{OP}}, {m_{1s}}^{\mathrm{OP}}, {m_{1c}}^{\mathrm{IP}}, {m_{1s}}^{\mathrm{IP}}\}^T$, where subscripts c and s stand for the cosine and sine components, respectively.

This mapping, which can be considered as a black box, is formulated as follows

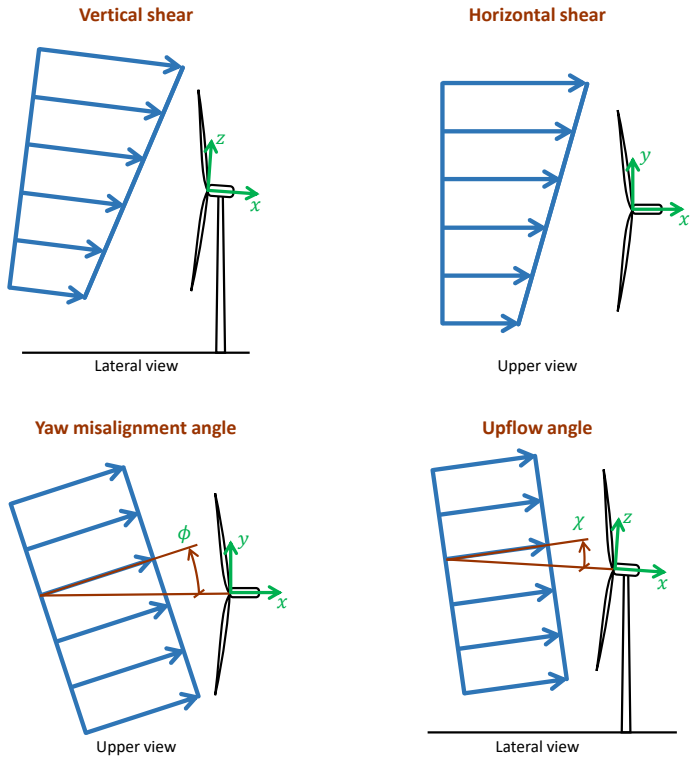

Figure 1. Wind state definition.

$$\boldsymbol{m} = \boldsymbol{F}(V)\boldsymbol{\theta} + \boldsymbol{m}_0(V) = [\boldsymbol{F}(V)\boldsymbol{m}_0(V)] \begin{bmatrix} \boldsymbol{\theta}^T \\ 1 \end{bmatrix} = \boldsymbol{T}(V)\bar{\boldsymbol{\theta}}, \tag{4}$$

with $\boldsymbol{F}(V)$ and $\boldsymbol{m}_0(V)$ the model coefficients scheduled with respect to the wind speed. This scheduling parameter is known in simulations, but can also be easily measured or even estimated in the field [14]. In details, $\boldsymbol{m}_0(V)$ represents the gravity-induced 1P loading, due for instance to coning or uptilt, whereas $\boldsymbol{F}(V)$ represents the derivative of the machine response with respect to the wind parameters.

The model can be readily identified just by collecting enough measurements of loads $\boldsymbol{m}_i$ and the respective wind inflow parameters $\boldsymbol{\theta}_i$, with $i = 1, \ldots, N$, N being the number of available datapoints. Defining $\boldsymbol{M} = [\boldsymbol{m}_1, \ldots, \boldsymbol{m}_N]$ and $\boldsymbol{\Theta} = \left[\bar{\boldsymbol{\theta}}_1, \ldots, \bar{\boldsymbol{\theta}}_N\right]$, focusing here for brevity on one wind speed $\bar{V}$, the system

$$\boldsymbol{M} = \boldsymbol{T}(\bar{V})\boldsymbol{\Theta}, \tag{5}$$

is inverted so that $\boldsymbol{T}$ can be computed in a least-square sense as

$$\boldsymbol{T}(\bar{V}) = \boldsymbol{M}\boldsymbol{\Theta}^T\left[\boldsymbol{\Theta}\boldsymbol{\Theta}^T\right]^{-1}. \tag{6}$$

An alternative identification strategy was described in [4] to face the possibility of an incomplete dataset, i.e. a dataset where not all required wind states are measured. In a nutshell, by exploiting the rotational symmetry of the rotor one can correlate the model coefficients depending on the horizontal wind direction to the ones depending on the vertical one, the same

holding for the shears. Therefore, first the coefficients of the measurable parameters are directly identified from Eq. (6), and then the missing ones are simply derived exploiting the rotor symmetry. This procedure can be particularly useful in a field test campaign, where usually only measurements of the horizontal wind direction and vertical shear are provided.

Once the coefficients have been identified, the wind states can be deterministically estimated in a least-squares sense from the measured response of the machine $\boldsymbol{m}_{\mathrm{M}}$, leading to the solution of the following simple problem

$$\boldsymbol{\theta}_{\mathrm{E}} = \arg\min_{\boldsymbol{\theta}} \Big((\boldsymbol{m}_{\mathrm{M}} - \boldsymbol{F}\boldsymbol{\theta} - \boldsymbol{m}_0)^T (\boldsymbol{m}_{\mathrm{M}} - \boldsymbol{F}\boldsymbol{\theta} - \boldsymbol{m}_0) \Big). \tag{7}$$

2.3. Non-deterministic observation

In order to increase the robustness of the estimation process, a Kalman filter is introduced allowing therefore for both a process and a measurement noise [11, 12]. At any time k, the estimate of the wind state vector is defined as

$$\boldsymbol{\theta}_k = \boldsymbol{\theta}_{k-1} + \boldsymbol{w}_{k-1}, \tag{8}$$

with $\boldsymbol{w}$ the process noise with covariance $\boldsymbol{Q}$, whereas the output equation of the filter writes

$$\boldsymbol{z}_k = \boldsymbol{m}_M - \boldsymbol{m}_{obs} + \boldsymbol{v}_k = \boldsymbol{m}_M - (\boldsymbol{F}\boldsymbol{\theta}_k - \boldsymbol{m}_0) + \boldsymbol{v}_k, \tag{9}$$

where $\boldsymbol{m}_{obs}$ represents the observed machine response and $\boldsymbol{v}_k$ the measurement noise, with covariance $\boldsymbol{R}$. Note that the filter output $\boldsymbol{z}_k$ is set to zero to enforce Eq. (4).

3. Results

To quantify the potential benefits of the Kalman-based formulation, several tests were run at different turbulence intensities (TI) with different mean wind speeds and mean inflows, i.e. setting the wind directions and shears to constant mean values but with a TI-dependent standard deviation.

In this work, a three-bladed, 3 MW machine, with cut in and cut out speeds of 3 and 25 ms^{-1} respectively and region $\mathrm{II}\frac{1}{2}$ between 9 and 12.5 ms^{-1}, was considered as reference model. Its aeroservoelastic behavior was simulated with `Cp-Lambda` [5], a modelling tool representing tower and blades as geometrically exact non-linear beams and including mechanical losses and a torsionally elastic drive train. The aerodynamic model is based on the Blade Element Momentum theory along with unsteady corrections, dynamic stall and tip and hub losses, and a collective LQR pitch and torque controller is used to regulate the machine [6, 13]. In addition, `TurbSim` [10] was used to provide as input to `Cp-Lambda` turbulent wind grids, computed according to the Kaimal model.

For each simulation performed, both a deterministic and non-deterministic wind observer were used to estimate the rotor effective wind parameters. Figure 2 shows an excerpt of the results obtained at 17 ms^{-1} and 12% TI with a *linear wind-response model*, i.e. a model that was identified with a dataset where measurements of all four wind parameters were available.

In each subplot, one per parameter, one can compare the reference wind condition (black) with the observed one with (red) or without (blue) a Kalman filter. The reference wind states, considered here as ground truth, were obtained fitting Eq. (1) and (2) on the rotor-swept area of the `TurbSim` generated turbulent grid, and therefore also represent a rotor-equivalent measurement.

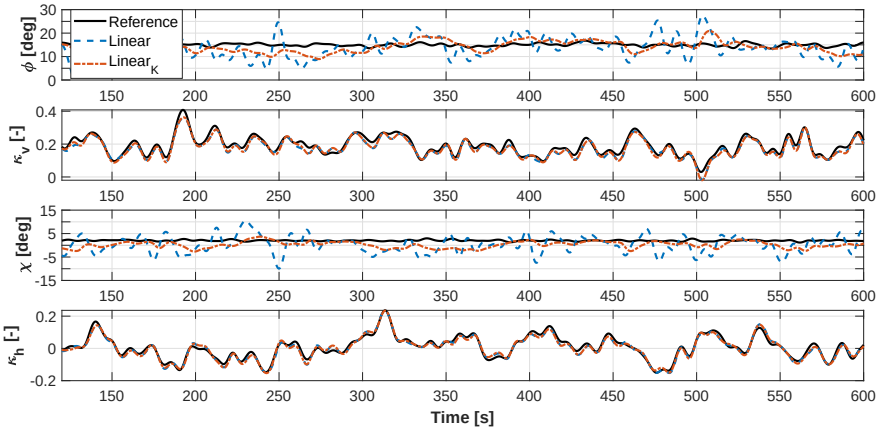

Figure 2. Wind parameters vs. time at 17 ms^{-1} and 12% TI for the linear model: reference condition (black), deterministic estimation (blue), non-deterministic estimation (red) for yaw misalignment, vertical shear, upflow angle, horizontal shear (top to bottom).

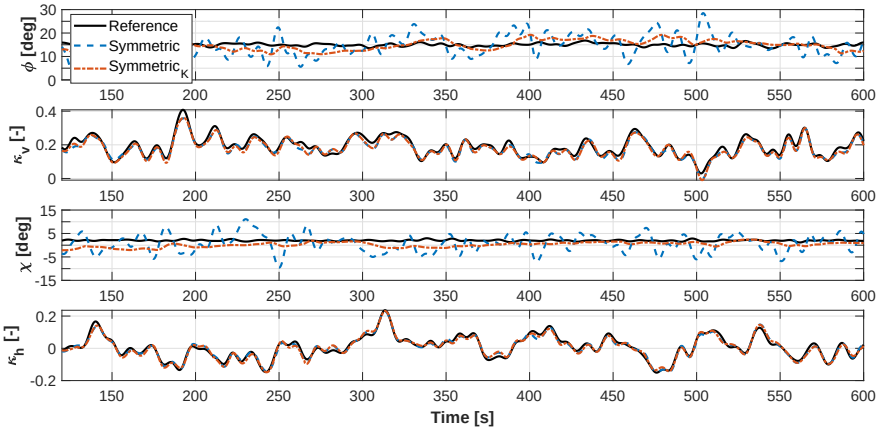

Figure 3. Wind parameters vs. time at 17 ms^{-1} and 12% TI for the symmetric model: reference condition (black), deterministic estimation (blue), non-deterministic estimation (red) for yaw misalignment, vertical shear, upflow angle, horizontal shear (top to bottom).

While the deterministic instantaneous estimation of both shears appears to be very accurate, the observation of both angles can only follow the mean value of the parameters, though with some fluctuations. The use of a Kalman filter appears to significantly reduce such fluctuations, especially for the vertical direction, thus improving the model performance. Such considerations apply also to the results obtained with a *rotationally symmetric model*, i.e. a model identified exploiting the symmetry of the rotor, as shown in Fig. 3. Here as well, the Kalman filter reduces the fluctuations in the angle estimation, whereas no margin of improvement can be noticed as far as the shears are concerned.

A statistical overview of the performance is presented next. For each chosen wind speed in the range $V \in [7,\ 17]$ ms^{-1}, given a TI level, three different mean inflows were considered, including

therefore different values of wind misalignments and shears. Moreover, for each mean inflow 4 different turbulent seeds were used: each marker in figures from 4 to 7 represents therefore a total of 12 10-minute long turbulent simulations.

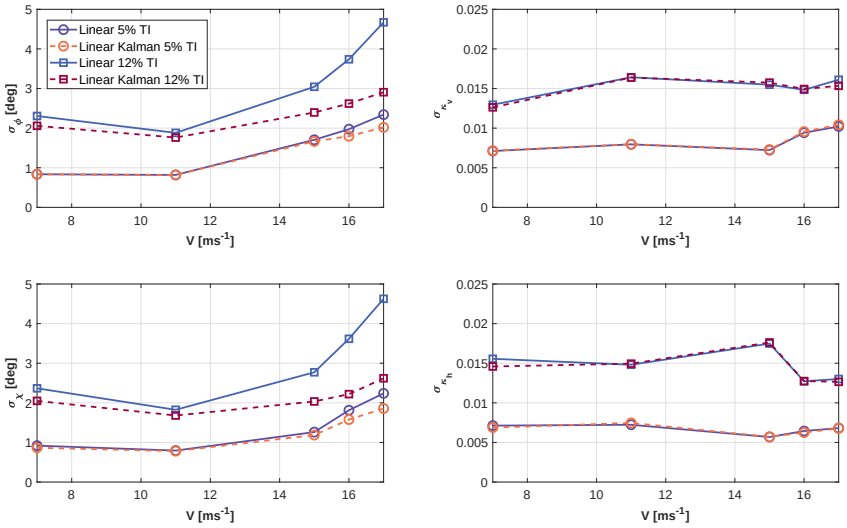

Figure 4. Standard deviation σ of the four wind states vs. wind speed for 5% and 12% TI levels for the linear model. Deterministic formulation: solid lines; non-deterministic formulation: dashed lines.

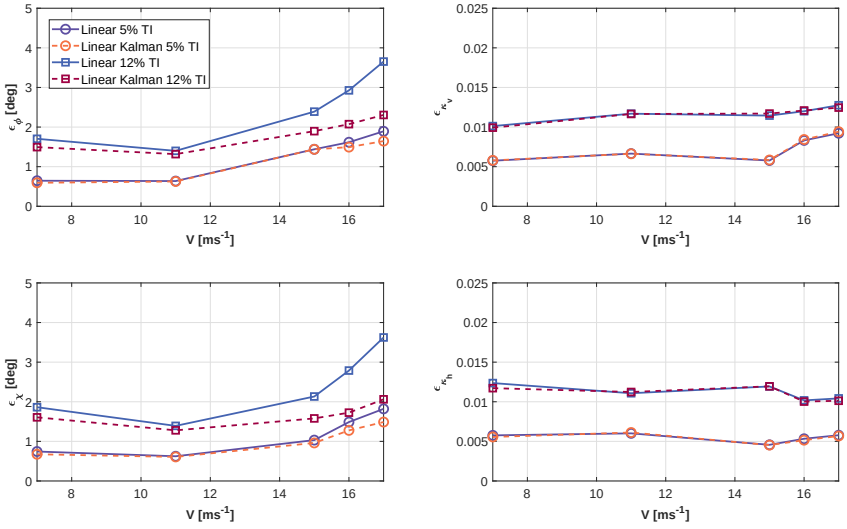

Figure 5. Mean absolute error ϵ of the four wind states vs. wind speed for 5% and 12% TI levels for the linear model. Deterministic formulation: solid lines; non-deterministic formulation: dashed lines.

Figure 4 and 5 show, respectively, for two different TI levels (5 and 12%), the standard deviation and the mean absolute error in the estimates of all parameters for both a deterministic

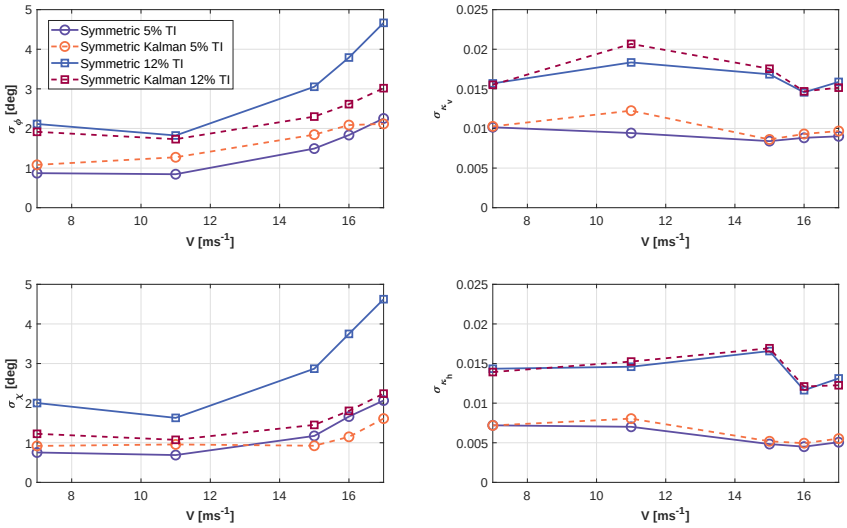

Figure 6. Standard deviation σ of the four wind states vs. wind speed for 5% and 12% TI levels for the symmetric model. Deterministic formulation: solid lines; non-deterministic formulation: dashed lines.

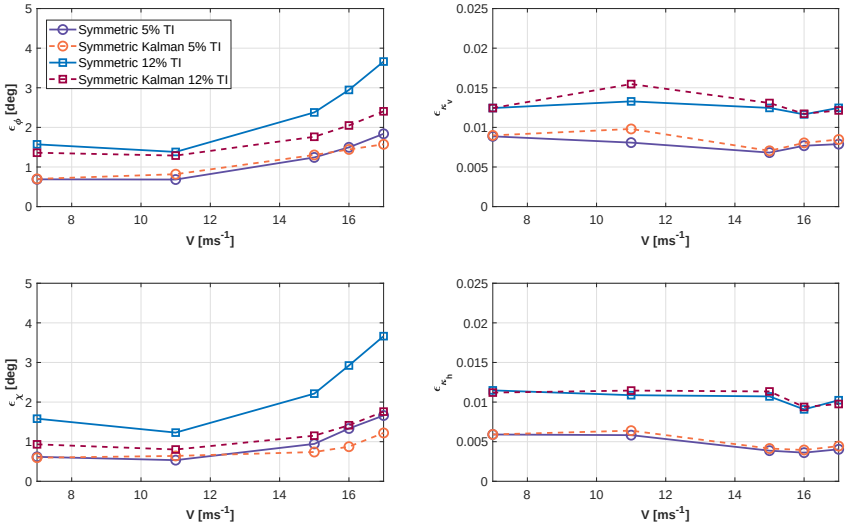

Figure 7. Mean absolute error ϵ of the four wind states vs. wind speed for 5% and 12% TI levels for the symmetric model. Deterministic formulation: solid lines; non-deterministic formulation: dashed lines.

(solid line) and non-deterministic (dashed line) linear model. Coherently to what seen in the exemplary time history, while no improvement in the accuracy can be seen in the shear estimates, a significant improvement can be noticed for the angles. A possible explanation for this behaviour lies in the physics behind the model.
As thoroughly discussed in [2], vertical and horizontal shears leave a clearer fingerprint on the machine response than upflow and yaw misalignment. In fact, to generate the same change in angle of attack, and in turn in blade loading, one needs a higher variation in wind directions than in shears. Similar results were confirmed by a singular value decomposition analysis [9, 2], which also showed that, while both shears are linearly independent parameters, a coupling is present between upflow and yaw misalignment: an error in the yaw estimate will also propagate in the upflow observation, and vice versa. The Kalman filter seems to be able to compensate for these issues, reducing the propagation of the error. Indeed, for higher wind speeds and turbulence levels, when the Kalman filter is employed the angle standard deviation decreases of almost two degrees, while the mean error of 1.5 deg, leading to a maximum absolute error in the estimation of 2.3 and 2.1 deg for yaw and upflow angle, respectively.
Similar considerations can be drawn for Fig. 6 and 7, which show standard deviation and mean error for a deterministic and non-deterministic rotationally symmetric model. No improvement in the shear estimation can be noticed, whereas higher accuracy can be obtained for the angles. Again, the most significant improvements can be noticed for higher wind speeds and higher turbulence, leading to a maximum estimation error of 2.4 and 1.8 deg for yaw and upflow angle respectively.

4. Conclusions and Outlooks

In this work, the wind sensing technology described in [2, 4] was further developed in order to include non-deterministic effects. A linear and rotor symmetrical model relating wind conditions and blade loads were identified; during operation, the inflow at the rotor disk was inferred from the machine measured loads. A Kalman filter was included in the estimation process in order to increase the robustness of the observations and, with it, their accuracy.

Based on a simulation study including several variations of mean inflow, wind speed and turbulence intensity, the following conclusions can be drawn:

- The non-deterministic wind observer is capable of capturing the instantaneous variations of both vertical and horizontal shear very accurately. Additionally, no significant improvement in the estimation can be noted with respect to the deterministic formulation.
- As far as the wind directions are concerned, the non-deterministic observer is capable of reducing the fluctuation in the estimates of the angle mean values, leading to significant higher accuracy. This is particularly the case when considering higher wind speeds and TI, where the mean absolute error can decrease up to almost 2 deg.
- While both the non-deterministic linear and symmetric observer prove better than their deterministic counterparts, no significant difference can be noted comparing their performance. This proves once again that one may simplify the model identification exploiting the symmetry of the rotor without decreasing the quality of the results. This is very valuable particularly for field test applications, where usually only information about the vertical shear and about the horizontal wind direction are available.
- Finally, the implementation of the described Kalman filter does not imply any significant addition to the computational cost of the observer. Indeed, considering that this methodology relies on simple linear models using as input blade load measurements, the observer still remains an easy-to implement solution for wind inflow estimation.

References

[1] Bertelè M, Bottasso CL 2020 Wind inflow observation from load harmonics: field test validation. *Wind Energ. Sci. Discuss.,* in preparation.

[2] Bertelè M, Bottasso CL, Cacciola S, Daher Adegas F, and Delport S 2017 Wind inflow observation from load harmonics. *Wind Energ. Sci. Discuss.*, https://doi.org/10.5194/wes-2017-23.

[3] Bertelè M, Bottasso CL, Cacciola S 2018 Simultaneous estimation of wind shears and misalignments from rotor loads: formulation for IPC-controlled wind turbines. *J. Phys. Conf. Ser* 2018, **1037**, doi.org/10.1088/1742-6596/1037/3/032007

[4] Bertelè M, Bottasso CL and Cacciola S 2019 Wind inflow observation from load harmonics: wind tunnel validation of the rotationally symmetric formulation. *Wind Energ. Sci. Discuss.*, https://doi.org/10.5194/wes-2018-61.

[5] Bottasso CL, Croce A Cp-Lambda: user's manual. *Technical Report*. Dipartimento di Ingegneria Aerospaziale, Politecnico di Milano; 2006–16.

[6] Bottasso CL, Croce A, Nam Y, Riboldi CED. Power curve tracking in the presence of a tip speed constraint. *Renewable Energy* 2012; **40**(1):1–12. DOI: 10.1016/j.renene.2011.07.045.

[7] Cacciola S, Bertelè M, Bottasso C 2016 Simultaneous observation of wind shears and misalignments from rotor loads. *J. Phys. Conf. Ser* 2016, **753**.

[8] Coleman RP and Feingold AM 1958 Theory of self-excited mechanical oscillations of helicopter rotors with hinged blades, Technical Report, NACA TN 1351.

[9] Golub, G.H. and van Loan, C.F.: Matrix Computations, Johns Hopkins University Press: Baltimore, MD, USA, 1996.

[10] Jonkman BJ, Kilcher L. TurbSim user's guide: version 1.06.00.

[11] Kalman RE, 1960 A new approach to linear filtering and prediction problems. *J. Basic Eng. Ser* 1960, **82**.

[12] Kalman RE, Bucy RS 1961 New results in linear filtering and prediction theory. *J. Basic Eng. Ser* 1961, **83**.

[13] Riboldi CED. Advanced control laws for variable-speed wind turbines and supporting enabling technologies. *Ph.D. thesis*, Politecnico di Milano, Milano, Italy, 2012.

[14] Soltani, M., Knudsen, T., Svenstrup, M., Wisniewski, R., Brath, P., Ortega, R. and Johnson, K.: Estimation of rotor effective wind speed: a comparison, IEEE Trans. Control Syst. Technol. 21 (4) 1155e1167, doi:10.1109/tcst.2013.2260751, 2013.

A.5 Paper V: Simultaneous estimation of wind shears and misalignments from rotor loads: formulation for IPC-controlled wind turbines

Reference: M. Bertelè, C. L. Bottasso, and S. Cacciola, "Simultaneous estimation of wind shears and misalignments from rotor loads: formulation for ipc-controlled wind turbines", *Journal of Physics: Conference Series*, vol. 1037, p. 032007, 2018. doi: 10.1088/1742-6596/1037/3/032007.

The Science of Making Torque from Wind (TORQUE 2018) IOP Publishing
IOP Conf. Series: Journal of Physics: Conf. Series **1037** (2018) 032007 doi:10.1088/1742-6596/1037/3/032007

Simultaneous estimation of wind shears and misalignments from rotor loads: formulation for IPC-controlled wind turbines

M. Bertelè[1], C.L. Bottasso[1,2], and S. Cacciola[2]

[1] Wind Energy Institute, Technische Universität München, Garching bei München, Germany
[2] Dipartimento di Scienze e Tecnologie Aerospaziali, Politecnico di Milano, Milano, Italy

E-mail: {marta.bertele, carlo.bottasso}@tum.de, stefano.cacciola@polimi.it

Abstract. In this paper, the turbine itself is used as an anemometer to estimate the inflow at its rotor disk. Indeed, given that any anisotropy in the wind will lead to periodic loads, by studying the machine response one can infer rotor-effective wind conditions and exploit such information for turbine and farm-level control applications. Specifically, expanding the idea of previous publications, the case of an individually pitch-controlled machine is considered herein: a linear implicit model is formulated to relate some characteristics of the wind —in the form of shears and misalignment angles— to the 1P harmonics of pitch angles and blade loads. The performance of the proposed algorithm is tested in a simulation environment, including both uniform and turbulent wind conditions.

1. Introduction

To improve the performance of a single wind turbine as well as of a wind farm, reliable information about the wind inflow can be of significant help. For example, accurate information about yaw misalignment can be used by a yaw control system to realign the turbine to the wind. When this information is of better quality than the one provided by the nacelle wind vane, this approach might lead to higher harvested power and lower fatigue loads. Similarly, the presence of a horizontal shear can be used for wake impingement detection, which can be used for the cooperative control of wind turbines within a wind power plant. Furthermore, measurements of the vertical shear can be used to better tune individual pitch control strategies (IPC) or to account for atmospheric stability, which has a strong effect on wake behavior and consequently on wind farm control strategies.

Unfortunately, accurate wind inflow measurements are still difficult to obtain. Commonly used devices such as met-masts measure an inflow that is not co-located with the turbine, and therefore is of only limited use. Wind vanes and anemometers, on the other hand, measure the wind at the nacelle, but this information is point-wise (as opposed to rotor-equivalent), and also affected by blade passage and nacelle interference effects. More accurate measurements can be obtained by LiDARs, which are however still not widely adopted and remain at the moment confined primarily to research applications. In general, it can be safely stated that wind turbines today are still largely unaware of the wind conditions in which they operate.

To overcome such hurdles, the idea of using the turbine as an anemometer was introduced in Ref. [1]. Following this approach, first in Ref. [2, 3] and then in [4, 5], the response of the

The Science of Making Torque from Wind (TORQUE 2018) IOP Publishing
IOP Conf. Series: Journal of Physics: Conf. Series **1037** (2018) 032007 doi:10.1088/1742-6596/1037/3/032007

machine was used to infer rotor-effective wind conditions. Specifically, since any anisotropy in the wind leads to periodic loads [6], by measuring the 1P harmonic components of the blade out-of-plane and in-plane root bending moment, one can infer the wind field, as described by four parameters: vertical and horizontal misalignment angles (upflow and yaw angle, respectively), and vertical and horizontal shears.

In this paper, the formulation proposed in Ref. [4, 5] is extended and adapted to IPC-controlled machines. Given that such control systems aim at decreasing the loading on the machine by individually pitching each blade, in this work both blade loads and pitch harmonics are used to estimate the inflow. Since the only required hardware consists of blade load and pitch sensors, the proposed wind inflow estimator amounts to a software upgrade when such sensors are already available (for example, for load alleviating closed-loop control).

2. Formulation

2.1. Wind field parameterization

Exposed to a non-isotropic wind field, i.e. an inflow constant in time but not in space, the loading experienced by a rotating blade will be periodic, since periodic are the changes in relative velocity and therefore in angle of attack experienced by its airfoils. To describe such anisotropy, four parameters are defined as shown in Fig. 1: the yaw misalignment ϕ, the vertical shear κ_v, the upflow angle χ, and the horizontal shear κ_h, grouped together in the wind state vector:

$$\boldsymbol{\theta} = \{\phi, \kappa_v, \chi, \kappa_h\}^T. \tag{1}$$

The wind field is described as

$$V(y,z) = V_h \left(\left(\frac{z}{z_h} \right)^{\kappa_v} + \frac{y}{R} \kappa_h \right), \tag{2}$$

where V_h and z_h are the wind speed and the vertical coordinate at hub height, respectively, while R is the rotor radius. The three wind speed components can then be expressed as

$$u(y,z) = V(y,z) \cos\phi \cos\chi, \tag{3a}$$
$$v(y,z) = V(y,z) \sin\phi \cos\chi, \tag{3b}$$
$$w(y,z) = V(y,z) \sin\chi. \tag{3c}$$

2.2. Blade load and pitch harmonics

Under a steady anisotropic wind, the response of a stable wind turbine will converge to a periodic motion [6]. Therefore a generic load m of the ith blade can be expanded in Fourier series as

$$m_{(i)} = m_0 + m_{1\mathrm{c}} \cos\psi_{(i)} + m_{1\mathrm{s}} \sin\psi_{(i)} + \ldots, \tag{4}$$

with ψ the azimuth angle, m_0 the constant amplitude, subscripts 1c and 1s referring to the 1P cosine and sine component, respectively. Once three measured blade loads are available, sine and cosine nP harmonics can be readily computed using the Coleman transformation [7] as follows:

$$\begin{Bmatrix} m_{nc} \\ m_{ns} \end{Bmatrix} = \frac{2}{3} \begin{bmatrix} \cos(n\psi_{(1)}) & \cos(n\psi_{(2)}) & \cos(n\psi_{(3)}) \\ \sin(n\psi_{(1)}) & \sin(n\psi_{(2)}) & \sin(n\psi_{(3)}) \end{bmatrix} \begin{Bmatrix} m_{(1)} \\ m_{(2)} \\ m_{(3)} \end{Bmatrix}. \tag{5}$$

The Science of Making Torque from Wind (TORQUE 2018) IOP Publishing
IOP Conf. Series: Journal of Physics: Conf. Series **1037** (2018) 032007 doi:10.1088/1742-6596/1037/3/032007

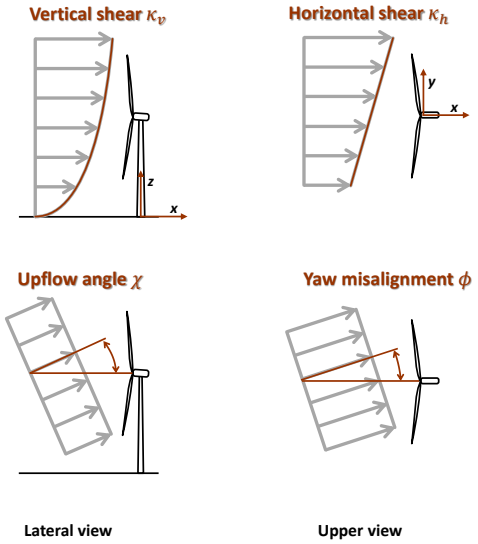

Figure 1. Parameterization of the wind inflow.

A similar approach can be used to extract the components of the blade pitch angle β. The 1P cosine and sine harmonics of both out- (OP) and in-plane (IP) loads and pitch are respectively grouped in vectors

$$\boldsymbol{m} = \{{m_{1\mathrm{c}}}^{\mathrm{OP}}, {m_{1\mathrm{s}}}^{\mathrm{OP}}, {m_{1\mathrm{c}}}^{\mathrm{IP}}, {m_{1\mathrm{s}}}^{\mathrm{IP}}\}^T \tag{6}$$

and

$$\boldsymbol{\beta} = \{\beta_{1\mathrm{c}}, \beta_{1\mathrm{s}}\}^T. \tag{7}$$

2.3. Wind state estimator

In this paper the idea of inferring the rotor effective inflow from the machine response is applied to the case of an IPC-controlled machine. When an IPC controller is used for load reduction, a different pitch demand is computed for each blade, exploiting the fact that each blade has its own independent pitch actuator. The blade pitch frequency is limited by the maximum pitch speed, and it is typically further limited to the 1P harmonic, since this allows for a reduction of the 1P blade loads and, in turn, of the 0P (constant) loads in the fixed frame. In the present work, the controller is implemented by combining a collective pitch and torque LQR formulation [8, 9] together with the proportional integral (PI) 1P IPC controller of Refs. [10, 11].

The linear model relating the response of the IPC-controlled machine to the wind parameters is formulated as follows

$$\boldsymbol{m} = \boldsymbol{F}(V)\boldsymbol{\theta} + \boldsymbol{G}(V)\boldsymbol{\beta} + \boldsymbol{m}_0(V), \tag{8}$$

where $\boldsymbol{F}(V)$, $\boldsymbol{G}(V)$ and $\boldsymbol{m}_0(V)$ are the model coefficients scheduled with respect to the wind speed V. The effect of wind parameters on blade loads, i.e. the derivative of the latter with respect to the former, is represented by the coefficients grouped in matrix $\boldsymbol{F}(V)$, while the effect of the controller cyclic pitching is represented by matrix $\boldsymbol{G}$. Finally, vector $\boldsymbol{m}_0(V)$ accounts for loading induced by gravity [5]. This formulation represents an extension of the one proposed in Refs. [4, 5], which now includes also the effects of pitch harmonics.

To identify the model coefficients given a specific wind speed, a rich enough set of measured $\boldsymbol{m}_j$ and $\boldsymbol{\beta}_j$ at the respective known $\boldsymbol{\theta}_j$ has to be available. Grouping the $j = 1, \ldots, N$

The Science of Making Torque from Wind (TORQUE 2018) IOP Publishing
IOP Conf. Series: Journal of Physics: Conf. Series **1037** (2018) 032007 doi:10.1088/1742-6596/1037/3/032007

experiments together, i.e. $\boldsymbol{M} = [\boldsymbol{m}_1, \ldots, \boldsymbol{m}_N]$, $\boldsymbol{B} = [\boldsymbol{\beta}_1, \ldots, \boldsymbol{\beta}_N]$ and $\boldsymbol{\Theta} = [\boldsymbol{\theta}_1, \ldots, \boldsymbol{\theta}_N]$, focusing here for brevity on one single wind speed $\bar{V}$, the system can be rewritten as

$$\boldsymbol{M} = \boldsymbol{F}(\bar{V})\boldsymbol{\Theta} + \boldsymbol{m}_0(\bar{V}) + \boldsymbol{G}(\bar{V})\boldsymbol{B} = \boldsymbol{T}(\bar{V})\bar{\boldsymbol{\Theta}}, \tag{9}$$

where $\boldsymbol{T} = \left[\boldsymbol{F}(\bar{V})\ \boldsymbol{G}(\bar{V})\ \boldsymbol{m}_0(\bar{V})\right]$ and $\bar{\boldsymbol{\Theta}} = [\boldsymbol{\Theta}\ \boldsymbol{B}\ \mathbf{1}]^T$, $\mathbf{1}$ being the unit vector. Finally, the model coefficients grouped in $\boldsymbol{T}$ can be identified in a least-square sense as

$$\boldsymbol{T}(\bar{V}) = \boldsymbol{M}\bar{\boldsymbol{\Theta}}^T\left[\bar{\boldsymbol{\Theta}}\bar{\boldsymbol{\Theta}}^T\right]^{-1}. \tag{10}$$

Once the coefficients are known, one can exploit the model to infer the wind state parameters from the machine response. Indeed, given the measured $\boldsymbol{m}_\mathrm{M}$ and $\boldsymbol{\beta}_\mathrm{M}$, the estimated wind states $\boldsymbol{\theta}_\mathrm{E}$ can be computed in a least-square sense as

$$\boldsymbol{\theta}_\mathrm{E} = \left(\boldsymbol{F}(V)^T\boldsymbol{F}(V)\right)^{-1}\boldsymbol{F}(V)^T\left(\boldsymbol{m}_\mathrm{M} - \boldsymbol{m}_0(V) - \boldsymbol{G}(V)\boldsymbol{\beta}_\mathrm{M}\right). \tag{11}$$

3. Results

3.1. Simulation environment

To characterize the performance of the proposed formulation, the flexible multibody aeroservoelastic model of a 3 MW three-bladed horizontal-axis wind turbine was simulated. The machine hub height and rotor diameter are 80 and 93 m, respectively, while the cut-in, rated and cut-off wind speeds are 3, 12.5 and 25 ms^{-1}, respectively, which include a wide region II1/2 from 9 to 12.5 ms^{-1}. The aeroelastic behaviour of the machine was simulated with the code `Cp-Lambda` [12], modeling blades and tower as geometrically exact non-linear beams, including a torsionally elastic drive-train and rotor-speed-dependent mechanical losses. The aerodynamics is rendered with the classical Blade Element Momentum theory, including hub and tip losses, unsteady corrections and dynamic stall.

Wind time histories were generated with the code `TurbSim` [13], for both turbulent and non-turbulent conditions. In the turbulent case, the wind histories were generated at a rotor-attached grid by adding turbulent fluctuations according to the Kaimal model to a steady flow characterized by given values of the four wind states. At each time instant, reference $\boldsymbol{\theta}$ values were then extracted by fitting Eq. (1) to the wind grid. Such reference values are considered as the *ground truth*, and they are subsequently used as terms of comparisons for the corresponding quantities computed by the estimator.

Several 3-minute long steady simulations were run with the IPC controller on and off, considering the combinations of the following parameter values:

$$V = \{11,\ 12,\ 15,\ 16,\ 17,\ 19\}\ \mathrm{ms}^{-1}, \tag{12a}$$
$$\phi = \{-16,\ -12,\ -8,\ -4,\ 0,\ 4,\ 8,\ 12,\ 16\}\ \mathrm{deg}, \tag{12b}$$
$$\kappa_v = \{0.0,\ 0.1,\ 0.2,\ 0.3,\ 0.4\}, \tag{12c}$$
$$\chi = \{0,\ 4,\ 8,\ 12\}\ \mathrm{deg}, \tag{12d}$$
$$\kappa_h = \{-0.1,\ -0.05,\ 0.0,\ 0.05,\ 0.1\}. \tag{12e}$$

The results of the simulations were then used to identify the model as described in §2.3. After having identified the model coefficients, the same set of simulations was then used to observe the wind conditions given measured blade loads and pitch angles.

Figure 2 shows the accuracy of the wind estimation in steady conditions for tests performed at 15 ms^{-1} with the IPC controller turned on. Each subplot represents a different wind state. The reference wind parameter, i.e. the ground truth, is reported on the x-axis, while the observed one on the y-axis: ideally, results should fall exactly on the bisector line. Analyzing the results,

The Science of Making Torque from Wind (TORQUE 2018) IOP Publishing
IOP Conf. Series: Journal of Physics: Conf. Series **1037** (2018) 032007 doi:10.1088/1742-6596/1037/3/032007

one can notice that the model is capable of correctly observing both shears, with a slight decrease in accuracy in the vertical shear observation when high positive yaw angles are considered. The upflow angle can as well be estimated with only slight inaccuracies, which nevertheless do not exceed 2°. Finally, the estimation of the wind direction appears to be very precise for angles that do not exceed ±12°, after which a deviation of about 3° from the reference can be observed. A similar overall behaviour was noted at different wind speeds from the one considered here. Such inaccuracies, specifically the one concerning the yaw angle, are due to non-linearities in the load-wind relationship, which cannot be captured by the present linear formulation. This problem can be easily addressed by the use of a model with a prescribed level of non-linearity, which still results in a linear model-estimation problem [5].

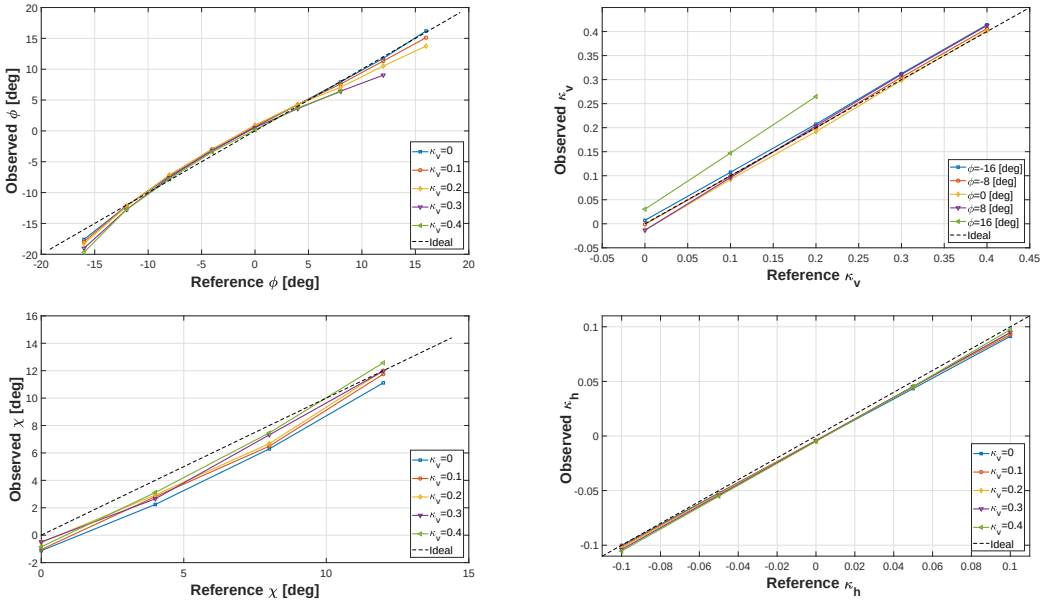

Figure 2. Wind states observed using the linear model for different steady inflow conditions at 15 ms^{-1}: yaw misalignment ϕ at $\chi = 8$ deg and $\kappa_h = -0.1$ (top left), vertical shear κ_v at $\chi = 8$ deg and $\kappa_h = -0.1$ (top right), upflow angle χ at $\phi = -8$ deg and $\kappa_h = -0.1$ (bottom left), horizontal shear κ_h at $\chi = 8$ deg and $\phi = -8$ deg (bottom right).

3.2. Non-turbulent wind conditions

To test the ability of the wind estimator in detecting changes in the wind parameters, different simulations were performed in non-turbulent wind conditions with the IPC controller turned on. In each simulation the wind speed was kept constant, whereas the wind parameters were varied independently from one another.

Figure 3 shows an excerpt of the results at 17 ms^{-1}. Wind parameters appear to be correctly estimated, with a very good accuracy as far as shears are concerned, and with only relatively small errors, not exceeding 3°, in the case of the angles. Similar results were obtained for different wind speeds, with an increase in accuracy at higher wind speeds. To ease the comparison, delays in the observed states induced by the 1P harmonic extraction procedure were eliminated from the figure.

The Science of Making Torque from Wind (TORQUE 2018) IOP Publishing
IOP Conf. Series: Journal of Physics: Conf. Series **1037** (2018) 032007 doi:10.1088/1742-6596/1037/3/032007

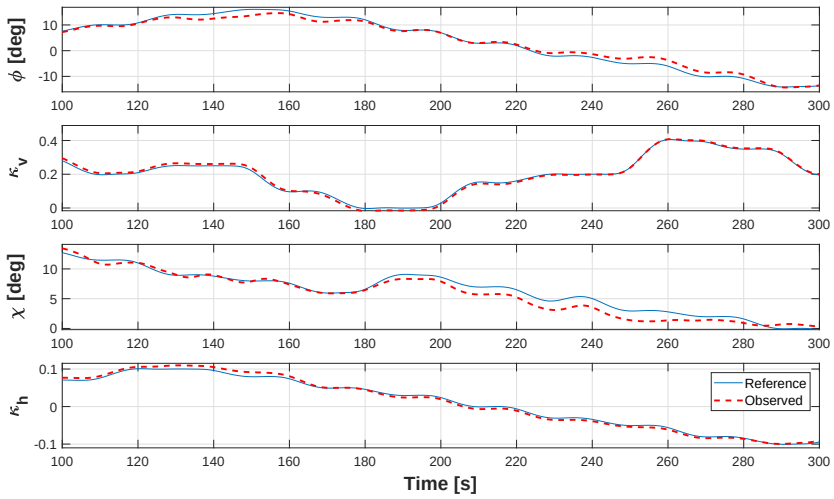

Figure 3. Wind state estimates in non-turbulent wind conditions with variable wind parameters at 17 ms^{-1}. Solid thick blue lines: reference wind parameters; dashed thick red lines: observations by the linear model.

3.3. Turbulent wind conditions

To test the estimator performance in more realistic wind conditions, several 10-minute long turbulent simulations were also considered. Starting from mean values of wind speed and inflow parameters, `TurbSim` was used to generate wind histories at 5 and 10% turbulence intensity (TI). To account for changes in the rotational speed of the machine due to turbulence, an adaptive filter was employed to extract the loads and pitch 1P harmonic components.

Figure 4 shows results at 11 ms^{-1} and 5% TI. Despite the filter-induced delay, one can notice that the estimator is capable of nicely following the fluctuations of both shears, particularly the horizontal one. On the other hand, only the mean values of the angles are well captured. A justification of this phenomenon is given in Ref. [5], where it is shown that the velocity triangle at the blade, and with it the angle of attack, is more affected by the presence of wind shear than of wind misalignment. It follows that the moments at the blades are more sensitive to shear rather than misalignment, carrying therefore more information about the first than about the latter. To better quantify the model performance, Tab. 1 and 2 show the standard deviation and the mean absolute estimation error at 5 and 10% TI. The yaw mean error for the lower turbulent case is about 1°, whereas for the higher turbulence level the mean error is about 2.4°. For yaw control, such performance should be enough, as the controller typically does not try to follow fast wind direction changes.

The model coefficients were identified starting from a set of simulations where the IPC controller was both on and off. Therefore, one should expect the linear model to be able to estimate the wind inflow both if the IPC controller is used or not. To test this hypothesis, additional 10-minute long turbulent tests were performed, using only the collective pitch controller. The standard deviation and mean absolute error with IPC off at 11 ms^{-1} with 5 and 10% TI are reported in Tab. 1 and 2. In this second scenario, the estimator seems to be slightly more accurate in computing shears and particularly angles, since now the mean error in yaw misalignment is less than 0.5 and 1.3° for low and high turbulence levels, respectively.

The Science of Making Torque from Wind (TORQUE 2018) IOP Publishing
IOP Conf. Series: Journal of Physics: Conf. Series **1037** (2018) 032007 doi:10.1088/1742-6596/1037/3/032007

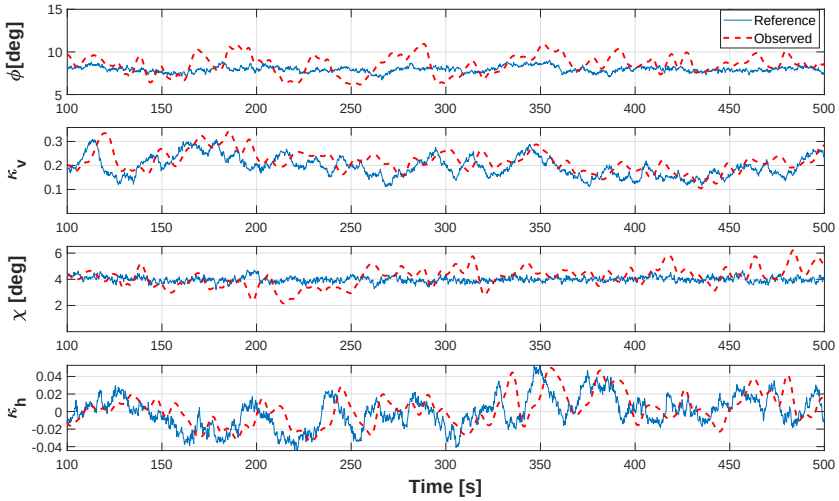

Figure 4. Wind state estimates in turbulent wind conditions with variable wind parameters at 11 ms^{-1}. Solid thick blue lines: reference wind parameters; dashed thick red lines: observations by the linear model.

Table 1. Wind state estimate standard deviation at 11 ms^{-1} and 5 and 10% TI.

Standard deviations	5% TI		10% TI	
	IPC on	IPC off	IPC on	IPC off
σ_ϕ[deg]	1.26	0.56	3.55	1.98
σ_{κ_v}	3.88e-2	3.33e-2	6.77e-2	6.27e-2
σ_χ[deg]	0.76	0.66	2.16	1.75
σ_{κ_h}	1.42e-2	1.32e-2	2.92e-2	2.6e-2

Table 2. Wind state estimate mean absolute error at 11 ms^{-1} and 5 and 10% TI.

Mean absolute error	5% TI		10% TI	
	IPC on	IPC off	IPC on	IPC off
ϵ_ϕ[deg]	1.04	0.46	2.42	1.3
ϵ_{κ_v}	3.1e-2	2.58e-2	5.44e-2	4.94e-2
ϵ_χ[deg]	0.6	0.52	1.57	1.27
ϵ_{κ_h}	1.12e-2	1.03e-2	2.35e-2	2.04e-2

4. Conclusions

In this work, a linear formulation was proposed to relate the machine response to the wind inflow, parameterized by a vertical and horizontal misalignment angle and by a vertical and horizontal shear. Extending the idea of Ref. [5], the case of an IPC-controlled wind turbine was considered, by using the 1P harmonic of in- and out-of-plane blade bending moments and blade pitch to infer the wind conditions at the rotor disk.

The model was tested first in uniform and then in turbulent wind conditions. Based on the reported results, the following conclusions can be drawn:

- In uniform wind conditions, the model is capable of estimating the instantaneous value of both shears and angles with good precision. Small inaccuracies decrease with wind speed and are due to the linearity of the model. This can be improved with a quadratic model, as shown in Ref. [5].
- In turbulent conditions both shears can be accurately estimated, although with a delay due to the 1P extraction process. Errors of about 1.3° can be noted in the estimation of the yaw angle for 5% TI. Given that such errors increase with TI [5], only a mean value of such quantities can be estimated with sufficient accuracy, while instantaneous values are polluted by significant fluctuations. This problem requires further investigations to be corrected, and its origin has been explained in Ref. [5].
- The proposed formulation expands the one presented in Refs. [4, 5] to IPC-controlled turbines, but nevertheless is still capable of estimating the wind inflow even if only a collective controller is used.

Acknowledgments

This work has been partially supported by the CL-Windcon project, which receives funding from the European Union Horizon2020 research and innovation program under grant agreement No. 727477.

References

[1] Bottasso CL, Croce A and Riboldi CED 2010 Spatial estimation of wind states from the aeroelastic response of a wind turbine. *The science of making torque from wind TORQUE* 2010 Heraklion, Crete, Greece.
[2] Bottasso CL and Riboldi CED 2014 Estimation of wind misalignment and vertical shear from blade loads *Renew. Energy* **62** 293-302.
[3] Bottasso CL and Riboldi CED 2015 Validation of a wind misalignment observer using field test data *Renew. Energy* **74** 298–306
[4] Cacciola S, Bertelè M, Bottasso CL 2016 Simultaneous observation of wind shears and misalignments from rotor loads. *J. Phys. Conf. Ser* 2016, **753**.
[5] Bertelè M, Bottasso CL, Cacciola S, Daher Adegas F, and Delport S 2017 Wind inflow observation from load harmonics. *Wind Energ. Sci.*, https://doi.org/10.5194/wes-2017-23.
[6] Eggleston DM and Stoddard FS 1987 *Wind Turbine Engineering Design* (New York: Van Nostrand Reinhold Company Inc).
[7] Coleman R.P. and Feingold A.M. 1958 *Theory of self-excited mechanical oscillations of helicopter rotors with hinged blades, Technical Report* NACA TN 1351.
[8] Bottasso CL, Croce A, Nam Y and Riboldi CED 2012 Power curve tracking in the presence of a tip speed constraint. *Renew. Energy* **40** 112.
[9] Riboldi CED 2012 *Advanced control laws for variable-speed wind turbines and supporting enabling technologies* Ph.D. thesis Politecnico di Milano.
[10] Bossanyi E 2003 Individual blade pitch control for load reduction *Wind Energy*, **6** 119-8.
[11] Bossanyi E 2005 Further load reductions with individual pitch control *Wind Energy*, **8** 481-5.
[12] Bottasso CL and Croce A 2006-12 *Cp-Lambda: User's Manual. Technical Report* Dipartimento di Ingegneria Aerospaziale, Politecnico di Milano.
[13] Jonkman BJ and Kilcher L 2012 *TurbSim User's Guide: Version 1.06.00* NREL Technical report.

A.6 Paper VI: Automatic detection and correction of pitch misalignment in wind turbine rotors

Reference: M. Bertelè, C. L. Bottasso, and S. Cacciola, "Automatic detection and correction of pitch misalignment in wind turbine rotors," *Wind Energy Science*, vol. 3, no. 2, pp. 791–803, 2018. doi: 10.5194/wes-3-791-2018.

Wind Energ. Sci., 3, 791–803, 2018
https://doi.org/10.5194/wes-3-791-2018

WIND ENERGY SCIENCE
Open Access
eawe european academy of wind energy

Automatic detection and correction of pitch misalignment in wind turbine rotors

Marta Bertelè[1], Carlo L. Bottasso[1,2], and Stefano Cacciola[2]

[1]Wind Energy Institute, Technische Universität München, 85748 Garching bei München, Germany
[2]Dipartimento di Scienze e Tecnologie Aerospaziali, Politecnico di Milano, 20156 Milano, Italy

Correspondence: Carlo L. Bottasso (carlo.bottasso@tum.de)

Received: 7 March 2018 – Discussion started: 3 April 2018
Revised: 11 September 2018 – Accepted: 3 October 2018 – Published: 25 October 2018

Abstract. In this work, a new algorithm is presented to correct for pitch misalignment imbalances of wind turbine rotors. The method uses signals measured in the fixed frame of the machine, typically in the form of accelerations or loads. The amplitude of the one per revolution signal harmonic is used to quantify the imbalance, while its phase is used to locate the unbalanced blade(s). The near linearity of the unknown relationship between harmonic amplitude and pitch misalignment is used to derive a simple algorithm that iteratively rebalances the rotor. This operation is conducted while the machine is in operation, without the need for shutting it down. The method is not only applicable to the case of a single misaligned blade, but also to the generic case of multiple concurrent imbalances. Apart from the availability of acceleration or load sensors, the method requires the ability of the rotor blades to be commanded independently from one another, which is typically possible on many modern machines. The new method is demonstrated in a realistic simulation environment using an aeroservoelastic wind turbine model in a variety of wind and operating conditions.

1 Introduction

The pitch system has the highest failure rate of all wind turbine components (Wilkinson et al., 2010). Issues can include, among others, faults of the pitch actuators or of the pitch angle sensors, but they can also be caused by an imperfect installation of the blades. In general, rotor asymmetries represent a significant problem for wind turbines, as also witnessed by the fact that certification guidelines require the verification of the effects of even relatively small pitch misalignments (typically $\pm 0.3°$ for two blades; GL Standards, 2010, Sect. 4.3.4.1, pp. 4–20).

Irrespective of the specific type of fault, a pitch imbalance will have as a direct consequence not only a possible decrease in harvested energy but, most importantly, also an increased level of vibrations and rotor speed fluctuations (Hyers et al., 2006; Kusiak and Verma, 2011). In fact, when a pitch misalignment among the blades is present, the periodic aerodynamic, dynamic and gravitational loading experienced by the blades is not balanced. As a result, additional harmonic components are transferred from the rotating to the fixed frame, resulting in vibrations that may lead to the failure of other components of the machine and that may also affect its fatigue life if not promptly corrected for (Yang et al., 2008). Moreover, whenever vibrations are fed back to the turbine control laws, imbalances can also result in increased duty cycles for the machine actuators.

Currently, the downtime related to pitch failures is relatively high (Wilkinson et al., 2010). In fact, once an anomalous behavior has been detected – typically by higher than expected fixed-frame vibrations; see Hameed et al. (2009) – pitch correction operations are often initiated by a visual inspection. An operator (more recently with the possible aid of a drone) takes pictures or videos of the blades, which are later analyzed to reveal whether all blades have the same pitch angle. Once a pitch offset has been estimated, the blade pitch is reset to align it with the others. This operation will imply some downtime and may come at a non-negligible cost. Furthermore, the procedure might not always be able to produce an exactly balanced rotor. Clearly, more effective condition monitoring and correction strategies for the pitch system

of wind turbines should be developed. An ideal solution for correcting misaligned blades should be able to first identify when a rotor is unbalanced, and then it should be able to automatically rebalance it. This should be obtained without the need to shut down the machine, without the presence and supervision of an operator, and without the need for expensive extra hardware.

Imbalance detection and correction techniques have been developed both in the literature and in practical applications. For example, Pierce and Slack (2009) and Axelsson et al. (2014) report on methods that reduce a rotor imbalance by first arbitrarily setting a pitch offset and then measuring the resulting loads and accelerations on the shaft or on the yaw system. However, no mathematical formulation is provided by the authors, thus preventing a better understanding of the methodology and its limits. Niebsch et al. (2010) and Niebsch and Ramlau (2014) proposed a method to simultaneously estimate both mass and aerodynamic imbalance effects from nacelle vibrational measurements. The method considers a finite-element model of the turbine, and the imbalance terms are obtained by solving an inverse problem through nonlinear regularization theory. The results are interesting although not excellent, with errors in the estimation of the pitch misalignment up to 0.5°. However, the need for a detailed model of the machine may hinder the applicability of this method. A different approach was proposed by Kusnick et al. (2015). In this case, the blade misalignment estimation is performed by an ad hoc workflow using multiple measurements, including power output, blade loads and accelerations. Finally, a method based on system identification is presented by Cacciola et al. (2016). In that work, a neural network is trained based on nodding moment and power measurements from different experiments conducted for varying known pitch misalignments and operating conditions. After training, the network is able to detect the severity and location of the imbalance, even distinguishing effects caused by pitch misalignments from those induced by ice accretion.

Ad hoc controllers have also been formulated to correct for rotor imbalances (Kanev and van Engelen, 2009; Kanev et al., 2009; Petrović et al., 2015; Cacciola and Riboldi, 2017; Cacciola et al., 2017). In all these cases, the general idea is to develop a control law that compensates for a pitch misalignment by targeting imbalance-induced vibrations, typically by Coleman-transforming blade loads (Bossanyi, 2003). One possible drawback of such approaches is the resulting extra control activity necessary to rebalance the rotor, which will induce extra duty cycles in the pitch system.

The analysis of signals such as loads and accelerations measured on the wind turbine fixed frame provides a way to determine if a rotor is unbalanced. In fact, it is well known that the amplitude of the 1P (once per revolution) harmonic is an indicator of an unbalanced rotor. Recently, it was shown that the phase of that same harmonic can be used to identify the unbalanced blade(s) (Cacciola et al., 2016). Based on this simple signal analysis, a condition monitoring system can be developed to detect the severity and location of the imbalance in order to schedule appropriate maintenance and repair actions.

In the present work, the same concept is used to automatically rebalance an unbalanced rotor. In a nutshell, the method works as follows. First, an unknown linear relationship is assumed between pitch setting of the blades and the 1P amplitude of a signal measured in the fixed frame. Exploiting the radial symmetry of a rotor, the coefficients of the linear relationship are reduced to only two. In addition, this also has the effect of including the phase information in the model, which eventually allows one to correctly identify the pitch misalignment of each blade. Since the linear imbalance–disturbance model is determined by two parameters, one single additional measurement (in addition to the one performed on the currently unbalanced configuration) is necessary to identify the unknown imbalance–disturbance relationship. This is easily achieved by pitching the blades by some amount and measuring the resulting 1P amplitude. Once the linear relationship is known, it is trivial to compute the blade pitch offset that, by zeroing the 1P amplitude, balances the rotor. To account for possible small nonlinearities, the procedure can be iterated a few times as necessary. A similar approach was presented in Bertelè et al. (2017), which considered only the case of a pitch fault located in one single blade. The present work expands and generalizes this methodology, allowing for the detection and correction of multiple simultaneous pitch imbalances.

The paper is organized as follows. Section 2 formulates the proposed imbalance detection and correction procedure. In particular, Sect. 2.1 shows the mechanism through which a pitch imbalance causes a 1P load in the fixed frame by developing a spectral analysis of the relevant loads and explaining their origin. Next, Sect. 2.2 formulates the linear imbalance–disturbance model of an axial-symmetric rotor, while Sect. 2.3 shows how the model coefficients can be readily identified by using two fixed-frame measurements at two different pitch settings. Lastly, Sect. 2.4 explains the rebalancing procedure. Results are discussed in Sect. 3, which reports extensive numerical simulations performed with a state-of-the-art aeroservoelastic model operating in a variety of different turbulent winds. Tests are conducted in realistic scenarios, in the sense that rebalancing is performed while the wind turbine is operating in changing wind conditions, including modifications in air density, wind speed, shear, yaw misalignment, upflow angle and turbulence intensity. Details on the specific combinations of conditions used in the tests are reported in Appendix A. In addition, Sect. 3.4 presents a study assessing the effects of measurement noise on the method performance, with the goal of defining minimum specification requirements for the whole measuring chain. Finally, Sect. 4 draws conclusions and gives an outlook on future work.

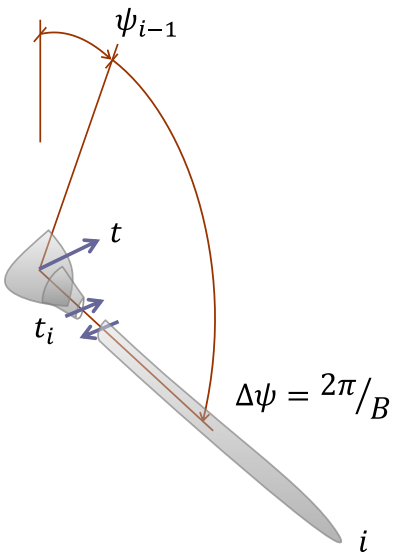

Figure 1. Thrust force t computed in terms of the shear forces t_i of the B blades. One single blade is shown for clarity.

2 Methods

2.1 Spectral analysis of an unbalanced rotor

In a balanced rotor with B blades, under the assumption of a periodic response, loads transmitted from the rotating frame of reference to the fixed frame contain only nBP frequencies. Indeed, the rotor acts as a filter: while the full spectrum of frequencies is observed in the rotating frame (1P, 2P, 3P, 4P, ...), in the fixed frame only frequencies that are multiples of the number of blades appear (BP, $2B$P, $3B$P, ...).

On the other hand, when an imbalance is present, other harmonic components can be detected in fixed-frame measurements, the most prominent typically being the 1P harmonic. Hence, detection and correction of rotor imbalances can be based on the analysis of the 1P harmonic measured in the fixed frame.

As an example, consider the measurement of nacelle fore–aft accelerations, which are primarily caused by fluctuations in the rotor thrust. The thrust force t on the rotor can be computed by summing up the out-of-plane shear forces t_i of the B blades, as illustrated in Fig. 1.

The shear force of the generic ith blade can be expanded in Fourier series as

$$t_i = t_{0_i} + \sum_{n=1}^{\infty} \left(t_{nc_i} \cos(n\psi_i) + t_{ns_i} \sin(n\psi_i) \right), \tag{1}$$

where $\psi_i = \psi_1 + 2\pi(i-1)/B$ is the azimuthal angle, subscripts $(\cdot)_{nc}$ and $(\cdot)_{ns}$ refer to the nP cosine and sine components, respectively, and t_0 is the 0th harmonic constant amplitude.

Assuming a periodic response, the harmonic amplitudes are the same for the various blades; i.e.,

$$t_0 = t_{0_i} = t_{0_j}, \tag{2a}$$
$$t_{nc} = t_{nc_i} = t_{nc_j}, \tag{2b}$$
$$t_{ns} = t_{ns_i} = t_{ns_j}. \tag{2c}$$

In the presence of an imbalance, the harmonic amplitudes of the kth (unbalanced) blade will differ from the other ones and can be expressed as

$$t_{0_k} = t_0 + \delta t_0, \tag{3a}$$
$$t_{nc_k} = t_{nc} + \delta t_{nc}, \tag{3b}$$
$$t_{ns_k} = t_{ns} + \delta t_{ns}. \tag{3c}$$

Inserting Eqs. (2) and (3) into Eq. (1) and using the properties of trigonometric functions, one can readily compute the thrust force t as

$$t = \sum_{i=1}^{B} t_i, \tag{4a}$$
$$= Bt_0 + B\sum_{n=1}^{\infty} (t_{nBc}\cos(nB\psi) + t_{nBs}\sin(nB\psi)), \tag{4b}$$
$$+ \delta t_0 + \sum_{n=1}^{\infty} (\delta t_{nc}\cos(n\psi_k) + \delta t_{ns}\sin(n\psi_k)), \tag{4c}$$

where $\psi = \psi_1$. Equation (4c) states that, when the rotor is balanced (i.e., when $\delta t_0 = \delta t_{nc} = \delta t_{ns} = 0$), then only nB harmonics are present in the spectrum of t. On the other hand, when the rotor is unbalanced

1. intermediate harmonics also pollute the spectrum, and
2. the phase of these harmonics indicates the unbalanced blade.

Limiting the analysis to the case of the lowest harmonics of both expansions in Eq. (4c), which are typically the most energetic ones, leads to

$$t = (Bt_0 + \delta t_0)_{0\mathrm{P}} + (\delta t_{1c}\cos\psi_k + \delta t_{1s}\sin\psi_k)_{1\mathrm{P}} + B(t_{Bc}\cos(B\psi) + t_{Bs}\sin(B\psi))_{B\mathrm{P}}. \tag{5}$$

This expression states that the 1P harmonic in the fixed frame is generated by the 1P harmonic of the unbalanced blade. This is not always the case, as the result depends on the considered fixed-frame load. For example, similar derivations performed for the nodding (overturning) moment show that the 0P of the unbalanced blade also contributes to the 1P in the fixed frame in that particular case. This is beneficial because, as shown later on, the 0 and 1P imbalance harmonics have a different aerodynamic origin. In fact, numerical experiments show that an improved performance and robustness of the detection algorithm can be obtained by using as an imbalance detection signal the overturning or yawing moments.

However, since load sensors in the fixed frame are typically difficult to install, a similar effect can be obtained by using the difference of two fore–aft accelerometers located in the nacelle at a distance between the two of them (which, depending on their positions, will measure nodding or yawing motions of the rotor or combinations thereof).

To better understand the effects of a pitch imbalance, the expression for the aerodynamic contribution to the shear in a blade can be worked out analytically. Following the approach of Manwell et al. (2009), which uses a one degree of freedom rigid body model of a flapping blade, the shear t_i of the ith rotor blade is found to be

$$t_i = t_{0_i} + t_{1c_i} \cos\psi_i, \tag{6}$$

where the 0 and 1P harmonic amplitudes are written as

$$= t_{0_i} - \bar{t}\left(\frac{\Lambda}{2} - \frac{\theta_i}{3}\right), \tag{7a}$$

$$t_{1c_i} = \bar{t}\left((\Lambda - \theta_i)\bar{V} + \frac{K}{3}\bar{U}\right). \tag{7b}$$

In these expressions, $\bar{t} = \gamma J\Omega^2/(2R)$, $\gamma = \varrho c C_{L,\alpha} R^4/J$ is the Lock number, ϱ the air density, c the blade chord, $C_{L,\alpha}$ the lift slope, R the rotor radius, J the flapping moment of inertia and $\Lambda = (1-a)U/(\Omega R)$ the nondimensional flow velocity at the rotor disk, with a being the axial induction, $\bar{V}_0 = V_0/(\Omega R)$ the nondimensional cross-flow and $\bar{U} = U/(\Omega R)$ the nondimensional wind speed; Ω is the rotor angular velocity and K the linear vertical wind shear.

Assuming a pitch misalignment $\delta\theta$, the resulting imbalance-induced 0 and 1P harmonic amplitudes are

$$\delta t_0 = \frac{\bar{t}}{3}\delta\theta, \tag{8a}$$

$$\delta t_{1c} = -\bar{t}\bar{V}\delta\theta. \tag{8b}$$

These expressions state that there is a linear dependency between a pitch misalignment and the resulting harmonic disturbances. In addition, the 1P imbalance harmonic δt_{1c} that – according to Eq. (5) – causes the appearance of a 1P harmonic in the fixed frame is proportional to the cross-flow. Although in operation there will always be some small misalignment between the rotor axis and the wind vector, this expression suggests that the 1P signal could be strengthened by operating at a slight yaw misalignment with the incoming wind when detecting an imbalance and correcting for it.

A word of caution is due in the interpretation of these analytical results. First of all, this analysis is based on the sole thrust force, while terms other than the cross-flow contribute to the 1P harmonic when considering yawing and nodding moments. In addition, the model is the simplest possible using one single degree of freedom and including various simplifications in the derivations. Nevertheless, the model is at least useful in qualitatively understanding the basic mechanisms by which fixed-frame vibrations are caused in an imbalanced rotor. After having served its purpose, the analytical model is dropped from the rest of the paper, the further developments of which are not based on it.

2.2 Linear imbalance–disturbance model

In this work, an imbalance–disturbance model is assumed in the form

$$\boldsymbol{s} = \mathbf{C}(\boldsymbol{b} - \boldsymbol{b}_\mathrm{m}), \tag{9a}$$

$$= \mathbf{C}\boldsymbol{b} + \boldsymbol{s}_\mathrm{m}. \tag{9b}$$

The 1P harmonic amplitude vector of the fixed-frame measured signal $\boldsymbol{s}$ is noted $\boldsymbol{s} = (s_\mathrm{c}, s_\mathrm{s})^T$, where s_c and s_s are the cosine and sine components, respectively. Considering here and in the following the common case of a three-bladed rotor ($B = 3$), vector $\boldsymbol{b} = (b_1, b_2, b_3)^T$ contains the pitch adjustments b_i for each one of the blades, while $\boldsymbol{b}_\mathrm{m}$ is the unknown pitch misalignment. Equation (9a) states that, if one knew the misalignment $\boldsymbol{b}_\mathrm{m}$, then by pitching the blades by $\boldsymbol{b} = \boldsymbol{b}_\mathrm{m}$ one would obtain $\boldsymbol{s} = 0$; i.e., the rotor would be balanced. On the other hand, before rebalancing, $\boldsymbol{b} = 0$ and hence, according to Eq. (9b), one measures a 1P signal equal to $\boldsymbol{s}_\mathrm{m} = -\mathbf{C}\boldsymbol{b}_\mathrm{m}$. In the model, the matrix of coefficients $\mathbf{C}$ links imbalance angles and 1P disturbances, and it is defined as

$$\mathbf{C} = \begin{bmatrix} c_{c_1} & c_{c_2} & c_{c_3} \\ c_{s_1} & c_{s_2} & c_{s_3} \end{bmatrix}. \tag{10}$$

The model coefficients $\mathbf{C}$ and $\boldsymbol{s}_\mathrm{m}$ are unknown. However, they can be readily identified from measurements. Once the model is known, one can use it to compute the pitch adjustment $\boldsymbol{b}$ that rebalances the rotor.

Note that the assumed imbalance–disturbance model implies a linear relationship between the pitch misalignment of the blades and the 1P harmonic component of a measured response signal (acceleration or load) in the fixed frame. As shown later on, this assumption is not a limitation of the model because in fact the model can be iteratively identified as the rotor is rebalanced, thus effectively removing the linearity hypothesis. However, linearity is confirmed by the previously derived simple analytical model, and it is indeed generally also observed in extensive numerical simulations conducted by using state-of-the-art aeroelastic models.

Since it is nearly impossible to guarantee that the whole model identification and rebalancing procedure will be conducted in exactly the same wind conditions, it is important to reduce the dependency of the model on the operating point. To this end, the harmonic amplitude vector $\boldsymbol{s}$ in Eq. (9) is scaled by the dynamic pressure

$$q = \frac{1}{2}\varrho U_\mathrm{a}^2, \tag{11}$$

where U_a is a moving average of the wind speed. The nondimensionalization by q has the effect of making the model coefficients $\mathbf{C}$ and $\boldsymbol{s}_\mathrm{m}$ largely independent from the operating condition. In the turbulent examples reported later on,

the moving average was computed over 10 min. To avoid the typical possible inaccuracies of nacelle-mounted anemometers, U_a might be based on estimates of the rotor-equivalent wind speed (Soltani et al., 2013).

To simplify the identification of the model coefficients, the radial symmetry of the rotor can be exploited. Assuming a periodic response, the effects of a misalignment in the second blade will be the same as those caused by a misalignment in the first blade, but shifted by $2\pi/3$. Hence, the model coefficients must obey the following relationship:

$$\begin{Bmatrix} c_{c_2} \\ c_{s_2} \end{Bmatrix} = \begin{bmatrix} \cos(2\pi/3) & \sin(2\pi/3) \\ -\sin(2\pi/3) & \cos(2\pi/3) \end{bmatrix} \begin{Bmatrix} c_{c_1} \\ c_{s_1} \end{Bmatrix} = \mathbf{R}\boldsymbol{c}. \tag{12}$$

Clearly, the same argument holds for the relationship between the response of blades two and three. Therefore, matrix $\mathbf{C}$ only depends on the two coefficients of vector $\boldsymbol{c}$ and can be written as

$$\mathbf{C} = \begin{bmatrix} \boldsymbol{c} & \mathbf{R}\boldsymbol{c} & \mathbf{R}^2\boldsymbol{c} \end{bmatrix}. \tag{13}$$

It is trivial to observe that this also implies the same relationship between the coefficients of blades three and one, thus closing the loop.

The imbalance–disturbance model might be affected by proximity to resonant conditions or by the presence of vibration control algorithms implemented onboard the turbine control system. The first problem is readily addressed by avoiding identifying the model and rebalancing the machine in the proximity of resonant conditions, which is easily done since these are typically well known. The second problem might require switching off these additional control loops during identification and rebalancing, although no general statements are possible here and the situation would have to be analyzed in detail for any specific implementation of such algorithms.

2.3 Model identification

Before computing the pitch adjustments that rebalance the rotor, one needs to identify the unknown coefficients in Eq. (9b). To this end, it is convenient to rewrite the imbalance–disturbance model as follows:

$$\boldsymbol{s} = \mathbf{C}\boldsymbol{b} + \boldsymbol{s}_m, \tag{14a}$$
$$= \mathbf{B}\boldsymbol{c} + \boldsymbol{s}_m. \tag{14b}$$

By simple algebraic derivations, one can readily show that matrix $\mathbf{B}$ is a sole function of the pitch adjustment $\boldsymbol{b}$ and is written as

$$\mathbf{B} = \begin{bmatrix} B_{11} & B_{12} \\ -B_{12} & B_{11} \end{bmatrix}, \tag{15}$$

where

$$B_{11} = b_1 + \cos(2\pi/3)b_2 + \cos(4\pi/3)b_3, \tag{16a}$$
$$B_{12} = \sin(2\pi/3)b_2 + \sin(4\pi/3)b_3. \tag{16b}$$

At the beginning of the procedure, one has not yet adjusted the rotor pitch, and hence $\boldsymbol{b} = \boldsymbol{b}^{(1)} = 0$. In this condition, a 1P harmonic equal to $\boldsymbol{s}^{(1)}$ is measured on the machine. Next, the pitch of the blades is changed by a chosen amount $\boldsymbol{b}^{(2)}$. In order not to upset the operating condition of the machine, this arbitrary pitch modification should be characterized by a null collective change. In correspondence to this new condition, one measures a 1P harmonic equal to $\boldsymbol{s}^{(2)}$. Considering the two measurements $\boldsymbol{s}^{(1)}$ and $\boldsymbol{s}^{(2)}$ together, one can write

$$\begin{Bmatrix} \boldsymbol{s}^{(1)} \\ \boldsymbol{s}^{(2)} \end{Bmatrix} = \begin{bmatrix} \mathbf{B}^{(1)} & \mathbf{I} \\ \mathbf{B}^{(2)} & \mathbf{I} \end{bmatrix} \begin{Bmatrix} \boldsymbol{c} \\ \boldsymbol{s}_m \end{Bmatrix}, \tag{17}$$

where $\mathbf{B}^{(1)}$ and $\mathbf{B}^{(2)}$ indicate matrix (15) evaluated in correspondence to vectors $\boldsymbol{b}^{(1)}$ and $\boldsymbol{b}^{(2)}$, respectively. Inverting this relationship, one readily obtains the unknown coefficients $\boldsymbol{c}$ and $\boldsymbol{s}_m$, which fully characterize Eq. (9b).

2.4 Rebalancing

Now that Eq. (9b) has been identified, it can be used to rebalance the rotor. Before doing so, however, one should note that only imbalances among the blades will produce a 1P harmonic in the fixed frame. In fact, a collective rotation of all blades by any given angle will not produce any imbalance, and therefore it cannot be detected by a method based on fixed-frame response signals. This implies that one cannot compute the full pitch adjustment vector $\boldsymbol{b}$, but only a zero-collective adjustment that satisfies the relationship $\sum_{i=1}^{3} b_i = 0$. This is also stated by Eq. (9b), which is in fact a rectangular system of two equations in three unknowns.

By appending the zero-collective constraint to the imbalance–disturbance model, one gets

$$\begin{Bmatrix} \boldsymbol{s} \\ 0 \end{Bmatrix} = \begin{bmatrix} \mathbf{C} \\ \mathbf{1}^T \end{bmatrix} \boldsymbol{b} + \begin{Bmatrix} \boldsymbol{s}_m \\ 0 \end{Bmatrix}, \tag{18}$$

where $\mathbf{1} = (1, 1, 1)^T$. Setting $\boldsymbol{s} = 0$, i.e., requesting a null 1P harmonic response in the fixed frame, one readily computes the necessary pitch adjustments as

$$\boldsymbol{b} = -\begin{bmatrix} \mathbf{C} \\ \mathbf{1}^T \end{bmatrix}^{-1} \begin{Bmatrix} \boldsymbol{s}_m \\ 0 \end{Bmatrix}. \tag{19}$$

Blades are now pitched by $\boldsymbol{b}$, as computed by Eq. (19). If, after application of the computed pitch adjustment, a 1P harmonic is still detected in the fixed frame, then this might be an indication of a non-exact linearity between pitch imbalance and fixed-frame harmonic amplitude. In this case, one can iterate the whole procedure. The measured amplitude in the current configuration becomes the new data point in the

model identification phase. This data point, together with the one measured just before adjusting the blade pitch, allows for the identification of a new model. Given the new coefficients, the zero-collective constraint is appended to the model, the inversion of which yields the new pitch adjustments. The process is repeated until only a negligible 1P harmonic signal is left in the fixed frame. Figure 2 gives a graphical representation of this algorithmic procedure.

Inspecting the values of the computed pitch adjustments $\boldsymbol{b}$, one may notice in some cases that two blades are characterized by the same correction, for example $b_1 = b_2 \neq b_3$. This means that only one blade (number 3 in this specific example) was misaligned with respect to the other two. In this case, one might choose to change the blade pitch of blade 3 by $b_3 - 2b_1$, which has the effect of realigning blade 3 with the others instead of adjusting all three at null collective change. This might be useful, for example, in the case that a blade has been mounted with the wrong pitch offset.

3 Results

3.1 Simulation environment

In this work, the proposed rebalancing procedure is demonstrated with the help of aeroservoelastic simulations of a 3 MW horizontal axis wind turbine. The machine, characterized by an 80 m hub height and a rotor diameter of 93 m, has cut-in, rated and cut-out speeds equal to 3, 12.5 and 25 m s^{-1}, respectively. The cut-in rotor speed is equal to 5.2 RPM, whereas the rated rotor speed is equal to 15 RPM. Both side–side and fore–aft tower frequencies are equal to 0.3 Hz. The first blade flap-wise frequency varies between 0.9 Hz at cut-in and 1 Hz at rated rotor speed. Finally, the first blade edge-wise frequency is about 1.5 Hz. The transient response of the machine is computed with the finite-element multibody code `Cp-Lambda` (Bottasso and Croce, 2006). The rotor blades and tower are modeled using a geometrical exact beam formulation (with torsion, axial, bending and shear deformability), resulting in a nonlinear finite-element model. The rest of the wind turbine is modeled by a combination of rigid bodies, joints and flexible elements to represent nacelle, drivetrain and foundations. Generator and pitch actuators are modeled by first- and second-order dynamical systems, respectively. The classical blade element momentum theory (BEM) is used to represent the aerodynamics, considering hub and tip losses, dynamic stall, unsteady aerodynamics and rotor-tower interference. A speed-scheduled linear quadratic regulator (LQR) (Riboldi, 2012) is used for the implementation of the pitch–torque controller. Turbulent wind time histories of 10 min duration are generated with the code `TurbSim` (Jonkman and Kilcher, 2012) based on the Kaimal turbulence model.

Different combinations of initial pitch misalignments in the range $\pm 2^\circ$ are considered, in which only one, two or even all three blades are simultaneously misaligned. To model finite resolution effects in the pitch system, the minimum resolution of the pitch motion is assumed to be 0.1°. Therefore, any blade movement smaller than the given resolution is rounded to the closest neighboring integer multiple. To quantify the effectiveness of the rebalancing algorithm, the absolute residual pitch misalignment angle ϵ is defined as

$$\epsilon = \max(\boldsymbol{b}_\mathrm{m} - \boldsymbol{b}) - \min(\boldsymbol{b}_\mathrm{m} - \boldsymbol{b}), \tag{20}$$

where $\boldsymbol{b}_\mathrm{m} - \boldsymbol{b}$ is the difference between real and computed misalignments.

Accelerometers are placed on the machine main bearing, with the goal of measuring the fixed-frame response of the system, and they are simulated in the mathematical model including the effects of measurement noise. Various tests were conducted in order to identify an optimal accelerometer configuration. Typically, the best results were obtained when two accelerometers are located to the two sides of the main bearing and spaced as far as possible from each other. The two accelerometer signals are subtracted one from the other, yielding a differential measurement proportional to the yawing accelerations of the rotor.

3.2 Linearity

The model described in Sect. 2.2 is based on the assumption that 1P harmonics in the fixed frame depend linearly on the pitch misalignment angle. To validate this assumption, simulations were performed to study the wind turbine fixed-frame response to blade misalignments. The simulations were performed in steady sheared wind conditions, misaligning one blade at a time.

Figure 3 shows the sine and cosine differential acceleration components at the main bearing for each one of the three blades. The plots correspond to a wind condition of 7 m s^{-1}, although similar results were obtained for different wind speeds. Accelerations were scaled with respect to the dynamic pressure and averaged over the simulation time. The relationship between 1P response and pitch misalignment appears to be linear to a very good approximation, with the correlation coefficient of the linear best fits differing from 1 by less that 10^{-3}.

It is interesting to observe that the misalignment of each different blade leaves a unique fingerprint on the measured signal. This means that the linear model not only contains information on the severity of the misalignment, but also on where the misalignment is located.

3.3 Performance assessment of the rebalancing algorithm

Next, the performance of the proposed algorithm is tested in a variety of different wind conditions. The model expressed by Eq. (17) is identified from accelerometer measurements recorded in 10 min turbulent conditions, characterized by different values of air density, wind speed, turbulence inten-

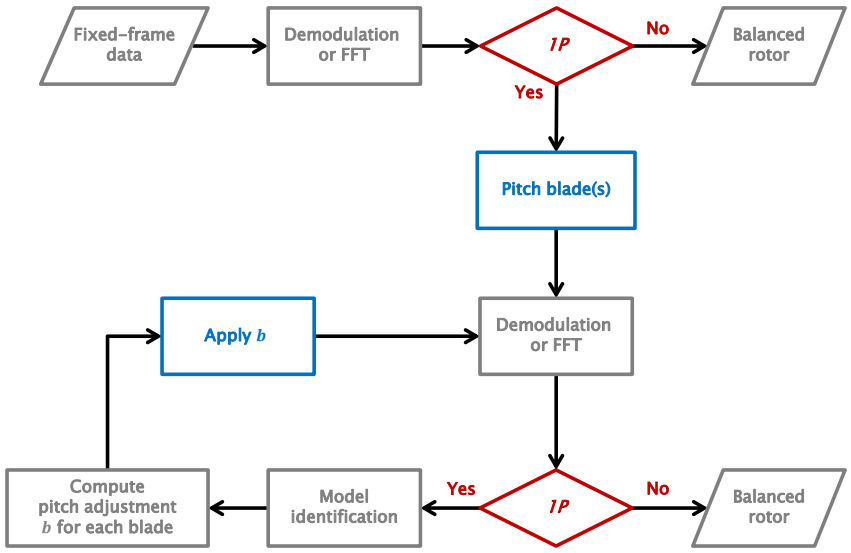

Figure 2. Graphical representation of the rotor rebalancing algorithm.

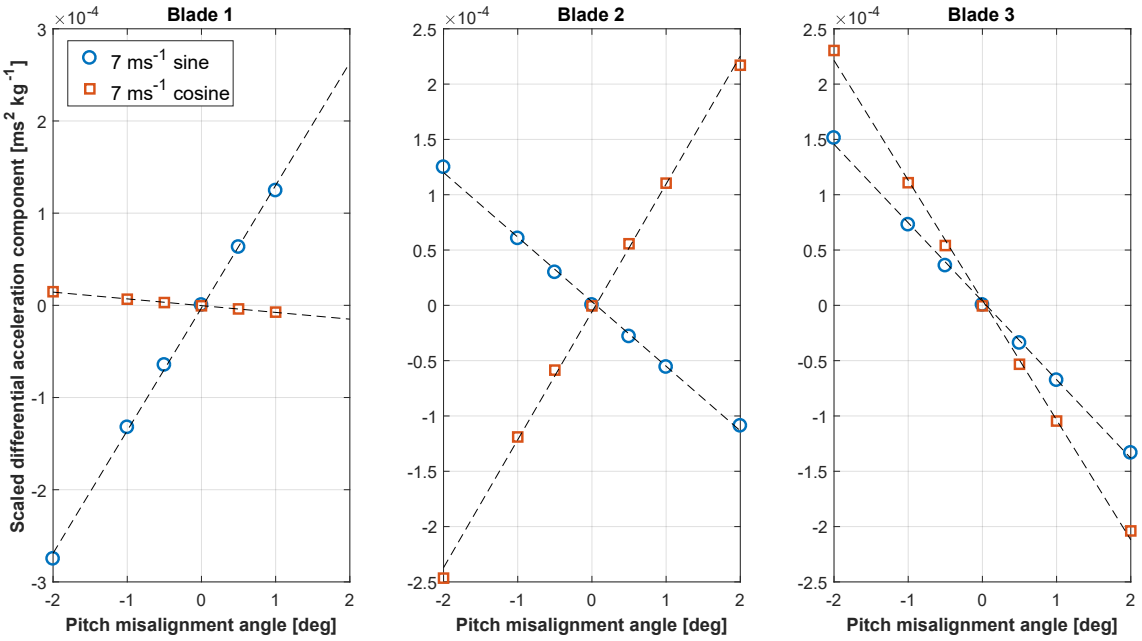

Figure 3. Cosine (squares) and sine (circles) 1P components of the main-bearing scaled differential acceleration as functions of pitch misalignment.

sity (TI), yaw misalignment, wind shear and upflow. These quantities are assumed to change according to a number of scenarios, termed series A through F, described in detail in Appendix A. Once the model is identified, the rotor is rebalanced by inverting the model itself. The procedure of identification–rebalancing is then repeated until the residual 1P harmonic is smaller than a given threshold.

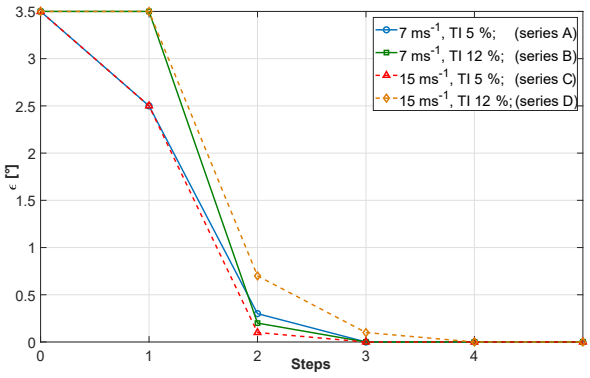

Figure 4. Residual pitch misalignment as a function of the number of steps for given wind speed and turbulence intensity, but variable conditions according to series A through D.

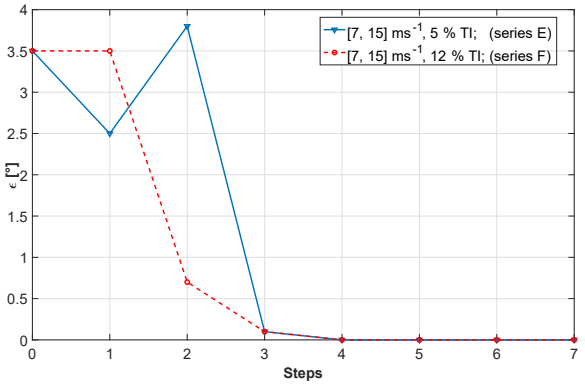

Figure 5. Residual pitch misalignment as a function of the number of steps for given turbulence intensity and variable wind speed, but variable conditions according to series E and F.

Figure 4 shows the absolute residual pitch misalignment ϵ after each iteration of the rebalancing algorithm. The specific cases reported in the figure correspond to situations in which wind speed and TI are kept constant, whereas mean values of yaw misalignment, vertical shear and upflow angle vary throughout the identification–rebalancing sequence according to what is specified for series A through D.

In the figure, the abscissa represents the various steps of the procedure. At the beginning (step 0), a 1P acceleration is measured in the fixed frame. Next, one or more blades are randomly pitched (step 1), while keeping the collective constant. In the resulting new configuration, a new 1P acceleration is measured. Since this step is random, the unbalance of the blades may worsen in this first step. The algorithm is now applied by first identifying the model and then computing the pitch adjustment $\boldsymbol{b}$ that rebalances the rotor. The blades are then accordingly pitched (step 2). If a residual 1P harmonic is still present, the algorithm is applied again using data from steps 1 and 2, resulting in a new pitch adjustment (step 3). The procedure is repeated until convergence.

The figure shows that the proposed algorithm is capable of rebalancing the rotor in a very small number of steps, typically ranging between three and four. It should be noted that during each one of these steps, the machine is operating in markedly different operating conditions, as described by the series reported in the Appendix. Notwithstanding these very significant operational changes, the procedure seems to be quite robust.

An important remark is due at this point. As wind conditions may change from one step to the next, in general it is not possible to guarantee that the imbalance will always diminish at each step of the algorithm. Indeed, some of the following numerical experiments show that the imbalance may occasionally increase. However, this happens only in the case of radical changes in wind conditions from one step to the next. It would be relatively straightforward to avoid such situations by implementing some simple logic in the procedure. For example, one might monitor the operating parameters and continue with rebalancing only when changes do not exceed a certain threshold. In addition, if one observes an increase in the 1P harmonic amplitude after a rebalancing step, then that step might be rejected and the blades could be pitched back to their previous setting. To consider a worst case scenario, in all numerical experiments presented here these simple precautions were not taken. Therefore, the algorithm was forced to continue irrespective of the severity of operating changes. Because of this, the results show occasional increases in the imbalance throughout the iterations. Nevertheless, these same results also show that the algorithm was always eventually able to successfully rebalance the rotor in a very small number of steps.

Figure 5 reports results obtained at different TI levels for cases characterized by changes in wind speed from 7 to 15 m s^{-1} and in density from 1.225 to 1.1 kg m^{-3} for series E and F. For the E series results, the situation temporarily worsens between steps 1 and 2. This may be due to the simultaneous change in air density, yaw misalignment and halving the shear from 0.4 to 0.2 in this step. Here again, very variable inflow conditions do not seem to excessively affect the performance of the algorithm, which is indeed able to completely rebalance the turbine rotor within four steps.

3.4 Effects of measurement noise

The effects of noise on the measurement of the accelerations driving the algorithm were then investigated. In fact, small imbalances induce only small 1P harmonics in the fixed frame so that the effects of noise on the measurements can be significant.

Measurement noise is modeled by adding a white Gaussian signal to the accelerations measured on the multibody wind turbine model. Five different signal-

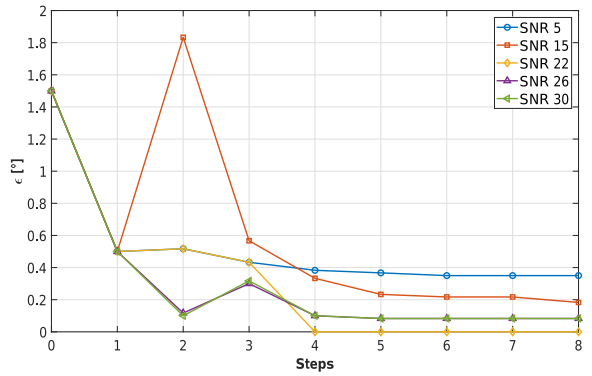

Figure 6. Residual pitch misalignment as a function of the number of steps for different SNRs in constant uniform inflow at $11\,\mathrm{m\,s^{-1}}$, $\phi = 0°$, $\kappa = 0.4$, $\chi = 0°$ and $\rho = 1.225\,\mathrm{kg\,m^{-3}}$.

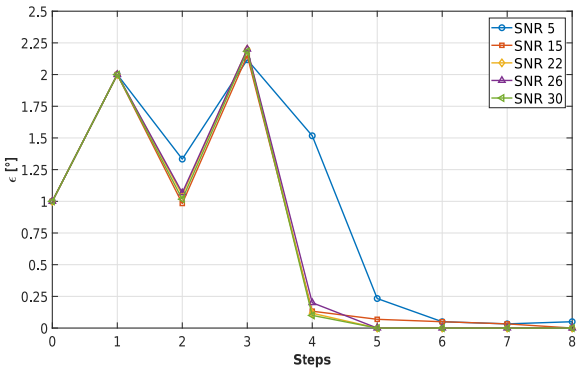

Figure 7. Residual pitch misalignment as a function of the number of steps for different SNRs for variable nonturbulent inflow (series G).

to-noise ratios (SNRs) are considered, namely SNR = [5 15 22 26 30] dB. To obtain statistically relevant results, for each SNR six different random noise realizations are used, and the results are then averaged.

In addition to acceleration noise, the study also considered the effects of errors in the measurement of the average wind speed U_a of Eq. (11), used for scaling the imbalance harmonic amplitudes. Such errors might be due to the well-known poor accuracy of nacelle-mounted anemometers. Results are not reported here for space limitations, but even errors of $\pm 20\,\%$ did not significantly affect the performance of the proposed algorithm.

3.4.1 Nonturbulent wind conditions

To separate the effects of measurement noise from the stochastic disturbances caused by turbulence, series composed of 3 min long nonturbulent wind conditions are considered first.

Figure 6 shows the average residual pitch misalignment for different SNRs for a case in which all wind parameters are constant and wind speed is equal to $11\,\mathrm{m\,s^{-1}}$. The results clearly illustrate the detrimental effects of decreasing SNR values on the quality of the rebalancing. For SNR = 5 dB, the residual ϵ converges to about 0.35°, which is nevertheless a good result considering that in this particular case the initial imbalance was of 1.5°. Increasing SNR, the residual misalignment improves as expected, showing that, from SNR $\geq$ 22 dB and higher, ϵ converges to values smaller than 0.1° (which is the assumed minimum resolution of the pitch system, and therefore past this value differences among the SNR levels become irrelevant).

Figure 7 shows results obtained in varying wind conditions. Specifically, wind speed and density change respectively from 11 to $15\,\mathrm{m\,s^{-1}}$ and from 1.1 to $1.225\,\mathrm{kg\,m^{-3}}$, while vertical shear and misalignment angles vary according to series G. Here again a temporary worsening of the rotor balancing can be observed between step 2 and 3, probably due to the halving of shear between these two steps, accompanied by simultaneous substantial increases in air density and wind speed.

It appears that the method very effectively reduces the initial misalignments. Indeed, results show a very modest effect of SNR, except for the lowest value of 5 dB that seems to take a bit longer to converge. The apparently surprising lack of sensitivity to SNR can be explained by the changing yaw misalignment within the steps. Indeed, as shown in Eq. (8b), the 1P harmonic measured in the fixed frame is related to the presence of a cross-flow component. Therefore, a bit of misalignment of the rotor axis with respect to the wind vector eases rebalancing because it makes the effects of an unbalance more prominent and therefore less affected by noise.

3.4.2 Turbulent wind conditions

Figure 8 shows the same simulation series as in Fig. 7 (i.e., wind speed and density changing from 11 to $15\,\mathrm{m\,s^{-1}}$ and from 1.1 to $1.225\,\mathrm{kg\,m^{-3}}$, respectively, with other wind parameters according to series G), but for a turbulent inflow characterized by TI = 5 %. Here again it appears that SNRs larger than 22 dB have very little effect on the speed of convergence of the algorithm.

It is also interesting to observe that convergence is actually faster in turbulent conditions (Fig. 8) than in nonturbulent ones (Fig. 7). This may be due again to the fact that turbulence implies a higher excitation of the 1P harmonic, making it more evident against the sensor noise.

A large number of tests performed in additional operating conditions and SNR values confirm the findings reported herein. Clearly, one should choose a sensor with the highest SNR possible in the frequency range of interest. However, these results suggest that even fairly limited values of SNR should typically be sufficient for the algorithm to completely rebalance a rotor in turbulent and varying wind conditions.

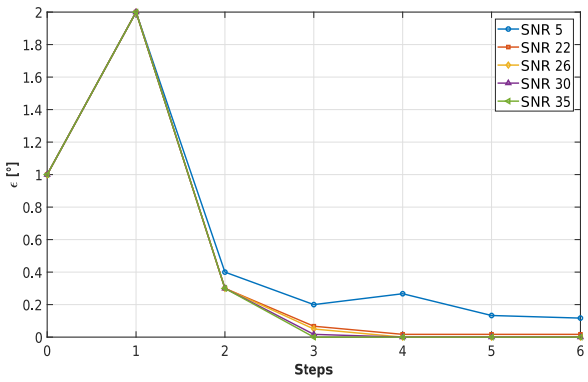

Figure 8. Residual pitch misalignment as a function of the number of steps for different SNRs with turbulent inflow at TI = 5 % (series G).

4 Conclusions

This paper has described a new method to detect and correct pitch imbalances in wind turbine rotors. The method uses a measured signal in the fixed frame, typically in the form of accelerations or loads. The signal is demodulated to extract the 1P harmonic, which is then related to the misalignment of the blades by a linear model. By exploiting the axial symmetry of the rotor, the phase of the signal is used to detect which blades are unbalanced. The use of the rotor axial symmetry has the additional effect of reducing the number of free parameters in the model to only two.

The model parameters are readily identified by measuring the signal and computing its harmonics at two different pitch settings, something that is easily achieved by simply pitching the blades by a small chosen amount. The procedure can be performed while the machine is in operation, without shutting it down. The method also works if measurements are taken at different operating conditions, which is indeed inevitable in the field. Once the model has been identified, its inversion readily yields the pitch adjustments of the various blades that rebalance the rotor. If, after rebalancing, some remaining 1P harmonic is detected, the whole procedure can be repeated, thereby eliminating the effects of possible small nonlinearities in the imbalance–disturbance relationship. The whole approach has fairly minimal requirements, as it only assumes the availability of a sensor of sufficient accuracy and bandwidth to detect the 1P harmonic to the desired precision and the ability to command the pitch setting of each blade independently from the others.

Extensive numerical simulations were conducted with the proposed procedure using a detailed aeroservoelastic model of a multi-MW wind turbine. The analysis considered realistic scenarios in which measurements and rebalancing were performed in operating conditions characterized by varying air density, wind speed, yaw misalignment, upflow, shear and turbulence intensity. The simulation environment also considered the modeling of measurement noise and disturbances.

Based on the results presented herein, the following conclusions may be drawn.

- The relationship between pitch imbalance and 1P fixed-frame harmonics appears to be linear and unique depending on the location of the misalignment. This allows one to not only quantify the severity of the imbalance, but also the unbalanced blade(s).

- In realistic wind conditions, i.e., with turbulent wind and variable air density, speed, vertical shear and wind rotor angles, the proposed algorithm successfully rebalances the rotor typically within four iterations. To account for possible changes in the mean value of wind speed and/or density, the simple scaling of the 1P input by the dynamic pressure was sufficient to guarantee a good performance in all tested conditions.

- Given the relatively small magnitude of the signals that are generated by small misalignments of the blades, one might expect that particular attention should to be paid to the selection of the installed sensors. However, results have shown that measurements are rather insensitive to SNR. Indeed, values of SNR $\geq$ 30 dB in the frequency range of interest are more than adequate for the present application, although even a significantly smaller value of SNR gives only a slight performance degradation. However, one should keep in mind that different results might have been obtained on different wind turbines and when placing the sensors at different locations than the ones considered here.

- Good results were obtained by using observation windows of 10 min. Although longer time windows might appear to be beneficial to smooth out fluctuations due to turbulence and noise, one should also consider that long time windows might also imply significant changes not only in the operating conditions, but also in rotor speed, which should also be duly accounted for.

Notwithstanding the very promising results obtained here in a simulation environment, a demonstration in the field remains indispensable to prove the actual effectiveness and applicability of the proposed method in practice. Finally, future studies should consider the case of simultaneous aerodynamic and mass imbalances.

Data availability. Data can be provided upon request. Please contact the corresponding author Carlo L. Bottasso (carlo.bottasso@tum.de).

Appendix A: Wind series

The following tables report the values of the relevant operational and wind parameters used for the verification of the rebalancing algorithm.

Table A1. Series A. Initial blade misalignment: $\boldsymbol{b}_{\mathrm{m}} = (2°, 0.5°, -1.5°)^T$.

Step	0	1	2	3
U (m s^{-1})	7	7	7	7
TI (%)	5	5	5	5
ρ (kg m^{-3})	1.225	1.225	1.225	1.225
ϕ (°)	0	10	0	10
κ (–)	0.2	0.4	0.2	0.2
χ (°)	0	0	0	0

Table A2. Series B. Initial blade misalignment: $\boldsymbol{b}_{\mathrm{m}} = (0.5°, -1.5°, 2°)^T$.

Step	0	1	2	3
U (m s^{-1})	7	7	7	7
TI (%)	12	12	12	12
ρ (kg m^{-3})	1.225	1.225	1.225	1.225
ϕ (°)	10	10	10	10
κ (–)	0.4	0.4	0.4	0.2
χ (°)	0	0	0	0

Table A3. Series C. Initial blade misalignment: $\boldsymbol{b}_{\mathrm{m}} = (2°, 0.5°, -1.5°)^T$.

Step	0	1	2	3
U (m s^{-1})	15	15	15	15
TI (%)	5	5	5	5
ρ (kg m^{-3})	1.225	1.225	1.225	1.225
ϕ (°)	0	0	10	10
κ (–)	0.2	0.2	0.4	0.2
χ (°)	0	0	0	0

Table A4. Series D. Initial blade misalignment: $\boldsymbol{b}_{\mathrm{m}} = (0.5°, 2°, -1.5°)^T$.

Step	0	1	2	3	4
U (m s^{-1})	15	15	15	15	15
TI (%)	12	12	12	12	12
ρ (kg m^{-3})	1.225	1.225	1.225	1.225	1.225
ϕ (°)	0	10	0	0	0
κ (–)	0.2	0.4	0.2	0.2	0.2
χ (°)	0	0	0	0	0

Table A5. Series E. Initial blade misalignment: $\boldsymbol{b}_{\mathrm{m}} = (2°, 0.5°, -1.5°)^T$.

Step	0	1	2	3	4
U (m s^{-1})	15	7	7	15	15
TI (%)	5	5	5	5	5
ρ (kg m^{-3})	1.225	1.225	1.1	1.225	1.225
ϕ (°)	0	10	0	10	0
κ (–)	0.2	0.4	0.2	0.4	0.2
χ (°)	0	0	0	0	0

Table A6. Series F. Initial blade misalignment: $\boldsymbol{b}_{\mathrm{m}} = (1°, 2°, -1.5°)^T$.

Step	0	1	2	3	4
U (m s^{-1})	15	7	7	15	15
TI (%)	12	12	12	12	12
ρ (kg m^{-3})	1.225	1.225	1.1	1.225	1.225
ϕ (°)	10	10	0	10	0
κ (–)	0.4	0.4	0.2	0.4	0.2
χ (°)	0	0	0	0	0

Table A7. Series G. Initial blade misalignment: $\boldsymbol{b}_{\mathrm{m}} = (-1°, 0°, 0°)^T$.

Step	0	1	2	3	4	5	6	7	8
U (m s^{-1})	15	11	11	15	11	15	15	11	15
ρ (kg m^{-3})	1.1	1.225	1.1	1.225	1.225	1.1	1.225	1.1	1.1
ϕ (°)	0	0	10	10	0	10	0	10	10
κ (–)	0.4	0.2	0.4	0.2	0.2	0.2	0.4	0.4	0.2
χ (°)	−4	0	0	0	0	0	−4	0	0

Appendix B: Nomenclature

a	Axial induction
b_i	Pitch adjustment that rebalances blade i
b_{m_i}	Pitch misalignment of blade i
s	Fixed-frame signal
t	Rotor thrust
t_i	Out-of-plane shear of blade i
B	Number of blades
$C_{\mathrm{L}\alpha}$	Slope of the lift coefficient
J	Flapping moment of inertia
K	Linear vertical shear factor
R	Rotor radius
U	Wind speed
V_0	Cross-flow speed
γ	Lock number
ϵ	Residual pitch misalignment angle
θ	Pitch angle
κ	Vertical shear exponent
ϱ	Air density
ϕ	Yaw misalignment angle
χ	Upflow angle
ψ	Azimuthal angle
Λ	Nondimensional flow velocity at the rotor disk
Ω	Rotor angular velocity
$\boldsymbol{b}$	Pitch adjustment vector
$\boldsymbol{b}_{\mathrm{m}}$	Pitch misalignment vector
$\boldsymbol{s}$	Fixed-frame signal vector
$\mathbf{I}$	Identity matrix
$\mathbf{R}$	Rotation matrix between two consecutive blades
$(\cdot)_0$	Zeroth harmonic
$(\cdot)_n$	nth harmonic
$(\cdot)_i$	Quantity related to the ith blade
$(\cdot)^{(j)}$	Quantity measured with the jth pitch setting
$(\cdot)_{\mathrm{c}}$	Cosine amplitude
$(\cdot)_{\mathrm{s}}$	Sine amplitude
$\bar{(\cdot)}$	Nondimensional quantity
nP	n times per revolution
BEM	Blade element momentum
SNR	Signal-to-noise ratio
TI	Turbulence intensity

Competing interests. The authors declare that they have no conflict of interest.

This work was supported by the German Research Foundation (DFG) and the Technische Universität München within the funding program Open Access Publishing.

Edited by: Joachim Peinke
Reviewed by: two anonymous referees

References

Axelsson, U., Bjork, M., and Haag, C.: Method for Balancing a Wind Turbine, US Patent No. 8683688 B2, 2014.

Bertelè, M., Cacciola, S., Bottasso, C. L., and Domestici M.: Automatic track and balance of wind turbine rotors, in: WCCM 2017 – 1st World Congress on Condition Monitoring, 13–16 June 2017, London, UK, 2017.

Bossanyi, E. A.: Wind turbine control for load reduction, Wind Energy, 6, 229–244, https://doi.org/10.1002/we.95, 2003.

Bottasso, C. L. and Croce, A.: Cp-Lambda: User's Manual, 2006.

Cacciola, S., and Riboldi, C. E. D.: Equalizing aerodynamic blade loads through individual pitch control via multi-blade multilag transformation, J. Sol. Energ., 139, 061008, https://doi.org/10.1115/1.4037744, 2017.

Cacciola, S., Munduate, I., and Bottasso, C. L.: Detection of rotor imbalance, including root cause, severity and location, J. Phys. Conf. Ser., 753, 072003, https://doi.org/10.1088/1742-6596/753/7/072003, 2016.

Cacciola, S., Riboldi, C. E. D., and Croce, A.: A new decentralized pitch control scheme for wind turbines, Wind turbine and wind farm control: control challenges and solutions, 20th IFAC World Congress, IFAC-PapersOnLine, 50, 9908–9913, https://doi.org/10.1016/j.ifacol.2017.08.1627, 2017.

GL Standards: Guideline for the Certification of Wind Turbines, Rules and Guidelines Industrial Services, Germanischer Lloyd, Hamburg, Germany, 2010.

Hameed, Z., Hong, Y., Cho, Y., Ahn, S., and Song, C.: Condition monitoring and fault detection of wind turbines and related algorithms: a review, Renew. Sust. Energ. Rev., 13, 1–39, https://doi.org/10.1016/j.rser.2007.05.008, 2009.

Hyers, R. W., Mcgowan, J. G., Sullivan, K. L., Manwell, J. F., and Syrett, B. C.: Condition monitoring and prognosis of utility scale wind turbines, Energy Materials, 1, 187–203, https://doi.org/10.1179/174892406X163397, 2006.

Jonkman, B. and Kilcher, L.: TurbSim Users' Guide: Version 1.06.00, 2012.

Kanev, S. and van Engelen, T.: Exploring the limits in individual pitch control, in: European Wind Energy Conference (EWEC), 16–19 March 2009, Marseille, France, 2009.

Kanev, W. E., Neilson, V., and Dominguez, S.: Alleviation of unbalanced rotor loads by single blade controllers, in: European Wind Energy Conference (EWEC), 16–19 March 2009, Marseille, France, 1296–1301, 2009.

Kusiak, A. and Verma, A.: A data-driven approach for monitoring blade pitch faults in wind turbines, IEEE T. Sustain. Energ., 2, 87–96, https://doi.org/10.1109/TSTE.2010.2066585, 2011.

Kusnick, J., Adams, D. E., and Griffith, D. T.: Wind turbine rotor imbalance detection using nacelle and blade measurements, Wind Energy, 18, 267–276, https://doi.org/10.1002/we.1696, 2015.

Manwell, J. F., McGowan, J. G., and Rogers, A. L.: Wind Energy Explained – Theory, Design and Application, John Wiley and Sons Ltd., West Sussex, UK, 2009.

Niebsch, J. and Ramlau, R.: Simultaneous estimation of mass and aerodynamic rotor imbalances for wind turbines, Journal of Mathematics in Industry, 4, 1–12, 2014.

Niebsch, J., Ramlau, R., and Nguyen, T. T.: Mass and aerodynamic imbalance estimates of wind turbines, Energies, 3, 696–710, https://doi.org/10.3390/en3040696, 2010.

Petrović, V., Jelavić, M., and Baotić, M.: Advanced control algorithms for reduction of wind turbine structural loads, Renew. Energ., 76, 418–431, https://doi.org/10.1016/j.renene.2014.11.051, 2015.

Pierce, K. G. and Slack, R. P.: Methods and Apparatus for Balancing a Rotor, US Patent No. 0035136, 2009.

Riboldi, C.: Advanced Control Laws for Variable-Speed Wind Turbines and Supporting Enabling Technologies, PhD thesis, Politecnico di Milano, Milano, Italy, 2012.

Soltani, M. N., Knudsen, T., Svenstrup, M., Wisniewski, R., Brath, P., Ortega, R., and Johnson, K.: Estimation of rotor effective wind speed: a comparison, IEEE T. Contr. Syst. T., 21, 1155–1167, https://doi.org/10.1109/TCST.2013.2260751, 2013.

Wilkinson, M., Hendriks, B., Spinato, F., and Harman, K.: Methodology and results of the Reliawind reliability field study, in: European Wind Energy Conference, 20–23 April, Warsaw, Poland, 2010.

Yang, W., Tavner, P. J., and Wilkinson, M.: Wind turbine condition monitoring and fault diagnosis using both mechanical and electrical signatures, in: 2008 IEEE/ASME International Conference on Advanced Intelligent Mechatronics, 2–5 July, Xian, China, 1296–1301, https://doi.org/10.1109/AIM.2008.4601849, 2008.